9-29-2017 10:00 AM

Petrophysical Investigations of the Marathon Cu-PGE Deposit, Marathon, ON

Hiruni Gunawardana, *The University of Western Ontario*

Supervisor: Phil J.A MaCausland, *The University of Western Ontario*
Co-Supervisor: Gerhard Pratt, *The University of Western Ontario*
A thesis submitted in partial fulfillment of the requirements for the Master of Science degree in Geophysics

Abstract

Drill core samples obtained from four mineralized zones of the Marathon Cu-PGE deposit in the Coldwell igneous complex have been investigated for their petrophysical characteristics. Remanent magnetization was used as a possible tool to reorient core samples but a drilling induced overprint magnetization dominated the record. Anisotropy of magnetic susceptibility was measured to provide a proxy for the petrofabric of samples obtained from oriented drill cores; a well-defined planar fabric was found to strike 177 and dip 25°W, with down-dip lineation, in excellent agreement with inferred magmatic flow direction based on 3D modeling of mineralized footwall troughs. Magnetite rich lithologies of the deposit show anomalous magnetic susceptibilities, natural remanent magnetizations, chargeabilities and resistivities which can be used as a resource vectoring tool to guide geophysical surveys in defining new feeder channels and conduit systems. Acoustic impedance contrasts between lithological units and highly mineralized zones indicate the possibility of employing seismic methods (reflection, tomography) to investigate the subsurface distribution of mineralization.

Key words- induced magnetization, remanent magnetization, AMS, anisotropy, petrofabric, magnetic, susceptibility. chargeability, resistivity, P-wave velocity, petrophysics, gabbro, Marathon, Ontario, Cu-PGE

Acknowledgements

I wish to extend my sincere gratitude to Dr. Phil McCausland for his unwavering support throughout the course of this thesis. His guidance, advices and expertise in the subject matter helped in structuring this thesis to a great deal.

I am much obliged to Dr. Gerhard Pratt for giving me the opportunity to get involved in this Masters project and providing me with helpful feedback on the thesis related work.

I would also like to thank Dr. David Good for imparting his wisdom on the Marathon deposit. His helpful guidance in geochemical analysis and data processing is greatly appreciated.

I would also like to thank the staff of Stillwater Canada Inc., especially John McBride for the insightful conversations and providing me with drill core samples to analyze in this thesis!

Lastly, I would like to thank my parents and Fabio for being a constant support system throughout the past two years!

Table of Contents

Table of Figures

List of Tables

List of Appendices

Chapter 1
Introduction

The Marathon Deposit, hosted in the Coldwell Alkaline Complex, is studied for its platinum group elements, (PGE/PGM) and copper (Cu) content hosted in a magmatic sulphide deposit. This thesis is a study of the petrophysical characteristics and their variations in the mineralized zones of the Marathon deposit.

Platinum Group Elements (PGEs) and Cu are valuable and important resources; high in demand in the current technologically and industrially developed society. PGEs consist of the elements platinum (Pt), palladium (Pd), iridium (Ir), osmium (Os), rhodium (Rh) and ruthenium (Ru) which are chemically similar and often tend to occur in the same mineral deposits alongside Ni, Cu and as elements typically associated with valuable minerals such as gold.

In 1920, sulphide mineralization was discovered during prospecting work at the Marathon deposit which eventually led to extensive exploration for copper and titanium (Barrie et al., 2002; Good, 1992). Later on, in the 1960s, exploration continued under Anaconda Canada Exploration Ltd, leading to 171 drill holes with an estimated total of 36,000 m in depth. The subsequent prospecting, field mapping and other geophysical surveys outlined a significantly economic deposit of Cu along with other minerals such as Pd, Pt, Au and Ni. In 1985, due to the escalated prices of PGE, Fleck Resources reactivated the project with further exploration done on the mineralization units. Again in 1989 and then in late 1990s, other exploration companies carried out reassaying programs of existing drill cores, accompanied by drilling, trenching and more geophysical surveys with the hopes of estimating and penetrating other ore bodies lying within the region (Barrie et al., 2002; Shaw, 1997). In late 1999, Geomaque Explorations Ltd. and other exploration companies reactivated the project due to another escalation of PGE demand. A nearly continuous stream of research has been conducted on the Marathon deposit over the past 50 years, resulting in an extensive database of over 40,000 assays, obtained from over 750 drill cores (Good et al., 2015; Barrie et al.,2002).

1.1 Mining for PGE

Chemical and physical properties of PGEs have vital commercial importance in the chemical, electrical, medical, glass and motor vehicle industries, used for resistance to corrosion and oxidation, high melting points, electrical conductivity and catalytic activity. Most recent applications are associated with motor vehicle industry from increase in the global emission controls, development of Pb free petrol and efforts to improve fuel efficiency. Other applications include the use of platinum-rhodium alloys to oxidize ammonia to nitric acid in the production of fertilizers, as electrode coatings, in electronics (LCD displays and fiber optic cables), multilayer ceramic capacitors, thermocouples for science and steel industries and for medical drugs and implants. Platinum is also used in high demand for jewelry. Therefore, the six PGE minerals have unique properties that will sustain their long term demand. As a result, PGEs are used in the manufacturing industries up to 20% on the world's consumer goods and are often alloyed with other metals including combinations of other PGEs. An increasing amount is being used for investment purposes in the form of bars and American Eagle coins (Ruthart at al., 2012).

The largest manufacturer of PGEs is South Africa, dominating up to 60% of the world market. Russia, Canada, United states and to smaller proportions Finland, Yugoslovia and Australia, contribute to the global manufacturing of PGEs. Canada's sole PGE producing mine is located in Lac des Iles, 80 km north west of Thunder Bay, Ontario. Ni mining operations in Sudbury, Ontario produces PGEs as byproducts. The only other sole large scale PGE operation in North America is the Stillwater mine located in Montana, USA (Geoscience Australia website).

PGE markets saw an exponential growth in demand for the past 25 years, due to the vastly expanding, industrially and technologically dependant society. Yet, last few years observed falling prices in all precious metals including PGEs and Cu although demand trends are positive.

Total supply of platinum by the end of 2016 was 6,106, 000 oz against a total net demand of 6,099,000 oz. Palladium supply was 6,390,000 oz with a total net demand of 7,233,000 oz. Rhodium supply was 739,000 oz against a total net demand of 755,000 oz (British geological survey). In 2014-2015, most PGM prices dropped almost 20-30% in its value, forcing most producing companies to stock pile in anticipation for higher prices in the future. Platinum price is currently at $920 per oz, a stark contrast from 2013 prices which ranged around $1600 per oz.

Palladium prices range around $806 per oz and Rhodium prices are at $950 per oz. Iridium and Ruthenium ranges at $945 and $65 per oz (from Johnson Matthey Precious Metals Management website). The PGM industry has been negatively affected due to a slowdown of the world economic growth, increased uncertainty in the key Chinese market and low recovery in the South African supplies. This also implies lower cash flows for mineral exploration and development work in the industry. Therefore, a dire need for less expensive means of innovative research programs is in need to ensure an adequate supply of PGEs for future usage.

1.2 Mining for Cu

From the discovery of copper alloying with tin to produce bronze, marking the beginning of Bronze Age, the use of copper had been one of the most commonly relied metals in human history. Uses of copper as a metal and as an alloy are invaluable and extremely important in today's society. Copper's excellent electrical and thermal conducting properties are used in many of the industrial machinery and equipment, electric and electronic products, power generation and transmission. For instance, copper wiring and plumbing are integral to appliances, heating and cooling systems and telecommunication links. It is also a good corrosion resistant, quite ductile, tough and alloys easily with other metals and therefore is used in many of the building- transportation products and general consumer goods.

World demand and consumption of copper have increased dramatically in the past 25 years. Copper is a material used in great quantities and therefore, demand for new constructions and remodeling of infrastructure correlates greatly with the demand for copper (USGS website, commodities information). Yet, due to the present state of the global economic slump, the demand for copper has lagged behind for the past few years. Globally, the market for copper is one of the largest behind iron and aluminum. South America dominates as the largest copper producers in the world, followed by United States and China. By the end of 2016, the worldwide production of copper was at 23,308,000 tons against a demand of 23,437,000 tons for the last year and shows an overall trend of decrease in supply. Copper prices saw a significant dip compared to the last 4 years, trading at US$ 4,863 per a ton of copper by the end of 2016. This is almost a 50% drop in prices compared to 2011's US$ 8,811 per ton (Geoscience Australia website).

1.3 Ore deposit chemistry and processes associated with Cu-PGE ores

PGEs and Cu mineralization is usually associated with mafic or ultramafic rocks from mantle derived magmas which segregate to immiscible sulphide liquid from the surrounding mafic melt. Such magmas are formed through melting of the mantle and raised to the crust and crystallize as intrusive bodies in structural traps to be later accessed by mining (Barrie et al., 2001; Good, 1992; Miller and Nicholson, 2013). Various factors such as the composition of the mantle source, degree of partial melting, timing and mechanisms of crystallizations and contamination of crustal rocks, must favor sulphide saturation and deposition in structural trappings for the Cu-PGE deposit (Mungall & Naldrett, 2008; McDonald,1987; Arndt et al., 2005; Mungall et al., 2004; Godel & Barnes, 2007; Driscoll &Jimenez, 2016). A key point to note is that during the process of the crystallization sequence, the magma must be sulphide saturated and contain chalcophile/PGE elements to the degree of forming a large amount of immiscible sulphides, enough to be economically viable.

The factors to form an economic Cu-PGE deposit depends on the abundance of ore metals in the magma, sulphide saturation state in magma, the ability to interact with the surroundings wall rocks as well as the mode of emplacement composition, temperature, viscosity and volatile content of the magma. For instance, solubility of sulphides in mafic- ultra mafic magmas increases with increasing temperature and decrease with increasing pressure (Mungall et al., 2004; Godel & Barnes, 2007; Peach et al., 1990).

1.3.1 Partial melting for accumulation of ore metals

Degrees of partial melting of mantle derived sources have a strong control over Ni-Cu-PGE content of a sulphide deposit. At equilibrium, concentrations of the PGE composition are at least 10,000 higher in sulphides than in a coexisting silicate melt. This makes sulphides an extremely powerful agent for segregation and collection of PGE and chalcophiles from most silicate magmas (Arndt et al., 2005). This is due to the preference shown for covalent bonding with sulphide ions in sulphide melt over ionic bonds that form the structure of most molecules in the silicate melt (Mungall & Naldrett, 2008; McDonald,1987; Arndt et al., 2005; Mungall et al., 2004). Geochemical behavior of the PGEs in magmatic settings is of a highly chalcophile nature such that

PGEs have a high partition coefficient for sulphides in magmatic environments (Driscoll & Jimenez, 2016). At high degrees of partial melting of the mantle, most of the sulpher is dissolved from the mantel source region, in to the silicate melt and PGEs and Cu are liberated out into the melt which leads to create fertile magmas (Mungall & Naldrett, 2008).

1.3.2 Accumulation

Most sulphides must interact with and extract ore metals from a much larger volume of silicate liquid. This accumulation of ore metals and increase of sulphur content probably occurs within magma channels or conduits during the ascent of the magma. Large, dense sulphide droplets can effectively scavenge ore minerals during the transportation of the magma is these conduits and eventually collect at the base or structural trappings of these magma channels (Mungall & Naldrett, 2008; Driscoll &Jimenez, 2016; Arndt et al., 2005). Therefore, separation, accumulation and crystallization of sulphide liquid in silicate magma systems with respect to the timing of PGM fractionation and accumulation is a crucial matter.

1.4 Geophysical and petrophysical characteristics of sulphide ores

Economic concentrations of sulphide deposits have quite distinctive geophysical and petrophysical properties and give great indicators of deposit locations. Yet, due to the non-uniqueness of responses from geophysical anomalies, geological and structural information need to be integrated together to explore sulphide deposits. For instance, sulphide ores which are commonly associated or hosted by conductive, dense, magnetic mafic/ultramafic rocks can also be mistaken for barren minerals such as pyrrhotite, magnetite and graphite and makes the responses non-unique (Kerr and Leitch, 2005). Physical properties of ore minerals and associated host rocks give prominent geophysical signatures which, combined with their physical properties provide invaluable information for exploration of sulphide deposits.

Density can be used to detect mafic or ultramafic rocks which hold dense sulphide deposits and also play an important factor in acoustic velocity variations within sulphide deposits. Since gravitational acceleration responds to local variations of density, gravity prospecting is analogous to assessing the rock densities. Therefore, a gravity anomaly is a result of a density anomaly formed from highly dense rock bodies. Estimates of bulk densities of different lithological units are

necessary to carry out Bouguer corrections in gravity surveys. In general, when exploring for mineral deposits, a high gravity anomaly indicates the presence of denser mafic, ultramafic rocks possibly hosting sulphide deposits (Chapin, 1996). But, iron oxides, barren sulphides and highly dense ultramafic rocks can also produce anomalies with respect to lower density host rock, and can interfere with detecting Cu-PGE sulphide deposits. As an alternative measure, resistivity and electrical conductivity can be employed to discriminate between these dense barren rock types against dense sulphide bearing rock types. Therefore, gravity measurements can be used as a follow up method to compare and contrast with other geophysical measurements and surveys.

Magnetic field methods are another technique to assess sulphide bearing host rocks. Magnetically susceptible rock types create a measurable magnetic disturbance in the local magnetic field. Even though sulphides themselves are not highly magnetic, their mafic and ultra mafic host rocks are usually highly magnetic and provides a useful tool to detect whereabouts of sulphide deposits. The presence of highly magnetically susceptible minerals such as magnetite, hematite or pyrrhotite can be used as locators for host rocks of sulphide deposits. Combined with density/ gravity data, use of magnetic susceptibilities of sulphide bearing host rocks can be used to successfully identify and delineate deposits. Magnetic surveys can be carried out easily from land or air and the resulting magnetic anomalies are extremely easy to detect.

Pyrrhotite dominates most sulphide ore bodies. Pyrrhotite and other ore bearing sulphides also has a high conductivity and very low electrical resistance compared to their host rocks and therefore is a great target when manipulating these two physical properties of various ore bearing rock types. Electrical resistivity of crystalline rocks is of the order of 10^-4 compared to the 10^-9 of sulphide bearing rocks, making electrical resistance the largest contrast as a diagnostic property.

Sulphide hosting disseminated host rock also has a very high chargeability, making these rocks great targets for Induced Polarization (IP) assessments. Also, most economically significant sulphides have very low acoustic velocities and are great targets for crosshole transmission seismic tomography that measures velocities in rock units. Yet, they are also anomalous in density and hence can be resulted in reduced reflectivity. This is due to the fact that the reflectivity is proportional to the acoustic impedance, which is the product of velocity and density. Yet, petrophysical assessments of acoustic velocities such as P-wave velocities in various rock units is

an excellent strategy for distinguishing sulphide bearing low velocity host rocks from high velocity mafic/ ultramafic rocks.

1.5 Statement of the thesis

The work in this thesis will discuss petrophysical assessments in four mineralization zones of the Marathon series deposit. The partner of this work, Stillwater Canada Inc., is seeking innovative methods to explore and create 3D models of the mineralization zones and associated subsurface structures of the Marathon Cu-PGE deposits. Although much conventional research has been conducted on the nature of mineralization (ore petrography, geochemistry), petrophysical assessments haven't been conducted in great detail as of yet. Such information could be used in conjunction with other geophysical surveys and geological characteristics to create better 3D models to understand the subsurface of the Marathon deposits. Other deposits may benefit from this form of petrophysical assessment. In this thesis, petrophysical characteristics of the Marathon deposit will be assessed to further understand the model of mineralization and introduce new exploration strategies to seek new mineral deposits. The drill core samples obtained from the Marathon deposit has been measured for magnetic, electrical and acoustic properties and a comprehensive discussion of these petrophysical properties will be pursued in three parts.

The first portion of this work (Chapter 4) will employ the technique of orienting drill core samples using remanent magnetization ingrained in the Marathon deposit rocks, first from fully oriented drill core as a test case and then with application to core samples that are only oriented along the core axis. The second portion of the thesis (Chapter 5) will assess the Anisotropy of Magnetic Susceptibility (AMS) to observe magnetic petrofabric foliation and lineation distribution in the lithological units in the deposit, as a possible proxy for magmatic flow fabric.

The third portion (Chapter 6) will contain an analysis and discussion of petrophysical property variations observed within the lithological units from four mineralized zones of the Marathon deposit. These observations will be discussed in relation to the mineralogical and textural variations in lithological units of the Marathon deposit. Exploration strategies that can be implemented within the Marathon mineralization zones will be further discussed with relation to the petrophysical properties.

Chapter 2
Geology of the study area

This thesis is intended to examine petrophysical characteristics of the host rock and sulphide mineralization hosting platinum group elements (PGEs) and copper (Cu) in magma conduit type deposits in the Coldwell Complex near Marathon, Ontario. The Coldwell alkaline complex is a multiphase intrusion, emplaced into the North American Mid Continental Rift system.

2.1 Mid Continental Rift (MCR)

The tectono-magmatic evolution of the 1.1 Ga Mid Continental Rift (MCR) system in the Lake Superior region led to the magmatic and hydrothermal development of economically viable ore deposits in the region. Considered as a failed rift, the 3000 km North American Mid Continental Rift system extends across central North America (Figure 2.1). The mid continental rift system hosts several world renowned ore deposits which has been mined for many centuries. Keweenaw Peninsula and Isle Royale were first mined in the mineral rush in 1841 (Miller and Nicholson, 2011). Increase in global demand for base and precious metals over the decade initiated a surge in exploration for these ore deposits of various kinds associated with the Mid Continental Rift system.

Large gravity and magnetic anomalies on the path of the MCR easily distinguishes the southwest to the southeast extensions of the structure. Reflection seismic data of the MCR show volcanic layers 20 km in thickness, overlain by 5-8 km of sedimentary rocks (Stein et al., 2016). The rift cuts across the Late Archean granitic greenstone terranes near the Lake superior region and continues on to crosscut several terranes within the Penokean Orogen (1.85 Ga). The eastern arm of the MCR is buried beneath Paleozoic rocks of the Michigan basin and the gravity and magnetic anomalies of the MCR end at the Grenville front tectonic boundary towards the southeast. It is considered that the rift failed to extend further due to the compression episodes initiated from the Grenville orogeny which assembled Laurentia and other continental terranes into the

supercontinent Rodinia (Miller and Nickolson, 2011; Cannon, 1994; Green et al., 1994; Swanson et al., 2014; Sengor and Burke, 1978).

The rift is defined by three major lithological components; thick subaerial lava flow, local concentrations of plutonic-hypabyssal intrusive rocks and sedimentary rocks of the Bayfield and Oronto Groups. Considering the large volume of magma that was emplaced during the crustal separation, the MCR is considered to be an excellent source for a large igneous province (Miller and Nickolson, 2011; Green et al., 1994).

Stratified volcanic and sedimentary rocks of the MCR are collectively called the Keweenawan Supergroup. One of the most distinctive features of the MCR is the prolonged period of magmatism, close to 30 million years (Miller and Nickolson, 2011; Stein et al., 2016; Cannon, 1994). The volcanic sequences of MCR are composed of tholeiitic flood basalts but also include intermediate and felsic rocks. Intrusive igneous rocks of the MCR are importantly the host of Ni-Cu-PGE mineralization. An increasing number of small ultramafic to mafic intrusions related to the MCR have been discovered as potential hosts for Ni-Cu-PGE deposits (Cannon, 1994).

MCR-hosted hydrothermal and magmatic deposits are world renowned and most mineral production of the area are from well-established hydrothermal deposits. Keweenaw Peninsula's long history of mining was the principal source of copper for United States for many years (Miller and Nickolson, 2011). Native copper and silver are found in abundance in most exposed mafic volcanic sequences related to the MCR. MCR adjacent Oronto and Sibley group sedimentary rocks are also well known for their large Cu and silver deposits (Miller and Nickolson, 2011; Swanson et al., 2014; Sengor and Burke, 1978). Some of the smaller scale magmatic deposits associated with the MCR are well under final stages of advance exploration and mine planning / resource estimation. MCR related hydrothermal rocks are hosts for native copper and silver deposits in basalt and interflow sediments, copper sulphides and native copper ores and polymetallic veins surrounding Archean and Proterozoic rocks.

The ore deposits related to MCR are mostly low grade Cu-Ni-PGE sulphide deposits, hosted in gabbroic to troctolitic rocks, mainly in Duluth and Coldwell Complex, Great Lakes Nickel deposit in the Crystal Lake gabbro and Mineral Lake intrusion at the Mellen Complex (Green et al., 1994). Other deposit types such as stratiform PGE reef deposits in layered mafic intrusions in the Duluth

complex and small high grade Ni-Cu-PGE occurrences in ultramafic rocks, Ti-Fe oxide gabbroic intrusions, U-REE carbonatites in the Kapuskasing structural zone of the north of Lake Superior as well as Prairie Lake deposit in the Coldwell complex and Cu-(Mo) bearing breccia pipes surrounding felsic intrusions in the Mamainse Point in Ontario are also being explored and developed in the MCR related rocks (Miller and Nickolson, 2011; Swanson et al., 2014).

The richest Ni-Cu-PGE deposit related to MCR system was discovered at the Eagle Deposit of Upper Michigan (Figure 2.1) which is formed in a narrow funnel-shaped intrusion, similar to the Marathon deposit at the Coldwell Complex. Other smaller, yet notable intrusions such as the Bovine intrusion and Tamarack intrusion have also been proven to host significant amounts of Cu and PGE and are in the stages of advanced exploration (Stein et al., 2016; Cannon, 1994; Green et al., 1994).

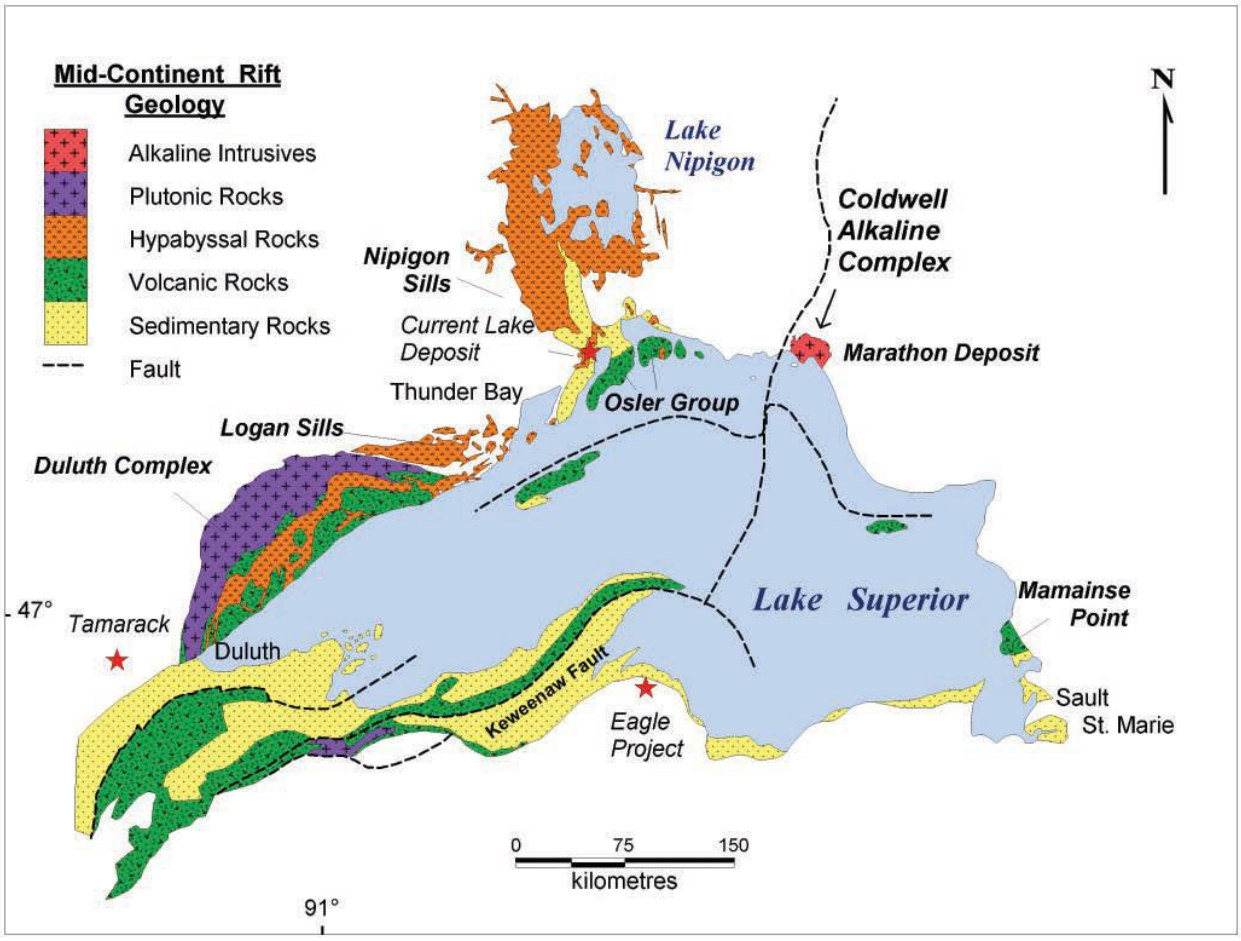

Figure 2.1- Location of the Coldwell Alkaline Complex and the Marathon deposit within the Midcontinent rift (adopted from Good et al., 2015)

2.2 Geology of the Coldwell Alkaline Complex

The Coldwell complex is sub circular in map view (Figure 2.2) with a diameter of 26 km and a total area of 580 km^2, making it the largest alkaline complex in North America (Shaw, 1997). The complex is a part of the ~1.1 Ga Keweenawan igneous rocks and the associated North American MCR event, along the western Great Lakes and into the Midwest U.S. (Good et al., 2014; Barrie et al., 2002; Dahl et al., 2002; Good, 1992).

The Coldwell complex intrudes the Archean Schreiber-Hemlo greenstone belt and the southern margins of the Black Batholith of the Wawa subprovince of the Superior province (Barrie et al., 2002; Miller and Nicholson, 2013). The mid continental rift system and the associated plutonic intrusions cross-cut the regional trend of the Archean and Proterozoic structures, including reactivated pre-existing faults and fractures (Dahl et al., 2002). These Archean supercrustal rocks are mainly mafic and felsic volcanic subjected to at least two large deformation events distinguished by a penetrative foliation-lineation and a second deformation event transposing the first (Dahl et al., 2002).

The complex is considered to have been intruded as sub horizontal sheet- or sill-like bodies and the overall structure was controlled by the preexisting fault systems and cauldron subsidence of the area (Good et al., 2015). (Dahl et al., 2004) indicate that the intrusion was emplaced relatively early in the magmatic history of the mid continental rifting, approximately around 1108 Ma (Barrie et al. 2002; Shaw, 1997).

The Coldwell complex is an alkali intrusion mainly consisting of gabbroic to syenitic rocks but has over saturated, saturated and under saturated intrusive units. The rocks of the eastern portion of the complex are considered to represent deeper levels, consisting of low amounts of xenoliths and metasomatism whereas the western portion of the complex shows extensive metasomatism implying a higher crustal setting (Ruthart, 2012). The whole of the complex has been sub divided into three superimposed intrusive centers I,II and III.

The oldest unit, Centre I consists of western syenodiorite unit, the east and northeast rimmed gabbroic unit named Eastern Gabbro. The Marathon deposit is hosted in the Eastern Gabbro with

minor intrusions of ferroaugite syenite and distinctive iron enrichment in the unit. Centre II consists of under-saturated alkaline rocks such as massive alkali gabbro and several phases of layered nepheline and natrolite syenite. The dominant mafic phase is amphibole and pyroxenes are also observed. Centre III, devoted to western half of the Coldwell complex, comprises of over saturated residue including barkevikite syenite, quartz syenite and granite with a wide range of amphiboles, minor biotite and quartz. The centre has been intruded, contaminated and brecciated multiple times by plutons; intrusive rocks of this centre crosscut other phases in the complex (Mitchell and Platt, 1982).

Within the Centre I and along the eastern and northern boundaries of the complex occurs a belt of gabbroic to ultramafic rocks with Cu and PGE bearing magmatic sulphides (Dahl et al, 2002; Good et al., 2015). Regarded as the oldest intrusive unit of the Complex, this sulphide bearing gabbroic suite is named Eastern Gabbro and is the primary host for the mineralized Two Duck Lake gabbro unit in the Marathon deposit. Most of the structural elements and lithological units of the Centre 1 unit strikes north-south and consists of rheomorphic intrusive breccia near the contact of the Archean footwall with the Eastern Gabbro. Given the long history of research conducted on the Coldwell complex and Marathon mineralization, complex cross cutting relationships of the magmatic intrusions in the Eastern Gabbros have been identified in fine detail and have been divided into three major magmatic series, categorized by their geochemical characteristics, physical conditions of emplacement and order of formation (Good et al., 2015; Ruthart, 2013). These magmatic series are the Fined grained series, Layered series and the Marathon series.

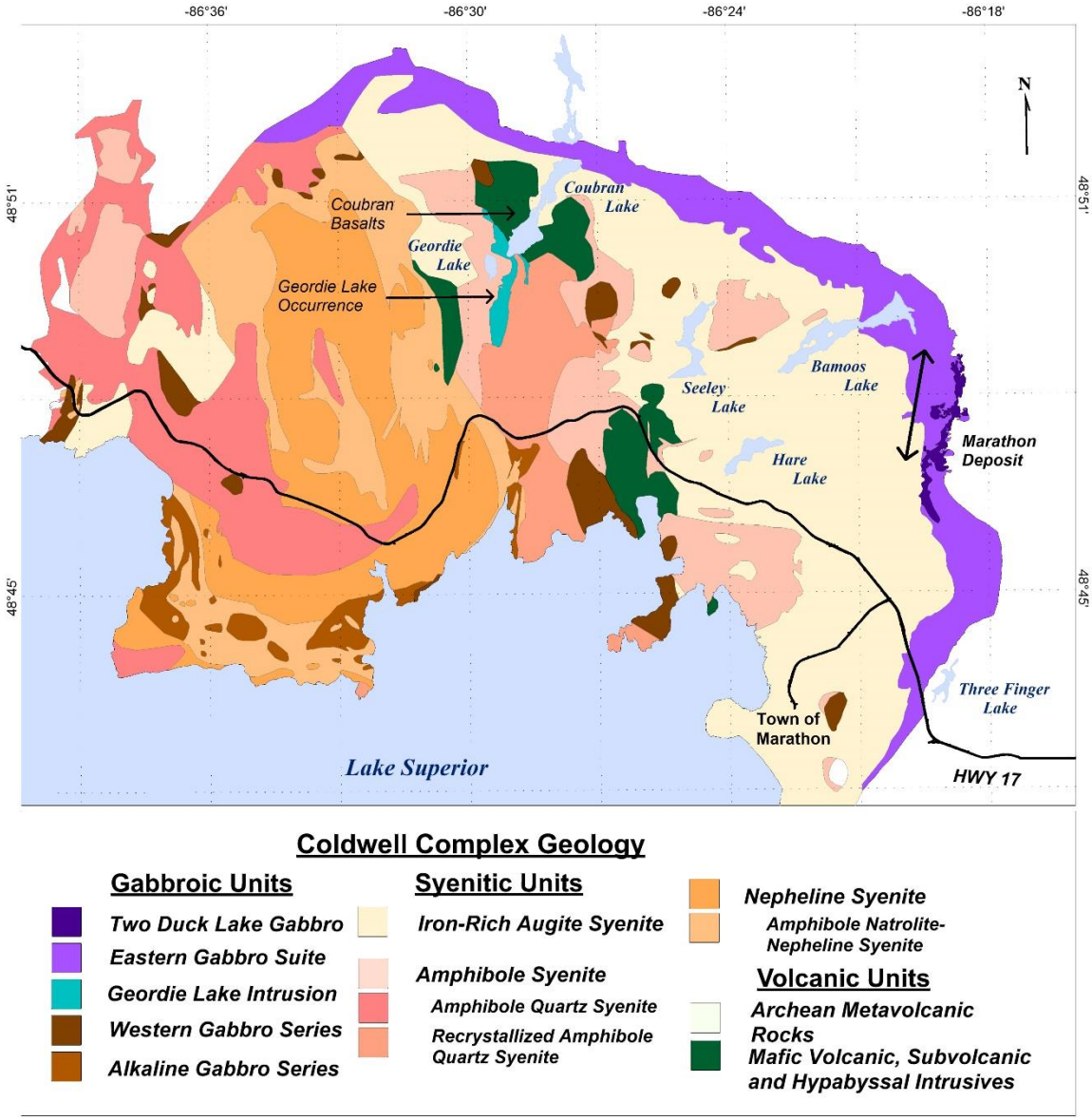

Figure 2.2 – Geology of the Coldwell Alkaline Complex. The legend of the main magmatic series in the Coldwell Complex has been indicated at the bottom of the figure. Adapted from Good at al. (2015)

2.3 Marathon Deposit

Much documentation of Cu and PGE mineralization in Coldwell Alkaline Complex (Figure 2.2) exists and comprehensive assessments of the geochemical, petrographic and geophysical signatures are available due to many years of research conducted on the area. As with many large igneous provinces, PGE and Cu enrichment of the Coldwell Alkaline complex is not surprising. Most of the significant Pd-Cu mineralization residing in the complex is concentrated along its eastern half, mainly in Eastern gabbroic suite or the Geordie Lake Gabbro. The Eastern Gabbros host the Marathon Cu-PGE deposit, located near Marathon, Ontario.

The Coldwell alkaline complex is considered to be a large tholeitic to alkali sill or lopolith. Geochemically, a large intrusive sill has the ability to partially melt super permeable mantle, resulting in siliceous, volatile rich melt accumulating in fine grained margins of the newly formed intrusion. Large intrusive complexes tend to circulate hydrothermal and magmatic fluids efficiently and can alter the products of primary magmatic processes, leading to further metal and sulphide enrichments (Good et al., 1992).

The Cu-PGM mineral deposit occurs within several areas of the Coldwell complex. Marathon Main zone upholds 97.4 million metric tons consisting of 0.27% Copper, 0.75 ppm Pd, 0.23 pp, Pt, and 0.09 ppm Au and 32.42 metric tons from the Geordie Lake deposit (Ruthart, 2013). Although hydrothermal origins have been proposed for the mineralization of these PGE and Cu deposits, the general consensus is now towards a model with magmatic origins (Good, 1992; Ruthart, 2013; Watkins and Jones, 1995; Good et al., 2015; Dahl et al, 2002; Good and Crocket, 1992). Most magmatic Ni-Cu-PGE sulphide deposits are considered to form within magma pathways and concentrated by the segregation and accumulation of immiscible sulphide liquid droplets from ultramafic and mafic magmas (Barnes et al., 2015). The latest of the models on the Marathon deposit have proposed the mineralization model to resemble a magma conduit style setting (Good et al., 2014; Barnes et al., 2015). Magma conduits are mostly feeder channels or tube like pipes delivering magma to intrusion complexes. The deposition of these sulphide liquids in the long lived vertically extensive conduits are driven by density contrast with the surrounding silicate magma (Barnes et al., 2015; Kerr and Leitch, 2005).

2.4 Mineralization zones

The four mineralization zones discussed in this thesis and the distribution of these deposit areas with relation to the Coldwell Complex has been plotted in Figure 2.3. These zones which are illustrated as red star marks in Figure 2.3 have been recognized by the exploration conducted on the Eastern Gabbro to host Cu and PGE rich mineralization and will be the focal points in petrophysical assessment throughout this thesis.

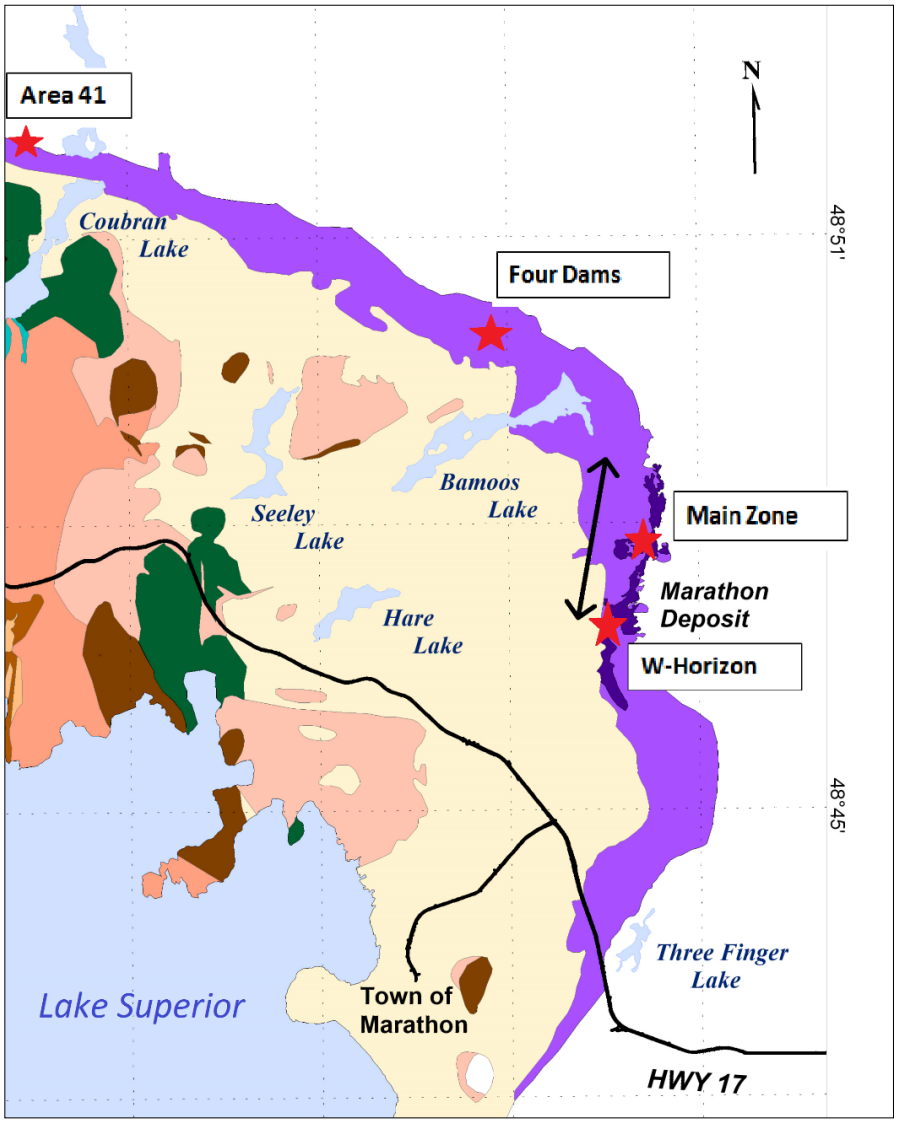

Figure 2.3- The figure is modified from Figure 2.2 and the main mineralization zones discussed in this thesis is marked with red stars. These mineralization zones are Area 41, Four Dams, Main Zone and W-Horizon

2.4.1 Main Zone

The Main Zone is the thickest and the most continuous zone of mineralization in the Marathon deposit. The most dominant sulphide minerals in the deposit are chalcopyrite and pyrrhotite with trace amounts of bornite, pentlandite and pyrite. The modal abundance of sulphides in the mineralization unit varies from 5-7%. Hydrous minerals such as chlorite are seen locally in the Main Zone. The mineralization is hosted by the Two Duck Lake Gabbro unit which has an average thickness of 35m. The unit strikes south and dips moderately to the west and the higher grade regions within the Main Zone follow troughs and ridges along the footwall contact. The sulphide assembledges at the base of the unit is pyrrhotite rich and the top of the unit is chalcopyrite rich (Good et al., 2015, Good et al., 2017, Cao, 2017).

2.4.2 Four Dams

The mineralization unit in the Four Dams area is located 3 km northwest of the Marathon Main Zone and contains Layered and Marathon series, similar in composition to the Main Zone. The Cu-Pd mineralization at Four Dams area is hosted in the Two Duck Lake Gabbro, mainly in apatitic clinopyroxenite and in small amounts of ophitic gabbro units. The Four Dams area has a significantly elevated Cu/S ratio compared to the other zones and the oxide melatroctolite is distinguished by a great abundance of disseminated magnetite (10-20%). Mineral abundance of the mineralized unit composes if olivine, plagioclase, clinopyroxene, magnetite and apetite. The unit contains disseminated sulphides that are dominantly fine grained pyrrhotite with trace amounts of chalcopyrite (Good et al., 2017, Cao, 2017).

2.4.3 W-Horizon

The Cu-Pd enrichment in W-Horizon is quite extraordinary with 67 ppm Pd and 39 ppm Pt over 2 m, and 42 ppm Pd and 12 ppm Pt over 8 m ranking it among the world's highest grade localities of PGE in disseminated sulphides. The discovery of the W-Horizon was made in 2004 and the first comprehensive mineralogical study was published Ames et al. (2017). W-Horizon consists of only minor to trace amounts of finely disseminated sulphides; chalcopyrite, bornite, pentlandite and millerite without much Fe-rich sulphides. The Two Duck Lake Gabbro that hosts this mineralization distinguishes primary magmatic textures and characteristics. Primary mineral assemblages consist of olivine, hornblende, biotite, magnetite-illmentite and apatite (Good et al.,

2015; Good et al., 2017; Cao, 2017; Ames et al, 2017). Local alteration is visible and secondary magnetite is a product of serpentinization of olivine and the breakdown of Ti-magnetite rimming sulphide blebs against silicates (Ames et al., 2017).

2.4.4 Area 41

Located in the northern contact of the Coldwell Alkaline complex, Area 41 is 16 km along strike to the northwest of the Marathon deposit. The Area 41 intrusion is approximately 100 m thick and extends for at least 1200m. The contact with the Archean foot wall dips at 30-60 degrees towards the south and the intrusion includes several units that resemble the Two Duck Lake gabbro. For instance, olivine gabbro, pegmatitic gabbro, oxide melatroctolite and apatitic clinopyroxinite units are also found in the Area 41 mineralized intrusion. The intrusion consists of Archean footwall xenoliths and the mineralization in hosted by chalcopyrite, pyrrhotite and pyrite and associated with a range of altered to unaltered silicates minerals. Mineralization is hosted by apatitic clinopyroxenite or olivine/pegmatitic gabbro (Good et al., 2017; Cao, 2017).

2.5 Previous Work conducted on the Marathon deposit

An extensive amount of geochemical research has been conducted on the Marathon deposit for the past 40 years. This is a summary of the development and evolution of the present state of thinking on the mode of mineralization and ore deposit model for the Marathon deposit.

Previous work on the Marathon deposit indicates that PGEs and Cu occur in complex alloys of Te, Sb and As and are mostly associated with sulphides such as chalcopyrite. Wilkinson (1983) conducted a detailed mapping and sampling of the Marathon deposit and the associated property, leading to the assaying of the samples and detailed descriptions of the petrography of the various gabbroic suites of the deposit. He proposed that the intrusion of Two Duck Lake gabbro and the mineralization associated with it is of magmatic origin and the addition of wall rock material lead to the increase in oxygen fugacity. This was proposed to initiate precipitation of massive magnetite layers leading to the increase in sulphur content and to precipitate sulphide minerals.

Good (1992) conducted detailed petrography and geochemical work on the Two Duck Lake intrusion and other parts of the Eastern Gabbro, elaborating on the genesis of copper-precious metal sulphide deposits in the Coldwell Alkaline complex.Good and Crocket (1994) in the proposed model for crystallization history of Two Duck Lake gabbro, stated that the initial

crystallization of plagioclase and olivine occurred in a deep magma chamber. Due to density contrasts, the magma chamber became compositionally stratified with denser olivine sinking to the bottom of the chamber. Migration and contamination of sulphur from the country rock resulted in the plagioclase mush being sulphide saturated, leading to the segregation of sulphide droplets. Later the plagioclase crystal mush was forced out of the magma chamber to form the Two Duck Lake gabbro at its present state.

Petrogenesis of four units in the Eastern Gabbro unit at Coldwell Alkaline Complex was investigated by Shaw (1994) in a petrographic and geochemical study. The most primitive of the magma compositions at the Eastern Gabbro was found to belong to the Two Duck Lake Gabbro unit.

Barrie et al. (2002) published results of a relogging and assaying study of the drill cores from the Marathon deposit, observing that the primary magmatic textures are common in all of the mineralized zones. They proposed that the initial melt enrichment was due to the accumulation of immiscible sulphides in a magmatic system. As observed by previous researchers, they have reported that the very coarse to pegmatitic gabbros contain disseminated primary magmatic sulphides and has replacement textures of silicate minerals. Barrie et al. (2002) propose a zone defining model where the intrusion of the gabbro caused a release of volatile rich fluids from a felsic volcanic source to become enriched in sulphur and precipitate chalcophile elements in the coarse grained to pegmatitic textures. The authors also stated that the lithological divisions which were mainly based on the textural evidence alone do not provide sufficient criteria for separating out intrusions as there were no chemical, isotopic, mineralogical or temporal distinctions between the pegmatitic gabbros and medium grained gabbro. They recommended against the use of ‘Two Duck Lake Gabbro’ for the pegmatitc hosts of mineralization (Barrie et al., 2002).

Dahl et al. (2002) completed large scale field mapping, documenting geological field relations along with petrological study to assess the geology of the Two Duck Lake gabbro and the Marathon Cu-PGE deposit. The study found that the Two Duck Lake gabbro consists of a main body of coarse grained pegmatitic gabbro and is identified to have three units: lower, middle and upper sub units. The field relationships and geological characteristics of the Two Duck Lake unit indicate that it is a separate and distinct intrusion. The Eastern Gabbro contains stratiformed and

differentiated internal structures whereas the Two Duck Lake intrusion appears to be a smaller igneous body closely resembling a sill swarm. Dahl et al. (2002) propose that the textural and petrological differences existing within the intrusion are due to the interactions with the wall rock, involving both magmatic and hydrothermal processes. Incorporation of xenolithic material in the intrusion exhibit evidence of partial melting and assimilation which is also commonly associated with the contacts of the Two Duck Lake intrusion and the pegmatites observed within the intrusion.

Good (2010) presented data of logs and assays from diamond drill cores of the Marathon deposit which involves the proposition of a multistage dissolution upgrading model. He proposed a model of sulphur-undersaturated magma feeding into Magama conduits, to become progressively sulphur saturated to the point of sulphide segregation and subsequently getting trapped within the troughs of the conduit.

Ruthart (2013) characterized the high PGE, low sulphur mineralization at the Marathon deposit in four drill holes selected from the W-Horizon mineralization zone. W-horizon is characterized by the high grade PGE zone with low S, low Cu/Pd and high Cu/Ni ratios.

Good et al. (2015) published an extensive study on the evolution of the Main Zone of the Marathon Deposit and the 3D spatial relationships were observed to compliment the proposed magma conduit model. The study also focuses on a viable deposit model that could be tested against other mineralization zones such as W-Horizon and Area 41 locations at south and north ends of the Eastern Gabbro, respectively. The paper reports deeply eroded lineaments that dominate the topography if the Complex and east-west keel shaped trough in the Main zone, filled with more than 100 meters of mineralization and interpreted to be the main feeder channel for the Two Duck lake intrusion. Primitive mantle normalization of abundances of Nb, Ce, Zr and Y also confirms that there are significant differences between Fine Grained, Marathon and Layered series. Therefore, the study proves that such large ranges and differences in elemental values cannot be generated by in situ crystal fractionation or contamination but most likely is due to intrusion of magma with different compositions and also that the fine grained series is not the chilled equivalent of the layered series or the Two Duck Lake Gabbro. Good et al. (2015) note that the sulphide mineralization is disseminated and occurs within Two Duck Lake Gabbro as continuous, shallow

dipping lenses, parallel to the foot wall. The sulphides consist of chalcopyrite, pyrrhotite with minor amounts of cubanite, bornit, pentlandite cobaltite and pyrite.

The shapes of Main Zone and W-Horizon strikes near north, parallel to the major N-S oriented topographic lineaments. The main zone dips 10-20 degrees towards the west and the keel shaped E trending extensions are parallel to the major E-W lineaments. Trends for higher grade Cu and Pd mineralization mimic the numerous troughs and ridges which are also parallel to the topographic lineaments, striking 350 in the Main zone and 90 at W-Horizon. These higher grade mineralization channels are interpreted to represent sulphide enriched crystal mush that imitated the footwall topography to form the mineralized unit.

Finally, the paper discusses the evidence pointing to the conduit style mineralization existing at the Marathon deposit. Assay results show a high proportion of sulphides relative to the host silicate rock which defines a conduit system. The paper proposes that the sulphides formed in a deep magma chamber which was probably orders of magnitude larger than the Two Duck Lake gabbro and were then instilled through magma pulses, intruding through a fault controlled system.

Good et al. (2017) published a paper on PGM facies variations in several deposits of the Coldwell Complex including the Main Zone, W-Horizon and Area 41, discussing the petrogenetic processes involving the concentration of PGE. Lithogeochemical observations and Sm-Nd isotopic compositions for the lithological units show similar patterns for Two Duck Lake as well as area 41 mineralize gabbroic units which indicate co genetic origins. The paper notes an increase in the copper tenor for sulphide assemblages in the order of deposits, Area 41, Main Zone and W-Horizon and an increase in the Pd enrichment in the order of Main zone, Area 41 and W-Horizon. When considering inter deposit metallogeny, there is a distinct lack of correlation for PGM mineral assemblages in Main Zone, W-Horizon and Area 41 and considering the geochemical implications, the authors suggest that the mineralization processes in each of these deposits have undergone different and dynamic intrusive histories with multiple injections of magma that had slightly different compositions in each of these deposits. The deposits have likely undergone similar processes for Cu and PGE concentrations which can be linked to a flow through mechanism for upgrading PGE enrichment in a magma conduit setting.

Ames et al. (2017) recently published on the extreme PGE enrichment of the W-Horizon mineralization zone and one of the key aspects of the research was to reiterate the fact that conduit style mineralization is capable of producing extremely enriched bodies of PGE. The W Horizon ore body has a more diverse array of PGE mineral assemblages and is mostly found in the late magma pulses of the intrusion.

2.5 Deposits with similar characteristics to Marathon mineralization

The Duluth complex is a contemporaneous member of the magmatic intrusions associated with the 1.1 Ga North American mid continental rifting event. The Duluth complex is explored for Cu-Ni sulphide deposits and the mineralization is known to have been developed by the multiple intrusions of anorthosite, troctolite and gabbroic rocks and is stated to have formed by multiple feeders through highly faulted rocks, similar to the Coldwell alkaline complex (Chandler, 1990). The mineralization of the Soju lake intrusion is proposed to be formed from differences in parent magma compositions, the efficiency of fractional crystallization and due to the conditions associated with crystallization (Riply et al., 1987; Riply et al., 1998; Paces, 1993).

The Skaergaard intrusion represents fractional crystallization of a closed system that contains low amounts of S and extremely high grades of PGE tenor and is somewhat similar to the mineralization at W-Horizon of the Marathon deposit (Nielsen et al., 2005). Considered to be the model example for a strongly differentiated layered intrusion, the Platinova reef in the Skaergaard intrusion contains economically viable mineralization of Au and PGE (Andersen et al., 1996; McBirney, 1996).

The Bushveld Complex situated in South Africa, is derived from repeated injections of magma and is enriched in economic deposits for PGE minerals. The PGE minerals are associated with magmatic sulphides deposited in the layered intrusion complex (Ballhaus and Sylvester, 2000).

Stillwater Complex situated in Montana USA, is a large magmatic intrusion hosting the world's largest PGE mining camp. The complex is a large layered mafic intrusion and several pulses of magmatic intrusions and mixing of magma have been proposed for the enrichment of ore grade

mineralization. In similar geological settings, conduits systems related mineral deposition have been proposed for Voisey's Bay, Thunder Bay North deposit and Eagle deposit (Ruthart, 2012).

Chapter 3
Lithological units and criteria for sampling

3.1 Magmatic series and rock types of Eastern Gabbro

The Eastern Gabbroic suite has been recognized with several different magmatic series events and brecciated lithologies (Good et al., 2015; Ames et al., 2017, Ruthart et al., 2014). These lithological units have been categorized by mineralogical compositions, textures and inferred petrogenetic histories. For the purposes of classification, the different lithological units and magmatic series have been given numbered letters by the geologists at Stillwater Canada Inc., which shall be used throughout this thesis for the identification of lithological units. A description of the lithological units is indicated in the following section for each magmatic series.

3.1.1 The Fine grained series (metabasalts)

Fine grained series metabasalt consists of gabbro to olivine melagabbro and is considered to be the oldest intrusive series at Marathon. The entire series is considered to be equigranular and homogenous, dominated by clinopyroxene, olivine, plagioclase and magnetite. Considered to be an intensely recrystallized to pyroxene hornfels grade unit, the metabasalt fine grained series of the Marathon deposit appears light grey to light green with a picritic to gabbroic composition (Ames, 2017). Layering is not readily visible and contacts between other magmatic series are usually readily observed by abrupt changes in the grain size. Thin intrusions of the coarser grained Two Duck Lack gabbro are visible in fine grained series rocks. Different lithological units related to the composition and textures have been identified during drill core logging, making for the numbers and short descriptions of the lithological units shown below.

2a	Fine grained homogeneous gabbro
2c	Fine grained gabbro with clinopyroxene, olivine porphyroblasts
2d	Fine to medium grained gabbro with Marathon series intrusions

2i	Feldspathic clinopyroxenite
2k	Medium grained homogeneous gabbro

3.1.2 Layered series

The Layered series makes up most of eastern gabbros, and occurs in a gross stratigraphic sense above the Fine grained series at the mineralization zone, dominated by massive to layered olivine gabbros. Cu sulphide mineralization occurs within rocks of Layered series but does not contain any PGEs. Layers range composition from olivine melagabbro to olivine gabbroic anorthosite. Contacts are defined by compositional variations in plagioclase, clinopyroxenes and magnetite. Layers dip moderately towards the middle of the Coldwell complex. Medium to coarse grained interstitial and/or poikilitic magnetite is distinctive in Layered series rocks.

Third and youngest of the magmatic intrusions, the Marathon series is associated with most of the copper and PGE mineralization in the Marathon deposit and includes gabbroic to ultramafic intrusions that crosscut both Fine grained and Layered series. Notably, the Two Duck Lake gabbro unit is encompassed in the Marathon series and hosts a very distinct geochemical signature unique to the Marathon series (Good, 1992). The series also include layered troctolite sill and oxide melotroctolite and apatite olivine clinopyroxenite as pod-like bodies. The following lithological units from the Layered series shall be discussed in this thesis.

2b	Coarse grained olivine gabbro with modal layering
2f	Medium to coarse grained oxide augite melatroctolite

3.1.3 Two Duck Lake Gabbro

The Two Duck Lake Gabbro is host to the Marathon Deposit. The Two Duck Lake gabbro unit, which in the Main Zone is a 4 km long and 250 m thick unit of the Marathon series, is the primary host of most of the Marathon deposit (Good et al., 2015, Barrie et al.,2002) and is mostly comprised of olivine gabbro and ferrogabbro units (Dahl et al., 2002). Two Duck Lake Gabbro intrusion is a

slightly flattened tube shaped body which spans on the eastern and northern borders of the Coldwell Complex and has been intruded into a thick pile of pyroxene hornfels grade metabasalts near the contact of the Archean basement rocks (Good et al, 2017).

Four feeder channels have been identified in the vicinity of the Two Duck Lake intrusion that coincides with topographic lineaments on the footwall contact (Good et al, 2015). Considered to be contemporaneous with the main gabbroic and syenitic units of the Coldwell Complex, the Two Duck Lake gabbro unit occurs within the larger Eastern Gabbro unit and Marathon series of the Coldwell complex. The texture most representative of the original intrusion is of a coarse grained, ophitic to hypidiomorphic granular rock hosting sulphides that are mostly concentrated in the lower sub unites of the gabbroic suite including pyrrhotite, chalcopyrite, pentlandite, cubanite, sphalerite and pyrite. The PGE minerals are exclusively associated with copper sulphide assemblages (Good and Crocket, 1994; Shaw, 1994; Dahl et al., 2002). The unit at the Main Zone strikes approximately north-south and dips shallowly towards the west and intrudes earlier fine grained series close to the contact of the Archean Metavolcanic rocks. The crystallization sequence of major minerals of this unit is plagioclase plus olivine followed by interstitial clinopyroxene plus magnetite and biotite with apatite as a fine grained accessory phase. Local alteration is seen in phases such as actinolite, chlorite, epidote, serpentine and carbonate occurrences. The lithological units of the Two Duck Lake Gabbro unit discussed in this thesis will comprise of:

3a	Medium grained, ophitic gabbro (<5mm) in grain size
3b	Coarse grained, ophitic gabbro (>5mm) in grain size
3c	Ophitic gabbro intermixed with leucogabbro
3d	Very coarse grained to pegmatitic, ophitic gabbro

3.1.4 Layered Troctolite sill

This feature is distinguished as an important marker horizon due to the fact that it is recognized just above the top of the Main Mineralized zone and is used as an indicator of the relative fault offsets of the E-W trending normal faults. An exact magmatic event for this unit is still unresolved

and the geochemical properties indicate that the unit is either a member of the Marathon series or of a transition between Layered series and the Marathon series (Good et al., 2015). The unit is recognized by the mottled texture of the augite troctolite layers, a sub unit of 1 cm subrounded clinopyroxene crystal distribution layer and thin layers of augite melatroctolite, oxide augite melatroctolite and oxide gabbro.

3l	Coarse grained augite troctolite with clinopyroxene, olivine magnetite oikocrysts

3.1.5 Oxide and apatite cumulate rocks

These lithological units are a part of the Marathon series intrusion. Sills and pods of apatitic olivine clinopyroxenite and oxide melatroctolite intrude the Fine grained series and can be seen stratigraphically above or as dikelets within the Two Duck Lake Gabbro. These units do contain disseminated chalcopyrite and pyrrhotite with high levels of PGE concentrations. They grade into thin zones of semi-massive to massive grains of magnetite. Oxide melatrctolite pods are medium to course grained and composed subhedral magnetite, olivine and clinopyroxene plagioclase and 2-30% fine grained apatite. The unit also locally grades into semimassive to massive magnetite zones.

3g	Medium to coarse grained oxide melatroctolite with >40 magnetite
3h	Apatitic clinopyroxenite with high percentages of apatite and magnetite
3i	Apatitic olivine clinopyroxenite with high amounts of apatite and magnetite

3.1.6 Footwall contacts

The eastern margin of the Coldwell Alkaline Complex comprises of the foot wall of the Archean intermediate pyroclastic rocks which has undergone hornfels metamorphism due to the contact of the intrusion of the Eastern Gabbro. At the contact of the Two Duck Lake Gabbro, blocks of these Archean foot wall material can be found as intrusions and is called as Rheomorphic Intrusive

Breccia. Down dip, the foot wall forms paleo surfaces with basins and ridges with well-defined trends and structural prominence.

1a	Footwall rheomorphic intrusive breccia
1b	Archean granitoids

3.1.7 Brecciated and other intrusive units

Three types of breccia units are found at the Marathon deposit. The first type consists of gabbro matrix and angular xenoliths of Fine Grained series rocks and another type is of xenoliths from the foot wall material. Two Duck Lake gabbro units and oxide melotroctolites are also intruded as versions of brecciated units in statigraphic Fine grained series rocks. These brecciated units also contain sulphide-bearing Two Duck Lake gabbro units and other sulphide-bearing lithologies.

4a	Marathon Series (MS) hosted breccia with Fine Grained gabbro xenoliths
4b	MS hosted breccia with Fine Grained gabbro and footwall xenoliths
4c	MS hosted breccia with Layered Series xenoliths
6a	Aphanitic to porphyritic mafic dykes

3.2 Drilling and sample preparation

Petrophysical measurements were conducted on drill cores samples obtained from drill cores which sampled four different mineralization zones. To conduct these petrophysical measurements, the drill cores were carefully selected in order to best represent the main lithological units of the mineralization zones. These drill core has been produced during exploration projects conducted by Marathon-PGM and later on by Stillwater Canada Inc from 2005-2013.

The **Main Zone** was represented by three drill cores: KP-01, KP-02, KP-03. **Four Dams** mineralization zone was represented by B-05, B-06 and FD-13-34, **W-Horizon** was represented by M-07-238, M-07-239 and M-07-249 and **Area 41** mineralization zone was represented by SL-13-32, SL-13-36, SL-13-44 and SL-13-56 (Table 3.1). Altogether there are 13 drill holes representing various mineralization zones at the Eastern Gabbro. An average sample obtained from a drill core is usually 15-20 cm in length. All samples were chosen in order to accurately represent and identify the lithological units of the Marathon deposit.

The drill tubes used in the drilling project were NQ size with 75.8 mm diameter to produce drill cores with a 47.6 mm diameter. During core logging, some parts of the drill cores have been sent for geochemical analysis and therefore has been split in half along the drill core axis. Therefore, some samples from W-Horizon drill cores M-07-238, M-07-239 and M-07-249, Four Dams drill cores B-05-15, B-06-16 and Area 41 drill cores SL-13-32, SL-13-36, SL-13-44 and SL-13-56 have been sampled as split cores. The specimens obtained from split cores are smaller in dimensions compared with standard specimens from a full drill core. A list of drill holes, specimen sizes and amount of specimens obtained from the samples have been listed in Table 3.1.

Figure 3.1- A) 10 cm3 specimens which have been obtained by drilling perpendicular to the drill core axis as is seen in B). The up direction of the drill core is marked on all samples as well as the depth from which the samples were obtained.

These drill cores have been sampled from the top of the drill core to the base, at approximately 10 meter intervals to represent the main lithological units and mineralized areas. The drill cores have been previously logged and relogged by Stillwater Canada Inc. and the lithological units were recognized with the consultation of drill logs provided by the Stillwater Canada Inc. The samples were chosen to accurately represent different lithological zones, silicate mineralogy, sulphide content and abundance, textures and fabric elements such as foliations and lineations.

3.2.1 Specimen drilling criteria

Figure 3.2- A drill press is used to obtain specimens from drill core samples. The samples are drilled perpendicular to the drill core axis as seen in A). The specimens obtained from this drilling procedure will be subjected to petrophysical assessments. A figure of the drill press in indicated by B)

The samples from drill cores were further drilled with the use of a drill press to obtain smaller cylindrical specimen for the petrophysical measurements (Figure 3.2). The specimen dimensions were drilled to resemble an equidimensional object or a sphere. The orientation of the drill core axis, drill core identification name as well as the sample depth and specimen number is written on each specimen (Figure 3.1 A). The up direction of the drill core is also indicated on the specimen for the purposes of orienting the drill core for petrophysical measurements. (Figure 3.1 B).

3.2.2 Main Zone samples

The samples that are obtained from the Main Zone are pristine, full core samples and therefore the specimens drilled are larger in size compared to the specimen obtained from half cores. For geo-engineering purposes, Main Zone drill cores have been drilled, fully oriented and the orientation markings have been drawn on the longitudinal surface of the drill cores. The laboratory drilling is done perpendicular to the drill core axis with the orientation marking-line centered on the circular specimen surface facing the up-core axis direction (Figure 3.1). The cylindrical specimens are approximately 10 cm^3 in volume and best resemble the dimensions of a sphere. This specification of dimensions is mainly to use samples for anisotropic work related to magnetic susceptibility of specimen. Each sample was drilled to obtain three to four specimens.

3.2.3 W-Horizon, Four Dams and Area 41 samples

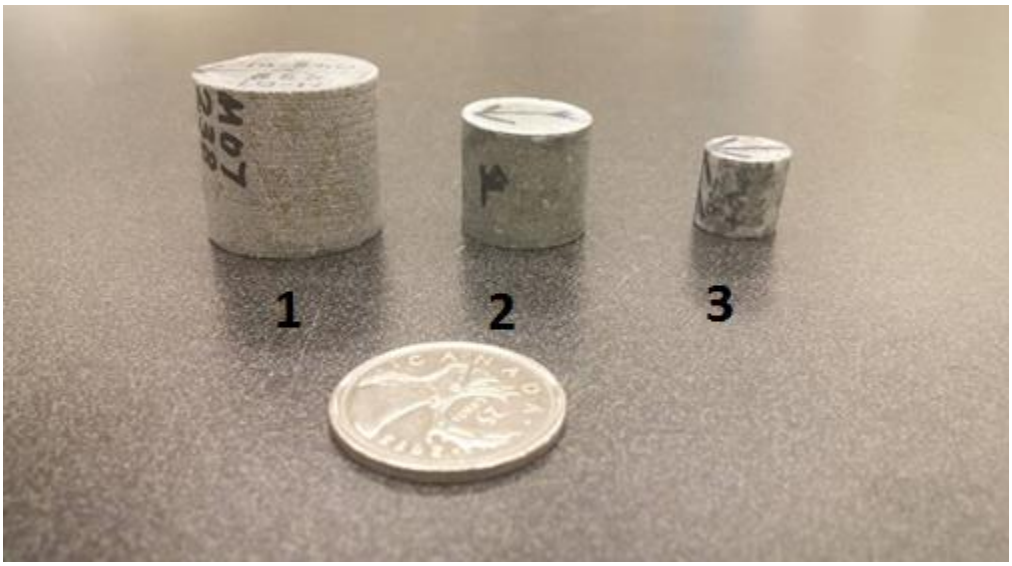

Figure 3.3- The three specimen sizes used in this study. 1- indicates a large specimen, obtained from a full drill core with a volume close to 10 cm^3. 2- is of a medium sized specimen obtained from a split core with a volume close to 7 cm^3. 3- is a small specimen, obtained from a split core with a volume close to 1 cm^3.

Samples obtained from these drill cores are only partially oriented with the plunge and the azimuth of the diamond drill cores, known. The perpendicular orientation to the drill core axis is unknown and therefore in situ orientation markings are not available. An arbitrary line, parallel to the drill core axis is drawn across the longitudinal surface of the drill cores before drilling perpendicular into the drill core axis (Figure 3.2 A). The standard specimen volume from a full drill core sample is 10 cm^3 (large). If the drill core samples are halved, the specimens which are drilled from these

samples are smaller in dimensions and are either 1 cm^3 (small) or 7 cm^3 (medium) in volume (Figure 3.3). These specimens were then subjected to petrophysical measurements to assess electrical, magnetic and acoustic properties which shall be discussed in later parts of the thesis.

Table 3.1- The four Marathon mineralization zones investigated in this study, with representative drill cores sampled for each specific mineralization zone, total depths of the drill cores, the specimen sizes obtained from each of the drill cores and the number of specimens for each drill core and specimen size.

Zone	Drill core	Depth (m)	Specimen Size	Number of specimens
Main Zone	KP-13-01	356	Large	45
	KP-13-02	281	Large	54
	KP-13-03	260	Large	40
W-Horizon	M-07-238	15-115	Large	56
	M-07-238	115-259	Small	45
	M-07-239	12-29	Large	34
	M-07-239	29-157	Small	94
	M-07-239	170- 239	Medium	32
	M-07-249	0 - 256	Small	123

	M-07-249	256 - 269	Large	21
Four Dams	B-5-15	292	Small	131
	B-6-16	276	Small	121
	FD-13-34	336	Large	93
Area 41	SL-13-34	0-234	Medium	102
	SL-13-34	234-252	Large	21
	SL-13-36	228	Medium	92
	SL-13-44	303	Medium	82
	SL-13-56	291	Medium	91

Chapter 4

Reorienting Drill Cores with the use of paleomagnetic techniques

Precise orientation of drill cores is of great importance and interest to mineral exploration and development of hydrocarbon reservoirs. Host rock structures and cross cutting relationships can be more reliably known if core samples can be oriented not only along the drilling axis, but also azimuthally about the drilling axis. With fully oriented cores, the surrounding geology, distribution of fault zones, joint structures and fractures can be well studied. In mining and civil engineering industries, oriented cores assist in the assessment of slope stability for site safety, maximum ore removal and for limited interruptions on production (Ureel et al., 2013). Assumptions made on the structures within the subsurface can be applicable for further analysis, only if the drill cores are oriented in their in-situ coordinates. Consequently, drill core data and structural information from oriented drill cores will enable more accurate resource estimations, help in designing future exploration and drilling work and resolve complexities arising in mine planning and other geotechnical problems.

Drilled cores need to be oriented when analyzing fabric orientation of ore related rock. Rock fabrics can give important indications of magmatic or hydrothermal flow directions and stress/ strain directors of altered and metamorphosed rocks when analyzing for directionality in resource exploration. This directional information can be used for subsequent planning of drilling programs and exploration projects. Magnetic fabric assessments done on the oriented cores of the Marathon deposit will be discussed in the coming chapters.

There are three methods for precisely orienting a drill core. Two of the techniques comprise of either using special tools for the conventional scribing technique where the outside of the core is scribed in situ as the drill core is recovered from the sub surface or the use of micro imaging (FMI) logs to match the features of the drill cores with the imaged drill hole to orient them to the correct position. In the scribing tool technique, there is an overall 11° error in the orientation procedure

and only 26% of the analyses follow the guidelines for an accurately oriented core (Rolph et al, 1995).

The technique discussed in this chapter is of an alternative orientation tool provided by paleomagnetism. The recovered core is analyzed to determine the remanent magnetization direction which usually tends to be the paleomagnetic field direction of the earth at the time of the acquisition of the magnetization of the rock. This analysis is done with reference to the axis orientation of the drill core which acts as a reference frame to later orient the drill core. The direction obtained from the core samples are then compared with previously established remanent magnetization direction characteristic for the site locality and the geological age of the rock formation. This information is usually acquired from the previously done paleomagnetic studies of the given rock strata. The directional information is then used as an ancient "compass" to reorient the drill core magnetization direction to the already established Characteristic Remanent Magnetization (ChRM) direction.

The objective of this work is to assess if this technique can be applied to the drill core samples obtained from the Marathon deposit. The pilot sample collection is obtained from the Main Zone drill cores which are already mechanically oriented. The subsequent analysis will assess the accuracy and the ability of the paleomagnetic techniques to correctly obtain a remanent direction for the drill core samples. Similarly, the technique can then be used in unoriented samples to revert them back into their natural geological position.

4.1 Previous Work

Lackie and Schmidt (1993) successfully reoriented drill core samples obtained from the Sydney-Bowen Basin with the use of paleomagnetic work. They utilized the consistent magnetization directions present on the region to reorient the non-oriented drill cores. The age of the remanence direction of the Sydney basin is Cretaceous which is determined to be from an over printing event but is still possible to use for reorienting work. The Natural Remanent Magnetization for the majority of the samples is northwards and steeply upwards which was used as the reorienting direction for the drill cores. The study used Alternating Field (AF) demagnetization to single out the remanent magnetization from the samples.

Rapalini et al. (2013) published another successful study of orienting drill cores with the use of Characteristic Remanent Magnetization (ChRM) directions acquired from AF demagnetization. They used 193 drill core samples from Neuqueb Basin in Argentina which were subjected to stepwise AF demagnetization that revealed a very well defined stable magnetization. The previously acquired directions were used in order to reorient the drill cores to their in situ geological position.

Kulakov et al. (2014) did an extensive paleomagnetic study of the Coldwell Complex and studied the ChRM directions of samples obtained from the three intrusive centers of the complex which were discussed in Chapter 2. The study reported results that point to a single geomagnetic reversal during the emplacement of the Coldwell Complex, indicated by the sample sites from Centre I and II. The polarity reverts back to geomagnetic normalcy in the Centre III and the results of the ChRM directions are similar to the other Keweenaw basalts and Mamainse Point sequence. The positive reversal test conducted on the site localities of the study indicate that the reversal was symmetric and support the validity of the geocentric axial dipole assumption for the 1.1 Ga. The magnetic remanence was removed stepwise with AF and thermal demagnetizations and nearly all samples contained two components to their ChRM: a low coercively component with variable directions which were removed at 10-15 mT or 250-300° C and a secondary component with a demagnetization trajectory heading towards the origin on a Zijderveld diagram which was removed by 575-590° C or by 60-70 mT. Centers I and II (defined according to the Good et al., 2015 geological map of the Coldwell Complex and Figure 2.2) gave group mean ChRM directions of D = 115, I = -66.1° and D= 114.6, I = -61.6° respectively. Sites from Centre III yielded well defined normal polarity directions with a group mean of D = 297.5, I = 56.3°. In this Chapter, we will be using these ChRM directions for the subsequent reorientation of the ChRM directions obtained from the drill cores.

4.2 Paleomagnetic theory

The main objective of a paleomagnetic research is to study the previous records of geomagnetic information ingrained in a rock's magnetic memory. From the two types of magnetization instilled in a rock record, remanent magnetization plays the key role in understanding the magnetic record of the past. The other type, induced (temporary) magnetization will be discussed in length in the upcoming chapters.

A material or rock acquires a magnetization when exposed to a magnetic field and this magnetization is called the induced magnetization which is a vector containing directionality (Equation 1).

$$M_i = kH \qquad (1)$$

M_i is the acquired induced magnetization, H the applied magnetic field and *k* is the magnetic susceptibility, unique to the given rock type or substance. Magnetic susceptibility is regarded as the magnetization ability of a rock. The *k* is usually a scalar quantity without directionality, but the anisotropic qualities of magnetic susceptibility will be discussed in detail in the next chapter.

In addition to the induced magnetization, rocks can contain a remanent magnetization (M_r) which is a record of the past magnetic field(s) that have acted on the material. This occurs when a magnetization is acquired permanently so that even if the inducing field changes, the remanent primary magnetization remains, more or less, a constant.

When a rock sample is left in the ambient geomagnetic field (H_g), the magnetization (M) of the rock therefore consists of the induced magnetization, induced by the geomagnetic field and the remanent magnetization ingrained in the rock from the records of past geomagnetic fields (Equations 2 and 3).

$$M = kH_g + Mr \qquad (2)$$

$$M = Mi + Mr \qquad (3)$$

Paleomagnetic work is based mostly on the intensity and the direction of the remanent magnetization which can provide information for tectonic reconstruction work and unraveling past geologic movements such as plate motions, knowledge on past geomagnetic fields and potentially provide a handy tool for the search of minerals and hydrocarbons!

The Geocentric Axial Dipole hypothesis states that the paleomagnetic field, when averaged over a sufficient amount of time, will conform with the field expected from a geocentric axial dipole (Irving, 1964; Butler, 1998). In this hypothesis, the earth's magnetic field is considered to be produced by a single magnetic dipole at the center of the earth that is aligned with the rotation axis. Therefore, the geomagnetic and geographic axes are considered to coincide with one and

other. The geomagnetic field lines will always point towards the north in normal polarity (as it does in the present) and the inclination as seen locally at the Earth's surface will vary from -90° (vertically up) at the south pole to +90° (vertically down) at the north pole and 0° (horizontal, directed north) at the equator. The hypothesis does require that a paleomagnetic result should consist ideally of samples that span at least several thousand years for the purposes of averaging to produce a good time-averaged pole.

The origin of the geomagnetic field has been of debate for many years. The theory involves the generation of the geomagnetic field within the fluid outer core of the Earth by the form of a magnetohydrodynamic dynamo. The Earth's core has the ability to operate as a self-exciting dynamo with the interaction of the magnetic field and the electrically conducting iron-nickel alloy in the outer core. The fluid motion of the outer core controlled by the rotation of the Earth acts to instigate hydrodynamic processes involving the generation of the geomagnetic field. The magnetohydrodynamic dynamo can operate in either polarity of the dipole and therefore the magnetic reversals observed in the history of the Earth's paleomagnetic record is quite plausible with this theory.

A pole position is derived from assessing paleo magnetic directions acquired during a paleo magnetic analysis. In such an analysis, measurements of a rock sample's magnetization are expressed by three values consisting of two angles of the magnetization vector and the scalar magnetic intensity of the magnetization vector. The declination will indicate the direction of the magnetic north pole and the inclination is the angle of the magnetization vector made with regards to the horizontal.

Paleopoles and latitudes for a site are calculated by determining the primary magnetization direction. Complexities may arise in the form of secondary overprinting magnetizations that could affect the natural magnetization to give altered magnetic directions that are not representative of the rock's true geographic position or primary magnetic direction at the time of the formation (Van der Voo, 1993; Butler, 1998).

4.3 Magnetic carriers

Magnetic carriers in gabbroic rock seen in the Marathon deposit usually consist of ferromagnetic minerals such as titanomagnetite, magnetite and ferromagnetic iron sulphides such as pyrrhotite. If ferromagnetic minerals dominate more than 0.1 volume percentage of a rock, the magnetization is to be dominated by the ferromagnetic minerals (Honsho et al., 2016). Most lithological units of the Marathon deposit are dominated by magnetite and in some cases pyrrhotite and hence the samples assessed in this study can be considered to be dominated by ferromagnetic minerals (Good et al., 2015; Ruthart, 2012; Ames et al., 2017).

Magnetism of the rocks is controlled by assemblages of fine ferromagnetic minerals dispersed within a matrix of diamagnetic and paramagnetic minerals. Ferromagnetic minerals have various energies which control the behaviors of the magnetization and the grain seeks the configuration of magnetization which minimizes the total energy of the grain.

It is important to be able to establish whether the carriers of remanence are in single domain or multi domain grains. With decreasing grain size, the number of magnetic domains within a grain decreases. Below a certain particle size, the domain division is not energetically favorable and the grain remains as one magnetic domain. These are single domain (SD) grains and their magnetic properties are quite different from a larger, multi domain (MD) grain. Fine grained magnetite grains, with a diameter smaller than 0.1 μm are considered single domain magnetite grains. Therefore, in magnetite, it appears that the grain is energetically favorable when it is not large enough to contain multiple domain walls. In single domain particles, the remanent magnetization parallel to the long axis of the grain is equal to the saturation moment. A large energy barrier must be overcome to separate and change the long axis direction of the magnetization which is the stable energy state of the single domain and therefore the SD grains are very efficient remanence carriers.

In large enough ferromagnetic grains, application of a magnetic field will produce preferential growth of domains with magnetization parallel to the field but with the removal of the external magnetic field, the domain walls are reassigned at their lowest energy positions. Due to domain reformations and higher imperfections of the domain walls, the removal of the applied magnetic field will not result in moving the domain walls into their original natural positions and the retained

remanent magnetization is lower than expected. Secondary magnetizations can easily influence most multidomain grains to reassign to a secondary magnetization due to the lower energy threshold barrier.

If the magnetic carriers have not been altered and overprinted with a secondary field or in the successful removal of these secondary components, the rock's characteristic magnetization (ChRM) will represent the ancient geomagnetic field present during the formation of the rock.

4.4 Finding the remanent magnetization

Natural Remanent Magnetization (NRM) of a rock consists of the primary magnetic component acquired during the formation of the rock and possibly one or several secondary magnetization components acquired at a later time in the rock's history. The resulting NRM that we measure in laboratory treatments are a composite vector sum of primary as well as secondary magnetic components. During favorable conditions in the formation of the rock, magnetization induced from the earth's field is recorded as a vector parallel to the magnetization elements. Later changes in the magnetization field, tectonic movements and chemical/thermal alteration events can induce secondary magnetizations on the rock record, largely depending on the single or multi domain state of the magnetic carriers.

4.4.1 Characteristic Remanent Magnetization (ChRM)

Components that are easily removed in a demagnetization process are the low stability components, mostly held by high coercive multi domain magnetic careers. These tend to be remanent magnetization portions obtained during later events of the rock's geological history. Removal of these low stability components will allow for the isolation of the more resistant high stability components. These components can be logically inferred to be the primary magnetization. However, this is not always the case and some of these high stability components can be secondary over print magnetizations which have successfully erased the primary magnetization. In such cases when the high stability magnetization components are uncertain of being primary or otherwise, they are inferred as Characteristic Remanent Magnetizations (ChRMs).

Our goal in laboratory work of paleomagnetic analysis is to isolate the ChRM of a rock and eradicate the secondary magnetic components acquired during later magnetic overprinting events of the rock's history.

Stepwise demagnetization is the laboratory technique used to gradually erase secondary magnetic components in the Natural Remanent Magnetization (NRM) of a rock. Therefore, demagnetization is a vital part of a paleomagnetic analysis to remove unwanted secondary magnetic information and viscous magnetization components in order to isolate primary magnetic information. Measurements of remaining magnetization of a rock is conducted after each controlled demagnetization step which indicates the progressive striping of secondary magnetic components to isolate the magnetic information held by more stable magnetic carriers.

In this study, AF (alternating field) demagnetization was conducted at the University of Windsor paleomagnetic lab which hosts a Sapphire Instrument (SI-4) AF demagnetizer with a peak field of 180 mT for alternating field demagnetization.

The pilot specimens were subjected to alternating field magnetization in stepwise increments which would remove secondary magnetization components to isolate the primary characteristic magnetization. With the aligning of mobile magnetic domains along the axis of the applied field, the sample will be cleaned of magnetization related to low coercivity magnetite domains, which are less than the peak intensity of the applied AF field. Equal number of domains will be magnetized in the positive and negative directions giving a net zero remanent field on the sample while a small percentage of magnetic domains with larger coercive forces than the applied field remains. AF demagnetization is quite effective at removing weakly-held secondary magnetizations. These secondary components are mostly held by low coercive multi domain magnetic grains and high coercive single domain grains hold the more stable primary or characteristic magnetization and often require thermal demagnetization to assess their magnetic information.

During thermal demagnetization, specimens were heated to an elevated temperature below magnetic carriers' Curie temperature (maximum temperature endured by a specific magnetic mineral before the magnetic information is lost).

The selective removal of secondary magnetization is based on fundamental principles that govern the acquisition of magnetization during a rock's history. We assume that the secondary magnetization acquired later on in the rock's history is held mostly as viscous magnetic components that's easily removable during the lower temperature steps of the demagnetization.

The assumption that the thermos-remanent magnetization acquired during a certain temperature (mostly in igneous or plutonic rocks) is also removable in that same temperature range (or temperatures above this limit) while being subjected to thermal magnetization is an important aspect of analysis (Irving, 1964). This reciprocity implies that very high temperatures associated with the formation and crystallization of rocks can also be used to isolate the primary magnetization of a specimen in a thermal demagnetization analysis.

Figure 4.1 is of a photograph of the University of Windsor paleomagnetic lab consisting of a thermal demagnetizer, AF demagnetizer and a cryogenic magnetometer for the stepwise demagnetization and measurement of specimen magnetization data. These instruments are all set within a magnetically-shielded room which has an ambient field of 0.2% of the Earth's magnetic field, to reduce the contribution of multidomain magnetite sprurious magnetizations during specimen handling and measurement.

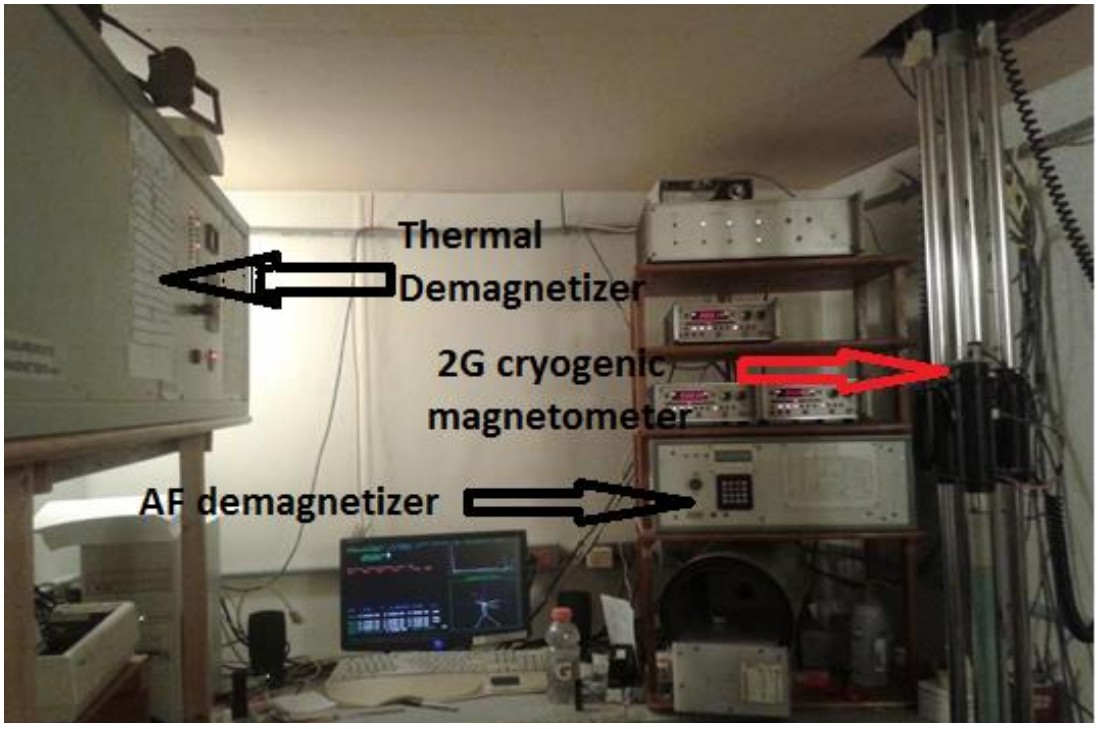

Figure 4.1- The picture is of the paleomagnetic lab of University of Windsor. The lab is situated in a field free room. To the left of the room is a Thermal demagnetizer, bottom right an AF demagnetizer and top right, a cryogenic magnetometer. Picture taken by author on 18/12/2015

2.4 Demagnetization analysis

Stepwise demagnetization processes are used to obtain primary magnetization direction of a rock. After each demagnetization step, the remaining remanent magnetization and the composite vector direction is measured with a magnetometer (Figure 4.1) Usually, the end of a demagnetization process for a sample is marked by the sample losing more than 90-95% of its NRM intensity, indicating the successful removal of most viscous magnetic components and isolation of stable components during the higher demagnetization steps.

With each demagnetization step, the magnetic intensity of a rock will diminish (in most cases) while each demagnetized vector component will indicate any corresponding changes to their directions until the total intensity of the rock's magnetization reaches near zero. A univectorial decay in the magnetization directions is the simplest situation. More complex problems will showcase changes in net directional record with each stepwise removal of secondary magnetic elements.

A statistical analysis of directional data of remanent magnetizations obtained at the end of a demagnetization process is necessary to gain an understanding of the behaviors of a demagnetization trajectory. Least square best fit lines are constructed to the trajectory of the end components of the magnetization vectors which indicate the directional information retained during higher demagnetization steps.

4.4.3 Zijderveld plots (Orthogonal demagnetization diagrams)

The most common form of demagnetization analysis is to visualize intensities of magnetization directions and their corresponding changes in inclination and declination of the vector in orthogonal decay plots or Zijderveld diagrams (Figure 4.2A). A Zijderveld diagram plots the end points of a three dimensional magnetization vector on to two orthogonal plots by projecting the three dimensional directional information onto two dimensional planes.

Vertical and horizontal planes are chosen for the orthogonal plots on most occasions. The horizontal plot is similar to a plan or map view and corresponds with a component of declination relative to north whereas the vertical planes show another component of the inclination of the

magnetization. The magnetization left over from the corresponding demagnetization step will match with the distance to the origin. The directions given in the demagnetization 'trajectory' of a Zijderveld plot indicates the opposing direction of the magnetization of the sample.

A decay plot displays the loss of magnetic intensity with each demagnetized step and is constructed for each demagnetized specimen (Figure 4.2B). An equal area stereonet plot is constructed alongside for each demagnetized specimen with a projection of the direction of each demagnetized vector component (Figure 4.2C).

4.5 Results

In this section, data obtained from AF and thermal demagnetization techniques are presented and methods of data analysis and basics of statistical interpretations are discussed. Magnetization behaviors and directional components of each site is assessed with the use of Zijderveld orthogonal diagrams, equal area stereographic projections and magnetization decay curves plotted in DAIE Open source software (Sagnotti, 2013). Least square regression lines (Kirschvink, 1980) were fitted to linear components of the Zijderveld diagrams for purposes of statistical analysis of remanence directions. These components are normally line segments trending toward the origin in the last few demagnetization steps. Directional information from each specimen was used to compute a mean directional value for its respective drill core. Mean magnetic directions for each site were computed using Fisher (1953) statistics of the dispersion of directions on a sphere.

Pilot sample collection of the Main Zone area of the Marathon deposit consists of three drill cores which have been sampled at various depths to represent the different lithological units. Altogether, 75 samples were demagnetized for the purposes of this analysis. Samples for this comprehensive step wise demagnetization study was chosen by assessing previously conducted anisotropy of magnetic susceptibility measurements. Samples that showed prominent fabrics were chosen to represent the demagnetization study for the purposes of orienting the fabric in drill cores.

Six samples were chosen with their accompanying sister specimen for each of the drill cores from the Main Zone. Two or three sister specimens are accompanied for each sample. All samples from each drill core were demagnetized with stepwise AF demagnetization using a Sapphire Instruments SI-4 alternating field demagnetizer. The demagnetization was conducted with 10 mT increments of the alternating field. After each demagnetization step, the remanent magnetization was

measured with a 2G Enterprises 755R DC-SQUID superconducting rock magnetometer. Samples were demagnetized further up to 90-120 mT in increments and any remaining magnetization was removed in a stepwise fashion. The measurements were carried out until the magnetic intensity of the specimen fell below noise level or until the measurement remanence direction became erratic. Most samples lost nearly 90% of their magnetization intensity by 70 mT.

Two thermal demagnetization steps were also conducted using a Magnetic Measurements MMTD-80 thermal demagnetizer on the already demagnetized samples to assess any possible influences from the mineral geothite, which unblocks below 130°C. Thermal steps at 260°C and 340°C were also performed subsequent to the AF demagnetization.

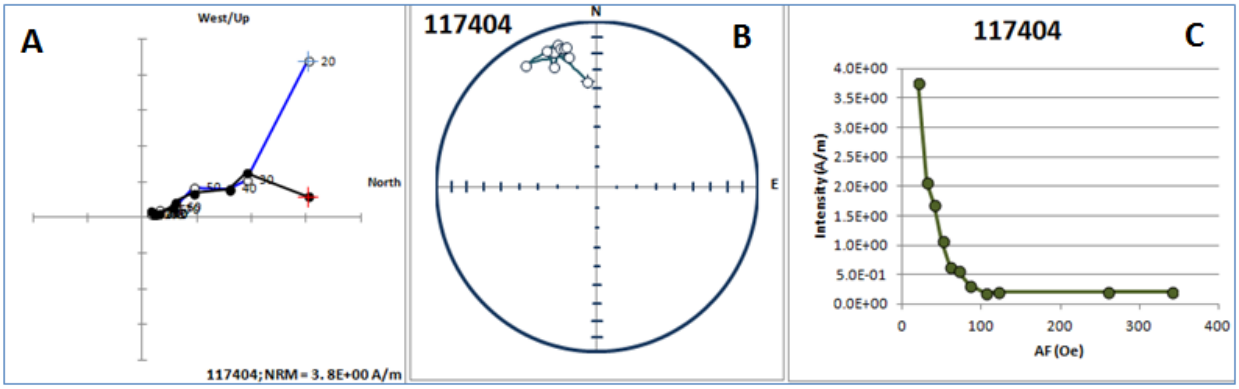

Figure 4.2 – A: KP-01 Zijderveld diagram B: Stereonet projection C: Intensity decay plot for KP-01-174 specimen

KP-01 drill core samples

For most of the KP-01 drill core samples, we observe that the magnetization was removed from a steep up directions to a shallower westward direction and the ChRM direction for each sample was identified by a straight, linear demagnetization trajectory towards the origin of the Zijderveld plot (Figure 4.2A). The remanence directions were projected onto a stereonet after each demagnetization step to follow the demagnetization direction trajectory (Figure 4.2B) Intensity decay plots indicated in an example in 4.2C figure shows the decrease of the magnetization intensity of 50-60 % by 40 mT of AF demagnetization. The decay plots from most samples indicate psedo single domain to multi domain behavior of the magnetite holding the remanence. The magnetization was removed to nearly 5% of its value by 90 mT of AF demagnetization. The ChRM

direction of the KP-01 samples was analyzed with least square best fit lines fitted to the last five consecutive demagnetizations steps until the trajectory reached origin. The trend lines were accepted for the assessment of ChRM directions since the maximum angle of deviation ranged from 4°-7° and is in at an acceptable range.

The last two steps of the demagnetization trajectory were contributed by thermal demagnetization but any changes in the direction of the demagnetization trajectory or the decaying intensity was indistinguishable.

The group mean ChRM for KP-01 drill core was calculated with the use of Fisher (1953) statistics and the mean was calculated with the use of 12 specimens. The 95% confidence circle for the mean of ChRMs was at 11° (Figure 4.5A) which is an acceptable range for the cluster analysis of ChRM directions of the KP-01 samples. The group mean direction gives a declination of 344.1 and an inclination of -9.5 with an α_{95} of 11°.

KP-02 drill core samples

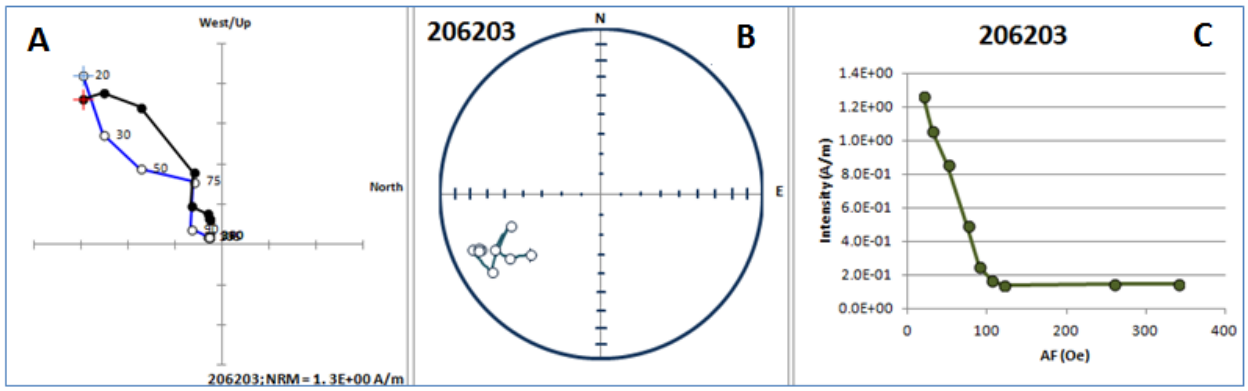

Figure 4.3- A: KP-02 Zijderveld diagram B: Stereonet projection C: Intensity decay plot for KP-02-062 specimen

The demagnetization trajectory for KP-02 core specimens are quite well established and the line decays towards the origin, starting from a south westerly up direction. The Figure 4.6 shows a specimen from a KP-02 specimen which gives an example of a demagnetization trajectory (4.3A,B) and intensity decay analysis plot (4.3C). The Figure 4.3A Zijderveld diagram indicates the directions to hardly change during the trajectory and this characteristic remains the same for most samples in the drill core. The directional change with every demagnetization step is also projected onto the stereonet seen in Figure 4.3B where the directions are of a south westerly up

direction. The NRM intensity decays up to 95% by 90 mT in AF demagnetization. A couple of samples from an augite syenite lithological unit showed coercively high samples with almost 30% of the magnetization intensity remaining by the end of the 120 AF demagnetization step. But most of the other samples show low coercivity multi domain to pseudo-single domain magnetite decay behavior.

The ChRM directions were assessed for each sample by fitting least square best fit lines. Once the ChRMs were calculated for all samples, the directions were plotted in a stereonet as in Figure 4.5B and the mean ChRM direction for the KP-02 drill core was calculated with fisher statistics. The mean direction was given at a declination of 250 and an inclination of -24° with a α95 value of 14.5°. The α95 value is acceptably below the usual critical value of 15° and the mean direction was acceptable for the scope of this project.**KP-03 drill core**

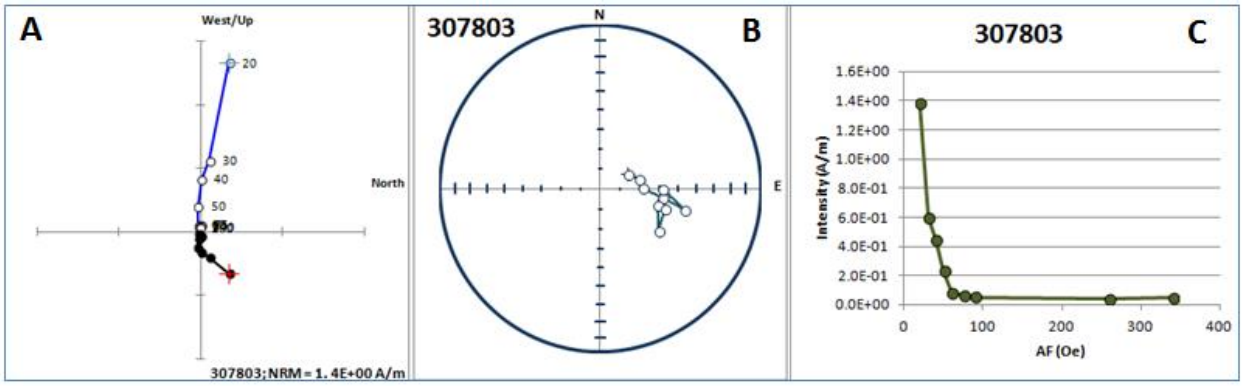

Figure 4.4- A: KP-03 Zijderveld diagram B: Stereonet projection C: Intensity decay plot for KP-03-078 specimen

Similar to KP-01 and KP-02 drill core samples, the KP-03 drill core samples were also demagnetized and an example of a KP-03 specimen has been displayed in the Figure 4.4. The first figure (4.4A) indicates the demagnetization trajectory to be of a straight linearly projected line towards the origin with a steep easterly up direction and the directions doesn't change with the progression of the demagnetization trajectory in much of the samples. The directional changes with each demagnetization step have been projected in the stereonet as indicated by Figure 4.4B. Nearly 60% of the NRM intensity was removed by 20 mT and the magnetization intensity was removed more than 95% at the end of 80 mT demagnetization step (4.4C).

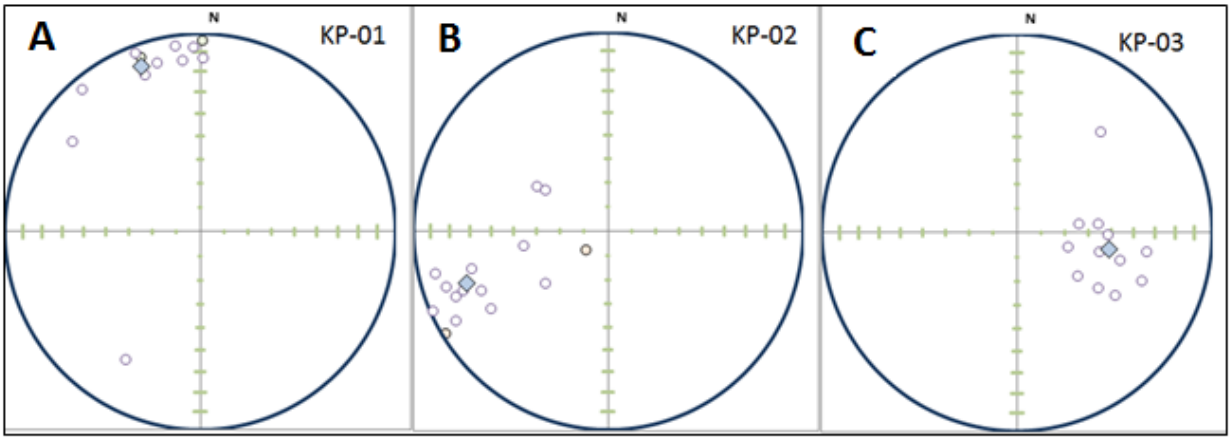

Figure 4.5- A: KP-01, B: KP-02, C: KP-03. The specimen ChRM directions are indicated as open circles and the corresponding fisher means are plotted as blue diamond signs.

A few samples from the fine grained homogeneous gabbroic units (2a lithology) showed a higher coercive magnetization with 60% of the magnetization still remaining at the end of 120 mT demagnetization step. These fine grained lithological units might contain single domain to pseudo-single domain behaviors in magnetite grains. Most samples tested in this study are from the Marathon series and Fine grained series lithological units that show a range of grain sizes from coarse to fine grained but most of the samples show multidomain to pseudo-single domain demagnetizing behavior.

Similar to samples from KP-01 and KP-02 samples, best fit least square regression lines were projected on demagnetization trajectories to calculate the ChRMs directions for each sample. The mean ChRM direction for the whole of the KP-03 drill core was computed with fisher statistics which gives a declination of 100 and an inclination of -50° with an α95 of 9.1°(Figure 4.5A).

ChRM directions obtained from all specimens from KP-01, KP-02 and KP-03 drill cores were plotted in three stereonet diagrams as observed in the Figure 4.5. The Fisher mean directions were plotted as blue diamond signs to distinguish the mean value from the individual ChRM directions of each drill core.

4.6 Discussion

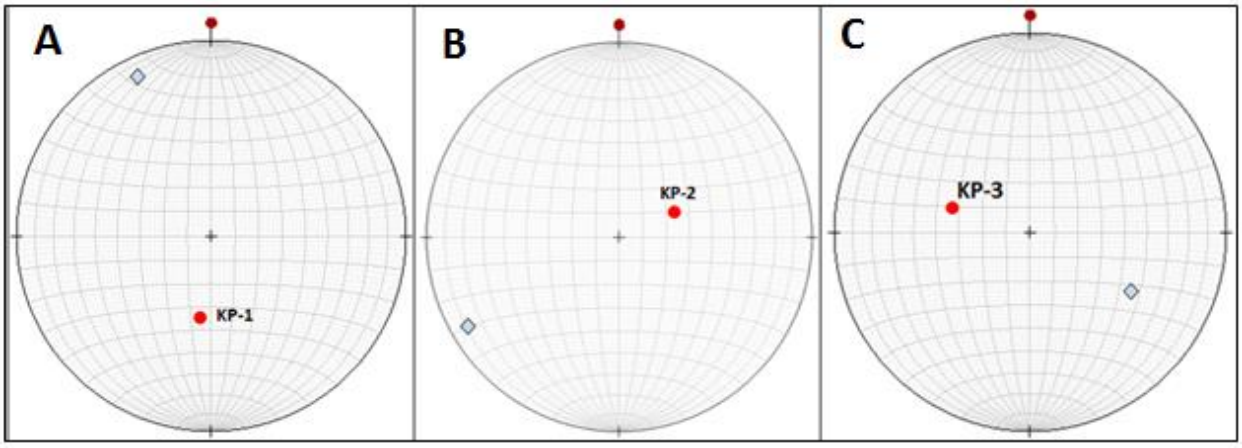

Figure 4.6- A: KP-01, B: KP-02, C: KP-03
The open blue diamond signs indicate the upwards-directed Fisher means for each of the drill holes and the red dots indicate the orientation of the drill core axis for the drill holes. The drill core orientation for KP-01: 188, 56°; KP-02: 069, 65°; KP-03: 289, 55°.

The results of the Main Zone drill cores indicate interesting results that doesn't show a uniform (ancient) ChRM direction as expected. Due to previous geotechnical work done on these drill cores, the cores are already oriented in in-situ geological position. Therefore, the samples have been subjected to AF demagnetization and other magnetic measurements, already oriented in its natural geological coordinates. Regardless of the drilling orientations, the samples should give a uniform ChRM direction, characteristic to the area and geology of the region. Kulakov et al. (2014) in their paleomagnetic study of the Coldwell Alkaline Complex states that the Eastern part of the complex is reversely magnetized with a mean declination of 114.8 and an inclination of -63.7°.

Yet, when the data are analyzed, the Main Zone specimens do not indicate ChRM mean directions obtained by Kulakov et al. (2014). When investigated further into the differing ChRM directions for each of the drill cores, a correlation with the drill core axis was noticed. In Figure 4.6, the mean ChRM direction and the azimuth and plunge of each drill core axis are plotted in separate stereonets. As observed, there is a correlation of the mean ChRM direction with the drill core axis orientation. The results indicate a possible tampering of the remanent magnetization during the drilling process which has overprinted the directions of the magnetization. In all three instances, we observe that the mean ChRM direction has an angle of close to ~120° made with the drill core axis orientation.

In literature, this phenomenon is named drilling induced magnetization, which is sometimes observable in drill cores that have been obtained during mineral exploration. Audunssin and Levi (1989) has noted that this is possibly due to the strong non-uniform field concentrated during the initial drilling process near the cutting rim of the drill string, creating a secondary magnetic field from the core barrel. Studies have shown that in most cases multidomain to single domain magnetite have been equally influenced by the drilling induced magnetization. But, drilling induced secondary magnetization is usually characterized by low coercivity and low blocking temperatures and Van Alstine and Gilbert (1981) reported that the basaltic drill core they used was severely affected by drilling overprinting. Many speculations are still rife in the scientific community as to what causes the drilling induced magnetization but many have agreed that the drilling induced magnetization has a closer resemblance to secondary VRM or isothermal remanent magnetization.

Based on the results, it's not evidently distinguishable as to why the ChRM direction is magnetized with respect to the drill core axis.

Main Zone drill cores were demagnetized to obtain the ChRM direction as a feasibility study to check if the drill core samples gave similar results as the Kulakov et al. (2014) and from there on be used to independently orient the core. Since the samples have been overprinted by a drilling induced magnetization, we were unable to compare the ChRM directions obtained in this study with the Kulakov et al. (2014) study conducted on the Coldwell Complex lithologies.

Apart from the Main Zone drill cores, the other three mineralization zones discussed in this thesis are only azimuthally oriented (orientation perpendicular to the drill core axis is unknown). This study was to assess the feasibility of orienting the rest of these azimuthally oriented drill cores using the present day over printing of viscous remanent magnetization or the ChRM. Since the over printed nature of the rest of the mineralization deposits and drill cores are unknown, a pilot sample collection was demagnetized to find the ChRM directions for the partially oriented drill cores obtained from W-Horizon and Area41. Three samples from W-Horizon and seven samples from the Area 41 were demagnetized and the ChRM directions were plotted in stereonets along with the drill core axis orientations of the respective drill holes (Figure 4.7).

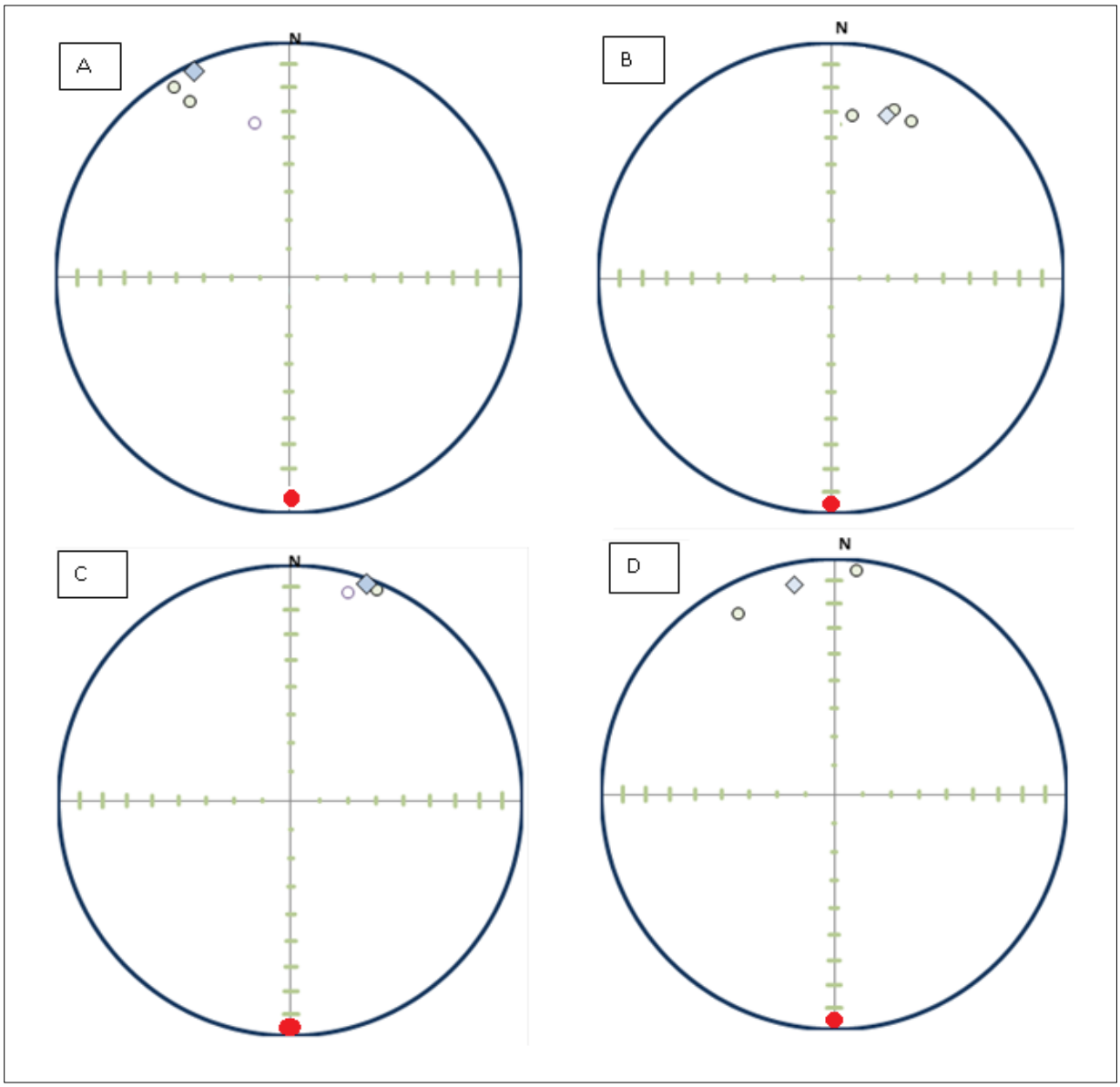

Figure 4.7- The red dots indicate the drill hole axis orientation which is plotted as 180, 0 by definition due to the specimens having been measured in specimen coordinates. The blue diamonds indicate the Fisher mean directions and the specimen demagnetization directions are displayed as open circles.
A:drill core M-07-238 (W-Horizon); B: drill core SL-13-44; C:drill core SL-13-36; D: drill core SL-13-56 (Area 41)

Since these samples from W-Horizon and Area 41 are only oriented azimuthally, the samples can be rotated at any given angle around the axis of the drill core. Therefore, the in-situ geological positions of the specimen are unknown. If the drilled samples are rotated randomly at any given angle around the axis and if these samples are not induced by the drilling, the ChRM obtained

from the samples will not have any directional correlation with the drill core axis. Figure 4.7A shows the ChRM directions obtained from the M-07-238 drill core of the W-Horizon mineralization zone and the other three stereonet projections are for drill cores from Area 41 zone. The red dots of the Figure 4.7 indicate the down hole axis orientation of the drill core which by definition plots as a pole south and 0°. This is due to the fact that the specimens were analyzed for the magnetization directions in their specimen coordinates, which is perpendicular to the drill core axis. The clusters of light coloured open circular dots indicate the ChRM for each specific specimen. The open blue diamond sign shows the mean upwards ChRM direction calculated for that particular drill hole which is the average of ChRM directions from all specimens for the drill core.

The ChRM directions are mostly similarly distributed in relation to the drill core axis and has a ~170-180° relationship which is directly opposing the drill core axis direction. ChRMs from SL-13-36 drill has a distribution slightly different to the rest of the ChRM directions with an angle of close to 160-170 degrees. These pilot studies of drill cores from W-Horizon and Area 41 provides ample evidence of the dominance of drilling induced magnetization and the induced remanent magnetization seems to distribute parallel but in opposing directions to the drill core axis.

The drilling induced magnetization has dominated most of the remanent magnetization observed in the specimens from all mineralization zones observed. A larger suite of samples and specimens can potentially contain coercively high magnetite carriers that might have retained the original ChRM or the primary magnetization of the rock unit but further studies need to be conducted to assess this phenomenon. Alternatively, drill cores can be oriented with the use of structural inversion methods. Reorienting drill cores has been successfully conducted with previously determined structural features of the area such as joint sets and fractures.

Conclusion

Drilling induced magnetization seems to dominate the remanent magnetization that has been obtained from Main Zone, W-Horizon and Area41 specimens. The samples from Main Zone has been induced at a slightly different angle in relation to the drill core axis, compared to the directions obtained from the samples of W-Horizon and Area41. Alternative drilling mechanisms are recommended to be used to orient the drill cores for the Marathon deposit and further analysis of

ChRM directions for a larger suite of samples is also recommended to assess if any samples have retained the primary remanence found in coercively hard magnetic grains.

Chapter 5
Use of Anisotropy of Magnetic Susceptibility (AMS) to analyze petrofabrics

5.1 Introduction

Magma conduit models have been proposed for many of the Cu-PGE mineralization zones in the Marathon deposit. Magma conduits are structurally controlled pipe-like bodies that magma passes through to reach intrusive complexes. The deposit itself is located in the Coldwell Alkaline complex, formed during several intrusion events in the Mid Continental rifting event of North America, at 1.1 Ga. Therefore, the prominent ore forming mechanisms of the deposit have been proposed to involve structural controlled magmatic flows which controlled the progressive enrichment and deposition of ore minerals. Deep seated lineaments and troughs that dominate the topography of the complex have been associated with faulting that provided the magma into the complex. These have been associated with directionally coherent feeder channels that brought magma into the Two Duck Lake Gabbro mineralization (Good et al., 2015).

The geochemical and field studies of the area indicate evidence of mineralization governed by magma flow. Experimental studies have shown that the anisotropic crystal growth could be interpreted in terms of direction. Use of classical methods such as the microscopy or other textural analysis is difficult in many cases when three dimensional interpretations need to be done to categorize flow directions. Anisotropy of Magnetic Susceptibility (AMS) provides quantifiable directional analysis that reflects the distribution of mostly ferromagnetic minerals in rocks, that can act as a proxy for the three-dimensional fabric which is a record of flow directions in magmatic systems.

Magnetic susceptibility is not always uniform in all directions in a rock. This anisotropy can be detected by applying an external magnetic field and measuring the induced magnetization in a number of orientations. This property of the directional distribution of magnetic susceptibility can be used to study petrofabics. One of the most important aspects of this technique is that it is

nondestructive, fairly straightforward, cost effective and can assess microscopic fabrics or weak foliations/lineation that are invisible or difficult to recover by other structural assessment methods.

Some materials display magnetic anisotropy is such a way that when an external magnetization is applied, the induced magnetization direction in not parallel to the exposed magnetic field. For an anisotropic substance, a magnetic field applied in a direction will induce a magnetization not only in that direction but also in other directions and therefore for an anisotropic rock type, magnetic susceptibility is expressed as a tensor, requiring a 3 x 3 matrix for full description of the distribution of the susceptibility in the cartesian coordinates (Guo, 2015, Jetlinek, 1981, Dubey, 2014).

Magnetic susceptibility of a rock varies depending on the bulk mineral content, ferromagnetic, paramagnetic or diamagnetic minerals of the rock. In the absence of strongly ferromagnetic minerals such as titanomagnetite, magnetite or pyrrhotite, paramagnetic minerals will dominate the contributions to the magnetic susceptibility. Specimens from the Marathon deposit are mafic-gabbroic with a considerable presence of ferromagnetic minerals such as magnetite and titanomagnetite. Therefore, a resounding magnetic response is to be expected. Susceptibility also depends on the temperature as well as the strength of the magnetization field but the measurements are all made in a constant room temperature and a low applied field of 1mT.

In an isotropic medium, induced magnetization in symmetric specimens are independent of the direction of the weak magnetization field that is applied to the sample. But for most rock types, the orientation of the sample within the field affects the strength of the induced magnetization. These rocks types are mostly anisotropic.

Magnitude of the anisotropy of magnetic susceptibility depends on the anisotropy of the particles themselves and the degree of their alignment. Individual particles can have shape anisotropy or crystalline anisotropy. Crystalline anisotropy depends mostly on the lattice forces that result in directing magnetization in specific directions whereas the shape anisotropy depends on the induced magnetization, oriented along the long axis of the grain. In magnetite for instance, the shape anisotropy is dominant and therefore is a great indicator of orientation of grains that can depict magmatic flow movements or flattened and metamorphosed fabrics (Borradaile, 1987; Dubey, 2014).

When the strength of the magnetization field intensity, H, is directly proportional to the induced magnetization, M, the susceptibility can be written as

$$K = M/H \qquad (1)$$

And the variations of the susceptibility *K* can be described as a symmetric second rank tensor where,

$$(K) = \begin{pmatrix} K(11) & K(12) & K(13) \\ K(21) & K(22) & K(23) \\ K(31) & K(32) & K(33) \end{pmatrix} \qquad (2)$$

Therefore,

$K_{ij} = K_{ji}$ (i, j = 1,2,3)

This symmetric matrix *K* is called the susceptibility tensor and can be transformed to another frame where the components are diagonalized to calculate the principal values of *K*.

$$K = \begin{pmatrix} K(11) & K(12) & K(13) \\ K(21) & K(22) & K(23) \\ K(31) & K(32) & K(33) \end{pmatrix} \rightarrow K' = \begin{pmatrix} K(1) & 0 & 0 \\ 0 & K(2) & 0 \\ 0 & 0 & K(3) \end{pmatrix} \quad .(3)$$

The Cartesian coordinate axes of the corresponding frame are known as the principal axes. Since susceptibility (*K*) is symmetric, the principal values can be expressed as the three eigenvalues of K and is possible to calculate the three eigenvectors which are orthogonal to each other. These principal values are the eigenvalues corresponding to the matrix K and the principal axes are given by the eigenvectors.

Here, *K*(1), *K*(2), *K*(3) along the three main orthogonal axis are the principal susceptibilities and the populations of induced magnetization can be expressed as

$$M_i = K_i H_i \,, \qquad (i = 1,2,3) \qquad (4)$$

The three principal susceptibilities are parallel to the corresponding populations of magnetic fields and since the fields are orthogonal, no interactions occur.

In practice, the susceptibility tensor can be calculated by means of the least square method from a set of *K*(H) measured along different directions. Reading from at least six different directions is necessary to obtain the three eigenvectors coinciding with the principal susceptibilities (Guo, 2015).

5.2 Magnetic susceptibility ellipsoid

The magnitude of the three eigenvalues and the orthogonal eigenvectors can be used to construct a standard ellipsoid called the magnetic susceptibility ellipsoid. The half lengths of the three susceptibility ellipsoid axes correspond with the magnitudes of the three principal susceptibilities (Guo, 2015, Dubey 2014). The distribution of the orthogonal axes of the ellipsoid is defined by the eigenvectors (Figure 5.1). The shape, distribution and orientation of the susceptibility ellipsoid in the Cartesian coordinates directly shows the status and orientation of the Anisotropy of the Magnetic Susceptibility (AMS).

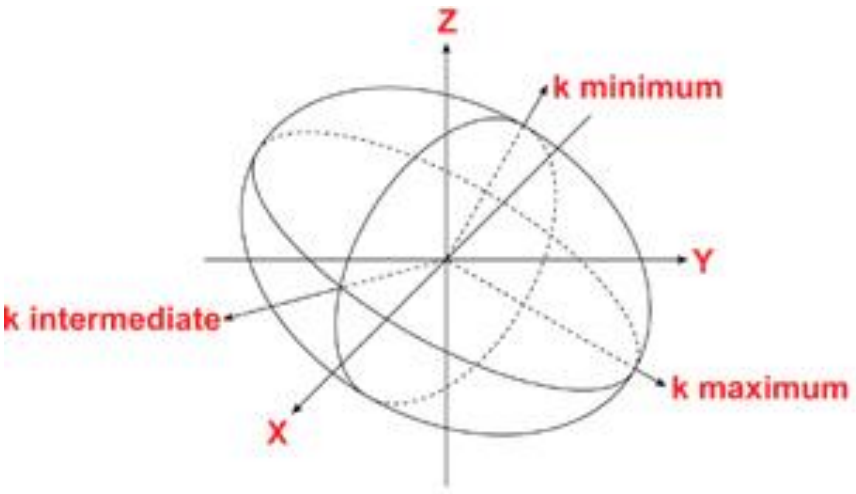

Figure 5.1- Magnetic Susceptibility ellipsoid. K (1), K (2) and K (3) eigenvectors are illustrated by K maximum, K intermediate and K minimum respectively. These axes are also called the principal susceptibility directions/ axes.(Figure adopted by Dubey, 2014

Therefore, the bulk susceptibility can be indicated by,

$$K = K(1) + K(2) + K(3)/\ 3$$

Where $K(1) > K(2) > K(3)$.

This is due to the fact that the ferromagnetic grain will have a lower magnetostatic energy if magnetized along its long length. Magnetostatic energy is the energy stored as the charge distribution on a grain surface. In a spherical grain, the same percentage of the grain surface is covered by the magnetic charge. The internal demagnetization field of a grain is proportional to this charge distribution of the grain and is always distributed such that the internal energy is the lowest. When the magnetostatic energy is distributed along the long axis of the grain, percentage wise, the surface covered by the charge is smaller and hence contributes to a lower internal demagnetization field. This magnetic energy distribution leads to the shape anisotropy seen in magnetite grains (Khan, 1962).

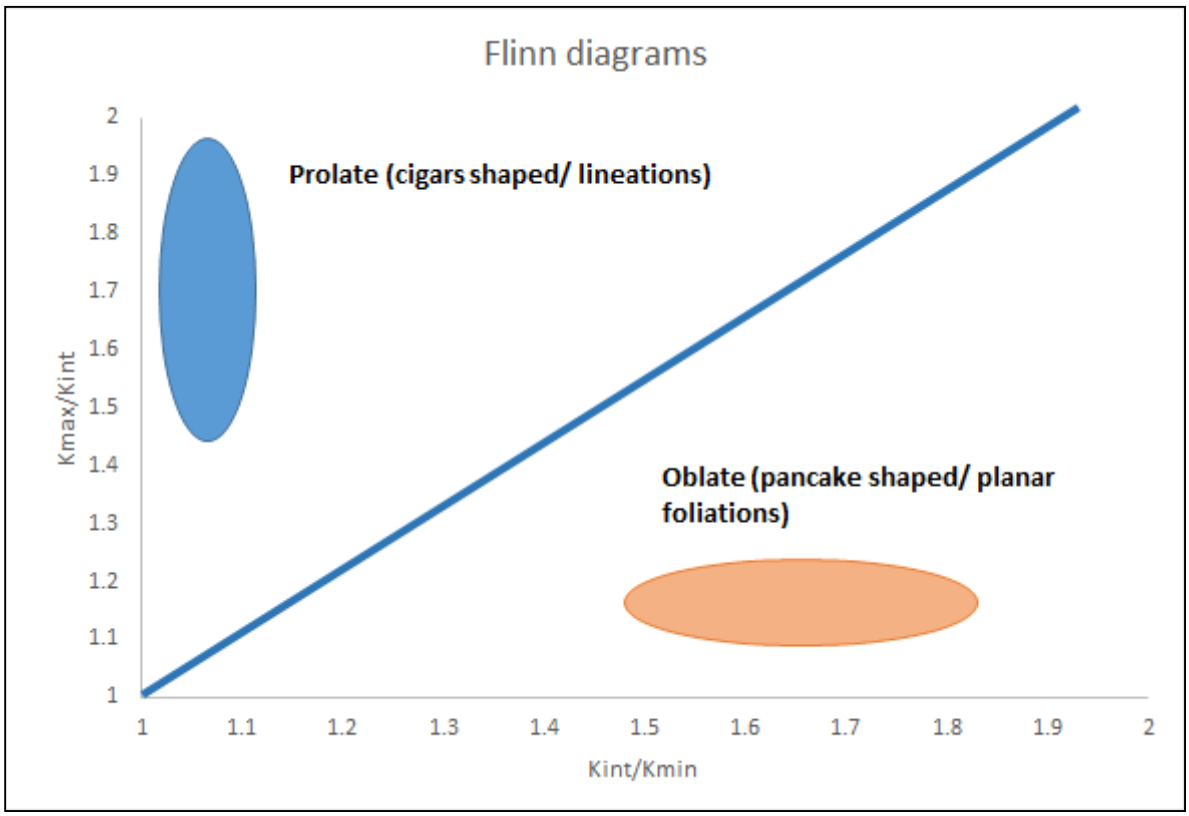

Figure 5.2- Flinn diagram constructed with x axis on ratios of K int/K min values for foliation and y axis on K max/ K int for lineation.

Anisotropy can be defined by A = $K(1)/K(3)$, Lineation property by L= $K(1)/K(2)$ and Foliation property by F = $K(2)/K(3)$.

5.3 Plotting of Magnitude and Shape of Susceptibility Ellipsoid

The ratios of principal susceptibilities are employed to represent the lineation and foliation qualities of an AMS fabric. The most commonly used diagram is the Flinn diagram (Figure 5.2) where the origin of the plot is representing an isotropic medium with no fabric. The horizontal axis is defined by the principal magnetic susceptibility ratios of $K2/K3$ and the vertical axis with $K1/K2$. Horizontal axis defines the properties of foliation textures and the vertical axis defines the properties of lineation texture in as AMS fabric. Therefore, plotting of ratios of principal susceptibilities in a flinn diagram provides a standard definition in understanding the fabrics developed in a rock. The 45°slope that runs through the origin divides the graph into oblate fabrics (foliations) plotted in the lower right portion of the graph and the prolate fabrics (lineations) plotted in the upper left potion of the graph. All ellipsoids with increasing axial ratios would plot at increasing distances away from the origin, governed by the increasing anisotropy. Depending on the magnitudes of principal susceptibilities and their ratios, the further the ratios are from the origin, the more oblate or prolate are the fabric textures.

The directions of the eigenvectors that represents the principal axis directions of the susceptibility ellipsoid are also plotted on equal area stereonets. The axes orientations of maximum susceptibilities ($K1$), intermediate susceptibility ($K2$) and minimum susceptibility ($K3$) are plotted as squares, triangles and circles respectively, in a stereonet to observe the distribution of directions of the principle susceptibilities in three dimensions.

5.4 Methodology

Drill core samples provided by Stillwater Canada Inc. were carefully selected in order to best represent the main lithological units of the mineralization zones.

These representative samples were assessed for anisotropy of magnetic susceptibilities and were measured with a Sapphire Instruments SI-2b magnetic susceptibility meter, located in the Western Paleomagnetic and Petrophysical Laboratory (WPPL), Western University. This technique

computes the orientation of the magnetic fabric existing within the rock, with the use of magnetic susceptibility, measured in six different orientations, in order to represent the magnetic anisotropy within the rock (Dubey, 2014). The output of the AMS measurements is an ellipsoid of magnetic susceptibilities indicated by the length and orientation of susceptibilities analyzed in three different principal axes directions of the rock fabric (Rochette et al., 1992).

5.5 Results

Specimens from three oriented drill cores of the Main Zone of the Marathon deposit were measured for AMS properties. Most lithological units described and stated in Chapter 3 were observed in the Marathon deposit and have been assessed in the AMS study, and the resulting principal susceptibilities have been plotted in corresponding Flinn diagrams for each of the drill cores (e.g., Figure 5.3A). The directions of the principal susceptibility axes have been depicted in stereo nets corresponding to each of the drill cores (e.g., Figure 5.3B). The principal susceptibility axes orientations in steronets indicate green squares for *K* maximum (*K*1) direction; blue triangles for *K* intermediate (*K*3) directions and pink circles for *K* minimum (*K*3) directions, calculated from each of the specimens of the study. The specimens have been measured in sample coordinates and the following stereonet projections have been plotted in specimen coordinates without being converted to the respective in-situ drill core coordinates.

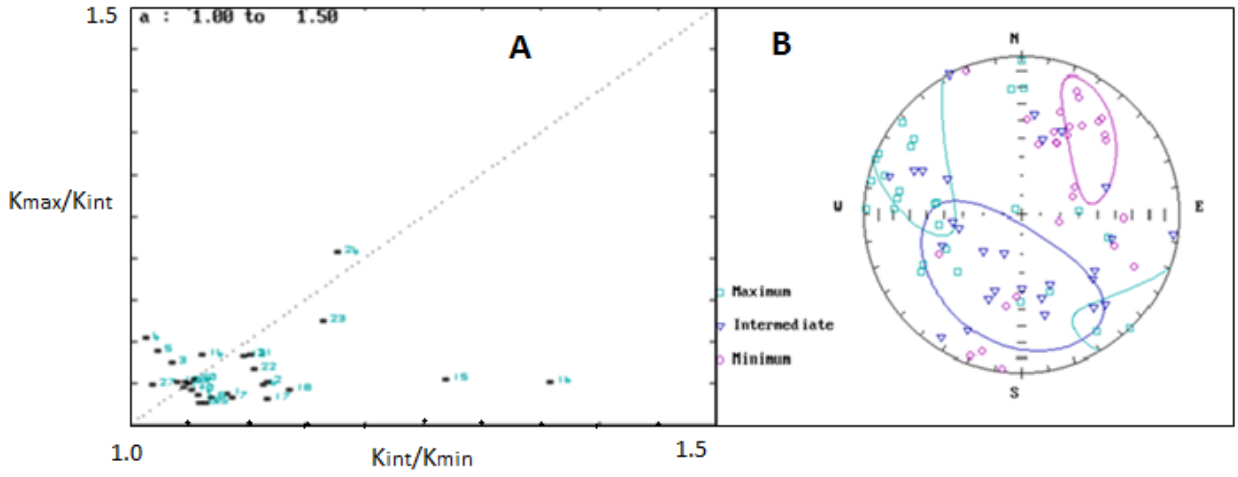

Figure 5.3- A: Flinn diagram for KP-01 specimens; B: Stereonet projections of principal susceptibility axis directions

KP-01 core from the Main Zone is represented by 35 specimens and represents Fine Grained, Layered as well as Marathon series lithologies. As observed from the distribution of the magnetic susceptibility ratios of KP-01 specimens in the flinn diagram, most specimens tend to distribute in close proximity to the x axis and four specimens have ratio values of 1.15 indicating a substantially dominant planar fabric feature. Two specimens from the collection are observed further along the direction of the y axis compared to the cluster near the origin which indicates the presence of some lineations. When the *K* min (K minimum), *K* int (K intermediate) and *K* max (K maximum) susceptibility directions were projected on to a streonet, we observe the *K* int and *K* max values to be projected in a well-defined great circle while the *K* min was projected in as a pole perpendicular to the great circle (Figure 5.3B). This distribution of the directions in a great circle can be analyzed for the directional assessment of the dominant fabric elements represented in the samples.

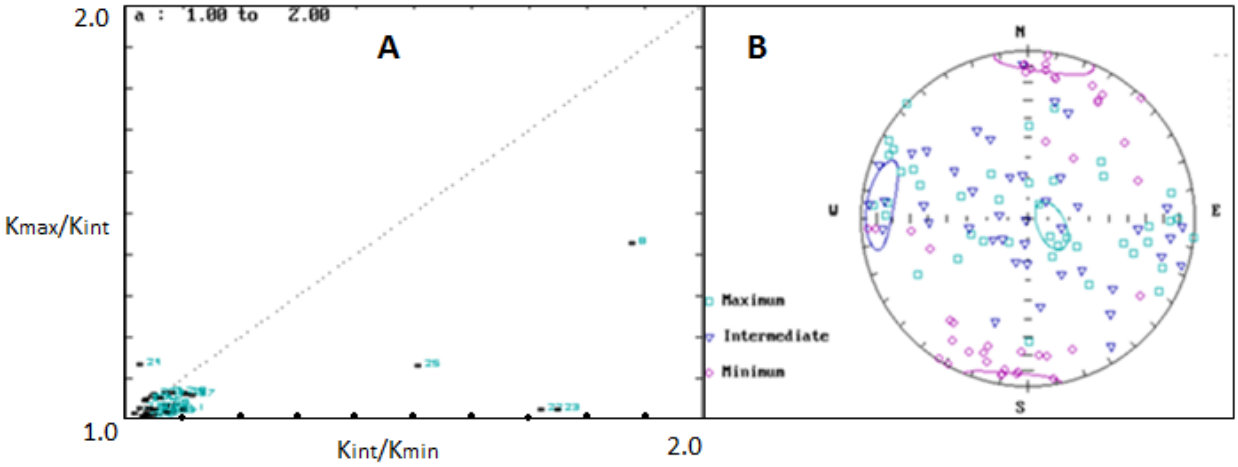

Figure 5.4- A: Flinn diagram for KP-02 specimens; B: Stereonet projections of principal susceptibility axis directions

KP-02 drill core is represented by 42 specimens and the principal susceptibility ratios have been calculated and plotted on a Flinn diagram (Figure 5.4A). Most specimens cluster close to the origin, indicating very little anisotropic distribution. Four specimens lie along the x axis indicating the presence of a planar fabric and the *K*int/*K*min values of these specimens range from 1.75-1.9 which is comparatively higher than KP-01 or KP-03 specimens that will be discussed next. The high values of the susceptibility ratios indicate somewhat of a stronger planar foliation fabric existing in KP-02 although not quite dominant. When the directions for the susceptibility tensors were projected on a stereonet, we observe a similar distribution of *K* max and *K* int as a great circle and the *K* min clustered perpendicular to the great circle (Figure 5.4B).

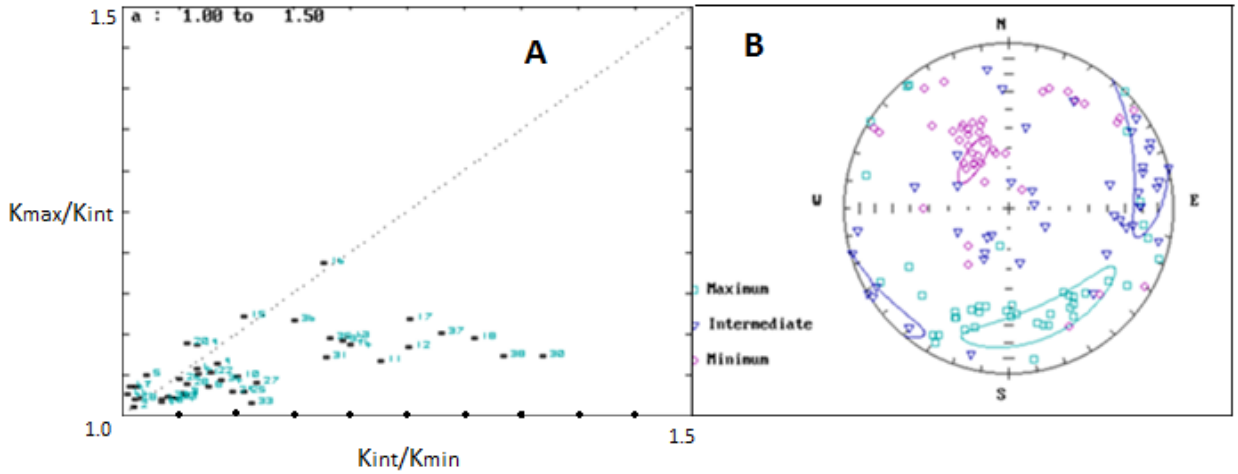

Figure 5.5- A: Flinn diagram for KP-03 specimens; B: Stereonet projections of principal susceptibility axis directions

KP-03 drill core has been represented by 42 specimens and their principal magnetic susceptibilities have been plotted as ratios in a flinn diagram (Figure 5.5A) and a substantial portion of the specimens (15 specimens) plot along the x axis, away from the origin, indicating the presence of a dominant planar foliation fabric. The *K*int/*K*min of the specimens furthest away from the origin give values close to 1.40 (Figure 5.5B). A few specimens also plot along the direction of the y axis, indicating some presence of lineations and the ratio of *K*max/*K*int of these specimens vary around 1.10-1.15. Similar to the other two drill cores, when the principal susceptibility axes are projected on a streonet, a great circle distribution is observed for *K*max and *K*int vector directions and the *K*min cluster is seen perpendicular to the great circle. The great circle distribution is substantially tighter and better defined in KP-03 drill core.

5.6 Reorienting the great circles

The three KP Main Zone, fully oriented drill cores were drilled for geoengineering purposes in different orientations but the specimens were measured in specimen coordinates without taking into consideration the in-situ drill core orientations. Therefore, the principal susceptibility vectors need to be corrected to their original orientation. Upon correcting each of the drill core samples to their original orientation, the three great circles coincide in their great circle distributions and fabric directions. The three drill cores indicate unanimously similar orientations.

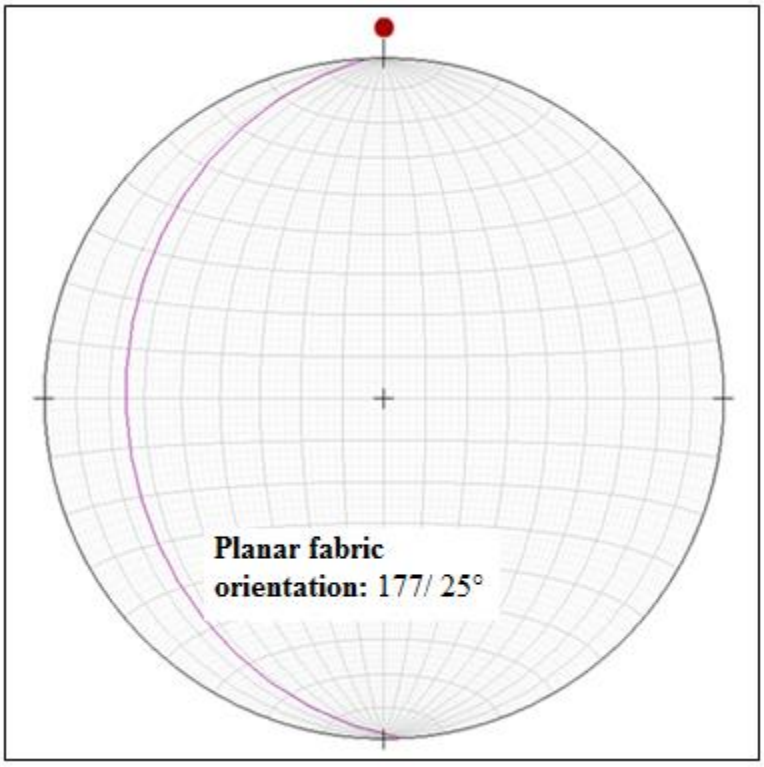

Figure 5.6- Fabric foliation direction observed in KP-01, KP-02, KP-03 drill holes. Fabric orientation of strike 177 and dip 25 ° is seen in all three KP cores after orienting the specimen to their original geological position.

Directional distribution of the three great circles gives a well-defined planar fabric orientation striking at 177 and dipping 25° to the west (Figure 5.6).

The few specimens that showed characteristics of a lineation fabric in the flinn diagrams were separated out and replotted on a stereonet. These specimens were mostly from the Two Duck Lake Gabbro lithologies and three specimens were indicated from the Fine Grained series grabbos. A Fisher (1953) statistical mean was computed for the lineation direction with a 95% confidence interval depicted in Figure 5.7. This fabric lineation direction gives an average trend of 295 and a plunge of 29° reflecting the likely direction of origin for the magma.

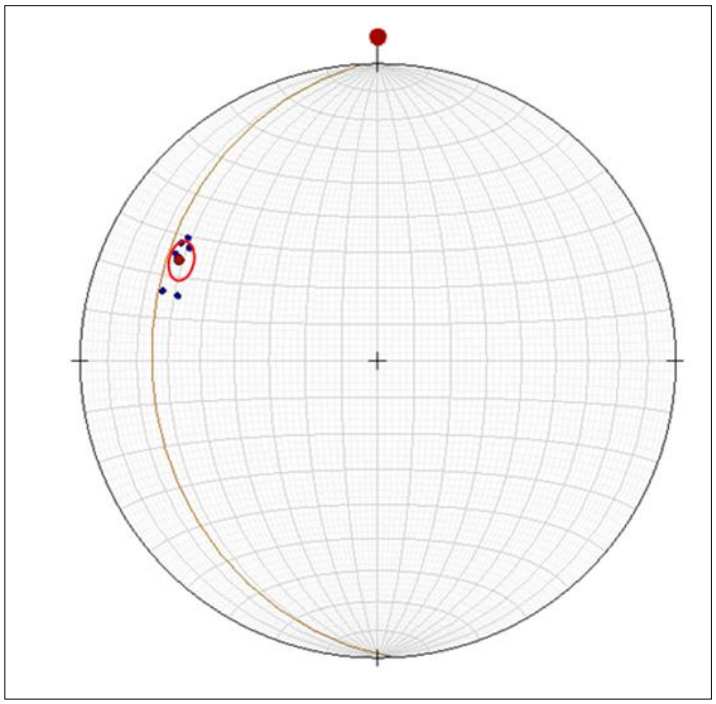

Figure 5.7 - lineation directions plotted alongside the Fabric foliation orientation of the KP specimens. The red dot and circle indicates the fisher mean of the lineations and the α95 confidence interval for the mean direction

5.7 Discussion

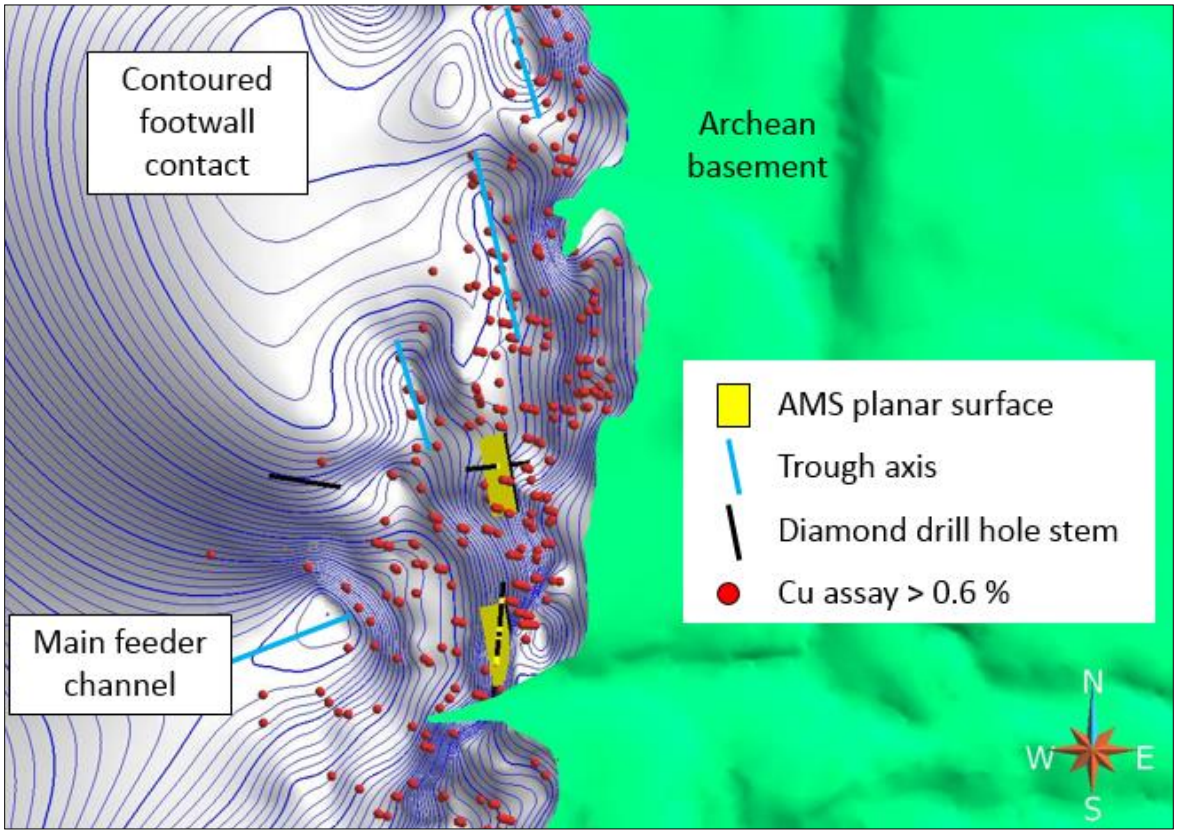

Figure 5.8 – The figure shows the contoured foot wall contact of the Marathon deposit against the Arcean basement. The surface lineaments and troughs have been plotted as blue lines and Cu assays above 0.6 ppm has been plotted as red dots. The surface lineaments mimic the directions and orientations of the main feeder zones which contains high copper content. The AMS planar surfaces has been plotted as yellow planes along with the drill cores axis orientations of the Main Zone drill holes. The AMS strike directions are extremely similar to the lineaments mimicking the feeder zones.

Main zone oriented drill core results which give a planar fabric orientation striking at 177 and dipping 25° to the west is in excellent agreement with proposed flow foliations based on 3D modeling of footwall troughs that contain higher grade copper mineralization (Figure 5.8). KP drill core samples show a dominant planar fabric and the most anisotropic samples are from the Two Duck Lake Gabbro lithologies which hosts the mineralization. Good et al. (2015) states that topographic lineaments, troughs and ridges observed on the footwall contacts of the Main Zone and W-Horizon are highly mineralized channels representing the feeder channels that brought sulphide ridden crystal mush into the Two Duck Lake Gabbro intrusion. A surface model of the

footwall has been projected on the Archean basement platform in Figure 5.8. Distribution of high grade copper assays have also been plotted in red dots with the axes of troughs and topological lineaments indicated in blue lines projected on to the foot wall. These troughs strike approximately at 170 (Good et al., 2015), extremely similar to the strike of the AMS planar surface (strike at 177), projected as yellow planes on the drill core axes.

Therefore, the planar AMS-defined surfaces seem to mimic the lineaments that brought the sulphide hosting magma flow into the deposit. This suggests that the AMS technique can be independently used to identify planar flow fabric that is following conduit structures. AMS can furthermore uniquely define possible local conduit flow directions to further assist mineral exploration work.

The specimens with highly anisotropic foliations and lineations were mostly from the Two Duck Lake (TDL) gabbroic unit and therefore can be of assistance in locating deposits hosted in this lithological unit. Since most mineralization is located in the TDL gabbro, further investigation in to the AMS technique could be of use in future exploration planning for the Marathon deposit.

While samples from the TDL gabbro has been dominant in indicating highly anisotropic mediums, some samples from Fine Grained and Layered series also illustrated similar fabric orientations. When these anisotropic Fine grained and Layered series samples were analyzed, both suits of specimens showed the same anisotropic distribution and similar fabric orientation to the TDL samples. Even though Fine Grained and Layered series were intruded prior to the Marathon series or TDL, these magmatic events seem to indicate similar flow directions and hence can be concluded as nearly contemporaneous, emplaced in similar magmatic intrusion events in nearly similar orientations to the TDL lithologies. This potentially indicates that the magmatism related to the different lithological units could have been emplaced in pulses from similarly oriented conduit type systems or feeder channels that transported the magma to the complex. This observation agrees with petrogenesis studies conducted on the Coldwell complex magmatism by Good et al., 2015; Ruthart, 2014; Good et al., 2017, Ames et al., 2017.

While further investigation needs to be conducted on the applicability of the AMS technique on other mineralization zones, Main Zone drill cores indicate anisotropic lithologies that shows a

direction quite similar to the directions of proposed feeder channels. From an exploration stand point, this technique can potentially be used to locate new feeder channels that harbor mineralized ore rock. Future work can include obtaining oriented drill cores for other mineralization units (Four Dams, W-Horizon and Area41) and testing the AMS method to find petro fabrics. The AMS technique could not be extended for drill cores from these mineralization units due to the fact the drill cores were only partially oriented and conducting AMS measurements would be futile without in-situ orientations of the specimens.

Even though the reorientation technique with the use of ChRM directions was not successful, structural features of the area can be used to obtain best fits for the partially-oriented drill cores which was discussed in Chapter 4. As a component of future work, these partially oriented drill cores can be oriented and then used for the assessment of AMS fabric directions.

Chapter 6
Physical Properties variations

Geophysical exploration methods effectively investigate an area or subsurface volume at a large scale and is considered an important aspect of a resource exploration program. Geophysical surveys are used to indirectly assess the subsurface geology and structures that can produce observable anomalies, which in turn are often directly related to the variations in petrophysical properties. An excellent understanding of the petrophysical characteristics in the area is important for the effective use of geophysical methods in mineral exploration. Physical properties of lithological units are variable in accords with changes in their mineralogical compositions and textures; geophysical results can, in turn, be inverted to estimate the 2D and 3D distribution of physical properties existing within the rock units. Properties vary within lithologies and also within different mineralization areas in the same deposit.

This chapter focuses on presenting the variations, means and relationships observed in different petrophysical quantities within lithologies and mineralization zones of the Marathon property. Such information can be used to improve geophysical model inversions and potentially be used to reduce the non-uniqueness of the geophysical models. Petrophysical information forms an important link between the geology and the geophysical anomalies observed in surveys.

Geophysics methods used in resource exploration exploits the fact that as lithologies vary, so do the physical properties of the rocks. Therefore, the main exploration methods are based on the physical properties associated with mineralization of economic commodities that are related to the density, magnetization, electrical and acoustic properties.

The gravity method uses the mass distribution of rock lithologies expressed as the density. The variations in the mass distribution results in small, localized changes of the Earth's gravitational field strength which can be observed and mapped. While gravity methods are not investigated or discussed in this thesis, changes in the spatial distribution of rock magnetization properties which corresponds to the magnetic susceptibility causes localized disturbances in the Earth's total

geomagnetic field strength and direction which is somewhat similar to spectral changes seen in gravity methods.

Electrical methods examine the subsurface distribution of the electrical resistance (or conductivity) of the rocks, investigated by electrical and magnetic responses in varying lithologies. These methods include resistivity and induced polarization surveys, electromagnetic responses, magnetotelluric and controlled source electromagnetic surveys. In this thesis, spatial distribution of resistivity and induced polarization response are discussed and analyzed in the mineralized zones of the Marathon property.

Acoustic properties are examined via the measurement of P-wave velocities and acoustic impedance of the rocks. The acoustic impedance is associated with the product of rock densities and the travel velocities of the elastic waves. Although the seismic method is the main source of exploration in the oil and gas industry, the mineral exploration industry is yet to instill a greater importance due to the expensive nature and limitations associated with the method. In this thesis, a spatial distribution of the acoustic impedance assessed by P-wave velocities of different rock types in the Marathon deposit is investigated.

An integrated approach is recommended for an effective assessment of the physical property variations existing within different lithologies. Therefore, a combination of petrophysical and geochemical properties will be used to better evaluate the variations observed in lithologies. This integrated interpretation approach uses petrophysical variations, structural variations and geochemical / assay data to generate a geological model that fits all data. This study could lead to recognition of petrophysical patterns and anomalies that could be used for resource vector exploration.

6.1 Physical rock property measurements

Physical rock properties have been systematically collected over fresh core from four different mineralization zones. The details of the drill cores, regions from where they were collected and number of samples used for the study have been described in detail in Chapter three. Magnetic susceptibility and NRM measurements have been provided in this chapter as cgs volume values. Resistivity has been reported as Ω-m and the integrated chargeability as (msec). The densities are indicated as kgm^{-3} and the p-wave velocities as ms^{-1}.

6.2 Electrical properties

Electrical properties of minerals create three main classes: insulators, electronic conductors (sulphides, oxides and graphite) and ion exchangers (clays). The two basic properties of electrical behavior analyzed in rocks are resistivity and dielectrical behavior pertaining to the polarization that occurs during charge separation. Electrical current can be flown through rocks. But most ore forming minerals are insulators and therefore when the current is flown through the rock, it is carried by the ions in the ground water that fill the pore spaces of the rocks. Earth materials are tested for the resistance for the current flow which ranges from very low resistivity rocks to very high resistivity rocks. Therefore, factors such as porosity, fracture density, pore fluid salinity, the presence of metalliferous minerals and graphite affect the resistivity and the conductivity of the rocks. Few minerals, mostly the naturally occurring metallic minerals such as the sulphides, oxides such as magnetite and conducting form of carbon, graphite are considered electrical conductors.

6.2.1 Resistance

The resistance is defined by the voltage drop when a current is passed through a given material when R is the resistance, ΔV the voltage drop and I the current (Equation 1),

$$\mathbf{R} = \frac{\Delta V}{I} \qquad (1)$$

The resistance is dependent on the material's geometrical factors and is proportional to the sample's length δl and inversely proportional to the cross section area A. Resistance is also dependent on the resistivity ρ of the target which is distinct for the material. The resistivity ρ is therefore an important factor in distinguishing electrical characteristics of a rock type (Equation 2).

$$\mathbf{R} = \rho \frac{\delta l}{A} \qquad (2)$$

Measuring of the resistivity is therefore done with the following relationship of the proportions of a specimen (Equation 3),

$$\boldsymbol{\rho} = \left(\frac{A}{\delta l}\right)\left(\frac{\Delta V}{I}\right) \quad (3)$$

Conductivity is the inverse proportion of the resistivity (Equation 4)

$$\sigma = \frac{1}{\rho} \quad (4)$$

6.2.2 Induced Polarization (IP)

Induced polarization is an excellent method to explore disseminated minerals such as sulphide deposits when the conductive mineral grains are not in contact electrically and is not detected through conventional electrical conductivity methods. This technique was used by Schlumberger (1920) where a voltage transient after a cut off of direct current pulse was observed at various electrical studies. This electrical phenomenon, Induced Polarization occurs when metallic minerals or clay minerals interact with an ionic current flow induced by ionic pore fluids in the rock material. Empirical results show that even small concentrations of metallic minerals such as sulphide minerals will result in recognizable induced polarization effects. The Marathon deposit in particular should respond to IP surveys quite effectively due to the disseminated nature of the sulphide grains detected (Good et al., 2015; Good et al., 2017).

IP effect shows a delayed decay in the voltage drop after the current is switched off and this effect is measured for the decay rate of the voltage. As seen in the Figure 6.1, the IP effect is observed both when the current is switched off and when the current is switched back on. Therefore, IP effect is described when a rock mass stores electrical energy when a current is flown through the material and the gradually release of energy when the current is turned off, resembling a battery.

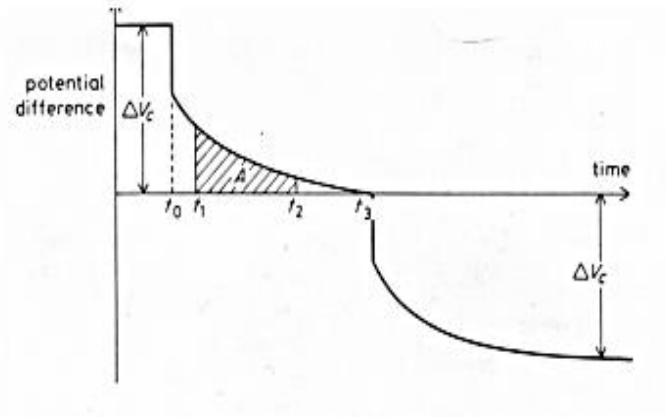

Figure 6.1 : At time t_0, the current is switched off and instead of an instantaneous decrease in the voltage, the potential difference decays gradually to zero. When the current is switched back on at time t_3, the voltage builds back up to a steady state value. The IP effect (chargeability) of the measured rock is calculated as the area under the curve from t_1 to t_2. The figure is adopted from Kearey and Brooks, 1991.

The electrode polarization plays an important role in detecting metallic mineral deposits. Current is usually conducted through groundwater movement of ions in interconnected pores, fractures, microcracks and mineral grains. When the passage of current is interrupted by particles such as sulphides, a charge pile-up occurs on particle-electrolyte interface. This piling of charges usually tends to occur opposing the flow of electrical current and when the current is interrupted, a residual voltage continues to exist across the particles, but decreases continuously as the ions slowly diffuse back into the surrounding electrolytes. The IP effect increases with the surface area of the grains due to increase in the ion accumulation on the available surfaces and therefore the IP effect is enhanced when the mineral grains are disseminated rather than connected and compacted. Therefore, depending on the polarizing properties of the minerals, a disseminated ore body most probably will show a much higher IP effect compared to their massive counterpart. Pyrite, pyrrhotite, chalcopyrite, graphite, galena and magnetite are some of the minerals that show high IP effects.

Four different measurement techniques have been developed to assess the IP effect of rocks. The Time Domain IP method uses a small direct current and measures the voltage drop after the current is terminated. The voltage drop is assessed for a given time frame after the DC current is terminated. The Variable Frequency IP method diagnoses the decrease in the apparent resistivity of the earth when the frequency of the applied alternative current is decreased. Instead of a DC

current, an AC current is used with varying frequencies to assess the voltage diffusions. In the Phase IP method, the presence of induced polarization is detected as a phase lag between the voltage measured across the rock and the applied current. As a continuation of this method, the Spectral IP method uses measurements of the phase and magnitude made over a range of frequencies. In this study, a time domain IP measurement process is used to calculate the IP responses of rock specimens from the Marathon deposit.

Induced polarization is defined as the chargeability of rocks, M, indicated by the Equation 5 and the relationship is established in the Figure 6.1 with the IP effect (chargeability) of the measured rock calculated as the area under the curve from t_1 to t_2.

$$M = \frac{1}{Vc}\int_{t1}^{t2} Vp(t)dt \qquad (5)$$

V_c = Voltage drop across the specimen during charge

V_p (t) = transient voltage drop across specimen after interruption of charging current
t_1 = start of measure time of the voltage drop after the interruption of charging current
t_2 = end of the measuring time of the voltage drop after the interruption of the charging current

It must be noted that for any polarized rock, the value of the resistivity and the conductivity will depend on the pore spaces, total concentration of the metallic minerals, the types of metallic minerals present and their grain textures. As a rule of thumb, increasing the metallic mineral content will decrease the resistivity and increase the chargeability or IP effect.

6.3 Electrical measurements

The Electrical measurements are made using a four electrode configuration; with two potential electrodes and two current electrodes in a wenner configuration. Current is supplied by a BRGM IP pulse system using a 2 second pulse time and 10 µA direct current (DC). The resulting voltage decay is measured with a digital oscilloscope. Commonly four complete cycles of on and off are recorded.

Resistivity measurements are made using a two-wire bridge and a high –impedance voltmeter capable of measuring milliohms. Uniform contact with the specimen is achieved using copper electrodes and copper sulphate saturated contact pads (Figure 6.2). Current is forced through the rock that acts as the resistive element for an electrical circuit. By measuring the voltage drop across the specimen, Ohm's law for electrical circuits can be used to determine the corresponding resistance. Electrical measurements were performed in time domain and a boxcar wave form was used to calculate the voltage drop during both the on-time and off-time of the DC current.

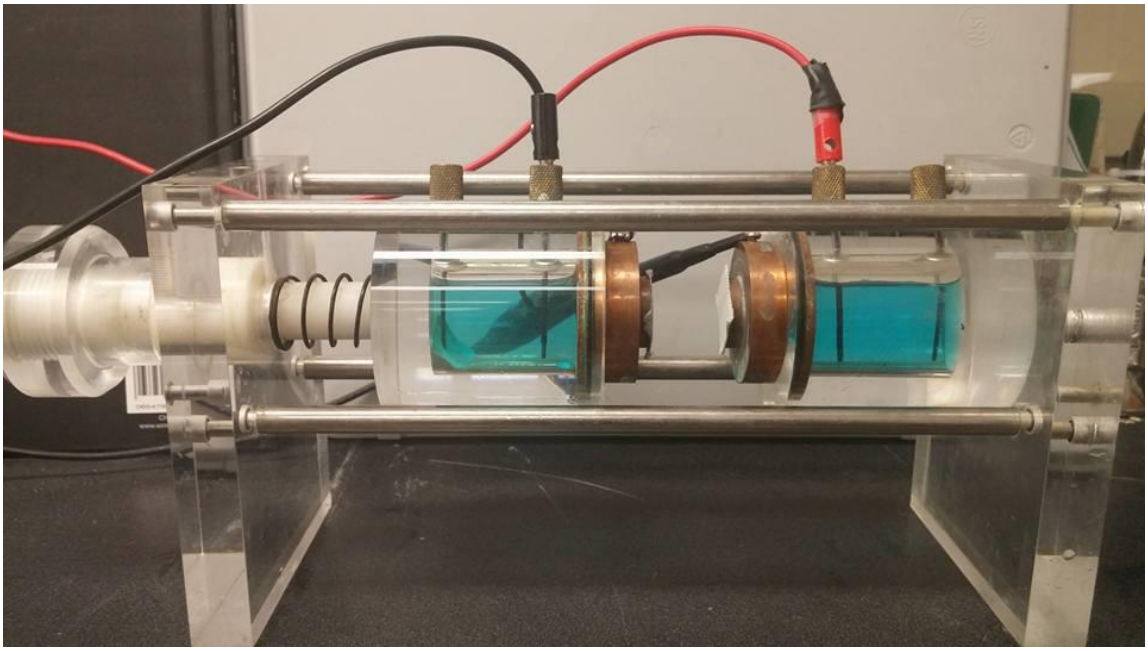

Figure 6.2 : Electrical measurement apparatus used for resistivity and IP measurements at Western Petrophysical laborotory

Passage of current in a specimen is very dependent upon the presence of water in the pores of the rock. Prior to any electrical measurements, all specimens were stored under water in a pressurized chamber for a minimum of two days. The intent is to water saturate the specimen. During measurements, the specimens start to dehydrate, hence it was optimal to take the earliest reading.

During the process of measuring the electrical properties, current initially flows through the rock sample with an instantaneous increase in measured voltage. Buildup of ionic charges results in a relaxation process where the measured voltage approaches a steady state DC voltage. After a sufficient time (for the purposes of this thesis, 2 seconds), the current source is switched off but due to the induced polarization effect, it takes a while for the rock to discharge the ionic buildup

of charge. As a result, there is a measurable voltage across the rock during the off time which is subsequently used to calculate the induced polarization property of the rock unit.

After acquisition, the voltage decay records were compiled in an Excel spreadsheet to provide information regarding the integrated chargeability of specimens. Cross section area and the lengths of the specimens were measured by a vernier caliper with a 10^{-3} cm precision to calculate the resistivities of the specimens.

6.4 Resistivity and Conductivity

Resistivity properties of rock lithologies varies according to the mineralogical variations and shows a direct relationship to the mineralogy and textures of the rock. Chargeability of the study indicates that the induced polorization properties correspond quite closely with the resistivity properties and show an inverse relationship at most times. As explained above, chargeability is dependent on the electrical conductive minerals, specifically the mineralogy and the textures of the lithologies and conductive minerals. In this chapter, chargeability, resistivity and density values measured for all rock samples have been averaged out with regards to their lithological units and mineralization zones and are summarized in the Table 6.1. Analysis of the IP and resistivity variations of each mineralization zone and the lithologies related to zones will be presented and discussed below.

6.4.1 Main Zone

The Main zone is represented by three drillcores and the samples measured for density chargeability and resistivities have been reported in the Table 1. In Main zone, resistivities are comparatively higher (in the ranges of 4000 Ωm and above) which correlates with the drill core assays indicating a lower sulphide percentage. The resistivities mainly vary inversely according to the amount of sulphide percentage ingrained in a rock specimen. Alongside higher sulphide content, coarser grained gabbros seem to show lower resistivities. The average value for Fine grained series lithologies is 6202.3Ωm and the Marathon series lithologies show an overall lower resistivity with an average of 4623.8 Ωm. The lowest resistivity 1042.3 Ωm is observed in the 3g lithology and the unit is described as medium to coarse grained oxide melatroctolite with extreme

Table 6.1 – Chargeability, resistivity and density average values for lithological zones found in the Main zone, W-Horizon, Area41 and Four Dams mineralization zones

Main Zone			W-Horizon			Area41			Fourdams		
Lithology	Chargeability (msec)	Resistivity (Ω.m)	Lithology	Chargeability (msec)	Resistivity (Ω.m)	Lithology	Chargeability (msec)	Resistivity (Ω.m)	Lithology	Chargeability (msec)	Resistivity (Ω.m)
1a	3.57	5080.01	1a	4.76	3694.26	1a	3.73	775.54	2a	11.42	532.52
2a	4.09	5691.43	2a	6.33	4412.05	1b	1.24	1039.73	2b	9.70	758.47
2c	1.30	8176.97	2d	4.01	3653.39	2a	17.85	1322.05	2f	81.72	215.49
2d	2.76	6907.88	3a	4.24	1719.18	2b	12.52	1435.87	3d	23.60	452.25
2k	8.76	5666.75	3b	8.04	1493.48	2f	24.33	1118.51	3g	43.17	297.19
3b	11.91	4789.44	3g	89.60	643.53	2i	32.17	576.42	3h	19.38	444.21
3c	5.91	7682.12	3h	22.91	962.07	3b	6.52	1148.38	3i	6.03	452.73
3g	46.85	1042.02	3i	54.24	835.13	3d	12.47	816.53	4a	15.49	486.60
3l	4.13	5339.50	4a	27.88	1225.74	3g	63.12	400.72			
4a	11.45	8034.12				3h	18.53	562.88	Fine Grained	12.68	601.08
						4a	10.45	817.91	Layered	45.71	486.97
Fine Grained	3.31	6206.29	Fine Grained	5.98	3955.43	4b	15.63	821.19	Marathon	23.04	487.77
Marathon	17.17	4623.86	Layered	18.42	1277.18	4c	11.97	467.78			
			Marathon	26.01	1226.65	6a	3.15	1425.98			
						Fine Grained	20.54	1217.86			
						Marathon	17.90	681.04			

gabbro with clinopyroxene/olivine porphyroblasts and shows an average resistivity of 8176 Ωm.

This mineralization unit shows chargeabilites in the ranges of 3-46 msec and has comparatively low chargeability properties compared with the other regions. The fine grained series lithologies, when combined gives an overall average of 3.30 msec and Marathon series lithologies show a higher chargeability with a 17.2 msec. The 3g unit shows the highest chargeability with a 46.8 msec and the lowest chargeability is represented again by 2c lithology which is a fine grained gabbro with clinopyroxene/olivine porphyroblasts with a 1.3 msec chargeability value. As observed in Table 1, the Marathon series lithologies show a higher chargeability, within the lithologies of the Main zone.

6.4.2 Area 41 mineralized zone

The mineralized zone is penetrated by four drill holes used in this work and the samples have been measured for the resistivity and chargeability properties and subsequently divided into different lithological elements. Similar to other zones, the resistivity is higher in the Fine grained and Layered series, compared to the marathon series lithologies. The resistivities are an order of a magnitude lower in the Marathon series compared with the Main Zone, giving a 681.2 Ωm as the mean resistivity. The 3g-Medium to coarse grained oxide melatroctolite unit shows the lowest resistivity with a 400.7. The highest resistivity is observed in 6a lithological unit, described as the aphanitic to porphyritic mafic dykes with a value of 1425.9 Ωm. The higher values are closely followed by 2b unit, stated as a coarse grained olivine gabbro with modal layering. These lithological units are deprived of sulphides or any other conducting minerals as depicted in Figure 6.6 indicating the amounts of sulphur found in different lithological units.

As observed from Table 1, the highest chargeability is seen in the 3g lithology, similar to the Main Zone with an average value of 63.1 msec. The rest of the samples representing Marathon series lithologies show values ranging from 6-18.5 msec, which are surprisingly not as high as the Fine grained and Layered series rocks of the Area 41 zone. The chargeabilities are noticeably higher in the 2a, 2b, 2f and 2i lithologies ranging in values from 12- 32 msec which does contain significantly higher amounts of disseminated sulphur ranging from 0.4-0.6% (Figure 6.6). The sulphur reported in Figure 6.6 is considered to represent sulphides in the rock units. The 4a, 4b and 4c lithologies that represent massive sulphide hosting xenoliths of the Fine grained series also

shows distinctively higher chargeabilities ranging in the values of 10.4-15 msec. The chargeabilities are directly correlated with the sulphides present in these lithological unit and therefore compared to Main zone, Area 41 lithologies host a higher percentage of sulphides. Hence the chargeability values are correspondingly higher to reflect the amount of electrically chargeable minerals.

6.4.3 W-Horizon

The W-Horizon mineralization zone is represented by three drill holes and the resistivity properties are carefully measured and allocated into their distinctive lithologies. The resistivity is higher in the Fine grained and Layered series and much lower in the Marathon series lithologies. Similar to other mineralization zones, lithology 3g shows the lowest resistivity with a 643.5 Ωm. Lower resistivities are also indicated in the 3h and 3i lithologies representing apatitic clinopyroxenite and apatitic olivine clinopyroxenite lithologies respectively. The values of resistivity for these two units are 962.1 Ωm and 835.1 Ωm indicating higher amounts of electrically conductive material in the rock types. Highest resistivities are observed in the 2a unit representing fine grained homogeneous gabbro with a resistivity value of 4412.1.

The W- Horizon drill core samples are assessed for the chargeability characteristics and the highest chargeability is observed in the 3g lithology with an average value of 89.60 msec. 3i lithology, described as an apatitic clinopyroxene unit also indicates high chargeability properties with a 54.23 followed by 3h unit (apatitic olivine clinopyroxenite) with a chargeability of 22.91. These units have been described in the drill core assays to indicate 3-5% disseminated sulphides which is comparatively a high sulphide percentage. The Fine grained lithologies all distribute in the low range of chargeability values, from 4-6.3 msec. Overall the Marathon series lithologies have a higher chargeability average of 26.01 msec compared to the Fine grained series which averages around 5.9 msec.

6.4.4 Four Dams

The Four Dams mineralization zone shows considerably low resistivity figures overall and the average resistivity for Fine grained series lithologies are 601.1 Ωm and Marathon series rocks are lower with resistivity of 487.7 Ωm. Notably, the highest average value for Four Dams is still lower than the other zones such as Main zone or W-Horizon. In Four Dams, the lowest resistivity

lithology is indicated by 2f Layered series lithology with medium to course grained oxide augite melatroctolite . The average value of resistivity for this unit is 215.4 Ωm closely followed by 3g Medium to coarse grained oxide melatroctolite unit and other Apatite bearing lithologies such as 3h and 3i. The 2f- layered series lithology has been geochemically tested for a high sulphide content and the drill core logging observations indicate almost 4-6% disseminated sulphide content in some portions of the rock samples. This is a lot higher compared to other units where the highest sulphide content ranges from 2-3% sulphides. The highest resistivity average is seen in the 2b rocks with a 758.4 Ωm which is still comparatively quite low compared to the other resistivity ranges observed in other mineralized zones.

Four Dams drill cores show chargeabilities in the higher range of values. The lowest chargeability mean value comes from 3i with a 6.2 msec and the highest from 2f unit of medium to coarse grained oxide augite melatroctolite with an average chargeability of 81.7 msec. This is one of the highest average chargeability figures observed for any lithological unit. When assessed for the Sulphur abundance and sulphide observations in the drill core, a substantial amount of disseminated sulphides were found. 3g unit also shows a considerably high chargeability value with an average figure of 43.1 msec. All Marathon series units show high chargeabilities compared to the Fine Grained and Layered series unit, as expected.

6.5 Chargeability variations across lithologies

From a lithological standpoint, it is quite clear from the data that the 3g unit dominates the low resistivities and high chargeability ranges observed in all the mineralization zones. The drastic increase in chargeabilities for 3g unit is better displayed in Figure 6.3 as average values for each lithological unit. The 3h and 3i units with extreme enrichment of apatite also indicates high chargeability ranges which is observant in Area41, W-Horizon and Four Dams mineralization zones. In Figure 6.3, the 2f unit of the Four Dams lithologies also show an increase in chargeability values although such an increase cannot be observed in other mineralization zones.

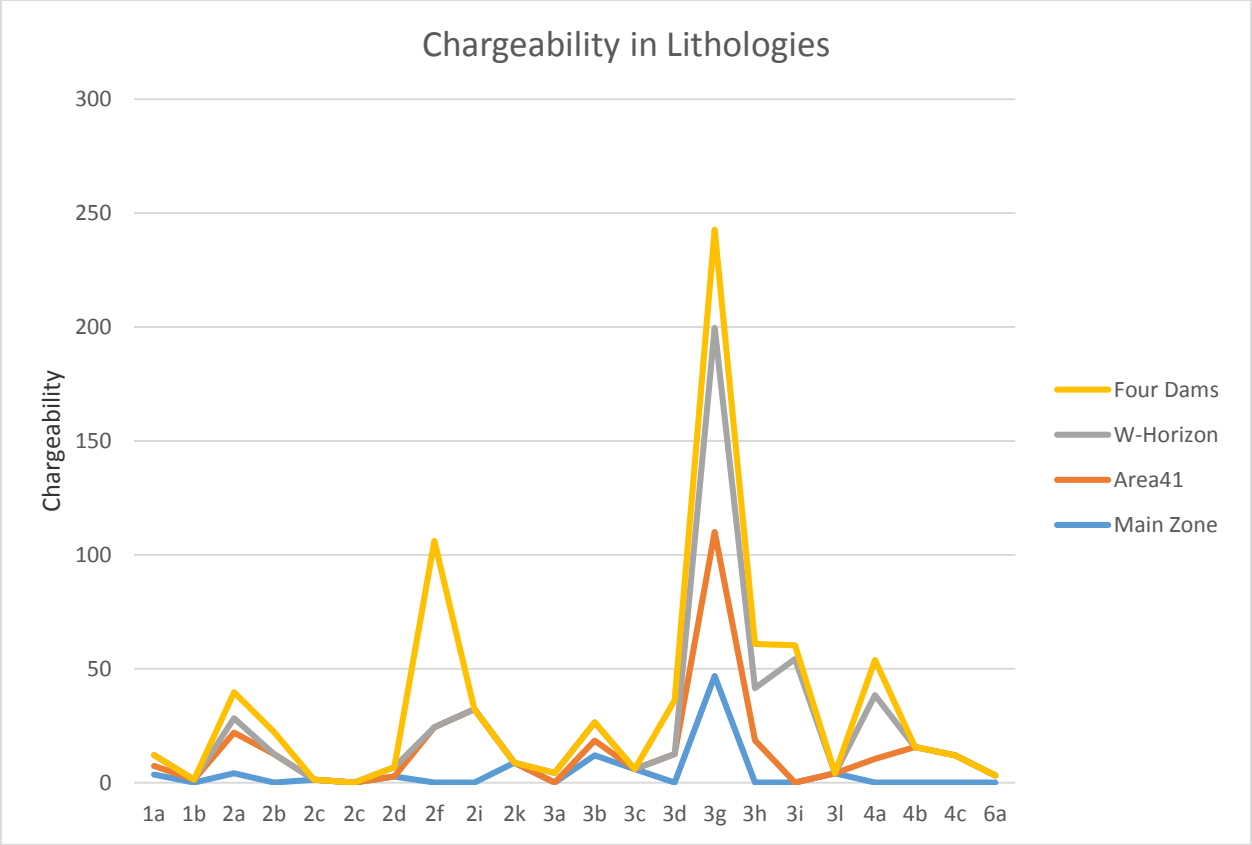

Figure 6.3 - Chargeability mean values displayed as lithological variations. The four mineralization zones are iin relation to the lithologies are indicated by coloured lines as reported in the legend.

6.6 Bulk Densities

Bulk densities of all specimens were calculated with measurements of mass and volume using the Archimedean (specific gravity) method. Large scale differentiations in density values cannot be observed within mineralization zones. Figures 6.4 indicates the different lithological distinctions seen in the marathon deposit and the chargeability values are plotted against the respective density values for each specimen. The variation in density depends on the samples' mineralogy, textures and pore spaces. Since most samples have very similar silicate mineralogy occupying much of the sample volume, large variations in bulk sample densities are unusual. While we observe tight clusters of densities for the individual lithological units, some variations from samples from the layered series unit can be observable.

Silicate minerals such as pyroxene, olivine and plagioclase have mineral densities of 3400, 3300 and 2650 kg/m^3 respectively (Beard et al., 2009), thus accounting for the tendency of bulk density values for the rocks in this study to fall in that range. Where large variations occur, it is most likely due to the enhanced presence of high-density minerals such as magnetite, apatite or sulphides such as chalcopyrite.

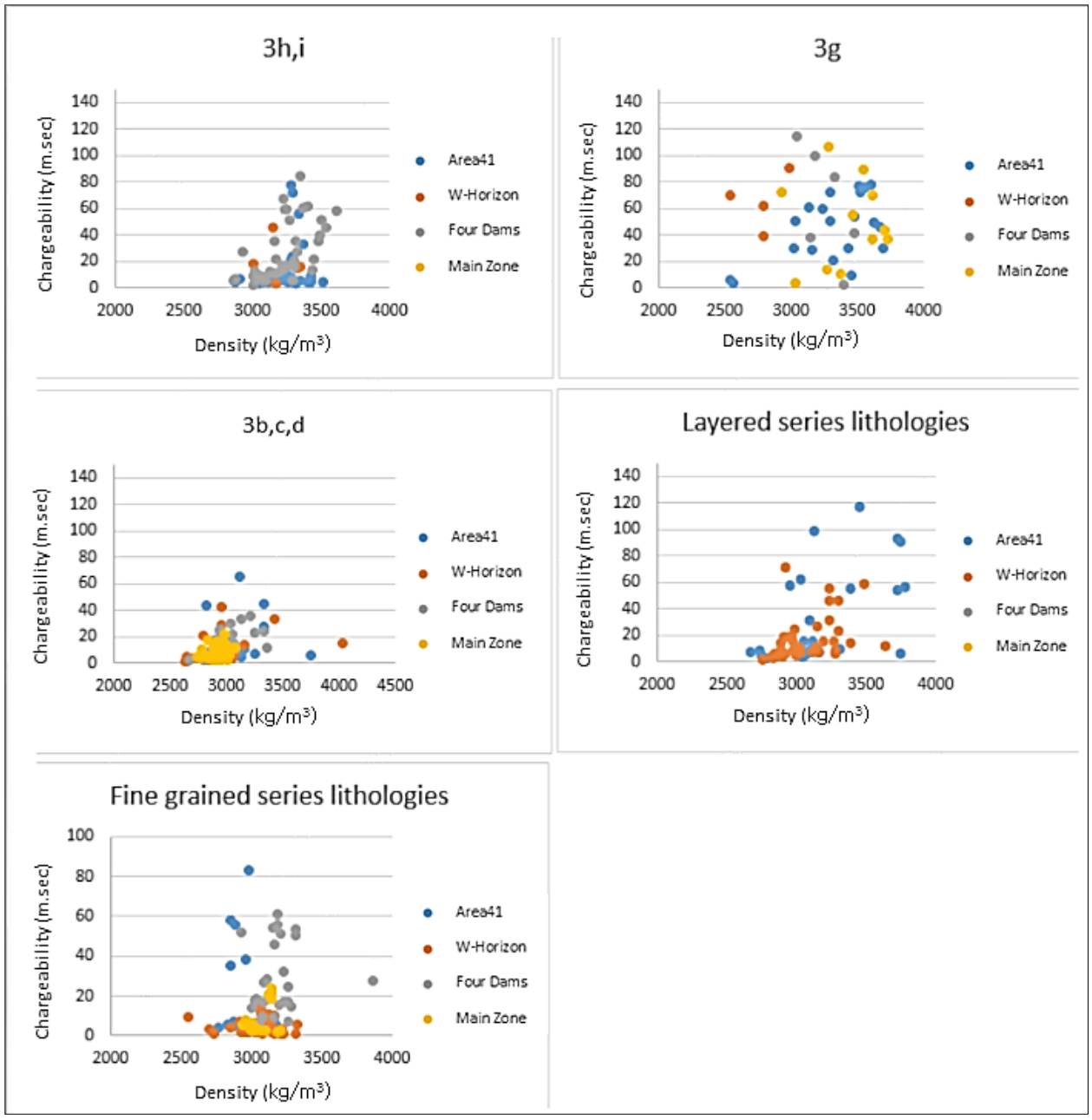

Figure 6.4 - Density and Chargeability of all specimens are divided into their respective lithological units and indicated as cross plots for each lithology

In most Fine grained series lithologies, the densities vary from 2981- 3185 kg/m^3 while the Layered series densities vary from 3056 to 3354 kg/m^3. Marathon series has a slightly higher range of values and samples vary from 2943 to 3481 kg/m^3 whereas the 3g lithologies specifically show a marginally higher density and much tighter spread of densities values 3262-3345 kg/m^3. As a commonly used rule of thumb, lithologies that show high chargeability and low resistivity also show high density values, especially in the Four Dams 2f lithology due to a higher magnetite content (magnetite has bulk density of 5100 kg/m^3 and sulphides with an average density of 5200 kg/m^3). The 3g lithologies also show slightly higher density values due to extreme enrichment of magnetite and W-Horizon 3h and 3i lithologies, possibly due to high amounts of sulphide and enrichment of apatite. The 3g units in W-Horizon and Area41 also show some chloritic alterations (chlorite has a considerably lower density, in the range of 2400 kg/m^3) which might result in a slight decrease in densities to what was expected for mafic rocks. Some specimen from Four Dams and W-Horizon seem to show significantly higher chargeabilities for similar density values as observed in Figure 6.3. The 3g oxide melatroctolite unit shows an erratic range of chargeabilites plotted against the density values, possibly implying a variable magnetite content in parts of the 3g lithology.

6.7 Resistivity and Chargeability Integrated results

Figure 6.5 displayed four graphs of resistivity and chargeability data plotted on a log x versus log y graphs. Each of the six plots show a lithological group within the mineralization zones of the Marathon deposit. The data from each mineralization zone has been fitted into a power regression model and least square best fit lines have been fitted to understand the relationships and trends of the chargeability and resistivity data.

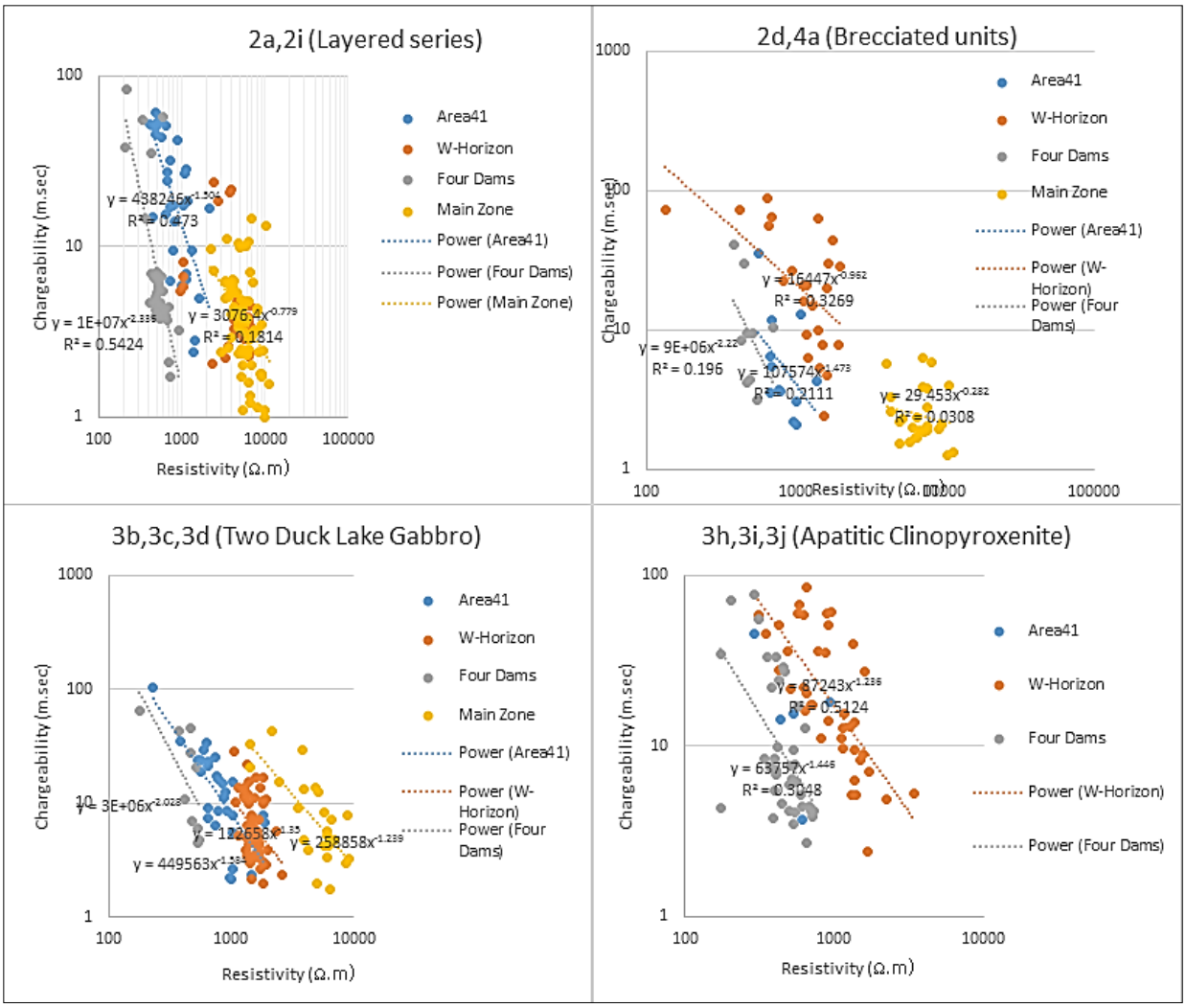

Figure 6.5- Resistivity and Chargeability of all specimens are divided into their respective lithological units and indicated as cross plots for each lithology. Least square best fit lines have been fitted as power curves to each lithological unit represented by the respective specimens.

The equations for the power law fittings of the data indicate the manner in which the decrease in chargeability occurs with increasing resistivity. Main zone samples do tend to have very high resistivities and low chargeabilities. Similarly, Area 41, W-Horizon and Four Dams data points all show the expected negative correlations for resistivity verses chargeability data.

And the slopes of W-Horizon and Area 41 are quite similar in most lithological units indicating that the decreasing rates of resistivity against chargeability are quite similar in both the zones. While both these lithological zones have similar ranges of chargeability values, higher y intercept values for W-Horizon samples indicate a higher resistivity value range while Area 41 values with

a lower y intercept shows a lower resistivity range. This indicates that Area 41 has a higher conductivity, possibly implying larger sulphide grains or the dominance of a different electricity conducting mineral leading to better conductivity while the chargeabilities remain essentially the same in both mineralization zones. Four Dams specimens have the lowest resistivity range observed among all zones but also indicate marginally lower values of chargeability indicating higher electrical conductivity usually observed with larger sulphide grains but displays a drop in chargeability due to the larger grain sizes and low dissemination of sulphide grains.

As mentioned earlier, these variations observed in different zones can be pointed toward the sulphide content as well as the textures and grain sizes. For a small to trace amounts of sulphides, the chargeability variations can be affected by the distribution of grain size of the sulphide minerals. Yet, presence of small amounts of sulphide material in a rock can only have a very minor decrease in the resistivity of the rock. Therefore, IP surveys would be effective for W-Horizon and Area 41 lithologies showing more disseminated textures and this fact is verified in hand samples.

This observation varies quite significantly in different mineralization zones. At Four Dams, most Marathon series lithologies show a large drop in the resistivities with increasing chargeability values. This is a direct contrast to the Main Zone values that show higher resistivity values with considerably smaller drops in chargeability.

In a summarized version of the above results and Figure 6.4, IP and resistivity values and relationships indicate that the Four Dams lithologies seem to generally have a higher electrical conductivity, potentially implying coarser sulphide grain textures while chargeabilities stays essentially the same as W-Horizon or Area41. Main zone with the lowest chargeability and the highest resistivities indicate extremely low electrical conductivity and chargeability due to the presence of low amounts of sulphides (Figure 16.6). Area 41 and W-Horizon zones in general have similar declination slopes with W-Horizon showing higher resistivity values with lower electrical conductivity which indicates the sulphides to represent a more disseminated texture compared to Area 41. An exact comparison of the sulphide content in Area 41 and W-Horizon was not made due to the unavailability of geochemical data for W-Horizon. But similar values of sulphide availability have been reported in drill core description logs.

6.7.1 Sulphides and Chargeability/Resistivity

Sulphide content and the type of sulphides can play a pivotal role in chargeability and resistivity values and their variations. Correlating the chargeability variations with the amount of sulphur present in each of the lithological units can be used as an important comparison. For this study, the Sulphur weight percentages obtained from the geochemical assays of the drill holes is considered to approximately represent the sulphide content of the rock specimens. In the Main zone, a high percentage of sulphur is present in the 3b unit, associated with the Two Duck Lake intrusion. Yet the extremely high values in chargeability seen in the 3g unit is not associated with an extreme enrichment of sulphur as observed in Figure 6.6.

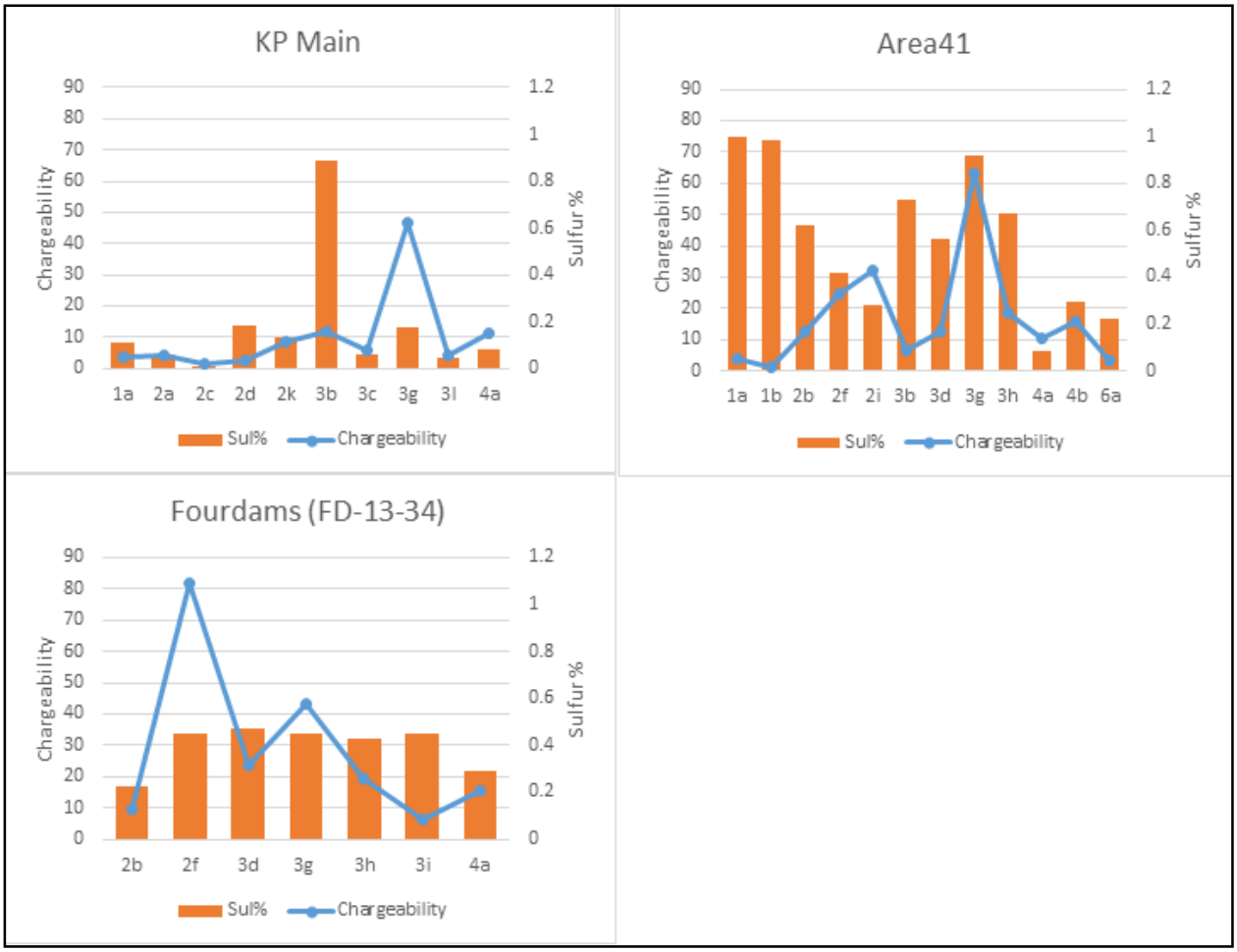

Figure 6.6- Chargeability averages for lithologies and corresponding mean sulphur % assay results have been plotted as bar charts. Corresponding chargeability variations are indicated as line graphs. KP Main represents the drill cores samples obtained for the Main zone. W-Horizon sulpher % are missing from the geochemistry assays. Only one drill hole has been reported from Four Dams (FD-13-34 drill core).

A general trend is observed in Area 41 as well as Four Dams, Main zone and W-Horizon where a higher sulphur percentage will result in a marginal increase in chargeability which is to be expected. But this observation doesn't stand correct for the 3g units in any of the mineralization zones. Also in Area 41, Footwall zones show extreme enrichment of sulphur with very low chargeability values which could be due to the presence of a different species of sulphur that does not participate in conducting electricity. A high chargeability increase in the 3g unit is also observed for surprisingly low amounts of sulphur, especially in the Main Zone and Four Dams units. Again, for Area 41, the sulphide percentage does not correlate with the fluctuation in chargeabilities for some of the lithological units such as 2i or 2b. In Four Dams FD-13-34 drill hole, again a large increase in chargeability can be seen in 2f unit compared to the other lithologies. All lithological units in Four Dams seem to have similar values of sulphur percentages in the rock masses but the extreme increase in chargeability is only visible in the 2f unit and to a lesser extent in the 3g unit.

Different types of sulphide minerals respond differently to electrical measurements. For instance, chargeability of pyrrhotite is 10.1 msec and chalcopyrite, 9.4 msec at 1% concentration in samples (King.et al., 2007; Pearce et al., 2006) for measurement conditions similar to those used in this study. Although the chargeability differences between these two minerals are not high, it would be important to note the proportions of different sulphides represented in the lithologies and the corresponding chargeability variations. To assess the relative contributions of types of sulphides existing in these rock units, weight values were calculated for chalcopyrite and phyrrotite. This was done by consulting the assay reports of copper ppm values of the respective drill holes which were expected to represent the chalcopyrite content. Once the required amount of sulphur was allocated for the copper to form chalcopyrite, the remaining sulphur was presumed to represent the pyrrhotite content. These two types of sulphides are the most dominant in the four mineralization zones (Good et al., 2015; Good et al., 2017; Ames et al., 2017) and therefore we will consider that the sulphides presented in the deposit to consist of only these two types of sulphides.

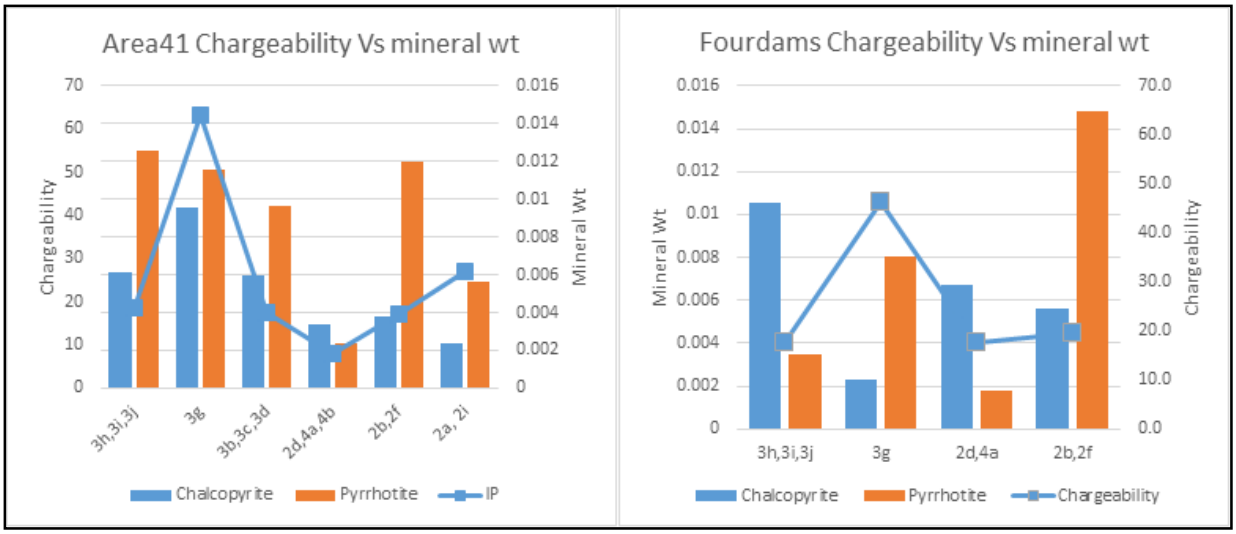

Figure 6.7- Chargeability and mineral weights have been calculated and plotted against the variations for chalcopyrite and pyrrhotite, reported by the drill core assays. For proprietary reasons, no copper% were reported in the assays for Main Zone or W-Horizon drill cores.

No specific correlations of chargeability can be found for different sulphide species types and chalcopyrite and pyrrhotite content plays close to equal roles (Figure 6.7). For instance, in Area 41, the combined Two Duck Lake unit represented by 3b, 3c, 3d lithologies show almost similar chargeability responses to the combined 2b, 2f unit although the pyrrhotite content is much higher in the 2b,2f unit. The same comparison can be made for the apatitic clinopyroxenite units represented by 3h,3i,3j which contains similar amounts of chalcopyrite to the Two Duck Lake unit but higher amounts of pyrrhotite, but show similar chargeabilities. But, an over simplification occurs when considering mean values of sulphide percentages that only represents smaller, distinct parts of a lithological unit and not the whole. This can obscure small scale variations within the lithological unit and highly sulphide rich areas.

The low chargeabilities observed for Area 41 footwall lithologies (1a, 1b) do have extreme values of pyrrhotite compared to chalcopyrite which might indicate a higher influence for chargeabilities. The unit is highly felsic and is also cross cut by syenitic dykelets and the high sulphide values are point values that do not represent the whole unit of the footwall. The drill core logs describe the units to have trace to 1% sulphides and therefore the geochemical estimates don't seem to add up to the low chargeabilities observed. 3g unit shows characteristic jumps in the values which cannot be correlated to an increase in any particular sulphide type. In Figure 6.6, low sulphide percentages

still correspond with a higher resistivity value range but a drastic drop in resistivities cannot be observed for the 3g unit as was observed in chargeability values.

6.8 Discussion and conclusions for electrical properties

Distinct relationships in chargeability and resistivity were observed for different lithologies in mineralized units. Main Zone lithology samples have the lowest chargeability range corresponding with the highest resistivity range. This can be correlated with the amount of sulphides present in the mineralization zone which ranges in the lower end of the sulphide percentage spectrum for the Marathon deposit (Figure 6.4) (Good et al., 2015).

W-Horizon lithologies tend to favor the second highest range of resistivities for a similar range of chargeabilities as Four Dams or Area41. Area 41 shows the third highest resistivity ranges for the respective conductivities, slightly higher than W-Horizon or Four Dams. Four Dams chargeabilities have a similar range to W-Horizon but has the lowest values in resistivities. The continued decrease in resistivity values as the chargeability values remain essentially in the same range of values indicate that the sulphides might be less disseminated and has better electrical attachment in increasing order from Main zone to W-Horizon, Area 41 to Four Dams.

Four Dams sulphide grains are possibly a lot coarser and larger compared to other units, providing better electrical contact among the grains hence lower resistivities. In descending order, Four Dams, Area 41, W-Horizon and Main Zone have electrical contact between the sulphide grains that enables electrical conductivity.

From hand sample examinations, Four Dams mineralization seems to indicate massive, less disseminated sulphide grains compared to the other mineralization zones. W-Horizon shows the most disseminated fine grained sulphide textures compared with Area 41 or Four Dams zones which seems to agree with our results in IP and resistivity response relationships indicated in Figure 6.6. Further petrological work and thin section examinations need to be conducted to understand the grain size variations of the sulphides and to assess if the petrophysical variations correspond with the petrological details.

Influences of different sulphide varieties that enable induced polarization characteristics and resistivities were difficult to determine from the available geochemical reports. In Area 41, we

observe footwall lithologies (1a, 1b) with extremely low chargeabilities but high enrichment of sulphur. The sulphur amount is considered to represent sulphides but there is a possibility that non-sulphide sources such as sulphates or native sulphur are represented in the assay reports.

Petrographic and geochemical analysis by Shaw (1997) indicate at least three separate intrusions of magma were injected into the layered gabbroic unit in the Eastern Gabbroic suite. When considering inter deposit metallogeny, there is a distinct lack of correlation for PGM mineral assemblages in Main Zone, W-Horizon and Area 41 as observed by Good et al., 2017 and considering the geochemical implications, the authors suggest that the mineralization processes in each of these deposits have undergone different and dynamic intrusive histories with multiple injections of magma that had slightly different compositions in each of these deposits. Therefore, the different trends of chargeabilities and resistivities observed for different deposits can be correlated to slight differences in composition and texture of suphides stemmed from the different petrogenetic histories of the four mineralization zones.

The consistent high chargeabilities observed in 3g unit can be correlated with the extreme enrichment of magnetite with the mineralization exceeding almost 35% of the rock mass. The 3g unit is described to contain extremely high cumulate magnetite content (Ruthart 2012; Good et al., 2015). Work by Vella and Emerson (2012) demonstrated that the magnetite rich rocks can be moderate to good conductors and show extremely high IP responses in barren rock types which in turn might indicate false positive anomalies in resistivity and IP surveys. Sagnotti (2004) and Johnson and Anderson (1981) have also reported anomalous IP responses with regards to enrichment of magnetite. Therefore, care should be taken when interpreting future electrical surveys of the Marathon deposit since low sulphide, high magnetite containing 3g oxide melatroctolite units seem to show falsely anomalous electrical responses. A similar response can be observed in 2f unit (medium to coarse grained oxide melatroctolite of the Layered series) at the Four Dams mineralization zone and drill core descriptions indicate that the unit contains almost 15-25% interstitial magnetite. Coupled with the high sulphide content of the unit, the chargeability response in this specific lithological unit is observed to be extremely high.

6.9 Magnetic Properties

Lack of knowledge of the geological factors and the mineralogical properties that cause magnetization becomes a hindrance in the interpretation of magnetic surveys. Rock magnetic properties can be used to improve the geological information that can be obtained from the magnetic anomaly patters in a conventional magnetic survey. Results obtained from a magnetic survey are correlated to an inversion process to investigate the source from which the magnetic anomaly was produced. Yet, the ambiguity and the non-uniqueness of these interpretations and mathematical models introduce problems when associating the results with a geological source or a structure in the subsurface. While geological constraints and integration of other geophysical methods can be used to narrow down the interpretations obtained from mathematical models, magnetic property measurements can be highly effective in interpreting an inversion from a magnetic survey. Therefore, a better understanding of the magnetic properties of rocks and the associated mineralogy is required.

Magnetic properties of rocks are broadly influenced by lithology, depositional environment, tectonic setting, geochemical affinities, hydrothermal alterations, metamorphic grade and rock age. The presence of magnetically susceptible minerals creates a measureable disturbance in the local magnetic field with just 0.1 percent of ferromagnetic minerals being enough to dominate the magnetic properties of a rock. Most rock types are associated with a broad range of magnetic susceptibilities mostly showing a strong bimodal distribution of values reflecting the paramagnetic and ferromagnetic minerals. Magnetic properties are usually dominated by ferromagnetic minerals, mainly magnetite. Most igneous rocks contain magnetite so that magmatic intrusions are shown clearly in a magnetic survey. Many metalliferous minerals and sulphides are often associated with magnetizable minerals and therefore the magnetic method is widely used in the mineral exploration to directly or indirectly detect mineralization or to help define subsurface structures.

There are two types of magnetizations found in a rock. These are induced magnetization (a detectable response to a magnetic field, such as the Earth’s field) and remanent magnetization

(magnetic memory acquired during previous exposure to a magnetic field) as discussed in Chapters 3 and 4. Magnetic susceptibility defines the ability of a rock to be magnetizable which is mostly unique for the given material or rock type. Knowing the exact nature of the magnetization of subsurface rocks, how the magnetization arises and is responding to the present day earth's field and past paleomagnetic fields is important in prospecting for mineral deposits.

6.9.1 Magnetism

Magnetic fields can be naturally occurring such as the earth's magnetic field but can also be created with electrical currents. The magnetic fields are examples of magnetic dipoles where magnetic field lines emerge from the north end and converge from the south end of the magnetic object. This is due to the combined dipolar fields arising from individual atoms and molecules. There are several types of magnetism that can happen as a response to an external magnetic field, with the responses governed by the differing material properties.

Diamagnetism arises when the net dipole moment is zero in minerals such as gypsum, salt quartz and graphite with low to no magnetic properties due to the elements having minimum dipole moment. Paramagnetism is caused by the presence of unpaired electrons in the electron shells which creates a net dipole effect and in the presence of an external applied magnetic field, the dipoles are aligned, resulting in a weak magnetic susceptibility. For both diamagnetism and paramagnetism, the magnetic response of the material disappears when the external magnetic field is removed.

In ferromagnetic minerals, the effect is caused by unpaired electrons. The adjacent atomic dipoles interact strongly, leading to a much stronger and non-linear response to an external field, producing magnetic memory. The dipole moment of the unpaired electrons is coupled by an external field to create domains where the dipole moment can be aligned to be parallel to the field. In such an instance, it creates a large positive susceptibility such as in iron, nickel or cobalt.

In naturally occurring rocks, ferrimagnetism is the most prominent. In such rocks, the magnetic domains that are created in individual mineral grains are anti parallel to the external field but the number of antiparallel domains are unequal, such as in magnetite or titonomagnetitie.

Two types of magnetizations contribute to the overall magnetization observed at a magnetic property investigation. When the two magnetizations are added as vectors, the resultant magnetization that is observed is M

$$M = M_i + M_r \qquad (6)$$

where M_i stand for the induced magnetization vector and M_r stands for the remanent magnetization vector, discussed in chapters 4 and 5 and in Equation 6.

Induced magnetization component is assumed to satisfy

$$M_i = kH \qquad (7)$$

And the H is the external ambient field intensity and k is the magnetic susceptibility (Equation 7). It has been established that the induced magnetization is usually parallel to the external field and the magnetization is proportional to the external field.

6.9.2 Magnetic Susceptibility measurements

All magnetic susceptibility measurements were made in a Sapphire Instruments SI-2B susceptibility bridge. The instrument assumes a specimen volume of 10 cm^{-3}, but this volume was adjusted during the use of different sample sizes as was discussed in Chapter 3. Susceptibility values are corrected for instrument drift and differences in specimen volume. The induced magnetization was measured for each specimen between two measurements made with applied magnetic field but with no sample present, to correct for the typically minor instrument drift in the ambient Earth's field between measurements. Typically, two measurement cycles were done to test for repeatability of the measurement. The induced magnetization of the sample was then used to obtain the magnetic susceptibility of the specimen. Common magnetic susceptibility measurements assume a uniform directional distribution of susceptibility, and this assumption was used here.

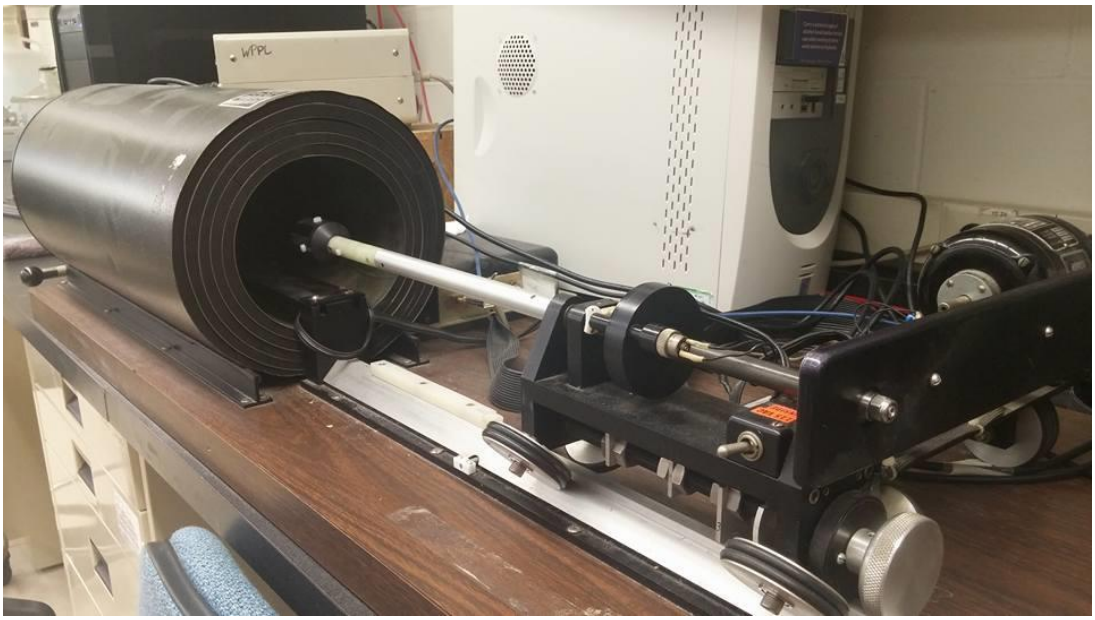

Figure 6.8 - Schonstedt SSM-2 spinner magnetometer at the Western Paleomagnetic and Petrophysical laboratory

6.9.3 Natural Remanent Magnetization (NRM)

Natural Remanent Magnetization (NRM) measurements were made on a Schonstedt SSM-2 spinner magnetometer using a six-spin configuration (Figure 6.8). The calculated intensity of the remanence vector in $1x10^{-6}$ emu was corrected for the volume of the sample to yield 10^{-6} emu/cm^3. These volumes were calculated using the measurements of the length and diameter of the cylindrical specimen. The remanence directions are calculated relative to the axis of the specimen. The up direction recorded during the logging of the drill core was used to establish positive or negative polarity for the remanence direction.

6.10 Magnetic properties of the Marathon deposit

Magnetic surveys have become an important tool in exploring for mineral resources, especially in large igneous intrusions. Geophysical inversion of the magnetic anomalies is dependent on correct and accurate information of the different lithological units. Reliability of interpretations therefore increase greatly by the knowledge of magnetic properties of the rock types in the region. The inherent non-uniqueness of predicted geophysical models can be resolved with the prior

information of the petrophysical characteristics of the geological units and different mineralization areas.

6.10.1 Magnetic Susceptibility

Magnetic susceptibility and NRM values are important in deciphering and analyzing magnetic surveys. The aim of this study is to understand the broader magnetic property distributions at the Marathon deposit which will assist in interpreting magnetic surveys and draw out interesting characteristics and relationships seen at the deposit. The attempt of this section is to assess the variations in magnetic properties existing within lithological units of different mineralization zones of the Marathon deposit. There is a large variation in magnetic susceptibility values, ranging from 10^2-$14x10^4$ (cgs units) and magnetite and pyrrhotite are the two magnetic minerals diagnosed in the Marathon deposit.

As observed from Table 2, data in the mineralization zones indicate that the highest magnetic susceptibility values are observed in 3g lithological unit which is unanimously high in

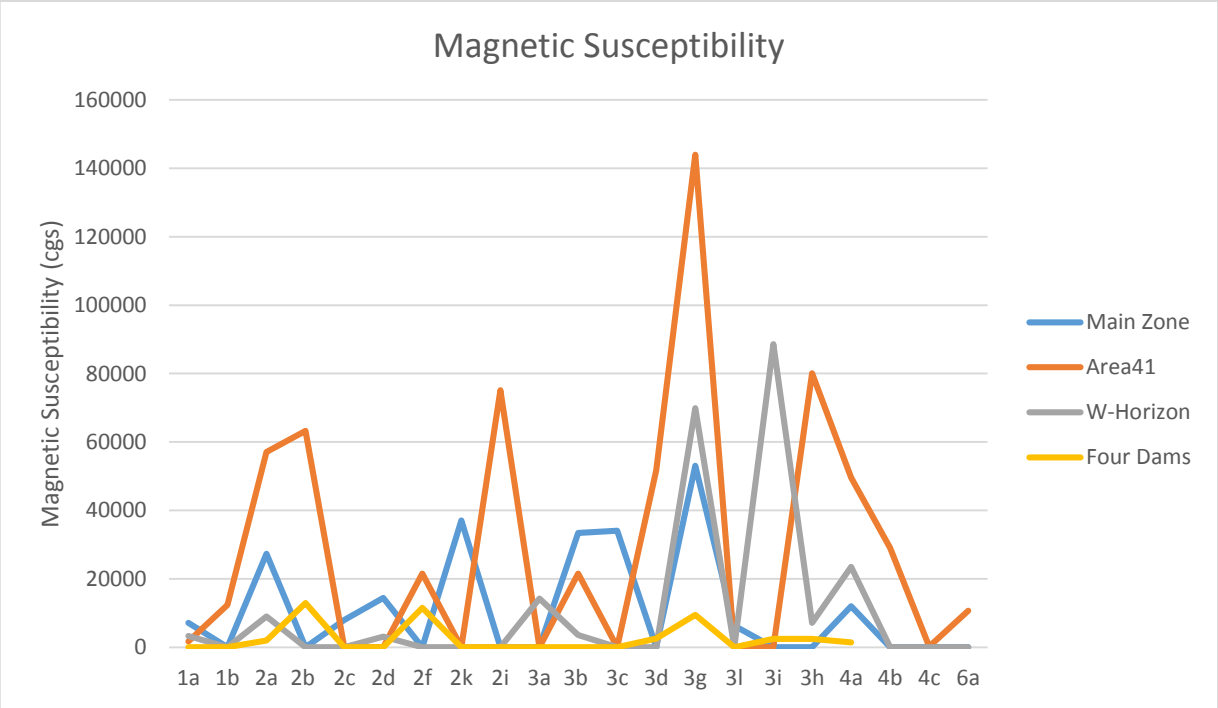

Figure 6.9- Magnetic Susceptibility values which have been averaged out for each lithological unit has been plotted as a variable diagram , indicated by the legend

ferromagnetic minerals and this characteristic is observed in all mineralization zones (Figure 6.9). Other Marathon series lithological units such 3b,3c, 3i, 3h also show high ferromagnetic susceptibilities in the range of $4x10^{4}$-$8x10^{4}$ (cgs). These high values are in direct correlation to the magnetic minerals associated with the deposit. Lithological units in Area41 mineralization zone in general seems to indicate extremely high magnetic susceptibilities compared to other mineralization zones which is shown in Figure 6.11. We observe Main Zone and W-Horizon to

indicate somewhat similar magnetic susceptibilities, specifically in the Marathon Series lithologies. Magnetic Susceptibilities in both Main Zone and W-Horizon are comparatively lower than Area41 magnetic susceptibilities. The lowest magnetic susceptibilities are observed in the Four Dams lithology which indicates values below $2x10^{-4}$ cgs giving comparatively moderate ferromagnetic signatures throughout all the lithologies.

Table 6.2 - Mean Magnetic Susceptibilities and NRM of lithological units and mineralization zones

Main Zone				Area41				W-Horizon				Four Dams			
Lithology	NRM (cgs)	MagSusc (cgs)	Q-Value	Lithology	NRM (cgs)	MagSusc (cgs)	Q-Value	Lithology	NRM (cgs)	MagSusc (cgs)	Q-Value	Lithology	NRM (cgs)	MagSusc (cgs)	Q-Value
1a	1.17E-04	7.08E-03	0.09	1a	4.25E-03	1.65E-03	2.43	1a	2.20E-04	3.31E-03	0.12	2a	3.05E-02	1.95E-03	2.56
2a	3.14E-03	2.73E-02	0.35	1b	3.58E-03	1.23E-02	1.95	2a	4.81E-03	8.96E-03	2.92	2b	2.61E-02	1.29E-02	2.31
2c	2.59E-03	7.95E-03	0.39	2a	5.01E-03	2.57E-01	0.03	2d	1.25E-02	3.07E-03	1.18	2f	8.67E-02	1.15E-02	1.75
2d	6.60E-03	1.44E-02	0.60	2b	6.77E-03	1.63E-01	0.23	3a	8.46E-04	1.42E-02	0.00	3d	5.87E-02	2.54E-03	2.34
2k	5.63E-03	3.70E-02	0.38	2f	3.35E-03	2.15E-02	0.56	3b	3.61E-02	3.57E-03	5.07	3g	1.73E-01	9.43E-03	3.39
3b	6.79E-03	3.34E-02	0.58	2i	8.97E-03	7.51E-02	0.32	3g	9.69E-02	6.99E-02	1.42	3h	5.76E-02	2.41E-03	4.65
3c	2.18E-03	3.40E-02	0.31	3b	1.26E-02	2.15E-02	2.55	3h	6.94E-02	7.10E-03	2.18	3i	5.72E-02	2.39E-03	4.26
3g	8.84E-03	5.31E-02	0.42	3d	1.91E-02	5.18E-02	0.82	3i	7.00E-02	8.86E-02	0.58	4a	2.44E-02	1.40E-03	2.82
3l	2.55E-03	6.28E-03	0.75	3g	2.61E-02	1.44E-01	0.37	4a	5.95E-02	2.35E-02	1.75				
4a	7.58E-03	1.19E-02	1.12	3h	1.56E-02	8.01E-02	0.45					Fine Grained	3.05E-02	1.95E-03	2.56
				4a	1.36E-02	4.96E-02	0.45	Fine Grained	7.26E-03	6.41E-03	2.05	Layered	5.64E-02	1.22E-02	2.03
Fine Grained	2.18E-03	2.17E-02	0.43	4b	3.50E-02	2.90E-02	2.90	Marathon	2.37E-02	3.12E-02	1.85	Marathon	4.52E-02	1.34E-03	3.66
Marathon	5.59E-03	3.04E-02	0.41	4c	3.16E-05	2.33E-04	0.31								
				6a	1.76E-04	1.06E-02	0.65								
				Fine Grained	6.99E-03	3.55E-02	0.18								
				Layered	5.06E-03	4.23E-03	0.12								
				Marathon	2.34E-02	1.42E-01	1.04								

6.10.2 Natural Remanent Magnetization

NRM is the remanent magnetization in a rock before it is subjected to any demagnetization treatment in the laboratory. It is usually a composite vector sum of ancient and modern remanent magnetizations, each of which were acquired parallel to the earth's ambient magnetic field at the time of the rock's formation but also represents portions of the ambient field as a component of the Viscous Remanent Magnetization (VRM). This is a component of magnetization which is based usually on the magnetic domains that are the most easily changed. As observed in Figure 6.12, NRM is particularly high in 3g, specifically in Four Dams unit with an average of 5.15 $x10^{-3}$ cgs which is not surprising considering the unit consists of more than 35% cumulate magnetite. This applies to magnetic susceptibility value as well since the magnetite content is usually proportional to the induced magnetization of the rock as well as the remanent magnetization portion. Other Marathon series lithologies such as 3b,3c,3d show considerably high NRMs and the Apetitic clinopyroxenite (3h) units indicate high NRM values. This observation is seen throughout all zones of the deposit in varying NRM values. 2f unit is also comparatively high in NRM values, specifically in the Four Dams zone which is observed to influence the electrical properties as well due to the high magnetite content (close to 20% magnetite). Second highest NRM values are observed in the W-Horizon with high NRMs observed in the apetitic clinopyroxinite (3h) units. Lowest NRM ranges are observed in the Main Zone and Area 41 which indicates a range from a low of $3.16x10^{-5}$ to a high of 3.50 10^{-2} (cgs) which are low in comparison to the other two mineralization units. The high remanent magnetization observed in some lithological units can be related to the domain states of the magnetization holding minerals or the presence of minerals such as pyrrhotite. The small domain walls indicating single domain behavior with higher magnetic coercivity and the presence of higher remanent magnetization.

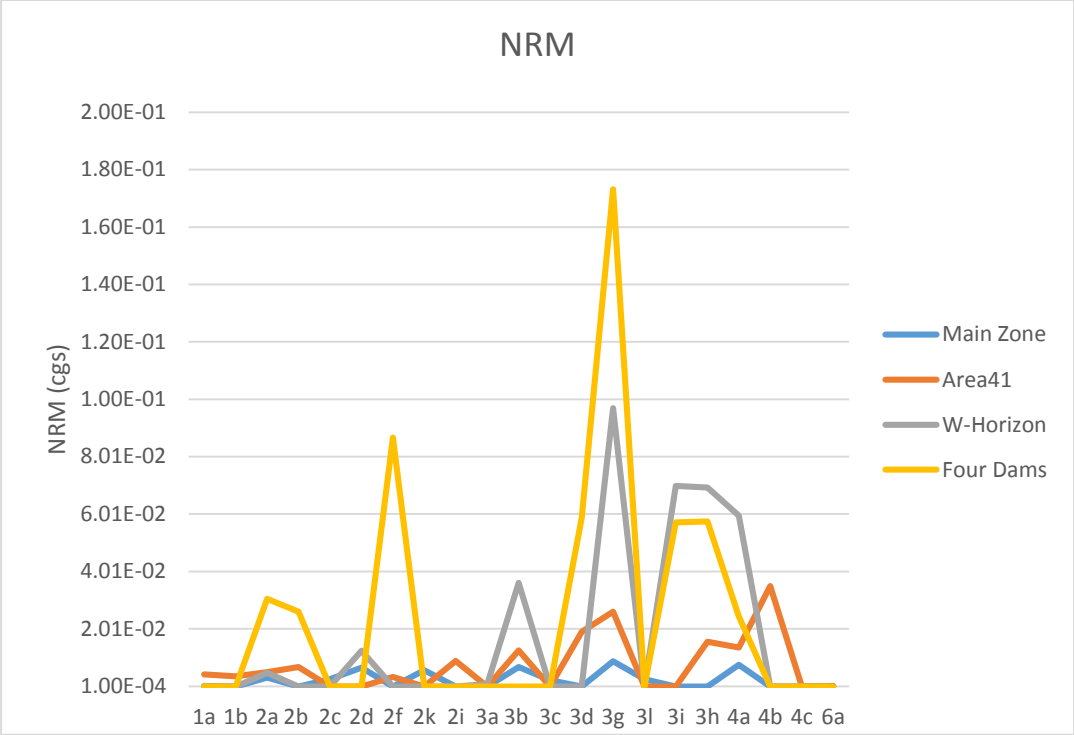

Figure 6.10- NRM values which have been averaged out for each lithological unit has been plotted as a variable diagram , indicated by the legend

NRM values depend not only on the minerals and grain sizes but also on the mode of remanent magnetization acquisition. Four Dams NRMs are observed to be higher compared to the other mineralization zone samples (Figure 6.10). An important point to be noted is to configure the viscous remanent magnetization (VRM) component in high NRM signatures. While magnetic surveys need to take into account the ancient remanent magnetization indicated by the NRMs that might potentially hinder the induced magnetization portion from being observed in a magnetic survey, an important sub component of the remanence is the VRM. This secondary remanent magnetization plays an important role in NRM signatures and is the only component of the remanence that gives an indication of how stable the remanent magnetization is with time. A significant portion of VRM can be expected in many of these coarse grained gabbroic samples due to the large domain sizes of the magnetite grains and VRM has the ability to obscure the faithful record of the ancient geomagnetic field represented by NRM. Since the highly viscose magnetization is acquired by multi domain magnetite, it also indicates that the VRM direction are easily influenced by the ambient field and mostly represents the present say geo magnetic field. This would be important when using NRM values to interpret geophysical anomalies and to configure if an ancient remanent magnetization is taking precedence over the induced

magnetization. The VRM component, if high, has the possibility to dominate the natural remanence and still provide a large enough magnetization with similar directions to the present day induced magnetic field. A possible way to assess the VRM component of the samples is to step wise demagnetize the samples containing high NRMs and observe the directional information of the ChRM. If the demagnetization curve indicates dominance in the direction of the present day geomagnetic field, it can be stated with some certainty that a large component of the NRM is dominated by VRM. Since most samples from the Marathon deposit was affected by the drilling induced magnetization, we were unable to assess the VRM dominance in samples.

6.10.3 Koenigsberger ratio (Q-values)

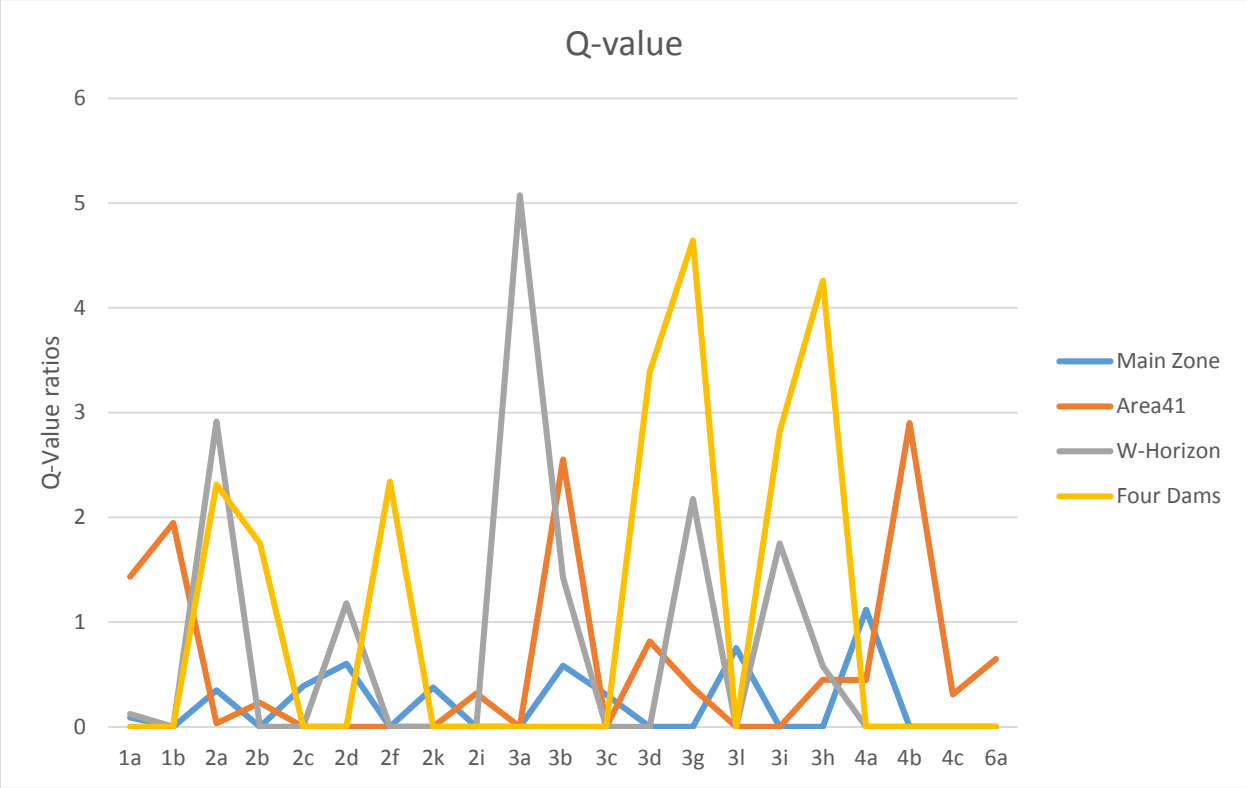

Figure 6.11 - Q values which have been averaged out for each lithological unit has been plotted as a variable diagram for the four different mineralization units, indicated by the legend.

Induced Magnetization is mostly proportional to the applied magnetic field and the constant of proportionality; magnetic susceptibility *k*. For most rocks, this induced magnetization is acquired parallel to the applied field. But in the case of a high remanent magnetization with direction

different to the induced magnetization, Koenigsberger ratio can be calculated to determine the relative induced and remanent magnetization proportions within a rock.

Koenigsberger ratio is usually calculated to examine the parameters that produce the most dominant signature out of the two components; induced (Mi) or remanent magnetization (Mr). Koenigsberger ratio is calculated by dividing the NRM by the induced magnetization (magnetic susceptibility x ambient geomagnetic field) (Equation 8).

$$\text{Q value} = \frac{Mr}{Mi} \qquad (8)$$

For the local geomagnetic field, 57000 nT was used as the inducing field in the calculations as that is an appropriate value for the Marathon location. When Q-values are less than 1, the magnetic response arises mainly from the induced magnetization of the rocks. When the Q values are higher than 1, the remanent magnetization is the dominant contributor to the anomaly or the magnetic response. Q-values are quite uniform and mostly less than 1 in Main Zone while high Q values are distinguished in some lithologies of Area41, W-Horizon and Four Dams samples, most notably Marathon series lithologies (3a, 3b, 3g, 3h) and Layered tractolite unit (2f) (Figure 6.11). Mineralization zones with high NRM values correspond with higher Q-values due to the remanent magnetization component being higher than the induced magnetization. In Four Dams and W-Horizon, the Marathon series lithologies in general seem to indicate high Q values. These samples likely contribute to a large and stable reversed NRM component in the magnetic anomalies seen in the area (e.g., Kulakov et al., 2015). Q-values in Area41 seem to show comparatively lower values but considerably higher than Main Zone Q-values. The Marathon series lithologies in general seem to indicate a higher Q-value in the range of 4-5.

6.10.4 Magnetic Susceptibility and NRM

The Magnetic susceptibility and NRM values seem to vary significantly and showed quite a wide range for different zones and lithological units. When NRMs and Magnetic Susceptibilities are plotted as depicted in Figure 6.12, a segregation of mineralization units within the data cluster can be observed. Figure 6.14 indicates lithologies represented in all four mineralization zones. Yet their magnetic characteristics seem distinctly different within these zonal distributions. The most interesting attribute is observed in the distinct clustering of different mineralogical zones which

are displayed in the data. In Figure 6.12 five different plots have been shown to indicate lithological varieties and how the magnetic susceptibility and NRM values vary within these lithologies and mineralization zones. As observed, we see a positive correlation between magnetic susceptibility and NRM. Increase of ferromagnetic minerals that influence the magnetization of a rock will induce magnetization as well as retain more remanent magnetization.

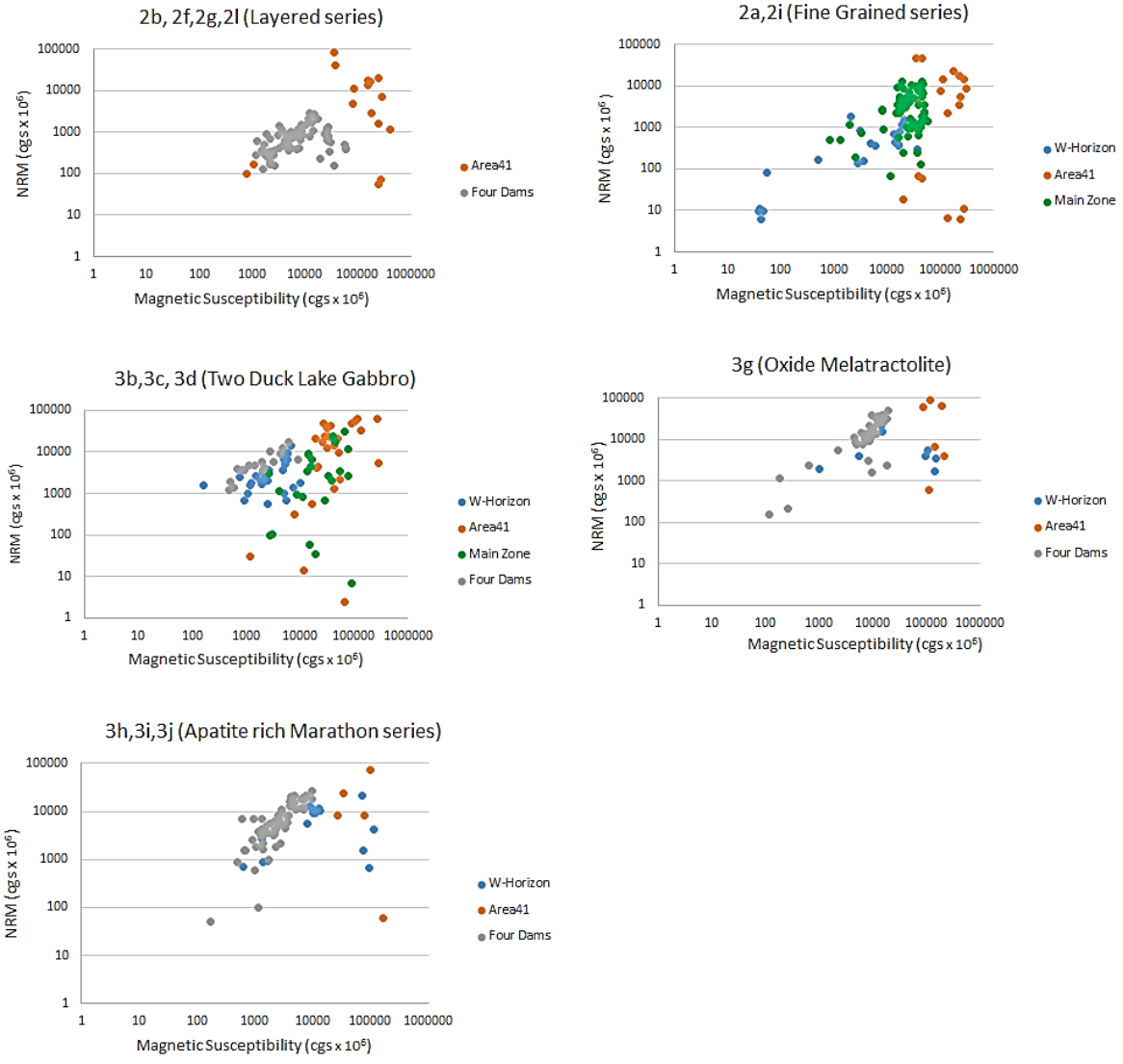

Figure 6.12- Magnetic Susceptibility and NRM values of specimen are grouped into their respective lithological units. Samples are also distinguished by their representative mineralization zones.

In most lithological units, two segments or clusters can be observed when mineralization zones were plotted with NRMs and the corresponding Magnetic susceptibilities. For example, in the Fine Grained lithologies, we observe that Area 41 data specimens distribute at a higher magnetic susceptibility values range, with considerably high NRM values compared to Four Dams data which show somewhat a lower magnetic susceptibility range corresponding with lower NRM values. These clustering effects are possibly due to the presence of different mineralogical elements and the internal petrological differences in the magnetization carrying grains.

6.11 Ferromagnetic Carriers

Brzozowski et al. (2017) studied magnetite species and textures of the Marathon deposit, noting that there are important and distinguishable textural differences in the magnetite grains found in different mineralization zones. The observed magnetite species and the distribution of different magnetite textures in the Marathon deposit can be correlated to the clustering effects seen in the NRM and magnetic susceptibilities data.

According to this study, Marathon deposit consists of two main types of magnetite varieties; primary (magmatic) magnetite and secondary magnetite which have different petrogenesis histories as was explained by Brzozowski et al. (2017). The magmatic magnetite has also been subdivided texturally into two end-member types; cloth-textured magnetite and trellis-textured magnetite, with a continuous solid solution between these two types (intermediate-textured magnetite). Cloth-textured magnetite contains fine lamellae of ulvospinel (Fe_2TiO_4), and can also contain coarse lamellae of ilmenite while the Trellis-textured magnetite contains fine and coarse lamellae of ilmenite ($FeTiO^3$).

Secondary magnetite usually occurs as a replacement of sulphide, is titanium deficient and does not contain any lamellae of ulvospinel or ilmenite. These secondary magnetites are significantly less abundant compared to primary magnetite and are presumed to not affect the magnetization as much as the primary magnetite textures.

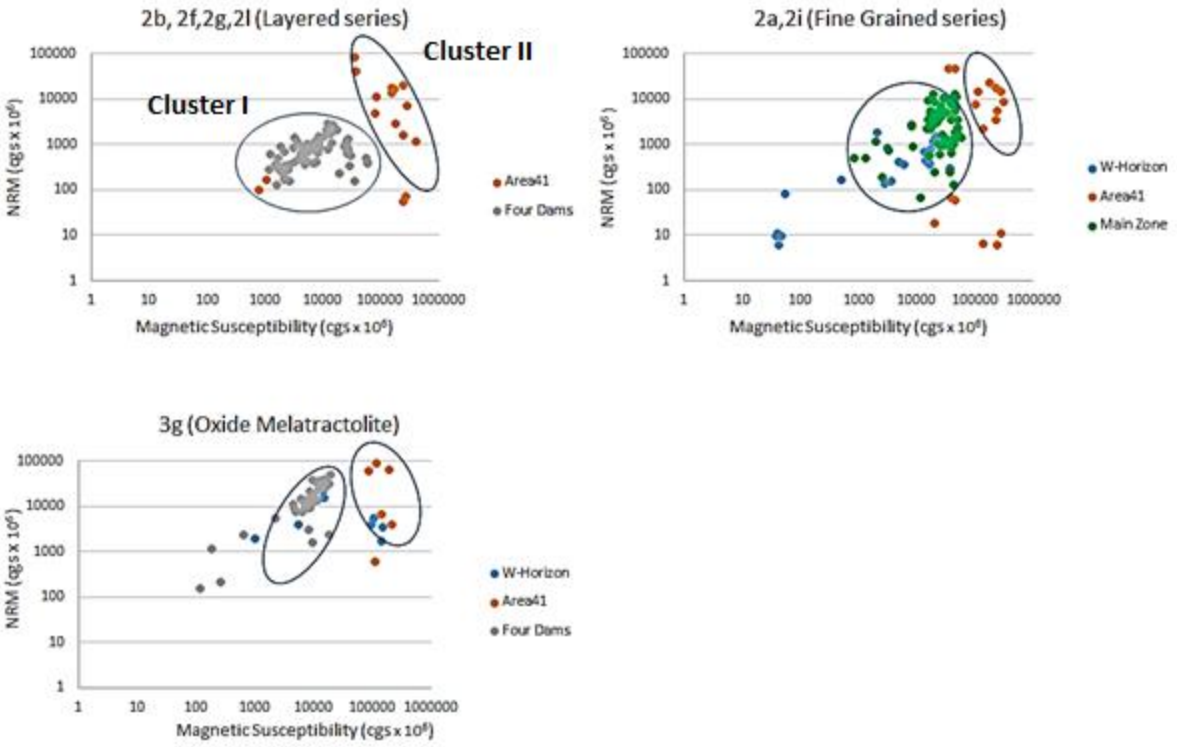

Figure 6.13 – Selected lithological units from figure 6.13 has been illustrated with circles to indicate the clustering effect as discussed in the text. Cluster I and cluster II has been labeled and demonstrates the two clusters observed in the magnetic susceptibility and NRM data

As discussed in the results and Figure 6.14, Magnetic Susceptibility and NRM form two cluster types, with some mineralization zones noticeably grouped into one cluster or another. Cluster I is distinguished by the Low NRM, Low magnetic susceptibility cluster and the Cluster II is the High magnetic susceptibility High NRM cluster (Figure 6.13) (Table 6.3).

Four Dams lithologies rests mostly in Cluster I and according to Brzozowski et al. (2017), consists of almost 85% cloth textured magnetite. W-Horizon falls in both cluster I and cluster II and has been reported to contain 65% trellis and 15% cloth textured magnetite. Area 41 specimens consists 70% trellis textured magnetite 10% cloth textured and 5% intermediate textured magnetite with most samples included in cluster II with a few scattered samples in the cluster I. Main Zone is dominated by trellis magnetite with 85-90% and also incidentally falls in cluster II (Figure 6.12, 6.13) and these results are summarized in (Table 6.3).

Zone	Magnetite (mt) Textures	MagSusc cluster	Properties
Four Dams	Cloth mt	Cluster I	Low NRM, Low Mag-Susc
W-Horizon	Cloth mt + Trellis mt	Cluster I and II	Both types
Area41	Mostly Trellis + some Cloth and intermediate mt	Cluster I and II	Both types
Main Zone	Trellis mt	Cluster II	High Mag-Susc, High NRM

Table 6.3 – Magnetite textures and the associated mineralization zones as observed by Brzozowski et al., 2017. The Textures are correlated with the Magnetic Susceptibility/NRM clusters observed in this study.

Domain state of magnetite is a fundamental element that needs to be taken into consideration when analyzing NRM and Magnetic Susceptibility values. Single domain magnetite grains are small and are in the range of 0.1-1 μm in diameter while multi domain magnetite grains are considerably larger and reaches close to 20 μm. As discussed in Chapter 4, rocks with multi domain magnetite will have a higher induced response to the present day geo magnetic field whereas the single domain and pseudo single domain (larger energy domains with controlled domain wall movement) are much more prone to having stable contributions from remanent magnetization (Butler, 1998).

With the consideration of petrological and geochemical assessments done on the wide spread distribution of magnetite species in the Marathon deposit, Cluster I mostly consists of cloth textured magnetite containing ulvospinel lamellae with overall more of a subdivision of the host magnetite into physical subgrains that are <1 μm in size, possibly representing a high NRM response. These grains are considerably smaller and more stable with regards to the domain wall movement, leading to a higher and potentially more stable NRM based on pseudo single domain to single domain behavior.

Cluster II represents magnetite with trellis and intermediate textured magnetite containing ilmenite lamellae which host magnetite grains that are more varied in the subdivision and the sub-grains are larger, between 10-50 μm and sometimes even larger (Brzozowski et al.,2017) The

mineralization zones that are predominant of trellis magnetite, display lower NRM values (Figure 6.14, 6.15). These larger magnetite sub grains would allow for more domain wall movement, displaying multi domain magnetite behavior. In the presence of multi domain magnetite, varied magnetic susceptibility responses are usually observed.

A similar observation has been made at the hemo-ilmanite ore deposit at Allard Lake, Quebec where hematite exsolution lamella was observed in ilmenite grains corresponding with high and stable NRM values (McEnroe et al., 2007). In another study, Fabian et al. (2008) suggest that the lamellar magnetism is indeed responsible for the stable and high NRMs observed at a large scale study done in titenomagnetite in Modum Norway.

6.12 Discussion and conclusions of magnetic properties

The mafic host rocks, which are already consisting of high magnetite content provides low comparison potentials to ore hosting rocks that contains sulphide minerals. Yet, we do find significant anomalies contributed by extreme enrichment of magnetite in certain lithological units of the Marathon deposit such as the 3g units and other apatitic clinopyroxenite units with an abundance of oxides. The magnetic susceptibilities of different zones of the deposit show characteristically different trends with regards to their magnetite varieties. Natural remanent magnetization shows interesting trends in the four mineralization zones with extreme values shown in Four Dams and W-Horizon lithologies. For some lithological units in Four Dams, NRM shows extremely high values and low magnetic susceptibility values indicating that the magnetization is almost entirely carried by NRM. These lithologies also carried the highest Q-Values observed for this deposit.

Four Dams and W-Horizon is predominantly observed to have clothed shaped magnetite with smaller, single domains due to the ulvospinel lamella. Single domain magnetite behavior usually indicates higher NRMs as diagnosed from the data. The higher Q-values are a telltale sign of the dominance of the remanent magnetization of these samples. A remanent magnetization with a direction different to that of the earth's induced magnetization shows high Q-values which can affect the shape and orientation of the magnetic anomalies in a magnetic survey. Of course, the portion of the viscous remanent magnetization that is instilled in the NRM component also plays a role in determining the magnetization response. Usually, the VRMs are much more prone to

being influenced and induced by the ambient field, i.e. the present geomagnetic field and if the NRMs are dominated by VRM, any ancient remanence with a different magnetization vector direction might be downplayed by being dominated by the VRMs of the sample. In such a case, the magnetic surveys would still represent mostly the magnetization induced by the present day geomagnetic field.

Pyrrhotite is another magnetic carrier that retains a substantial component of NRMs (Sagnotti 2004; Honsho et al., 2014; Butler, 1998). While the high Q-Values and NRMs distinguished in specimens are mostly from Four Dams and W-Horizon, any significant distinction of pyrrhotite distribution could not be found in these two mineralization zones.

When compared to the NRM values obtained for the Coldwell Complex and Eastern Gabbro in Kulakov et al. (2014), we observed that the effects of intensity from the drilling induced magnetization as detected in Chapter 4 was low to insignificant in the samples.

As indicated earlier, Main zone and Area 41 with lower NRMs are dominated by trellis textured magnetite containing larger titenomagnetite grains with behaviors possibly similar to multi domain magnetite. These samples are mostly dominated by induced magnetization and not as much influenced by the remanent magnetizations. This factor is also observable by lower Q values for these two regions. Therefore, when conducting magnetic surveys, it must be noted that Four Dams and W-Horizon have extremely high remanent magnetizations and must be taken into consideration when inspecting geophysical models.

As expected, extreme enrichment of magnetite seen in 3g oxide melatroctolite lithological units of all four mineralization zones are indicated to have high magnetic susceptibility as well as NRMs. Apatite clinopyroxenite units also indicated high NRM and magnetic susceptibilities on all four zones due to high percentage of magnetite. The effects of the magnetite enrichment also influence the electrical properties that has been discussed in another part of the chapter. Extreme values of Induced polarization and conductivity can be observed for the 3g units in general and previous studies have proved that more than 25% magnetite content can induce high electrical properties such as a large Induced Polarization response in ores that are otherwise barren.

6.13 Seismic Methods

Classical non-seismic geophysical methods include electromagnetism, induced polarization, potential field and radio metric techniques. These methods cannot resolve targets beyond about 500m. Therefore, with the pressing need to explore deep mineral deposits, the mineral exploration industry is turning towards reflection seismic exploration surveys which can resolve up to 3 km in depth. Classic hard rock techniques are constrained by inescapable limitations to their sensitivity and resolving power with increase in depth and distance from borehole intersections. These methods have been sufficient to meet the industry standards but with the decline and depletion in shallow deposits, deeper exploration strategies will be required to discover new deposits. The only surface method to this day that can successfully provide the required amount of depth penetration are the seismic and acoustic techniques. Eaton et al. (2003), have proposed the usefulness of integrating seismic and petrophysical methods to identify deep geological structures with a special interest in the seismic exploration methods to be used in the hard rock environment.

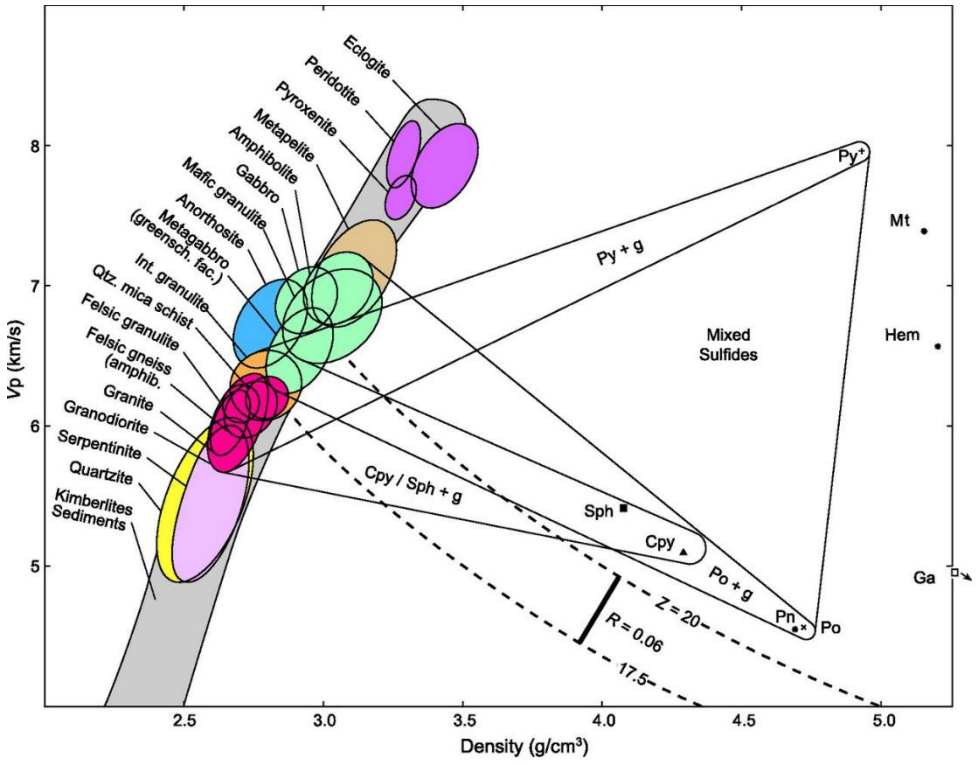

Figure 6.14- P-wave velocity and density cross plots for common rocks and minerals in hardrock terrain. Adopted from Salisbury and Snyder, 2007

Seismic exploration methods are based on P and S wave behavior in the subsurface mediums. The seismic signals correspond with the reflection, refraction and scattering of these waves at lithological and structural boundaries when changes in the medium are distinguished by the rock properties. Therefore, seismic interpretations require thorough understanding of rock properties such as the P and S wave velocity and densities of the different lithologies of the deposit (Table 6.4). Elastic properties and acoustic impedance of massive sulphides are significantly different from the other rock types yet at laboratory scale, samples may not be fully representative of the physical properties of ore deposits at seismic wavelength scales because of the presence of fractures, formation damage and ambient stress conditions.

Seismic exploration is extremely effective in hydrocarbon exploration in sedimentary rock units. But, reflective characteristics of the crystalline rocks can vary fundamentally from the reflectivity of sedimentary basins. Acoustic impedance varies largely by the velocity changes of the sedimentary rock units due to stark changes in mediums. But in hardrock settings, density plays an equally prominent role (Figure 6.14). The figure was derived from the Nafe Drake curve used as a standard for acoustic and p-wave velocity properties that distinguish characteristics of sulphide hosting rock types and other commonly found host rocks for ore bodies.

6.13.1 P-wave velocity measurements

In this study, the p-wave velocities of samples were measured with the use of an ultrasonic wave form that was propagated across the specimens. All measurements were conducted in room temperature and standard pressure conditions. Each specimen was mounted in an apparatus with metal rods to be clamped tightly while an ultrasonic wave was transmitted through the sample (Figure 6.15).

Travel time of the propagated wave form across a given sample is established using the first arrival time which uses a digital oscilloscope capable of 1 microsecond resolution. The travel time between two points is dependent upon the distance and the velocity of transmission in the medium. Therefore, length of each specimen was also measured using a digital Vernier caliper that gives values of 10^{-3} cm resolution. Therefore, the velocity can be calculated simply by Equation 9,

$$\textbf{P wave velocity = specimen length / first arrival time} \qquad (9)$$

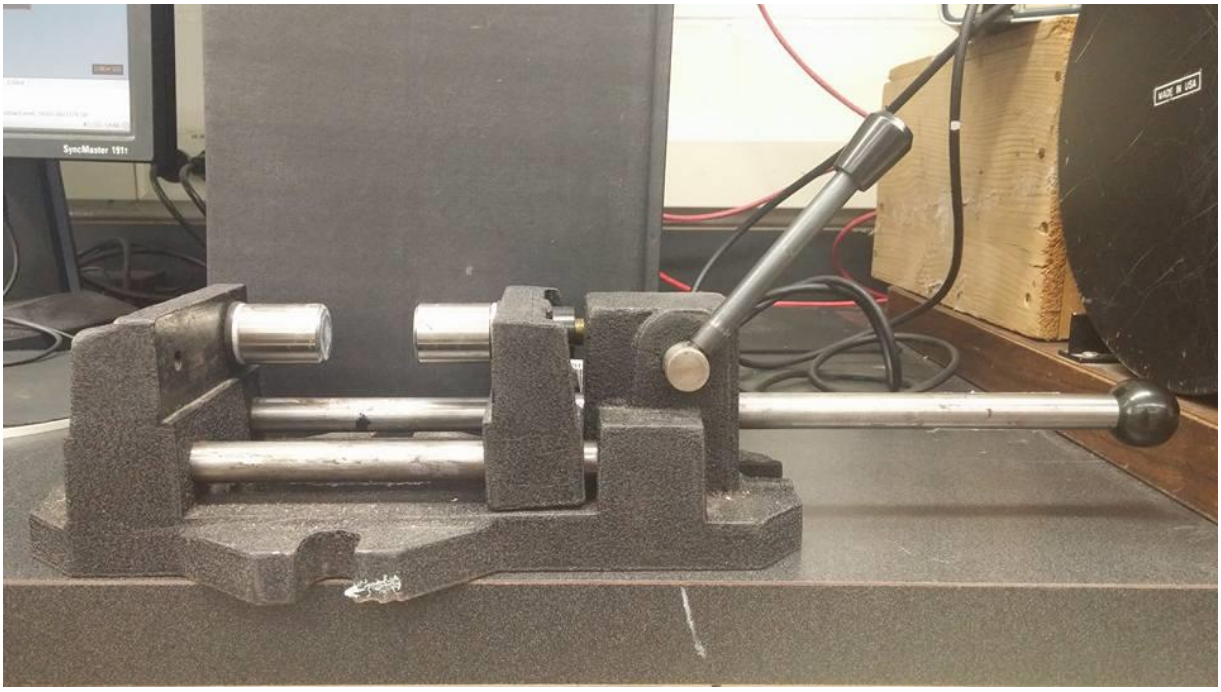

Figure 6.15- P-wave velocity apparatus with the specimen holder

Calibration of the oscilloscope parameters and the sonic wave measurement apparatus is established using a reference block of aluminium of known thickness and density. After subtracting for the apparatus baseline transmission time, the first arrival times were obtained, analyzed and documented with the use of PicoLog Data logging software.

Table 6.3 - Mean p-wave velocity, density and acoustic impedance of lithological units and mineralization zones

Main Zone				Area41				W-Horizon				Four Dams			
Lithology	P wave m/s	Density kg/m^3	Acoustic Impedence	Lithology	P wave m/s	Density kg/m^3	Acoustic Impedence	Lithology	P wave m/s	Density kg/m^3	Acoustic Impedence	Lithology	P wave m/s	Density kg/m^3	Acoustic Impedence
1a	5996.94	2767.70	16.77	1a	6235.78	2770.62	17.27	1a	4891.84	2805.42	13.75	2a	6797.03	2981.16	20.18
2a	6275.40	3028.86	19.04	1b	6148.58	2703.70	16.63	2a	6367.73	3039.02	19.38	2b	6613.62	3057.30	20.21
2c	7156.63	3184.52	22.79	2a	6526.65	3073.74	20.06	2d	6366.73	3126.65	18.60	2f	6830.49	3354.04	23.43
2d	6619.26	3060.13	20.35	2b	6554.67	3056.19	19.79	3a	5942.43	2916.75	17.33	3d	6339.29	3225.95	20.52
2k	5710.56	3097.22	17.66	2f	6366.06	3235.86	19.75	3b	5834.50	2911.25	16.91	3g	6450.49	3344.65	21.61
3b	6514.78	2982.99	19.34	2i	6558.16	3202.98	20.94	3g	6643.88	3481.09	23.12	3h	6843.76	3180.86	21.79
3c	6492.50	2790.24	18.12	3b	6690.27	2943.06	20.36	3h	6213.87	3224.27	19.93	3i	6771.81	3230.99	21.80
3g	6552.39	2785.40	18.18	3d	6745.14	2926.10	20.52	3i	6670.84	3348.98	23.19	4a	6701.87	3089.19	20.69
3l	6286.30	3005.52	20.01	3g	6576.83	3262.45	21.43	4a	6432.46	3167.56	20.45				
4a	6497.08	2914.69	18.94	3h	6649.72	3153.33	21.05					Fine Grain	6797.03	2981.16	20.18
				4a	6807.54	3115.73	20.27	Fine Grain	6234.39	3021.37	18.87	Layered	6722.05	3205.66	21.82
Fine Grain	6414.20	3057.22	19.44	4b	6993.16	3058.31	21.43	Marathon	6117.78	3101.52	18.77	Marathon	6552.26	3267.48	21.34
Marathon	6513.41	2932.27	19.14	4c	6052.26	2778.43	16.80								
				6a	5998.20	2739.91	16.50								
				Fine Grain	6542.40	3138.36	20.33								
				Layered	6460.36	3146.02	19.77								
				Marathon	6700.16	3036.47	20.51								

6.13.2 P-wave velocity results

Acoustic impedance is calculated by the product of P-wave velocity and density of the rock, and is a standard value assessed in a seismic study to understand the properties of the host rocks and ore bodies. A sufficient contrast in acoustic properties needs to be available for the detection of massive sulphide ores in igneous and metamorphic rocks. A sulphide ore body would be expected to reflect seismic energy yet there are a few fundamental implications that need to be considered. In most cases in crystalline rock, the velocities are faster, the targets are smaller and the structure more complex and the dips of the ore body boundaries are quite steep (Whiteley and Greenhalgh, 1979; Salusbury et al., 2000) Therefore, this requires shorter wavelengths (higher frequencies) and a broader range of source receiver offsets in the survey design. The reflection coefficients are low due to low impedance contrasts and therefore the acquisition parameters must be adjusted to ensure that the signal to noise ratio is large. Therefore, a significant acoustic impedance contrast needs to be present in the survey for the sulphide ore body to be detectable. Lowest velocities and acoustic impedances are observed in the footwall units in 1a,1b lithologies. The densities are important for the velocity values since higher densities tend to increase the P-wave velocities. Mafic or ultramafic rocks tend to have higher velocities in general but the presence of sulphides is bound to decrease the velocity as observed by the ore rocks containing high amounts of sulphide minerals (Nafe Drake curve in Figure 6.14).

Seismic methods have been slowly embraced by the mineral exploration community with the increase in the demand for exploration tools in deeper sources. The laboratory results presented in this section will discuss the feasibility of using seismic methods to identify strong sulphide-generated reflectors in the Marathon setting.

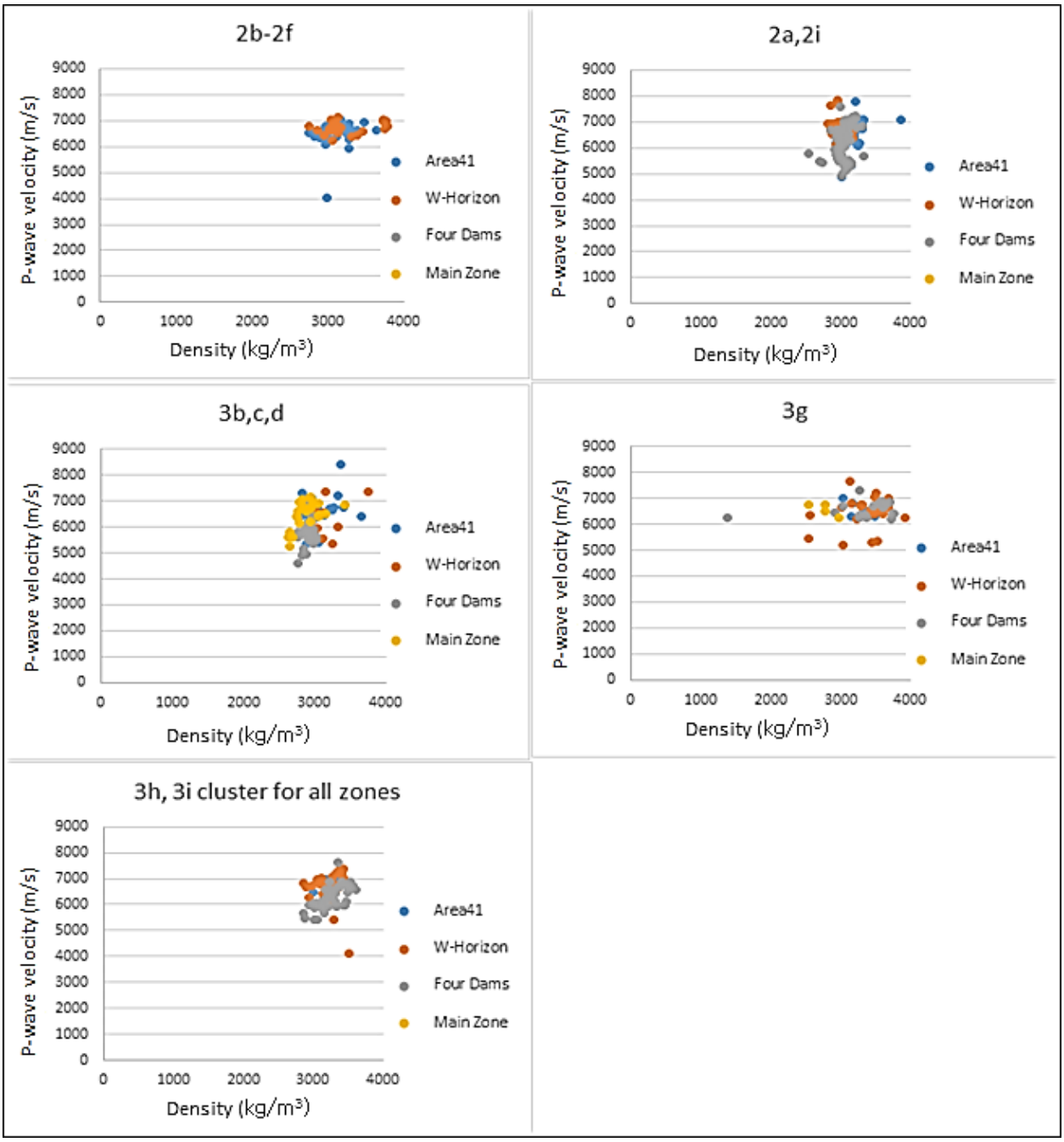

Figure 6.16- Density and P-wave velocity cross plots for the lithological units which are indicated in the headings of the plots. The respective mineralization zones are also indicated in the legends.

6.13.3 P-wave velocityes and the distributions in mineralization zones and lithologies

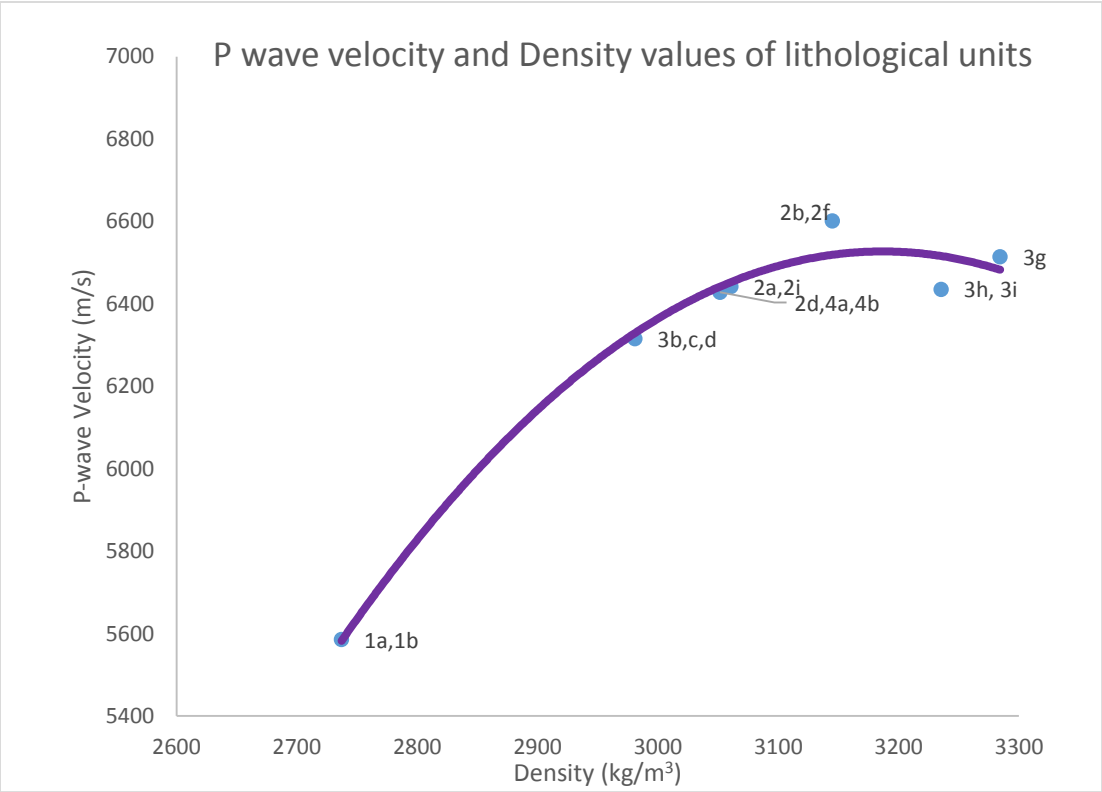

Figure 6.17-distribution of average values of density and P-wave velocities for lithological units. This diagram is to illustrate the density and velocity properties for the distinctive classes of lithologies where all lithologies except 1a,1b have distinctively similar P-wave velocities and densities.

Petrophysical measurements of P-wave velocity have been carried out on lithological units at the Marathon deposit. The findings can be further used for possible interpretations of the crustal reflectors and velocity distribution that can be used in future seismic surveys done on the area.

Density is a good indicator of the presence of sulphides since the inherent density of sulphides are a lot higher compared to the silicate mineralogy. P-wave velocities on the other hand, slows down in the presence of sulphides. Therefore, naturally, there is a negative correlation between the densities and P-wave velocities for sulphide bearing units. Densities within individual lithologies varied relatively little as observed in Figure 6.16 where densities and the corresponding p-wave velocities have been plotted with regards to the lithological units. The lithological units with similar compositions and petro-genetic history has been grouped together and considered as one

lithological unit for the depiction of results in this study. Within a lithological unit, the density values from all four zones show very little variations as well.

The P wave velocities distinguish lithological properties in the Marathon deposit and hence are a good way to identify mineralogical differences existing within lithological units. As indicated in the Figure 6.17, similar lithologies show similar p-wave velocity distributions regardless of the mineralization zones. 2b,2f layered series lithologies when combined together have a velocity of 6600 ms^{-1} while the Fine grained lithologies show a lower velocity of 6400 ms^{-1}. Highest velocity range observed in Marathon series lithologies are in 3h and 3i Apatitic clinopyroxenite unit at 6435 ms^{-1} with a close second observed in Two Duck Lake lithologies at 6410 ms^{-1}. Notably 3g unit shows lower P-wave velocities at a mean of 6350 ms^{-1}.

When average means for lithological units are calculated, the distribution of velocities with regards to their individual densities varies by very little. As observed in Figure 6.18, densities and p-wave velocities span within a very tight knit range of values. If the footwall rocks are disregarded since these lithologies are often not as highly represented, densities vary only within 3000- 3300 ms^{-1} and the p-wave velocities vary from 6350-6550 ms^{-1} for all other lithological units. In Figure 6.18, the average values of P-wave velocities and corresponding densities for each of the lithologies indicate that the range of values among lithological units is not characteristically different. When these mean values are superimposed in a Nafe-Drake curve (Figure 6.15), we see that almost all the lithologies plot within the fields of mafic gabbroic units with chalcopyrite and pyrrhotite mixture rock units (Figure 6.19). The curve indicates how simple mixing lines of end member sulphides with mafic or felsic gangue affects the P-wave velocities. Archean footwall rocks are extremely low in density as well as P-wave velocities and hence will not be discussed for any further purposes of sulphide bearing rocks.

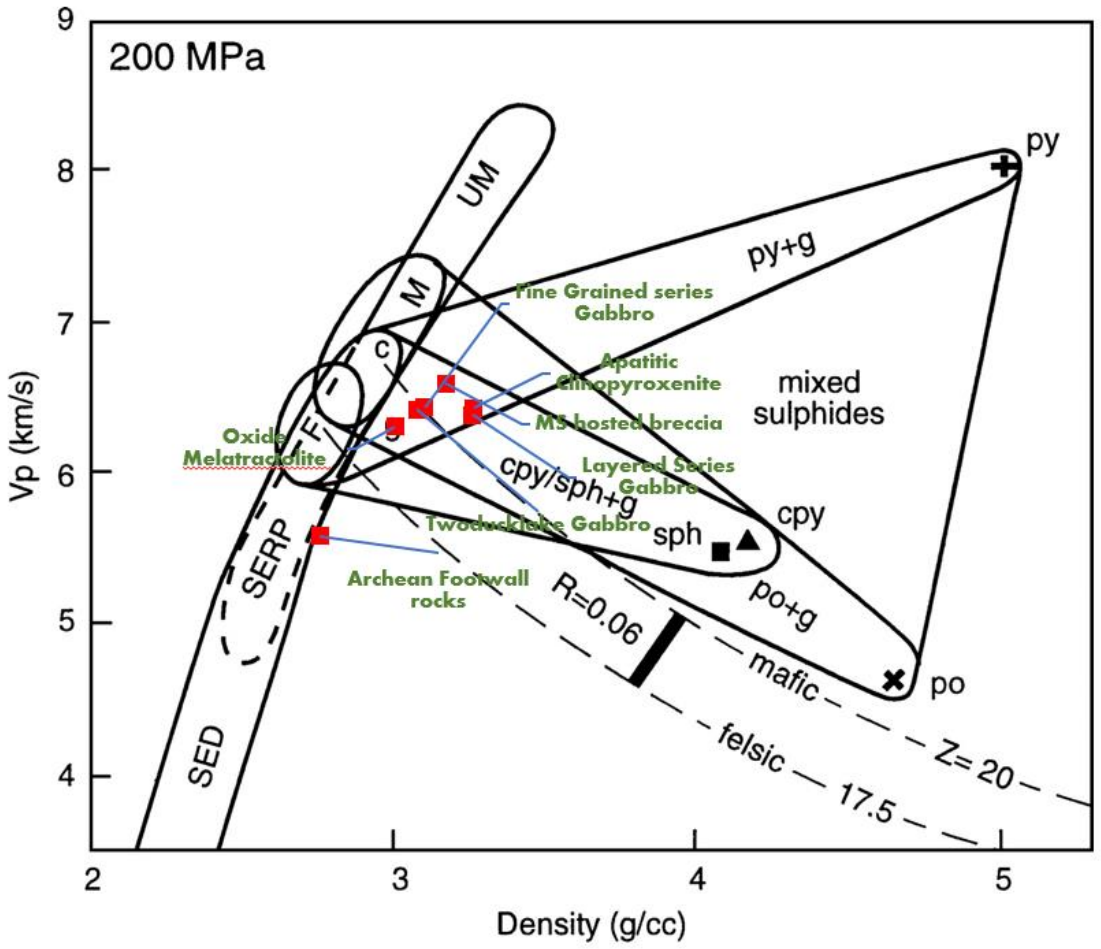

Figure 6.18- average values of P-wave velocities and corresponding densities superimposed in a Nafe Drake curve. Most lithological units are observed in the fields of Chalcopyrite, Sphelerite and Pyrrhotite mixed mafic volcanics.

6.13.4 Sulphide quantities and P-wave velocity

For this study, assay values of sulphur percentages have not been obtained for W-Horizon lithologies but the copper values have been provided and hence we were able to plot the corresponding p-wave velocities for whole rock sulpher percentages and copper values. In Figure 6.20, we observe that the copper values hardly change within the lithological units but a large fluctuation is observed for the p-wave velocities. This can potentially indicate the presence of sulphides that doesn't include copper (such as pyrrhotite) and possibly instrumental is decreasing velocities within the lithological units. Ames et al. (2017) and Good et al. (2017) indicate that W-Horizon has trace amounts of pyrite which could be influencing the variations observed in velocities.

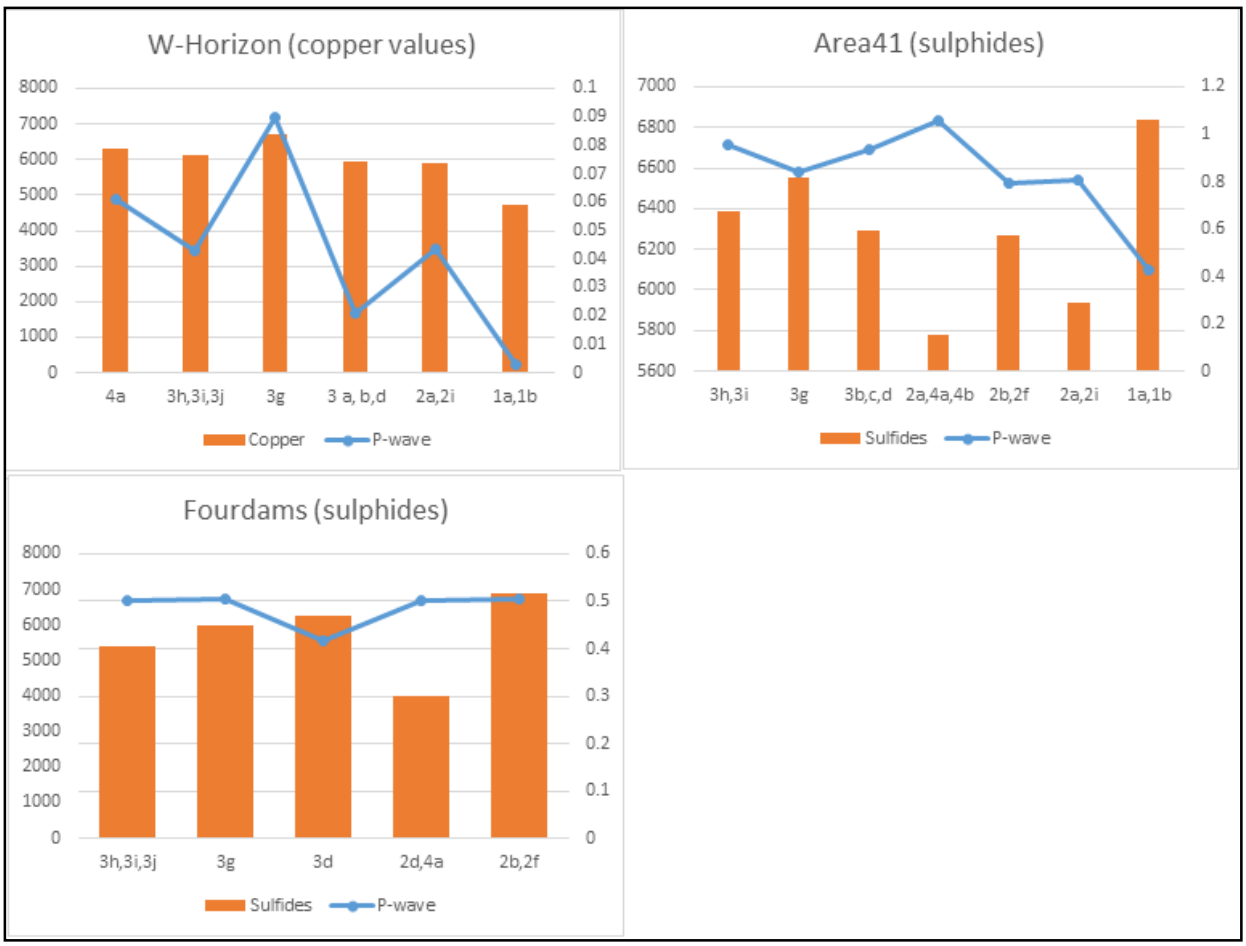

Figure 6.19- P-wave velocity distribution with regards to the sulphur content which is represented by the Sulphur values obtained by assay data for the drill cores

As seen from Figure 6.20, Sulphur content in Area41 does influence the velocity values when larger sulphur percentages are available. Higher presence of sulphides seem to influence the velocities to decrease as indicated by 3g unit in Area 41. Lower sulphur presence has increasing p wave velocities 2a,4a,4b in Area 41. Even in Four Dams, higher sulphur percentage visible in Two Duck Lake gabbro lithologies indicate a lower velocity but not by much. Therefore, a general trend can be observed where the velocities are observed to decrease with the increase in percentage of sulphur.

6.13.5 Acoustic Impedance

Lithology	Area41	Four Dams	Main Zone	W-horizon
3h,3i,3j	21.5	21.3	-	19.9
3g	21.4	21.6	18.1	23.0
3b,c,d	20.2	20.5	19.1	17.0
2d,4a	20.3	19.5	20.2	19.9
2b,2f	20.0	21.7	-	-
2a,2i	21.3	20.1	18.9	19.3
1a,1b	16.6	-	15.5	13.7

Table 6.5 – Average acoustic impedances of lithological units

Table 6.5 indicates the acoustic impedance calculated for each of the lithological groups. These lithologies have been subdivided for their minerelization zones. The acoustic impedance is the product of density and P wave velocity as was explained earlier. The impedance contrast between different lithologies is important to give a strong reflection across a lithological boundary in a seismic survey. The reflection coefficient which is derived as ratios of accoustic impedance was computed between different pairs of lithological units. Reflection co-officients are required to be 0.06 or more to cause a strong seismic reflection. W-Horizon lithologies do show a sizable reflection coofficent, probably due to the presence of pyrite as observed by Good et al. (2017) especially between the contacts of 3g unit and other fine grained and layered sereis units. Apart from these lithologies in W-Horizon, refelctions coofficients calculated amoung other litholgical zones do not give large enough values for a strong siesmic refection to be present between the lithological units.

6.14 Seismic discussion

The reflection coefficients calculculated for the lithological units are derived from mean figures for each of the lithologies (Table 6.4) that might not represent the accurate variations observed within a lithological unit. The sulphides in these lithological units show a great level of spread over a large range and using single values such as a mean P-wave velocity or a density value might not represent the small scale fluctuations observed within a lithological unit. For example, Figure 6.19 plots P-wave velocity variations and acoustic impedances observed through the length of the drill hole M-07-238. The blue highlighted areas indicate the lowest velocity regions and the corresponding impedance values. The impedance value fluctuations closely mimic P-wave velocity fluctuations indicating that the density fluctuations within the drill hole are almost negligible and acoustic impedance is controlled soley by the changes in the velocity. This characteristic is observed within all minerleization zones of the Marathon deposit due to the almost nonvarying densities of the rock units (Figure 6.17). Therefore, the minerlization zones that contain high amounts of disseminated sulphides with low P-wave velocities are often seen as units with low acoustic impedances that show a significant contrast with the surrounding high density, high velocity barren gabbroic units.

These low velocity regions are not represented by many samples in this work and hence large scale interpretations cannot be made. But, from the drill cores that has been analysed, low velocity, high sulphide content samples are analogous with slower velocities and lower acoustic impedance. The signal to noise ratio is also extremely low in such hard rock terranes and the targets thus far observed in the Marathon deposit appear to more likely be point sources or scatterers rather than the continous reflectors expected of massive sulphide.

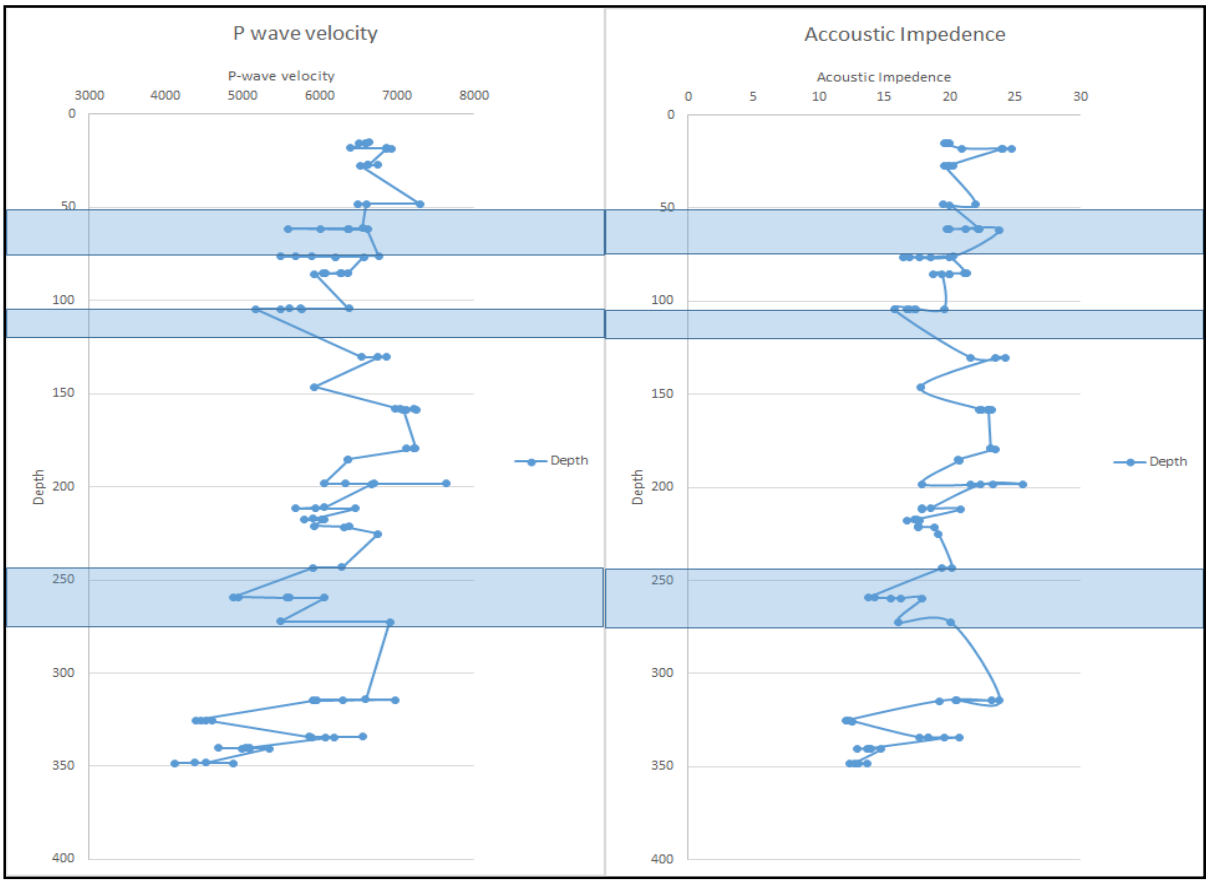

Figure 6.20- P wave velocity variations and Acoustic Impedance observed within the legth of the drill hole M-07-238 drill core. The blue highlights indicate the low velocity areas which correspond with high sulphur content

In the Nafe Drake curve (Figure 6.15), we observe that the velocities increase dramatically with pyrite content and decrease with pyrrhotite and chalcopyrite. Salisbury et al., 2000; Lalehmir et al., 2012; Leslie et al., 1999 states that strong reflectors are dependent on how comparatively different the host rock and the mineralized sulphide units are. This contrast is derived with the use of the impedance calculated by the density and P-wave velocity. As are observed from the data of the Marathon lithologies, large impedance contrasts are not seen within most lithological units. The mineralized zones that host sulphides have low acoustic impedance and the surrounding host gabbros tend to have higher acoustic impedances. A high acoustic impedance involving sulphide ores depend mostly on the amount of pyrite that is available in the mineralized unit and will give a strong to brilliant reflector (Salisbury et al., 2011) depending on the amount of pyrite available. This is due to the fact pyrite is one of the only sulphide minerals which tends to increase the seismic

velocity. Since Marathon deposit has negligible amounts of pyrite, large acoustic impedance values cannot be expected and this is seen in the computed values of acoustic impedance and reflection coefficients of all lithological zones.

A few of the best known examples such as the discovery of 6-8 Mt tons of massive sulphide lenses at a depth of 1.2 km in Halfmile Lake, New Brunswick (Salisbury et al 2000) and a 3D seismic survey in Sudbury complex with delineation of sulphide deposits are examples of the successful attempts at discovering mineralization zones with the use of reflection seismic. The characteristic of a lower acoustic impedance observed in a sulphide deposit will ensure that the sulphide body will be represented as a dark area in the seismic section compared to the brighter host lithologies with higher acoustic impedance.

Alternatively, seismic velocity tomography can be employed to characterize the low velocitiy units categorized by massive sulphides. This technique uses the P and S wave arrival times to determine the properties of the structure of the subsurface. Crosshole transmission tomography can be used to image subsurface features between boreholes and to map velocity fluctuations.

6.15 Discussion

6.15.1 Effects of the specimen sizes of the samples

Sample specimen that were used to analyze and measure the physical properties in this study are represented by three different specimen sizes. The largest specimen size is obtained by full (2.4 cm diameter) drill core samples taken from drill core segments that typically have not been split for geochemical assaying. The medium and small specimens are smaller in dimensions due to the fact that these specimens have been obtained from drill cores that were split in to half cores. One half of the core has been sent for geochemical analysis while the remaining half has been retained in storage and used to obtain specimens for this thesis. Therefore, the samples obtained from halved drill cores are smaller in dimensions compared to the large specimen (Table 6.6). A study of the sample specimen sizes and the effects of the different specimen dimensions on petrophysical measurements were investigated in this study.

Specimen size	Avg. length	Avg. diameter	Avg. volume
Large	2.2 cm	2.5 cm	11.5 cm^3
Medium	1.7 cm	1.7 cm	3.8 cm^3
Small	1.1 cm	1.0 cm	0.86 cm^3

Table 6.6- Specimen dimensions used in the petrophysical study

P-wave analysis and electrical property calculations relies on volumetric measurements and therefore, specimen dimensions become an important factor to consider. The length and the surface area of the specimens are important parameters in calculating the resistivity and the P-wave velocities. Therefore, the sample dimensions become important factors that might contribute to the source of error when assessing the physical properties of samples.

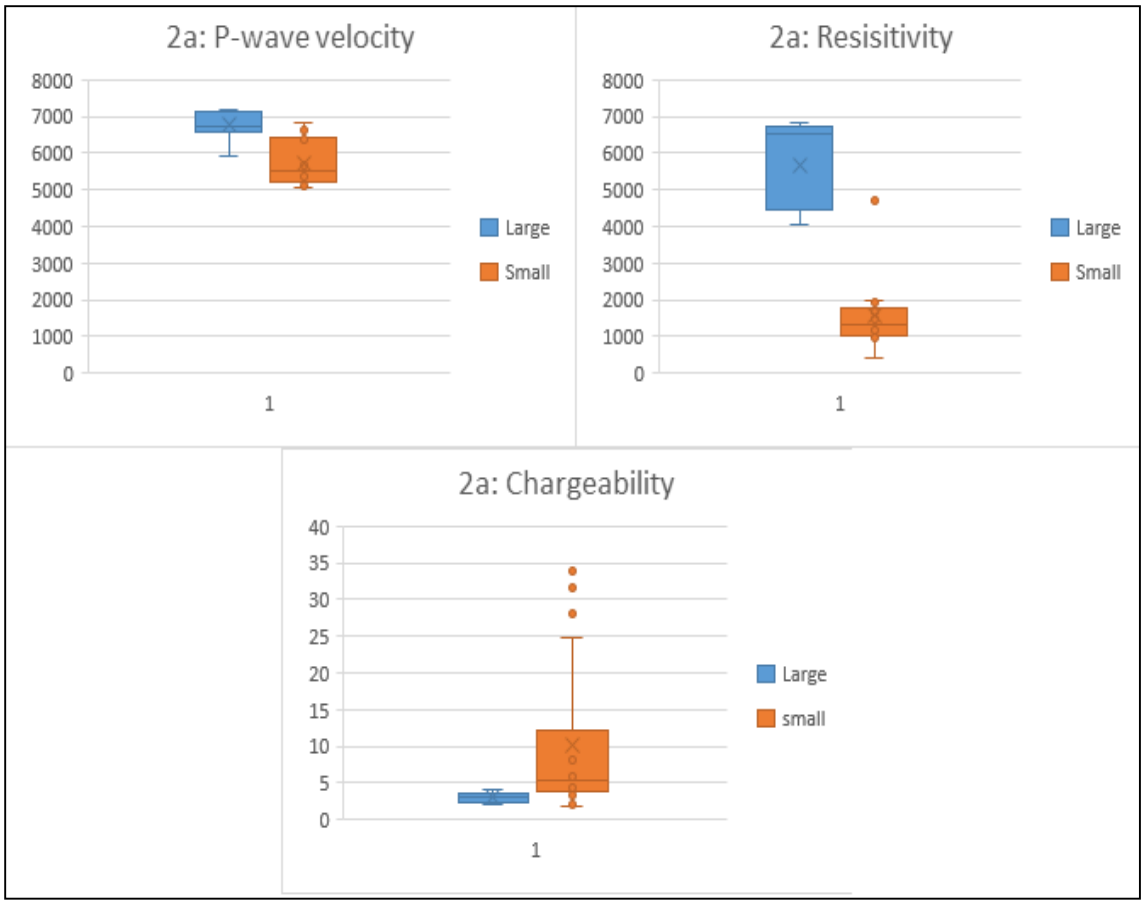

Figure 6.21- P-wave velocity(ms^{-1}), resistivity(Ω.m) and chargeability(m.sec) variations observed in the 2a lithological unit for large and small specimen sizes. The 2a lithological unit was assessed in W-Horizon mineralization zone.

Figure 6.22 indicates the P-wave, resistivity and chargeability variations observed for 2a – fine grained homogenous gabbro unit in M-07-239 drill core of the W-Horizon mineralization zone. The whisker plots show that there seems to be a larger variance in petrophysical values for the smaller samples in P-wave velocity measurements and chargeability. Average values of resistance and p-wave velocity are quite low in the smaller dimension samples and chargeability is comparatively higher as well. Such distinctly different behaviors are not observed for NRM and magnetic susceptibilities and therefore has not been reported here.

3h: apatitic clinopyroxenite lithological unit in the Area41 SL-13-34 drill core was assessed for variations observed in petrophysical values within two different specimen sizes as indicated by Figure 6.22. Similar results were observed where P-wave velocity and resistivities were comparatively lower in the smaller dimension specimens and the chargeabilities were marginally higher as well.

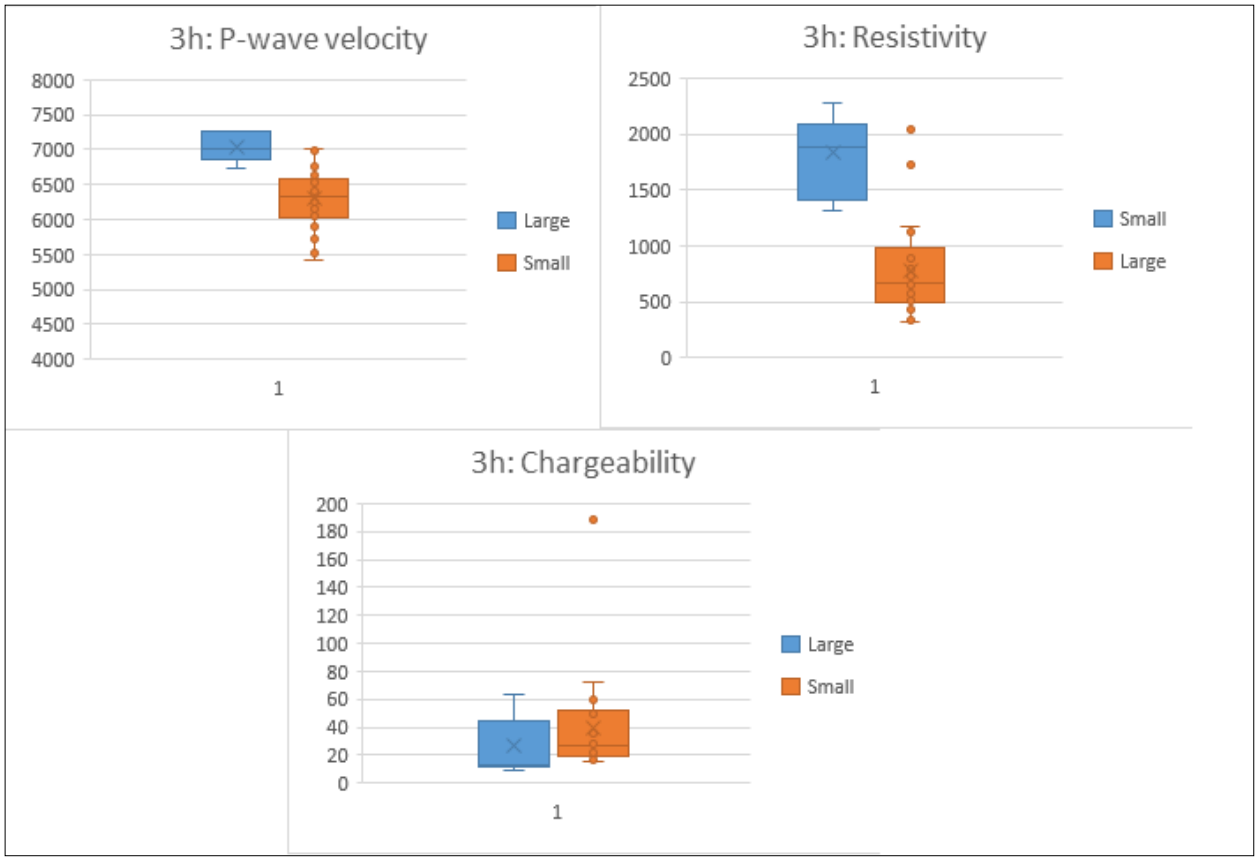

Figure 6.22- P-wave velocity (ms^{-1}) , resistivity(Ω.m) and chargeability(m.sec) variations observed in the 2a lithological unit for large and small specimen sizes. This 3h lithological unit was assessed for Area41 mineralization zone

6.15.2 Sampling bias

This comparison was done on a limited amount of lithological units due to the fact that not all lithological units were represented in each mineralization zone and not all three specimen sizes were observed for each lithological unit. Therefore, sample size comparisons for lithological units were conducted on a limited number of samples. Also, the number of specimens representing each of the three specimen sizes for a given lithology consisted of five to six samples. Most of the other

representative lithological units did not yield statistically reasonable number of samples for a comparison analysis.

The W- Horizon, Four Dams and Area 41 mineralization zones in Two Duck Lake lithologies are mostly represented by smaller specimens. With an extremely low count of representation from large specimens for these units, such a comparison regarding sample dimensions were not reasonable for most lithological units. Medium size samples were not represented by any other specimen size for a given lithology in W-Horizon and Area 41 drill cores and therefore a comparison was not discussed here.

The high variance observed for the smaller specimens might be due to the sensitive nature of the variations of lengths and areas impacting the measurement processes. Smaller specimens likely underrepresent homogeneity of the rock due to the fact that a lot smaller fraction of the lithological unit is measured and this is especially valid for in coarse grained lithologies.

The smaller specimens have been obtained from samples that have been tested for geochemical analysis and therefore have been singled out for higher sulphide content and higher potential for holding Cu and PGE hosting minerals. The large specimens have been obtained from drill cores that have not been sampled for geochemical analysis due to the lack of mineralization and other properties that might potentially hold viable information of the deposit characteristics. Therefore, it is reasonable to infer that the smaller specimens are more prone to represent electrically conductive and sulphide bearing zones. In such a case, high chargeabilities, low resistivities and low P-wave velocities observed in the smaller specimens are related to the selective sampling conducted on the more mineralized samples.

But, we cannot rule out the possibility of the sample dimensions affecting the measurement and calculation process of the physical properties. The contributions of small and large specimen sizes when calculating mean values for individual lithological units must be taken into consideration since different specimen sizes do seem to indicate considerably different petrophysical values. Specimen dimensions can be affecting the physical properties but further analysis with different size specimens need to be conducted to better understand the effects of sample sizes and dimension.

6.15.3 Petrophysical variations observed in extremely high sulphide bearing samples

Samples that indicated more than 3% volumetric sulphide content in core logs were handpicked from the sample collection for this study, with electrical, magnetic and acoustic properties analyzed to investigate the type of petrophysical responses observed from an enriched sulphide unit. It can be anticipated that that small scale fluctuations related to concentrated pod-like sulphide bodies may become diluted during the averaging of physical property values of a whole lithological unit.

Most highly sulphide enriched samples were found in the Two Duck Lake gabbro lithological units. Samples from oxide melotractolite units (3g) and other highly magnetite bearing units (2f, 3h, 3i) were not used for the subsequent comparisons in this section due to the anomalous responses brought in by magnetite. The highly magnetite-enriched rocks give anomalous electrical and magnetic signatures which need to be evaluated carefully with respect to rock units that bear high percentages of sulphides. A subsequent comparison of properties of highly magnetite bearing rock units will be discussed in this section.

A mineralized sample from the M-07-249 drill core obtained at the depth of 157 m contains 3-5% sulphide content in a coarse grained Marathon series gabbroic lithology (3b unit). The sample is enriched with some of the highest sulphide percentages observed in the Marathon drill cores. When compared to the adjacent 3b lithological units with no visible suphides, the resistivity was considerably lower in the sample specimens with high sulphide content due to the presence of electrical conducting minerals. Chargeability of the specimen are in the range of 20-30 msec which is higher than the barren 3b samples from the same drill core. But the high sulphide enriched samples are still considerably lower in chargeability values compared to the barren oxide melatroctolite (3g) units. P-wave velocities are quite low in these sulphide bearing samples, ranging in values of 6300-6400 ms-1 whereas barren Two Duck Lake lithological units and extremely magnetite enriched oxide melatroctolite units of the Marathon series show higher P-wave velocities in the range of 6800-7100 ms^{-1}. The lowering of the P-wave velocities is not surprising in the sulphide enriched samples since the presence of sulphides decreases the P-wave velocity.

Another 3b sample from the SL-13-44 drill core at the Area41 mineralization zone at a depth of 87m with high visible sulphide presence in the range of 3-4% volume was analyzed for petrophysical characteristics. While only 3-4 specimens represented that particular sample, distinctive variations were observed in the physical properties that differ from a barren sample of the same lithology in the same mineralization zone. The high sulphide content of the samples ensured higher chargeabilities and also very low resistivities. Samples from the oxide melotractolite units (3g) still gives extremely high chargeability values as was discussed in the earlier part of this chapter. Comparatively, chargeabilities for the highly sulphide mineralized samples are not as high, ranging in 20-30 msec. 3g oxide melatroctolite units indicate chargeabilities in the range of 100-200 msec which compared to the sulphide enriched samples, is a lot higher. Oxide melatroctolite and other dense lithologies give higher P-wave velocities in the range of 6800-7000 ms^{-1} in Area 41 mineralization zone. Comparatively, P-wave velocities in the sulphide rich specimens range around 6400-6600 ms^{-1}. As discussed earlier, the increase in the sulphide percentage influences the P-wave velocities to decrease, depending on the types of sulphide varieties found in the mineralization.

Magnetic susceptibilities and NRMs of oxide melatroctolite units and apatitic clinopyroxenite units are extremely high due to the enrichment of magnetite. Therefore, these units can be distinguished readily by a magnetic survey while such extreme enrichment cannot be observed in the mineralized units of the other Two Duck Lake gabbroic units. The above two samples discussed for the high sulphide content indicate lower magnetic susceptibilities compared to the highly magnetic, oxide melatroctolite units and apatitic clinopyroxenite units.

Most highly mineralized units are also chloritized to a certain extent and hence a decrease in density is observed in the ranges of 2800 kgm^{-3} which is a stark contrast to an unchloritized, Marathon series sample which ranges around 3300-3500 kgm^{-3}. The decrease in the densities affect the acoustic impedance contrasts in which case a contrast in impedance could be easy to notice between a sulphide rich and barren unit.

It is observed that the samples with trace to 1.5% sulphides differentiate very little from the barren, highly mafic host rocks and other Marathon series lithologies. The P-wave velocities are observed to be extremely high, in the range of 6900-7200 ms^{-1} in the trace-1.5% volumetric sulphides,

similar to other dense barren gabbroic lithologies. The chargeability values usually range around 3-5 msec and the resistivities are considerably higher in the ranges of 1000-1500 Ohm.m. But these values can vary within mineralization units according to the textures, dissemination and grain sizes of sulphides.

In a case of differentiating between low resistive units such as oxide melatroctolite and sulphide bearing gabbroic units, a mixture of different geophysical methods could be used to analyze lithological units. Oxide melatroctolite units show extremely high chargeabilities in the range of 150-200 msec and low resistivities (100-500 Ωm); a telltale characteristic in most mineralization zones to indicate the presence of magnetite bearing barren rock.

Therefore, an integrated geophysical approach, combined with geochemical and structural data need to be brought forth to investigate highly mineralized areas. Sulphide rich lithological units such as the Two Duck Lake intrusion unit indicates low to medium chargeability figures (10-20 msec) with low resistivity values in the range of 200-800 Ohm.m. P-wave velocities generally decrease to the range of 6400 ms^{-1} and magnetic susceptibilities are in the lower ranges compared to the oxide melatroctolite unit. Extremely high chargeability values and magnetic susceptibility values are a good indication of the presence of enriched magnetite related erroneous anomalies.

To predict whether two lithologies can generate significant reflections to be distinguished in a conventional seismic survey, we only require a knowledge of their densities and velocities from which the acoustic impedance and reflection coefficients can be calculated. With higher sulphide concentrations, the acoustic impedance contrasts and reflection coefficients change considerably, implying ore deposits with enrichment of suphides should be detectable as reflectors or scatterers. When we calculate the acoustic impedance for highly sulphide enriched rocks, the values range from 17-19 which is comparatively quite low due to the decrease in velocities associated with enriched sulphide content. The surrounding mafic gabbroic rocks in comparison, have acoustic impedances in the range of 20-22 implying that high sulphide content corresponds with lower acoustic impedances compared to the surrounding mafic host rock. Most Marathon series lithologies which are barren indicate higher p-wave velocities and high acoustic impedances due to the higher densities. In comparison, a sulphide rich rock unit decreases in the acoustic impedance and P-wave velocity.

It is also quite observable that the Fine grained series and Layered series rocks as well as the footwall and brecciated rock units indicate lower acoustic impedances compared to Marathon series lithologies. The key difference in mineralogical assemblages of these lithologies point towards the densities of the mineral compositions. Marathon series lithologies consists a lot more of magnetite (5315 kgm^{-3}) and apatite (3170 kgm-^{3}) with sulphide minerals (4200-5500 kgm^{-3}) in the mineral composition, alongside other common mafic sillicate minerals such as olivine (3300 kgm^{-3}), plagioclase (2610 kgm-3) and clinopyroxene (3200 kgm^{-3}). Layered and Fine grained series lithologies consists mostly of the common silicate minerals in varying quantities with less of the other dense accessory minerals and hence the resultant bulk densities vary from 1500 -2000 kgm-3.

Therefore, the acoustic impedances for barren lithological units in Fine Grained series and Layered series should be discernable from denser Marathon series lithologies. The calculated reflection coefficients for most lithological units with high apatite/magnetite content and other less dense Layered series or Fine grained series lithological units exceeds 0.06. In practice, a planar surface that reflects 6% incident energy can be readily detectable by conventional seismic reflection surveys (Salisbury et al., 2000). Therefore, the probability of distinguishing Marathon series lithological units from the rest of the barren Fine grained and Layered series lithologies is quite high.

Velocities decrease drastically as the sulphide percentage escalates to 3-5% volumetric sulphides as was discussed earlier. Therefore, a technique such as seismic tomography which assesses the three dimensional seismic velocity distribution, will provide a better correlation of sulphide enriched units between drill holes. The basic technique is to place explosives in drill holes and record the seismic wave transmission by the use of receiver strings in other drill holes. An integrated approach of seismic travel-times is recommended for a more cohesive approach towards assessing the lithological variations and assessment of sulphide rich mineralized units.

6.15.4 Oxide and apatite rich intrusions and implications for mineral exploration

An important spatial relationship of the oxide and apatite rich rocks in the Marathon deposit has been discussed by Good et al. (2015) with a model proposed of mineralization adjacent to the feeder channels in the Marathon magmatic intrusion. A possible mechanism has been explained

for the extreme enrichment of magnetite and apatite cumulates through density contrast where the dense crystals in a magma body settles at the base of feeder channels to form extremely magnetite and apatite enriched irregular pod like bodies. These feeder channels are filled with greater than 100 m of mineralized Two Duck Lake gabbro which makes up for the thickest zone of mineralization in the Main Zone and observations suggest that magma intruded into the intrusional complex with the faulting that occurred to form these feeder channels.

According to the magmatic intrusion model, the magnetite and apatite rich rocks were formed from the magma that escaped out the main magmatic body and deposited adjacent to the main feeder channels. Therefore, the occurrence of magnetite and apatite rich rocks are excellent markers for potential underlying mineralization and suggests as important components of the future exploration strategy for Coldwell complex (Good et al., 2015).

From the study of petrophysical characteristics of the Marathon deposit, the oxide melatroctolite and apatite clinopyroxenite units in particular show extreme enrichment in magnetite which in turn leads to interesting geophysical anomalies. Chargeability values for this unit is extremely high and the resistivities are quite low indicating highly distinguishable electrical properties as was discussed in the electrical portion of this chapter. The magnetic properties such as magnetic susceptibility and NRMs are also dominant in the oxide and apatite rich lithologies. Therefore, an assembly of electrical and magnetic properties can be used in geophysical surveys to delineate potential oxide and apatite rich rock units. With the integration of different geophysical surveys, mainly IP and magnetics, delineating these important oxide and apatite bearing units is quite plausible.

Chapter 7
Discussion and Conclusions

7.1 Anisotropy of Magnetic Susceptibility and petrofabric orientation

Anisotropy of Magnetic Susceptibility was employed to detect the petrofabrics existing within the rock samples of the Marathon deposit. While an AMS fabric was detected for the Main Zone, allowing a west-dipping plane of foliation and associated lineation to be identified, the technique couldn't be implemented for the other mineralization zones. This was due to the fact that the drill core samples which were obtained from W-Horizon, Four Dams and Area 41 were only partially oriented along the drill core axis. In the case of a partially oriented drill core sample, the results obtained from the AMS study/petrofabric could not be fully oriented in three dimensions. An attempt at independent drill core orienting was discussed in Chapter 4 with the use of Natural Remanent Magnetization components recorded within the rock samples. A pilot study on oriented drill cores from the Main Zone failed to independently orient the core samples, due to the high coercivity, high unblocking temperature remanence being apparently overprinted during the original drilling process. A similar effort was attempted to orient the drill core samples from the W-Horizon, Four Dams and Area 41 to their original geological position, but again a pervasive drilling overprint magnetization was encountered. Such an orientation would have paved way to orient the AMS fabric distribution and in turn observe the directionality of the AMS fabric distribution in those zones.

As a continuation of this study, a future project can employ the use of previously determined structural features to orient the drill cores. Fractures, joint sets, faults and marker horizons are some such features that can be used to orient the drill cores to a reasonably well-determined in situ position.

Magma conduit related mineralization was proposed by Good et al. (2015) at the Marathon deposit and the AMS planar fabric was diagnosed to follow a similar directionality to the feeder channels which are part of the magma conduit system that transported the magma into the intrusion. The

fact that the AMS fabric mimics these directions attests to the proposed model of mineralization for the Marathon deposit. These feeder channels have been found to be enriched with high mineralization (Good et al., 2015; Ruthart, 2012). Therefore, future exploration projects can employ the AMS fabric distribution and directionality to search for further conduit systems and exploration targets, provided some means of fully orienting drill core can be devised. Such geophysical vectoring methods can be employed during the search of feeder channels potentially containing high mineralization. The AMS fabric orientations with regards to the directional distribution of the feeder channels independently demonstrates conduit style mineralization of the Marathon deposit. (Good et al., 2015, Good et al., 2017)

Good et al. (2015) have also recommended exploring for highly oxide and apatite rich Marathon series units (3g, 3h, 3i units) to delineate these feeder channels since these units are usually found in the vicinity of feeder zones. From the petrophysical assessment of the units in this work, extremely high IP responses, magnetic susceptibilities and low resistivities can be used to describe these Marathon series units in all four zones that have been investigated. An integrated approach of electrical and magnetic surveys can be used to delineate the oxide and apatite rich rock units. Further use of AMS directions could also be employed to vectorize and delineate the search for these oxide and apatite enriched lithological units.

7.2 Petrophysical characteristics

While IP and resistivity are the primary surveying tools recommended for sulphide deposits, associated magnetite also acts as conductor which is often present with or without sulphide mineralization, potentially resulting in many spurious targets. A geophysical and petrophysical study done on the Bushveld complex indicates extremely high susceptibilities due to cumulous magnetite phases found between the upper and main zones of the units of the Nothern Lobe (Ashwal et al., 2006). This unit has similar values of magnetic susceptibilities to the oxide melatroctolite unit (3g) of the Marathon deposit.

A 3D IP survey was done at the Paleoproterozoic River Valley mafic intrusion, located 60 km northeast of Sudbury, Ontario, for the intensions of mapping lithological variations to identify structural trends that might be related to the extensions of the mineralization of the Platinum Grade Mineral deposit. In the survey, low to anomalous resistivities (300-1000 ohm.m) and moderate

chargeabilities were noted (13-20 msec) whereas alteration zones with high magnetite alteration within the mineralized zones gave values extremely high of chargeabilities (> 40 msec). The anomalous response corresponds with the IP values diagnosed for the oxide and apatite rich units of the Marathon deposit and the moderate chargeabilities of the Two Duck Lake intrusion seems to also display similar values to the sulphide-rich intrusions of the River Valley Intrusion (Geophysical report, SJ Geophysics., 2011). In a report presented by Mira Geoscience on geophysical interpretations of porphry deposits in British Columbia, similar high IP responses were noted at the highly magnetic rock units of the Mount Milligan deposit (Mitchinson, KEG conference 2012). These similar IP and magnetic anomalies found in the deposit is an excellent analogy for the magnetite rich oxide melatroctolites.

The ranges of magnetic susceptibilities fall under magnetite series igneous/ plutonic rocks in the range of $1x10^{-3}$- $1x10^{-4}$ cgs as was reported by Clarke et al. (1992). The paper states that the total magnetic susceptibility is dominated by the ferric iron content reflecting the presence of magnetite. Tholeiitic magma differentiation, as seen by the magmatic intrusions of the Eastern Gabbroic unit at the Marathon deposit is characterized by iron enrichment reflecting early crystallization of Mg-rich silicates. Examples such as the Bushveld, Stillwater and Skaergaard intrusions with magnetic gabbros and anorthosites contain intercumulous magnetite with magnetic susceptibilities of $1x10^{-3}$ – $1x10^{-4}$ cgs (Clarke et al., 1992) similar to the rock magnetic properties seen in the Marathon deposit (Table 6.2).

Clarke et al. (1999) discusses an idealised magmatic anomaly distribution at the Bushveld complex with modal layering of magnetite rich upper ferrogabbros with Fe olivine, plagioclase, pyroxene and magnetite cumulates giving an average susceptibility of $1.51x10^{-3}$ cgs. Apart from the similarities of the magnetic susceptibility signatures, the overall mineralogy and modal compositions of the silicate and oxides in the ferrogabbro unit at Bushveld is quite similar to the mafic-ultra mafic lithologies observed in the Marathon series lithological units such as the oxide melatroctolite unit and olivine gabbros of the Two Duck Lake intrusion.

A similar study conducted by Hankel (1991) as an attempt to illustrate a large data set of lithological units with different mineralogical compositions indicates that ferromagnetic mafic rocks are diagnosed with magnetic suscpetibilities in the range of $3.7x10^{-4}$-$1x10^{-3}$ cgs, similar to

the Marathon deposit. The study indicates that highly magmatic rock lithologies tend to show an increased Q-value, indicating that the increase in remanence usually corresponds with the increase in susceptibilities as observed in the magnetic property values of the Marathon deposit. The study has also stated that the increase in remanence in coarse grained magnetite grains is a consequence of the ilmenite exsolution lamellae partitioning the magmatic grains which pins the domain walls to behave as single/pseudo single domain. The petrophysical assessments at Marathon has displayed two types of ilmenite and ulvospinel lamellae which influence the domains to act as single/pseudo single or multi domain magnetite, depending on the physical size of the exsolution segregation of the host magnetite. Pyrrhotite-containing rocks also tend to show a higher remanence as observed by Hankel (1991) and are distinguishable in some samples from the Two Duck Lake intrusion rocks which indicates a higher remanence and higher Q-values (5-10 range in Q-values).

While seismic surveys are being used to search for geological features in the deposits, the acoustic impedance contrasts need to be taken into account when determining the eligibility of using seismic methods. The denser lithological zones of the deposit, mainly Marathon series lithologies with an abundance of magnetite, apatite and sulphides show higher densities. P-wave velocities which increase with the increase of densities, responds with a higher acoustic impedance relative to the surrounding less dense silicate lithological units. Therefore, Marathon series lithologies can be distinguishable from the Layered and Fine Grained series in a conventional seismic survey. This fact can be shown by calculating the reflection coefficients for different combinations of lithological units.

A similar case study was conducted in the Halfmile Lake copper- nickel deposit in the Bathurst camp in Canada where ore hosting rock units were clearly distinguishable with the reflection seismic surveys. (Salisbury et al., 1999). For the Marathon deposit study, seismic reflection survey can be used to extensively map out internal stratigraphy and structures of the igneous complex and their contacts with the country rock/wall rocks. This is due to the fact that highly mafic lithological units provide sufficiently large impedance differences with the mafic bodies at the base and against the Archean footwall contact.

At the Bushveld complex, 3D seismic reflection surveys were conducted for detection of cumulate stratigraphy and at the Trillabelle deposit in Sudbury where massive sulphides have been detected as an impedence feature along the footwall. Since massive sulphides have lower impedance than the highly mafic surrounding lithology, sulphide bodies were detected as dark patches in a seismic profile (Salisbury et al., 2007). Similar results and observations are possible for any highly sulphide rich or massive sulphide zones of the Marathon deposit where the acoustic impedance drops considerably, compared to the host mafic rocks.

Also, seismic velocity modeling of the Bushveld complex has been conducted with surface wave tomography to successfully differentiate lithological units with different velocities (Malchmir et al., 2012). With the use of travel time and wave form tomography, elastic parameters, mostly the velocities of different mediums (lithological unties with distinguishable velocity variations) were assessed and the waveform models were compared well with independently estimated petrophysical velocity data at the Voisey's Bay deposit (Afanasiev et al., 2014). Similar surveying methods could be used to detect highly sulphide rich zones in the Marathon deposit which will clearly distinguish the slowing of the seismic velocities as they propagate through a sulphide body and other seismically slow zones.

7.3 Limitations of the petrophysical work and future recommendations

Mineral compositions, soil heterogeneity, micro geometry of the geological units, chemical environment of the deposit etc might create complication when assessing results of geophysical ground surveys which are usually not highlighted in a laboratory petrophysical study. Therefore, previously acquired information of the lithological units with the aid of drilling, soil sampling and geochemical analysis etc needs to be integrated alongside petrophysical results to successfully interpret geophysical surveys. Moreover, pressures and temperatures at different crustal depths can be vastly different from the laboratory conditions. Therefore, the p-wave velocities, resistivities and IP effects can change significantly when assessing petrophysical properties in different conditions of the subsurface (Balog and Secco, 1999).

For the detection of accurate resistivity and chargeability, the specimens need to be fully water saturated. Even though an exact verification of the amount of water saturation is not assessed in this study, future studies can employ the use of Archimedean method to assess the density of water

saturated specimens and compare the density values obtained from helium pycnometry (Tamari, 2003). The volumes obtained from the two methods need to be equal for the specimens to be concluded as fully water saturated.

IP and resistivity data also depends on the concentration of ions in the pore spaces since the amount of ions present will affect the current density and the induced polarization effect observed in rock specimens. Therefore, it is imperative to regulate the ion concentration in the water used for saturation purposes of the specimens. For future work, we recommend using distilled water to produce a solution with a known chemical/ionic concentration to be used to water-saturate the specimens.

7.4 Exploration strategy and conclusions

While petrophysical properties are directly analogous to the responses obtained by a geophysical survey, geological variables such as the tectonic setting, composition and history of the source region, depth of emplacement, dimensions of the ore bodies etc. play important roles during exploring for ore deposits. Nevertheless, petrophysical properties are essential to evaluate and obtain insight into the important variables that decide the implementations of geophysical surveys. Marathon deposit consists of several gabbroic to ultramafic series which has led way to the differentiation of key lithological units. The sulphide bearing Two Duck Lake intrusion hosts most of the mineralization and a key part of the exploration strategy for Marathon deposit is to understand the distribution of these lithological units and the mineralization-associated marker units.

Magnetic responses and electrical responses have been able to differentiate Marathon series units from the other lithological units. In the Marathon series, notably the olivine gabbros, oxide melatroctolite and apatite clinopyroxenite units have distinctly noticeable electrical responses. The sulphide-bearing units show moderate chargeabilities and low resistivities whereas magnetic susceptibilities range in medium to high ferromagnetic responses. Therefore, IP and magnetic investigations as integrated surveys can be used to identify potential mineralization hosting lithological units.

As discussed earlier, refraction travel time seismic surveys and tomography studies can be utilized to assess low velocity zones to detect extreme sulphide enrichment while conventional reflection

surveys can be used to map internal geological units / structures quite effectively due to a considerable acoustic impedance difference noticeable between Fine grained, Layered and Marathon series rocks.

Oxide and apatite rich rocks have been identified previously to serve as detectors for feeder channels, hosting extreme mineralization. Chargeability in these rock units are also noticeably higher and should be detectable in an IP survey. Therefore, electrical surveys are recommended for the detection of these units. These highly ferromagnetic, cumulous magnetite rich rocks also indicate large magnetic responses. Therefore, magnetic surveys should also be integrated to delineate these marker units.

In future drilling programs, obtaining oriented drill cores are recommended for further investigation into the directionality of petrofabrics. The AMS fabric at Main Zone has been diagnosed as an excellent directional indicator for feeder channels and further investigations into fabric directions should be extended in mineralized zones such as W-Horizon, Four Dams and Area41 for potential indicators of magma conduit and feeder channels.

While drilling induced magnetization has eradicated the ChRM directions of the drill core, use of previously established directionality of structural features in the area (joints, fracture units, orientation of lithological units etc.) can be employed to reorient the drill cores to the original geological position. Therefore, an integration of geophysical, structural and geochemical methods is recommended to establish new drilling targets and explore new mineralized areas. AMS fabric as well as IP, magnetic and seismic responses can be used to delineate mineralization units in the Marathon deposit.

References

Afanasiev, M. V., Pratt, R. G., Kamei, R., & McDowell, G. (2014). Waveform-based simulated annealing of crosshole transmission data: A semi-global method for estimating seismic anisotropy. *Geophysical Journal International*, *199*(3), 1586-1607.

Ames, D. E., Kjarsgaard, I. M., McDonald, A. M., & Good, D. J. (2017). Insights into the extreme PGE enrichment of the W Horizon, Marathon Cu-Pd deposit, Coldwell Alkaline Complex, Canada: Platinum-group mineralogy, compositions and genetic implications. *Ore Geology Reviews*.

Andersen, J. C., Rasmussen, H., Nielsen, T. F., & Ronsbo, J. G. (1998). The Triple Group and the Platinova gold and palladium reefs in the Skaergaard Intrusion; stratigraphic and petrographic relations. *Economic Geology*, *93*(4), 488-509.

Arndt, N., Lesher, C. M., & Czamanske, G. K. (2005). Mantle-derived magmas and magmatic Ni-Cu-(PGE) deposits.

Ashwal, L. D., Webb, S. J., & Knoper, M. W. (2005). Magmatic stratigraphy in the Bushveld Northern Lobe: continuous geophysical and mineralogical data from the 2950 m Bellevue drillcore. *South African Journal of Geology*, *108*(2), 199-232.

Audunsson, H., & Levi, S. (1989). Drilling-induced remanent magnetization in basalt drill cores. *Geophysical Journal International*, *98*(3), 613-622.

Barnes, S. J., Cruden, A. R., Arndt, N., & Saumur, B. M., 2015, The mineral system approach applied to magmatic Ni–Cu–PGE sulphide deposits: Ore Geology Reviews.

Barrie C.T., MacTavish A.D., Walford P.C., Chataway R. and Middaugh R., 2002, Contact-type and Magnetitite Reef-type Pd-Cu Mineralization in Ferroan Olivine Gabbros of the Coldwell Complex, Ontario: Canadian Institution of Mining and Metallurgy Special Volume 54, p 321–337.

Bery, A. A., Saad, R., Mohamad, E. T., Jinmin, M., Azwin, I. N., Tan, N. M. A., & Nordiana, M. M. (2012). Electrical resistivity and induced polarization data correlation with conductivity for iron ore exploration. The Electronic Journal of Geotechnical Engineering, 17, 3223-3233.

Borradaile, G. (1987). Anisotropy of magnetic susceptibility: rock composition versus strain. *Tectonophysics*, *138*(2-4), 327-329.

British geological survey website, file:///C:/Users/user/Downloads/comm_profile_plat_group_ele.pdf

Brooks, C. K., & Gleadow, A. J. W. (1977). A fission-track age for the Skaergaard intrusion and the age of the East Greenland basalts. *Geology*, *5*(9), 539-540.

Brzozowski, M.J., *Samson, I.M., Gagnon, J.E., Good, D.J., Linnen, R.L.* (2017) Textural and chemical characteristics of oxide minerals as a record of postmagmatic processes in the Eastern Gabbro, Coldwell Complex, NW Ontario. GAC-MAC, Kingston, Canada, May 14-18, 2017.

Burtman, V., Zhdanov, M., Lin, W., & Endo, M. (2016). Complex resistivity of mineral rocks in the context of the generalized effective-medium theory of the IP effect. In *SEG Technical Program Expanded Abstracts 2016* (pp. 2238-2242). Society of Exploration Geophysicists.

Büyüksaraç, A., Jordanova, D., Ateş, A., & Karloukovski, V. (2005). Interpretation of the gravity and magnetic anomalies of the Cappadocia Region, Central Turkey. *pure and applied geophysics*, *162*(11), 2197-2213.

Calvert, A. J., & Li, Y. (1999). Seismic reflection imaging over a massive sulfide deposit at the Matagami mining camp, Quebec. *Geophysics*, *64*(1), 24-32.

Cao, Y. (2017). Cu-Pd mineralization and exploration geochemistry of the Eastern Gabbro, Coldwell Alkaline Complex, ON, Canada.

Chandler, V. W. (1990). Geologic interpretation of gravity and magnetic data over the central part of the Duluth Complex, northeastern Minnesota. *Economic Geology*, *85*(4), 816-829.

Chapin, D. A. (1996). The theory of the Bouguer gravity anomaly: A tutorial. *The Leading Edge*, *15*(5), 361-363.

Cheeke, J. D. N. (1961). The electrical and magnetic properties of magnetite at the low temperature phase transition (Doctoral dissertation, University of British Columbia).

Clark, D. A. (1999). Magnetic petrology of igneous intrusions: implications for exploration and magnetic interpretation. *Exploration Geophysics*, *30*(2), 5-26.

Clark, D. A., French, D. H., Lackie, M. A., & Schmidt, P. W. (1992). Magnetic petrology: application of integrated rock magnetic and petrological techniques to geological interpretation of magnetic surveys. *Exploration Geophysics*, *23*(2), 65-68.

Dahl, R., Watkinson, D.H., and Taylor, R.P., 2001, Geology of the Two Duck Lake intrusion and the Marathon Cu-PGE deposit, Coldwell Complex, northern Ontario: CIM Exploration and Mining Geology, v. 10, p. 51–65.

De Wall, H., & Worm, H. U. (2001). Recognition of drilling-induced remanent magnetization by Q-factor analysis: a case study from the KTB-drillholes. *Journal of applied geophysics*, *46*(1), 55-64.

Drenth, B. J., Anderson, R. R., Schulz, K. J., Feinberg, J. M., Chandler, V. W., & Cannon, W. F., 2015, What lies beneath: geophysical mapping of a concealed Precambrian intrusive complex along the Iowa–Minnesota border: Canadian Journal of Earth Sciences.

Drenth, B. J., Anderson, R. R., Schulz, K. J., Feinberg, J. M., Chandler, V. W., & Cannon, W. F. (2015). What lies beneath: geophysical mapping of a concealed Precambrian intrusive complex along the Iowa–Minnesota border. *Canadian Journal of Earth Sciences*, *52*(5), 279-293.

Dubey, A. K. (2014). *Understanding an orogenic belt*. Springer, Heidelberg, New York, Dordrecht, London.

Dubey, A.K., 2014. Understanding an Orogenic Belt: Structural Evolution of the Himalaya. Springer Geology. Chapter 2, The Anisotropy of Magnetic Susceptibility; p.7

Eaton, D., Guest, S., Milkereit, B., Bleeker, W., Crick, D., Schmitt, D., & Salisbury, M. H. (1996). Seismic imaging of massive sulfide deposits; Part III, Borehole seismic imaging of near-vertical structures. *Economic Geology*, *91*(5), 835-840.

Fernandes A.E (2015). Magnetic fabric study and the emplacement of sulfide deposits in the North Range offset dykes of the Sudbury Impact Structure, Ontario, Canada

Gallardo, L. A., & Meju, M. A. (2004). Joint two-dimensional DC resistivity and seismic travel time inversion with cross-gradients constraints. *Journal of Geophysical Research: Solid Earth*, *109*(B3).

Geoscience Australia website, http://www.australianminesatlas.gov.au/education/fact_sheets/copper.html

Godel, B., & Barnes, S. J. (2008). Platinum-group elements in sulfide minerals and the whole rocks of the JM Reef (Stillwater Complex): Implication for the formation of the reef. *Chemical Geology*, *248*(3), 272-294.

Good, D. J., Cabri, L. J., & Ames, D. E. (2017). PGM Facies variations for Cu-PGE deposits in the Coldwell Alkaline Complex, Ontario, Canada. *Ore Geology Reviews*.

Good, D. J., Epstein, R., McLean, K., Linnen, R. L., & Samson, I. M., 2015, Evolution of the Main Zone at the Marathon Cu-PGE Sulfide Deposit, Midcontinent Rift, Canada: Spatial Relationships in a Magma Conduit Setting: Economic Geology, V. 110, p. 983-1008.

Good, D.J., and Crocket, J.H., 1994, Genesis of the Marathon Cu-platinum group element deposit, Port Coldwell alkalic complex, Ontario: A Midcontinent rift-related magmatic sulfide deposit: Economic Geology, v. 89, p. 131–149.

Good, D.J., and Crocket, J.H., 1994, Genesis of the Marathon Cu-platinum group element deposit, Port Coldwell alkalic complex, Ontario: A Midcontinent rift-related magmatic sulfide deposit: Economic Geology, v. 89, p. 131–149.

Good, John David., 1991, Genesis of copper-precious metal sulfide deposits in the Port Coldwell alkalic complex, Ontario.

Guo, W. W. (2015). Mathematical Model of Anisotropy of Magnetic Susceptibility (AMS). *Journal of Applied Mathematics and Physics*, *3*(04), 399.

Hallof, H.G, (1983), An introduction to the se of the Spectral induced polarization method.

Hanna. F. H. (1977). Weak-Field Magnetic Susceptibility Anisotropy and its Dynamic Measurement

Helz, R. T. (1995). The Stillwater Complex, Montana: a subvolcanic magma chamber?. *American Mineralogist*, *80*(11-12), 1343-1346.

Henkel, H. (1994). Standard diagrams of magnetic properties and density—a tool for understanding magnetic petrology. *Journal of Applied Geophysics*, *32*(1), 43-53.

Honsho, C., Yamazaki, T., Ura, T., Okino, K., Morozumi, H., & Ueda, S. (2016). Magnetic anomalies associated with abundant production of pyrrhotite in a sulfide deposit in the Okinawa Trough, Japan. *Geochemistry, Geophysics, Geosystems*.

Ishikawa, M., & Arima, M. (2009). Laboratory measurements of ultrasonic wave velocities of crustal rocks at high pressures and temperatures: Petrological structure of Izu-Bonin-Mariana arc crust. *Physics and Chemistry of the Earth's Interior: Crust, Mantle and Core*, 143-52.

Jelinek, V. (1981). Characterization of the magnetic fabric of rocks. *Tectonophysics*, *79*(3-4), T63-T67.

Jelínek, V., & Kropáček, V. (1978). Statistical processing of anisotropy of magnetic susceptibility measured on groups of specimens. *Studia geophysica et geodaetica*, *22*(1), 50-62.

Johnson, G. R., & Anderson, L. A. (1981). *A laboratory study of some physical properties of sulfide ores in igneous and metamorphic rocks from the Burnt Nubble area, Somerset County, Maine* (No. 81-669). US Geological Survey,.

Johnson's metal management website - http://www.platinum.matthey.com/

Jones, W. R., Howland, A. L., & Peoples, J. W. (1960). *Igneous and tectonic structures of the Stillwater Complex, Montana*. US Government Printing Office.

Kerr, A. & Leitch, A. M., 2005, Self-destructive sulfide segregation systems and the formation of high-grade magmatic ore deposits: Economic Geology, V. 100, p. 311-332.

Kgaswane, E. M., Nyblade, A. A., Durrheim, R. J., Julià, J., Dirks, P. H., & Webb, S. J. (2012). Shear wave velocity structure of the Bushveld Complex, South Africa. *Tectonophysics*, *554*, 83-104.

Khan, M. A. (1962). The anisotropy of magnetic susceptibility of some igneous and metamorphic rocks. *Journal of Geophysical Research*, *67*(7), 2873-2885.

Kiberu, J. (2002). Induced Polarization and Resistivity Measurements on a Suite of Near Surface Soil Sampless and Their Empirical Relationship to Selected Measured Engineering Parameters. ITC.

King, A. (2007). Review of geophysical technology for Ni-Cu-PGE deposits. In *Proceedings of Exploration* (Vol. 7, pp. 647-665).

Kulakov, E. V., Smirnov, A. V., & Diehl, J. F. (2014). Paleomagnetism of the~ 1.1 Ga Coldwell Complex (Ontario, Canada): Implications for Proterozoic geomagnetic field morphology and plate velocities. *Journal of Geophysical Research: Solid Earth*, *119*(12), 8633-8654.

Lelièvre, P. G., Farquharson, C. G., & Hurich, C. A. (2012). Joint inversion of seismic traveltimes and gravity data on unstructured grids with application to mineral exploration. *Geophysics*, *77*(1), K1-K15.

Lenaz, D., Garuti, G., Zaccarini, F., Cooper, R. W., & Princivalle, F. (2012). The Stillwater Complex chromitites: The response of chromite crystal chemistry to magma injection. *Geologica Acta: an international earth science journal*, *10*(1).

Leslie, J. M., & Lawton, D. C. (1999). A refraction-seismic field study to determine the anisotropic parameters of shales. *Geophysics*, *64*(4), 1247-1252.

Li, Y., & Oldenburg, D. W. (1998). 3-D inversion of gravity data. *Geophysics*, *63*(1), 109-119.

Loncarevic, B. D., Feininger, T., & Lefebvre, D. (1990). The Sept-Iles layered mafic intrusion: Geophysical expression. *Canadian Journal of Earth Sciences*, *27*(4), 501-512.

Macdonald, A. J. (1987). Ore deposit models# 12. The platinum group element deposits: classification and genesis. *Geoscience Canada*, *14*(3).

Maier, W. D., 2005, Platinum-group element (PGE) deposits and occurrences: mineralization styles, genetic concepts, and exploration criteria: Journal of African Earth Sciences, V. 41, p. 165-191.

Malehmir, A., Durrheim, R., Bellefleur, G., Urosevic, M., Juhlin, C., White, D. J., ... & Campbell, G. (2012). Seismic methods in mineral exploration and mine planning: A general overview of past and present case histories and a look into the future. *Geophysics*, *77*(5), WC173-WC190.

McCallum, I. S. (2002). The Stillwater Complex: A review of the geology. *Stillwater Complex, Geology and Guide. Billings*, 21-25.

McEnroe, S. A., Robinson, P., Langenhorst, F., Frandsen, C., Terry, M. P., & Boffa Ballaran, T. (2007). Magnetization of exsolution intergrowths of hematite and ilmenite: Mineral chemistry, phase relations, and magnetic properties of hemo-ilmenite ores with micron-to nanometer-scale lamellae from Allard Lake, Quebec. *Journal of Geophysical Research: Solid Earth*, *112*(B10).

Milkereit, B., Salisbury, M., Eaten, D. W., & Wu, J. (1996, June). Seismic imaging of massive sulphide deposits. In *58th EAGE Conference and Exhibition*.

Miller, J., Nicholson, S. W., Easton, R. M., Ripley, E. M., & Feinberg, J. M., 2013, Geology and mineral deposits of the 1.1 Ga Midcontinent Rift in the Lake Superior region–an overview. Field guide to the copper-nickel-platinum group element deposits of the Lake Superior Region. Edited by Miller, J. Precambrian Research Center Guidebook

Mira Geophysics (2012), BC porphyry deposits: geological interpretation of geophysical data

Mitchell, R. H., Platt, R. G., Lukosius-Sanders, J., Artist-Downey, M., & Moogk-Pickard, S. (1993). Petrology of syenites from center III of the Coldwell alkaline complex, northwestern Ontario, Canada. *Canadian Journal of Earth Sciences*, *30*(1), 145-158.

Mitchell, R.H., Platt, R.G., and Cheadle, S., 1983, A gravity study of the Coldwell Complex, northwestern Ontario, and its petrological significance: Canadian Journal of Earth Sciences, v. 20, p. 1631–1638.

Mitchell, R.H., Platt, R.G., and Cheadle, S., 1983, A gravity study of the Coldwell Complex, northwestern Ontario, and its petrological significance: Canadian Journal of Earth Sciences, v. 20, p. 1631–1638.

Mungall, J. E., & Naldrett, A. J. (2008). Ore deposits of the platinum-group elements. *Elements*, *4*(4), 253-258.

Mungall, J. E., Andrews, D. R., Cabri, L. J., Sylvester, P. J., & Tubrett, M. (2005). Partitioning of Cu, Ni, Au, and platinum-group elements between monosulfide solid solution and sulfide melt under controlled oxygen and sulfur fugacities. *Geochimica et Cosmochimica Acta*, *69*(17), 4349-4360.

O'Driscoll, B., & González-Jiménez, J. M. (2016). Petrogenesis of the platinum-group minerals. *Reviews in Mineralogy and Geochemistry*, *81*(1), 489-578.

Oduduru, P. I., & Mamah, L. I. (2014). Integration of electrical resistivity and induced polarization for subsurface imaging around the Pond, Nsukka, Anambra Basin, Nigeria. *Pacific J Sci Technol*, *15*(1), 306-317.

Ohnenstetter, D. A. N. I. E. L. (1991). Hydrothermal origin of platinum-group mineralization in the Two Duck Lake intrusion, Coldwell Complex, northwestern Ontario. *Canad Mineral*, *30*.

Paces, J. B., & Miller, J. D. (1993). Precise U-Pb ages of Duluth complex and related mafic intrusions, northeastern Minnesota: Geochronological insights to physical, petrogenetic, paleomagnetic, and tectonomagmatic processes associated with the 1.1 Ga midcontinent rift system. *Journal of Geophysical Research: Solid Earth*, *98*(B8), 13997-14013.

Peach, C. L., Mathez, E. A., & Keays, R. R. (1990). Sulfide melt-silicate melt distribution coefficients for noble metals and other chalcophile elements as deduced from MORB: Implications for partial melting. *Geochimica et Cosmochimica Acta*, *54*(12), 3379-3389.

Pearce, C. I., Pattrick, R. A., & Vaughan, D. J. (2006). Electrical and magnetic properties of sulfides. *Reviews in Mineralogy and Geochemistry*, *61*(1), 127-180.

Pelton, W. H., Ward, S. H., Hallof, P. G., Sill, W. R., & Nelson, P. H. (1978). Mineral discrimination and removal of inductive coupling with multifrequency IP. *Geophysics*, *43*(3), 588-609.

Revil, A., Aal, G. Z. A., Atekwana, E. A., Mao, D., & Florsch, N. (2015). Induced polarization response of porous media with metallic particles—Part 2: Comparison with a broad database of experimental data. *Geophysics*.

Revil, A., Florsch, N., & Mao, D. (2015). Induced polarization response of porous media with metallic particles—Part 1: A theory for disseminated semiconductors. *Geophysics*.

Ripley, E. M., & Al-Jassar, T. J. (1987). Sulfur and oxygen isotope studies of melt-country rock interaction, Babbitt Cu-Ni deposit, Duluth Complex, Minnesota. *Economic Geology*, *82*(1), 87-107.

Ripley, E. M., Lambert, D. D., & Frick, L. R. (1998). Re-Os, Sm-Nd, and Pb isotopic constraints on mantle and crustal contributions to magmatic sulfide mineralization in the Duluth Complex. *Geochimica et Cosmochimica Acta*, *62*(19), 3349-3365.

Rochette, P., Jackson, M., & Aubourg, C. (1992). Rock magnetism and the interpretation of anisotropy of magnetic susceptibility. *Reviews of Geophysics*, *30*(3), 209-226.

Ruthart, R., 2012, Characterization of high-PGE, low-sulphur mineralization at the Marathon PGE-Cu deposit, Ontario: M.Sc. thesis, Waterloo, ON, University of Waterloo, 145 p.

Sagnotti, L. (2007). Iron sulfides. In *Encyclopedia of Geomagnetism and Paleomagnetism* (pp. 454-459). Springer Netherlands.

Salisbury, M. H., & Snyder, D. A. V. I. D. (2007). Application of seismic methods to mineral exploration. *Mineral deposits of Canada: A synthesis of major deposit types, district metallogeny, the evolution of geological provinces, and exploration methods: Geological Association of Canada, Mineral Deposits Division, Special Publication*, *5*, 971-982.

Salisbury, M. H., Harvey, C. W., & Matthews, L. (2003). The acoustic properties of ores and host rocks in hardrock terranes. *Hardrock seismic exploration: SEG*, 9-19.

Salisbury, M. H., Milkereit, B., & Bleeker, W. (1996). Seismic imaging of massive sulfide deposits; Part I, Rock properties. *Economic Geology*, *91*(5), 821-828.

Salisbury, M. H., Milkereit, B., Ascough, G., Adair, R., Matthews, L., Schmitt, D. R., ... & Wu, J. (2000). Physical properties and seismic imaging of massive sulfides. *Geophysics*, *65*(6), 1882-1889.

Schmelzbach, C., Simancas, J. F., Juhlin, C., & Carbonell, R. (2008). Seismic reflection imaging over the South Portuguese Zone fold-and-thrust belt, SW Iberia. *Journal of Geophysical Research: Solid Earth*, *113*(B8).

Scott, W. J., & West, G. F. (1969). Induced polarization of synthetic, high-resistivity rocks containing disseminated sulfides. *Geophysics*, *34*(1), 87-100.

Shaw, C. S., 1994, Petrogenesis of the Eastern gabbro, Coldwell Alkaline Complex, Ontario: Ph.D thesis, London, ON, Western University,

Shaw, C. S.,1997, The petrology of the layered gabbro intrusion, eastern gabbro, Coldwell alkaline complex, Northwestern Ontario, Canada: evidence for multiple phases of intrusion in a ring dyke: Lithos, V. 40, p. 243-259.

SJ Geophysics (2011), Geophysical report 3d induced polarization survey on river valley property.

Smith, R. J. (2002). Geophysics or iron oxide copper-gold deposits.

Stillwater Canada In, Environmental Assessement from the Marathon PGM-Cu project at Marathon, Ontario (2012)

Sun, J., & Li, Y. (2015). Advancing the understanding of petrophysical data through joint clustering inversion: A sulfide deposit example from Bathurst Mining Camp. In *SEG Technical Program Expanded Abstracts 2015* (pp. 2017-2021). Society of Exploration Geophysicists.

Watkinson, D. H., & Jones, P. C. (1996). Platinum-group minerals in fluid inclusions from the Marathon deposit, Coldwell Complex, Canada. *Mineralogy and Petrology*, *57*(1), 91-96.

Watkinson, D. H., & Melling, D. R. (1992). Hydrothermal origin of platinum-group mineralization in low-temperature copper sulfide-rich assemblages, Salt Chuck Intrusion, Alaska. *Economic Geology*, *87*(1), 175-184.

Webb, S. J., Ashwal, L. D., Nguuri, T. K., & Cawthorn, R. G. (2004, June). Geophysical constraints on the shape and emplacement of the Bushveld Complex. In *66th EAGE Conference & Exhibition*.

Whiteley, R. J., & Greenhalgh, S. A. (1979). Velocity inversion and the shallow seismic refraction method. *Geoexploration*, *17*(2), 125-141.

Zhao, D. (2009). Multiscale seismic tomography and mantle dynamics. *Gondwana Research*, *15*(3), 297-323.

Zhao, D. (2015). Methodology of Seismic Tomography. In *Multiscale Seismic Tomography* (pp. 21-54). Springer Japan.

Appendix A

Axis orientations of the magnetic susceptibility ellipsoid, calculated with AMS results

Specimen ID	Susc. Axis	Mag. Susc	Dec.	Inc.
KP1.1611	MAX	0.003965	309.2	85.7
KP1.1611	INT	0.00364	97.3	3.6
KP1.1611	MIN	0.003558	187.5	2.2
KP1.1612	MAX	0.066035	245.4	46.7
KP1.1612	INT	0.062935	72.6	42.9
KP1.1612	MIN	0.056554	339.2	3.6
KP1.1461	MAX	0.05609	285.8	10.9
KP1.1461	INT	0.054297	25.6	41.1
KP1.1461	MIN	0.049987	184	46.7
KP1.1462	MAX	0.064506	282.4	2.8
KP1.1462	INT	0.062449	15.7	48.9
KP1.1462	MIN	0.058427	189.9	40.8
KP1.1711	MAX	0.187916	0.1	3.7
KP1.1711	INT	0.181266	264.9	54.3
KP1.1711	MIN	0.171439	92.7	35.3
KP1.1712	MAX	0.106096	228.3	45.2
KP1.1712	INT	0.101727	7.2	36.7
KP1.1712	MIN	0.096725	114.5	21.7
KP1.1741	MAX	0.057521	280.8	22.5
KP1.1741	INT	0.054648	166.5	44.7

KP1.1741	MIN	0.052551	28.9	36.6
KP1.1742	MAX	0.065767	277	21.7
KP1.1742	INT	0.062887	157.9	50.6
KP1.1742	MIN	0.060131	20.9	30.9
KP1.1861	MAX	0.124141	277.5	44.6
KP1.1861	INT	0.114571	132	39.8
KP1.1861	MIN	0.104479	26.2	18
KP1.1862	MAX	0.109912	278.5	45.1
KP1.1862	INT	0.101263	127.6	41
KP1.1862	MIN	0.095455	24.1	15
KP1.1961	MAX	0.005354	272.1	20.7
KP1.1961	INT	0.005077	166.9	34.7
KP1.1961	MIN	0.004002	26.8	47.8
KP1.1962	MAX	0.008089	272	1.4
KP1.1962	INT	0.007693	179.9	51
KP1.1962	MIN	0.005665	3.2	38.9
KP1.2261	MAX	0.012638	1.1	20.5
KP1.2261	INT	0.011759	248.9	45.3
KP1.2261	MIN	0.011358	107.8	37.5
KP1.2262	MAX	0.021446	355.3	21.2
KP1.2262	INT	0.019415	104.5	40.2
KP1.2262	MIN	0.019163	244.6	42.1
KP1.2301	MAX	0.04358	104.6	42.3
KP1.2301	INT	0.042222	295.6	47.1

KP1.2301	MIN	0.037805	199.7	5.4
KP1.2302	MAX	0.058976	87.3	60.1
KP1.2302	INT	0.056595	292	27.5
KP1.2302	MIN	0.049822	196.4	10.6
KP1.2571	MAX	0.011242	307.8	4.9
KP1.2571	INT	0.010835	205.4	68
KP1.2571	MIN	0.010009	39.8	21.2
KP1.2572	MAX	0.020187	263.1	46.3
KP1.2572	INT	0.0192	142	26.2
KP1.2572	MIN	0.017193	34	31.9
KP1.2771	MAX	0.023215	290.6	0.8
KP1.2771	INT	0.022114	199.8	47.2
KP1.2771	MIN	0.021057	21.4	42.7
KP1.2772	MAX	0.02203	293.2	1.9
KP1.2772	INT	0.020886	201.5	42
KP1.2772	MIN	0.019812	25.3	47.8
KP1.2931	MAX	0.050275	305.5	18
KP1.2931	INT	0.046322	212.9	7.8
KP1.2931	MIN	0.042005	100.3	70.2
KP1.2932	MAX	0.038185	302	18.9
KP1.2932	INT	0.035785	204.7	20.4
KP1.2932	MIN	0.03238	71.3	61.5
KP1.3301	MAX	0.033663	240	28
KP1.3301	INT	0.029935	136.8	23

KP1.3301	MIN	0.025719	13.5	52.2
KP1.3302	MAX	0.047225	242.9	31.3
KP1.3302	INT	0.039095	333.1	0.1
KP1.3302	MIN	0.033237	63.2	58.6
KP1.3441	MAX	0.113424	147.3	13.1
KP1.3441	INT	0.11044	258.8	57.6
KP1.3441	MIN	0.103741	49.8	29
KP1.3442	MAX	0.101691	136.6	0
KP1.3442	INT	0.098968	226.7	62.4
KP1.3442	MIN	0.093489	46.5	27.5
KP1.3521	MAX	0.130149	160.2	47.8
KP1.3521	INT	0.124143	294.1	32.1
KP1.3521	MIN	0.121832	40.5	24.1
KP1.3522	MAX	0.126363	181.8	44.5
KP1.3522	INT	0.120106	286.7	14.6
KP1.3522	MIN	0.114767	30.2	41.7
KP2.0061	MAX	0.043273	79.9	13.4
KP2.0061	INT	0.041663	276.5	75.9
KP2.0061	MIN	0.03827	170.9	3.8
KP2.0062	MAX	0.018512	243.5	65.9
KP2.0062	INT	0.01782	105.9	18.2
KP2.0062	MIN	0.016736	10.8	15
KP2.0221	MAX	0.018801	274.9	7.8
KP2.0221	INT	0.018294	45	77.9

KP2.0221	MIN	0.01689	183.6	9.1
KP2.0222	MAX	0.018794	268.7	4.4
KP2.0222	INT	0.018301	21.8	78.6
KP2.0222	MIN	0.016867	177.9	10.3
KP2.0222	MAX	0.026305	61.1	47.1
KP2.0222	INT	0.025332	277	36.9
KP2.0222	MIN	0.023298	172.3	18.5
KP2.1281	MAX	0.090124	37.1	81
KP2.1281	INT	0.089446	274.9	4.7
KP2.1281	MIN	0.086619	184.3	7.5
KP2.1282	MAX	0.090973	132.4	70.5
KP2.1282	INT	0.090123	265.8	13.6
KP2.1282	MIN	0.087403	359.2	13.5
KP2.0241	MAX	0.021353	313.3	0
KP2.0241	INT	0.014942	223.7	88.7
KP2.0241	MIN	0.007958	43.3	1.2
KP2.0242	MAX	0.017844	96.7	0
KP2.0242	INT	0.017337	186.9	77.9
KP2.0242	MIN	0.01667	6.7	12
KP2.0271	MAX	0.044325	0.9	43.8
KP2.0271	INT	0.041586	171.8	45.8
KP2.0271	MIN	0.037737	266.5	4.5
KP2.0272	MAX	0.051961	240	50
KP2.0272	INT	0.049205	21	33

KP2.0272	MIN	0.04708	124.5	19.7
KP2.0451	MAX	0.032873	116.2	68.7
KP2.0451	INT	0.032376	299.3	21.2
KP2.0451	MIN	0.031281	208.9	1
KP2.0452	MAX	0.031381	119.6	62.1
KP2.0452	INT	0.030856	303.4	27.8
KP2.0452	MIN	0.029751	212.5	1.5
KP2.0621	MAX	0.021683	288.6	55.1
KP2.0621	INT	0.02112	95.5	34.1
KP2.0621	MIN	0.01987	189.7	6.1
KP2.0622	MAX	0.023783	52.3	43.9
KP2.0622	INT	0.020063	267.9	40.1
KP2.0622	MIN	0.003501	161.3	18.6
KP2.0721	MAX	0.012868	93.5	28.3
KP2.0721	INT	0.012644	295.9	59.7
KP2.0721	MIN	0.012452	188.8	9.6
KP2.0722	MAX	0.01241	101.1	27.8
KP2.0722	INT	0.012298	261.2	60.7
KP2.0722	MIN	0.011959	6.6	8.4
KP2.0841	MAX	0.05726	218.4	75.6
KP2.0841	INT	0.055948	93.1	8.3
KP2.0841	MIN	0.053879	1.4	11.5
KP2.0842	MAX	0.05559	147.1	67.7
KP2.0842	INT	0.054904	277	14.6

KP2.0842	MIN	0.053	11.4	16.2
KP2.1061	MAX	0.025311	243.3	27.1
KP2.1061	INT	0.024898	139.1	25.5
KP2.1061	MIN	0.024021	12.7	51
KP2.1062	MAX	0.019657	294.4	9.3
KP2.1062	INT	0.019124	197.7	35.5
KP2.1062	MIN	0.018668	37	52.8
KP2.1121	MAX	0.110076	90.8	11.9
KP2.1121	INT	0.107168	232.6	74.9
KP2.1121	MIN	0.062272	358.8	9
KP2.1122	MAX	0.118382	91.2	16.7
KP2.1122	INT	0.115419	239.3	70.5
KP2.1122	MIN	0.066005	358.2	9.6
KP2.1311	MAX	0.010121	254.9	60.9
KP2.1311	INT	0.009482	147	9.6
KP2.1311	MIN	0.008873	52	27
KP2.1312	MAX	0.022372	320	61.7
KP2.1312	INT	0.019746	85.8	17.4
KP2.1312	MIN	0.0131	182.9	21.4
KP2.1451	MAX	0.083076	179.4	27.4
KP2.1451	INT	0.078001	302.5	46.4
KP2.1451	MIN	0.070589	71.4	30.8
KP2.1452	MAX	0.10541	129.2	76.8
KP2.1452	INT	0.09944	357.8	8.7

KP2.1452	MIN	0.089054	266.3	9.6
KP2.1581	MAX	0.14369	137.9	45.1
KP2.1581	INT	0.135069	13.6	29.3
KP2.1581	MIN	0.128841	264.2	30.5
KP2.1582	MAX	0.128847	110.6	15.1
KP2.1582	INT	0.11345	336.1	68.8
KP2.1582	MIN	0.110654	204.6	14.3
KP2.1681	MAX	0.056265	276.2	16.4
KP2.1681	INT	0.05356	105.5	73.3
KP2.1681	MIN	0.051777	6.9	2.5
KP2.1682	MAX	0.058844	271.2	16
KP2.1682	INT	0.0561	38.4	64.5
KP2.1682	MIN	0.054346	175.5	19.2
KP2.1881	MAX	0.158097	297.8	10.2
KP2.1881	INT	0.153375	181	68
KP2.1881	MIN	0.147016	31.4	19.1
KP2.1882	MAX	0.161085	299.4	5.2
KP2.1882	INT	0.156818	196	68.4
KP2.1882	MIN	0.149199	31.4	20.8
KP2.2051	MAX	0.121807	290.7	20.4
KP2.2051	INT	0.117679	76.6	65.7
KP2.2051	MIN	0.109908	196	12.4
KP2.2052	MAX	0.112944	119.1	11.9
KP2.2052	INT	0.110819	353.9	69.8

KP2.2052	MIN	0.102653	212.6	15.9
KP2.2081	MAX	0.108147	287.2	33.2
KP2.2081	INT	0.106664	134.5	53.5
KP2.2081	MIN	0.101052	26	13.1
KP2.2082	MAX	0.133039	293.4	26.3
KP2.2082	INT	0.129505	149.4	58.4
KP2.2082	MIN	0.123453	31.6	15.9
KP2.2141	MAX	0.071713	303.5	73.3
KP2.2141	INT	0.070892	97.8	15.1
KP2.2141	MIN	0.067784	189.6	6.9
KP2.2142	MAX	0.004283	13.5	32.6
KP2.2142	INT	0.004236	129.8	34.6
KP2.2142	MIN	0.004072	253	38.3
KP2.2701	MAX	0.047553	104.2	40.6
KP2.2701	INT	0.045091	329.7	39.2
KP2.2701	MIN	0.042511	217.5	24.7
KP2.2501	MAX	0.031267	34.2	67.9
KP2.2501	INT	0.030431	289.6	5.7
KP2.2501	MIN	0.027686	197.4	21.1
KP2.2702	MAX	0.051754	108.3	33.5
KP2.2702	INT	0.048488	334.2	46.4
KP2.2702	MIN	0.044941	215.7	24.3
KP2.2502	MAX	0.025519	1.9	72.5
KP2.2502	INT	0.025044	107	4.6

KP2.2502	MIN	0.023357	198.4	16.7
KP3.0081	MAX	0.764581	57.3	15.8
KP3.0081	INT	0.748155	294.3	62.3
KP3.0081	MIN	0.736393	153.9	21.9
KP3.0082	MAX	0.730713	240.7	11.1
KP3.0082	INT	0.722003	117	70.3
KP3.0082	MIN	0.715121	333.9	15.9
KP3.0121	MAX	0.097367	239.7	30.6
KP3.0121	INT	0.094691	11.8	48.4
KP3.0121	MIN	0.0898	133.6	25
KP3.0123	MAX	0.173154	211.1	11.3
KP3.0123	INT	0.16364	5.9	77.5
KP3.0123	MIN	0.153539	120.1	5.1
KP3.0151	MAX	0.22035	145.5	36.1
KP3.0151	INT	0.209811	316.9	53.5
KP3.0151	MIN	0.205572	52.5	4
KP3.0153	MAX	0.199151	194.3	71.3
KP3.0153	INT	0.193802	58.5	13.5
KP3.0153	MIN	0.183529	325.4	12.5
KP3.0154	MAX	0.187999	138.6	31.1
KP3.0154	INT	0.181508	31.8	25.5
KP3.0154	MIN	0.179223	270.2	47.7
KP3.0152	MAX	0.089607	170.3	7.9
KP3.0152	INT	0.08642	261.4	7.7

KP3.0152	MIN	0.080341	35.2	78.8
KP3.0201	MAX	0.101588	209.5	13.1
KP3.0201	INT	0.095503	53.1	75.6
KP3.0201	MIN	0.088182	300.8	5.5
KP3.0202	MAX	0.068987	208.7	7.8
KP3.0202	INT	0.065794	81.1	77.3
KP3.0202	MIN	0.059723	300.1	9.8
KP3.0341	MAX	0.18285	163.8	27.3
KP3.0341	INT	0.171321	254.5	1.3
KP3.0341	MIN	0.139602	347.2	62.6
KP3.0342	MAX	0.165472	166.3	29.2
KP3.0342	INT	0.152615	76	0.3
KP3.0342	MIN	0.122001	345.5	60.7
KP3.0052	MAX	0.147275	321.4	4.6
KP3.0052	INT	0.134283	217.1	72
KP3.0052	MIN	0.112091	52.9	17.3
KP3.0051	MAX	0.154748	320.7	4.7
KP3.0051	INT	0.142347	213	74.5
KP3.0051	MIN	0.11858	51.9	14.6
KP3.0661	MAX	0.143978	176.4	36.9
KP3.0661	INT	0.12841	73.7	16.2
KP3.0661	MIN	0.116015	324.5	48.5
KP3.0662	MAX	0.156672	178.1	41.9
KP3.0662	INT	0.131923	80.7	8.2

KP3.0662	MIN	0.112116	341.8	46.8
KP3.0781	MAX	0.177056	197.9	38.5
KP3.0781	INT	0.158199	89.5	21.6
KP3.0781	MIN	0.126372	337.3	43.6
KP3.0782	MAX	0.179903	200.7	35.2
KP3.0782	INT	0.164217	77.3	37.8
KP3.0782	MIN	0.125483	317.6	32.5
KP3.0951	MAX	0.137448	179.2	35.4
KP3.0951	INT	0.126366	75.9	17.9
KP3.0951	MIN	0.118617	324.1	48.9
KP3.0952	MAX	0.137753	181.2	38.3
KP3.0952	INT	0.126393	82.7	10.6
KP3.0952	MIN	0.119613	339.9	49.6
KP3.1092	MAX	0.124338	196.5	35.2
KP3.1092	INT	0.118174	89.2	22.7
KP3.1092	MIN	0.110759	333.6	45.9
KP3.1091	MAX	0.138582	193.7	39.3
KP3.1091	INT	0.131618	83.9	22.4
KP3.1091	MIN	0.122094	331.9	42.2
KP3.1251	MAX	0.098009	207.3	29.9
KP3.1251	INT	0.095811	95.7	32.5
KP3.1251	MIN	0.091532	329.5	42.7
KP3.1252	MAX	0.093099	205.9	27.5
KP3.1252	INT	0.091079	99.2	28.8

KP3.1252	MIN	0.087074	331.3	48
KP3.1541	MAX	0.149144	302	1.2
KP3.1541	INT	0.144865	209.3	65.3
KP3.1541	MIN	0.130959	32.6	24.6
KP3.1542	MAX	0.128141	147.4	39.3
KP3.1542	INT	0.122589	283.1	41.1
KP3.1542	MIN	0.116706	36.1	23.9
KP3.1381	MAX	0.154497	200.2	23.7
KP3.1381	INT	0.14842	98.1	25.4
KP3.1381	MIN	0.13272	327.3	53.8
KP3.1382	MAX	0.146561	45	0.7
KP3.1382	INT	0.140889	135.4	28.8
KP3.1382	MIN	0.133266	313.7	61.1
KP3.1543	MAX	0.139752	123.9	15.3
KP3.1543	INT	0.135641	245.3	62.2
KP3.1543	MIN	0.1237	27.4	22.5
KP3.1544	MAX	0.129287	87.6	21.3
KP3.1544	INT	0.12045	351.2	16
KP3.1544	MIN	0.087966	227.1	62.8
KP3.1702	MAX	0.084383	146	30.2
KP3.1702	INT	0.078742	237.1	1.7
KP3.1702	MIN	0.066813	330	59.7
KP3.1701	MAX	0.105684	144.6	34.5
KP3.1701	INT	0.096727	239.4	6.9

KP3.1701	MIN	0.081023	339.2	54.6
KP3.1871	MAX	0.084741	158.6	31.9
KP3.1871	INT	0.083372	65.1	5.5
KP3.1871	MIN	0.074907	326.3	57.4
KP3.1872	MAX	0.077047	196.2	25.8
KP3.1872	INT	0.073829	102.4	7.6
KP3.1872	MIN	0.067923	357.1	62.8
KP3.1992	MAX	0.094269	161.5	26.1
KP3.1992	INT	0.086054	67.4	8.3
KP3.1992	MIN	0.072785	321.2	62.3
KP3.1991	MAX	0.104827	148.5	30.9
KP3.1991	INT	0.093851	54.9	5.9
KP3.1991	MIN	0.081542	315.2	58.3
KP3.2091	MAX	0.188413	126.7	26.6
KP3.2091	INT	0.171046	220	6.6
KP3.2091	MIN	0.133573	322.9	62.4
KP3.2092	MAX	0.167235	149.1	25.6
KP3.2092	INT	0.155792	239.3	0.2
KP3.2092	MIN	0.116704	329.8	64.3
KP3.2141	MAX	0.009775	206.2	27.5
KP3.2141	INT	0.009545	94	35.9
KP3.2141	MIN	0.009177	323.8	41.6
KP3.2142	MAX	0.010156	224.9	26.1
KP3.2142	INT	0.009984	114.8	34.8

KP3.2142	MIN	0.009652	343	43.7
KP3.2361	MAX	0.033456	283	12
KP3.2361	INT	0.032256	168.7	62.4
KP3.2361	MIN	0.032055	18.5	24.3
KP3.2362	MAX	0.025693	108.6	4
KP3.2362	INT	0.025166	206.3	62
KP3.2362	MIN	0.024324	16.5	27.5
KP3.2541	MAX	0.011849	97	18.2
KP3.2541	INT	0.011604	356.8	28.2
KP3.2541	MIN	0.011481	215.6	55.4
KP3.2542	MAX	0.011752	102.1	14.4
KP3.2542	INT	0.011449	194.6	9.6
KP3.2542	MIN	0.011396	317	72.5

Appendix B

Intensity of the Remanent magnetizations, the direction of the magnetization (in declination and inclination) with regards to each demagnetization step is reported in this diagram

Sample ID	Demag Step	Decl Specimen	Incl Specimen	Intensity (CGS)
116101	46	350.5	5.29	2.38E-03
116101	50	349.22	-12.98	1.26E-03
116101	75	351.1	-13.01	1.01E-03
116101	90	355.84	-15.44	8.57E-04
116101	105	353.83	-12.58	6.95E-04
116101	120	359.8	-12.98	6.29E-04
116101	260	0.73	-13.85	6.28E-04
116101	340	2.39	-14.9	6.21E-04
118602	20	335.26	-13.49	8.15E-03
118602	40	343.68	2.88	4.36E-03
118602	50	354.12	-1.64	2.97E-03
118602	75	354.46	9.98	1.76E-03
118602	90	0.16	4.39	1.13E-03
118602	260	359.68	4.21	1.12E-03
118602	340	2.69	3.95	1.13E-03
118603	46	354.13	-4.38	3.17E-03
118603	50	354.36	-16.19	2.23E-03
118603	75	351.49	-2.63	1.39E-03

118603	90	350.41	-21.25	7.79E-04
118603	105	343.55	-7.47	4.48E-04
118603	120	359.67	-8.2	2.71E-04
118603	260	358.34	-9.51	2.73E-04
118603	340	357.26	-8.31	2.70E-04
117402	20	335.04	-44.3	3.55E-03
117402	40	332.1	-15.45	1.35E-03
117402	50	342.45	-10.21	1.01E-03
117402	75	337.24	-0.69	5.66E-04
117402	260	338.23	-1.34	5.66E-04
117402	340	337.32	0.72	5.75E-04
117404	20	354.37	-35.66	3.75E-03
117404	30	341.72	-14.68	2.07E-03
117404	40	345.98	-13.79	1.69E-03
117404	50	339.43	-23.08	1.08E-03
117404	60	338.88	-12.48	6.40E-04
117404	70	343.87	-10.82	5.74E-04
117404	85	347.15	-19.83	3.23E-04
117404	105	328.56	-14.79	1.81E-04
117404	120	344.57	-13.52	2.17E-04
117404	260	346.05	-14.14	2.16E-04
117404	340	347.01	-13.39	2.12E-04
202203	20	254.19	-54.81	1.10E-03
202203	40	261.48	-14.07	4.36E-04

202203	60	243.37	-7.18	1.86E-04
202203	75	247.35	1.94	1.10E-04
202203	260	246.8	1.85	1.10E-04
202203	340	248.19	2.12	1.11E-04
305001	20	85.38	-68.49	2.42E-03
305001	40	153.83	-70.38	5.38E-04
305001	50	98.21	-71.25	3.38E-04
305001	60	109.3	-63.22	1.85E-04
305001	260	117.19	-62.39	1.85E-04
305001	340	111.76	-59.68	1.84E-04
307803	20	62.27	-74.46	1.38E-03
307803	30	75.91	-69.86	5.98E-04
307803	40	89.19	-68.49	4.43E-04
307803	50	98.32	-58.24	2.33E-04
307803	60	103.72	-45.27	7.95E-05
307803	75	89.73	-58.44	6.92E-05
307803	90	105.95	-59.74	5.25E-05
307803	260	125.27	-53.76	4.03E-05
307803	340	107.21	-55.28	4.70E-05
306602	20	19.95	1.63	1.74E-03
306602	260	22.22	-2.83	1.52E-03
306602	340	24.51	-4.81	1.21E-03
320901	260	309.89	-72.77	5.17E-03
320901	340	322.06	-77.33	4.37E-03

319903	20	87.68	-58.97	7.29E-04
319903	40	93.82	-43.89	2.30E-04
319903	60	104.76	-42.84	1.62E-04
319903	75	96.76	-36.04	9.42E-05
319903	90	131.24	-28.08	5.89E-05
319903	260	129.66	-28.25	6.12E-05
319903	340	119.38	-28.72	6.43E-05
310903	46	105.91	-57.19	2.08E-04
310903	50	108.8	-53.61	1.46E-04
310903	60	104.28	-49.9	1.37E-04
310903	75	109.19	-47.44	9.61E-05
310903	90	107.2	-42.92	7.54E-05
310903	105	102.4	-43.95	6.76E-05
310903	120	110.65	-47.61	6.06E-05
310903	260	98.75	-39.93	5.50E-05
310903	360	110.14	-50.84	5.83E-05
307804	20	1.99	-31.03	1.73E-03
307804	260	8.65	-34.78	1.47E-03
307804	340	12.84	-35.77	1.24E-03
220802	20	248.4	-50.38	6.14E-03
220802	40	264.41	-11.12	1.67E-03
220802	50	247.45	-13.77	9.17E-04
220802	60	248.5	-36.9	3.70E-04
220802	260	246.32	-36.93	3.71E-04

220802	340	250.6	-37.26	3.79E-04
320902	20	37.45	-31.24	2.18E-03
320902	260	43.41	-35.99	1.96E-03
320902	340	42.9	-35.38	1.96E-03
315403	20	119.35	-66.62	1.15E-03
315403	40	140.12	-55.44	6.46E-04
315403	60	117.61	-51.76	4.91E-04
315403	75	126.45	-47.61	4.05E-04
315403	90	128.38	-49.94	3.80E-04
315403	105	120.95	-49.16	3.11E-04
315403	120	124.54	-50.27	2.78E-04
315403	260	128.97	-48.43	2.75E-04
315403	340	122.43	-44.04	2.91E-04
303402	20	52.98	-41.47	6.23E-03
303402	30	54.45	-35.53	2.13E-03
303402	40	90.59	-50.3	1.08E-03
303402	50	96.55	-53.05	7.88E-04
303402	60	78.51	-43.69	3.30E-04
305003	46	298.87	-57.4	6.09E-03
305003	50	247.88	-72.04	5.03E-04
305003	60	151.25	-62.34	1.85E-04
318703	20	75.35	-42.13	4.64E-04
318703	40	94.86	-36.02	2.86E-04
318703	60	93.13	-34.48	2.50E-04

318703	75	97.73	-33.26	1.84E-04
318703	90	100.84	-35.23	1.62E-04
318703	105	99.34	-32.62	1.50E-04
318703	260	98.94	-31.81	1.48E-04
318703	340	95.62	-31.5	1.51E-04
306601	260	285.34	-64.33	3.28E-03
306601	340	292.16	-72.37	2.32E-03
320903	20	91.77	-65.17	2.76E-03
320903	30	86.4	-54.29	8.75E-04
320903	50	87.71	-49.63	5.04E-04
320903	75	95.52	-48.13	2.96E-04
320903	90	123.98	-39.02	1.19E-04
320903	260	119.55	-43.85	1.10E-04
320903	340	123.45	-35.91	1.13E-04
202702	20	97.74	-25.08	1.77E-02
202702	260	98.18	-26.34	1.72E-02
202702	340	99.68	-28.61	1.70E-02
315401	20	221.47	-67.12	1.11E-03
315401	30	173.15	-71.39	8.00E-04
315401	40	125.68	-63.26	6.17E-04
315401	50	125.26	-53.63	5.23E-04
315401	60	125.58	-52.9	3.88E-04
307802	20	92.56	-67.31	3.37E-04
307802	30	96.17	-63.23	2.53E-04

307802	40	86.64	-63.12	2.26E-04
307802	50	72.38	-55.74	1.72E-04
307802	60	110.39	-35.37	6.64E-05
307802	75	99.54	-62.11	4.21E-05
307802	90	64.83	-43.15	3.11E-05
307802	105	69.74	-54.32	2.32E-05
307802	340	102.72	-43.78	2.22E-05
123002	20	211.35	-24.04	1.86E-04
123002	260	208.53	-27.8	1.40E-04
123002	340	208.28	-26.84	1.27E-04
220803	20	304.57	-74.47	3.86E-03
220803	40	288.75	-28.92	1.43E-03
220803	60	252.51	-15.22	6.84E-04
220803	75	262.15	-3.25	2.96E-04
220803	260	265.13	-3.41	2.97E-04
220803	340	258.64	1.16	3.17E-04
212803	46	240.5	-22.69	1.10E-02
212803	50	238.48	-23.6	1.06E-02
212803	75	233.61	-22.39	8.84E-03
212803	90	235.61	-23.77	7.36E-03
212803	105	239.3	-11.52	4.67E-03
212803	120	238.9	-11.1	3.72E-03
212803	340	240.06	-11.32	3.72E-03
303403	20	59.75	-75.99	7.07E-03

303403	40	35.06	-65.54	1.28E-03
303403	60	84.48	-63.76	5.31E-04
303403	260	86.26	-64.44	5.35E-04
303403	340	78.24	-61.92	5.20E-04
202701	260	46.75	-77.44	4.34E-03
202701	340	51.4	-78.92	4.36E-03
125703	20	279	-18.54	4.99E-03
125703	30	339.5	-19.74	2.28E-03
125703	40	351.45	-16.82	2.30E-03
125703	50	348.17	-13.15	2.21E-03
125703	60	352.74	-13.46	2.19E-03
125703	75	349.84	-14.88	2.01E-03
125703	90	351.87	-10.14	1.71E-03
125703	105	351.37	-6.85	1.54E-03
125703	120	352.59	-6.62	1.28E-03
125703	260	353.63	-7.13	1.27E-03
125703	340	351.78	-6.6	1.27E-03
307801	260	310.98	-55.65	4.72E-03
307801	340	314.65	-55.37	4.33E-03
305004	20	272.48	-25.13	1.33E-02
305004	40	273.67	-37.59	4.74E-03
305004	60	280.38	-43.38	1.52E-03
305004	75	253.33	-61.43	2.00E-04
305004	260	251.83	-60.17	2.03E-04

213103	20	327.47	-66.1	1.14E-03
213103	40	314.55	-65.65	8.74E-04
213103	60	305.43	-65.21	8.58E-04
213103	75	315	-57.42	7.21E-04
213103	90	301.56	-64.51	7.15E-04
213103	105	313.35	-55.01	6.24E-04
213103	120	300.66	-53.49	5.04E-04
213103	260	295.32	-57.04	5.05E-04
213103	340	308.65	-55.78	4.98E-04
213101	20	333.12	-55.61	5.22E-04
213101	30	307.49	-63.12	5.56E-04
213101	40	302.13	-57.95	5.17E-04
213101	50	295.15	-56.58	5.09E-04
213101	60	301.98	-51.43	4.92E-04
213101	75	296.06	-57.99	4.73E-04
213101	90	291.5	-60.64	4.25E-04
213101	105	299.21	-57.97	4.37E-04
213101	120	305.31	-57.32	3.97E-04
213101	340	305.27	-61.93	4.04E-04
210603	20	255.54	-42.75	1.57E-03
210603	30	257.19	-36.2	1.33E-03
210603	40	254.17	-34.59	1.20E-03
210603	50	257.36	-36.89	9.86E-04
210603	60	251.64	-28.23	7.28E-04

210603	75	263.56	-34.35	6.18E-04
210603	90	271.61	-33.25	5.53E-04
210603	105	242.89	-24.67	4.40E-04
210603	340	241.9	-24.34	4.43E-04
210602	20	238.85	-39.11	2.05E-03
210602	260	244.08	-39.21	2.05E-03
210602	340	246.74	-38.79	2.06E-03
306603	20	168.28	-56.66	4.61E-04
306603	30	131.18	-53.24	2.07E-04
306603	40	100.15	-46.86	1.56E-04
306603	50	92.64	-40.12	1.25E-04
306603	60	111.99	-35.78	8.26E-05
306603	75	115.99	-35.82	7.69E-05
306603	90	98.55	-32.41	6.75E-05
306603	105	91.89	-27.87	5.71E-05
306603	120	115.87	-34.97	4.43E-05
306603	260	117.64	-24.88	4.35E-05
306603	340	129.42	-11.18	5.56E-05
133002	20	281.33	-4.8	1.29E-04
133002	260	292.01	-14.92	9.47E-05
133002	340	291.33	-15.09	9.20E-05
123003	20	211.83	-28.73	2.38E-05
123003	30	204.04	-34.18	1.33E-05
123003	40	247.96	-28.72	7.67E-06

123003	50	274.03	-66.48	5.79E-06
123003	60	225.11	-77.58	2.57E-06
123003	75	20.07	-19.1	1.52E-06
123003	260	344.12	15.87	4.62E-06
123003	340	335.37	-5.46	3.43E-06
202403	20	260.31	-36.56	1.74E-03
202403	40	266.98	-4.7	5.31E-04
202403	60	242.01	-7.01	1.80E-04
202403	75	235.67	9.01	1.23E-04
202403	260	234.88	9.37	1.24E-04
202403	340	236.2	8.32	1.24E-04
133001	260	270.39	-43.54	6.48E-04
133001	340	270.41	-46.82	4.56E-04
133003	20	311.28	-64.91	3.85E-05
133003	30	310.33	-35.65	1.39E-05
133003	40	333.28	-20.31	1.07E-05
133003	50	330.54	-30.08	7.35E-06
133003	60	337.42	-35.57	4.65E-06
133003	75	310.29	-14.49	3.17E-06
133003	90	336.59	-18.7	2.29E-06
133003	105	20.74	17.96	2.48E-06
133003	120	315.96	-9.86	2.86E-06
133003	260	330.66	-2	1.77E-06
133003	340	273.61	-48.51	2.23E-06

206201	260	228.57	-56.38	1.33E-03
206201	340	230.06	-55.52	1.31E-03
210601	260	258.97	-55.56	3.02E-03
210601	340	259.3	-53.4	3.00E-03
202703	20	221.91	-47.95	5.69E-04
202703	30	232.03	-28.59	1.98E-04
202703	40	245.2	-30.51	1.49E-04
202703	50	256.33	-34.83	1.25E-04
202703	60	256.01	-35.02	9.02E-05
202703	75	262.29	-41.72	7.22E-05
202703	90	263.82	-34.59	6.20E-05
202703	105	233.62	-21.26	7.87E-05
202703	260	233.46	-21.54	7.90E-05
202703	340	233.49	-21.46	7.91E-05
206203	20	230.67	-42.06	1.26E-03
206203	30	236.09	-31.15	1.06E-03
206203	50	243.04	-26.31	8.56E-04
206203	75	251.29	-39.6	4.95E-04
206203	90	235.49	-18.11	2.47E-04
206203	105	247.2	-13.78	1.72E-04
206203	120	245.64	-18.79	1.42E-04
206203	260	246.88	-17.89	1.44E-04
206203	340	245.85	-17.55	1.47E-04
202401	20	259.19	-37.73	2.00E-03

202401	40	263.54	-7.82	6.76E-04
202401	50	248.51	-8.67	3.12E-04
202401	60	262.17	-37.5	1.09E-04
202401	260	265.27	-36.4	1.10E-04
125701	260	225.29	-39.64	6.68E-03
125701	340	225.39	-38.97	6.22E-03
125702	20	299.66	-22.23	2.20E-03
125702	260	304.87	-22.89	1.98E-03
125702	340	304.36	-21.28	1.93E-03
206202	20	231.52	-28.77	1.53E-03
206202	260	235.12	-29.83	1.51E-03
206202	340	237.69	-29.5	1.50E-03
123004	260	239.89	-28.33	3.63E-05
123004	340	240.4	-25.21	3.60E-05
118604	20	341.97	-4.23	7.13E-03
118604	40	357.49	-7.1	4.79E-03
118604	60	355.84	7.8	2.51E-03
118604	75	0.96	3.42	1.70E-03
118604	90	356.04	-22.11	7.78E-04
118604	105	351.78	-2.15	3.38E-04
118604	260	351.05	-2.53	3.40E-04
118604	360	352.63	-1.5	3.51E-04
117103	20	184.36	-40.87	2.66E-04
117103	45	186.02	-39.26	5.23E-05

117103	60	209.49	-30.02	7.04E-06
117103	260	216.82	-34.38	6.12E-06
117103	340	233.22	-23.11	4.95E-06
117404	20	354.37	-35.66	3.75E-03
117404	30	341.72	-14.68	2.07E-03
117404	40	345.98	-13.79	1.69E-03
117404	50	339.43	-23.08	1.08E-03
117404	60	338.88	-12.48	6.40E-04
117404	70	343.87	-10.82	5.74E-04
117404	85	347.15	-19.83	3.23E-04
117404	105	328.56	-14.79	1.81E-04
117404	120	344.57	-13.52	2.17E-04
117404	260	346.05	-14.14	2.16E-04
117404	340	347.01	-13.39	2.12E-04
M238152	10	329.69	4.76	2.66E-03
M238153	15	326.45	6.07	2.41E-03
M238154	20	327.54	7.71	2.21E-03
M238155	25	331.26	7.5	2.01E-03
M238156	30	324.58	10.49	1.34E-03
M238157	40	332.28	11.56	1.01E-03
M238158	50	333.98	7.75	7.19E-04
M238159	60	319.01	18.29	3.04E-04
M238160	75	337.43	3.26	1.88E-04
M238161	90	332.3	11.56	1.02E-04

M238162	105	334.3	51.71	7.09E-05
M238483	10	327.3	14.8	1.49E-03
M238483	15	328.3	16.7	1.11E-03
M238483	20	333.3	17.9	8.63E-04
M238483	25	338.8	12.8	7.08E-04
M238483	30	335.1	16.3	4.38E-04
M238483	40	347.2	17.2	3.00E-04
M238483	50	345.9	10.8	2.08E-04
M238483	60	343.8	17.5	9.89E-05
M238483	75	348.8	15.4	6.88E-05
M238483	90	340.3	10.4	4.09E-05
M238483	105	348.3	18.0	2.25E-05
M238761	10	346.28	-33.36	6.43E-03
M238761	15	347.28	-37.5	5.19E-03
M238761	20	350.19	-36.14	4.33E-03
M238761	25	349.89	-25.62	3.09E-03
M238761	30	348.8	-35.8	1.78E-03
M238761	40	353.45	-34.36	1.23E-03
M238761	50	348.66	-18.6	8.30E-04
M238761	60	352.61	-17.78	4.69E-04
M238761	75	354.15	-34.51	2.30E-04
M238761	90	354.52	-11.91	2.52E-04
M238761	105	344.61	7.1	1.03E-04
SL362022	5	357.61	50.78	6.96E-03

SL362022	10	12.57	55.5	4.88E-03
SL362022	15	11.12	46.01	3.18E-03
SL362022	20	14.71	10.84	1.69E-03
SL362022	25	27.4	9.46	8.70E-04
SL362022	30	18.25	3.57	6.08E-04
SL362022	40	13.64	-12.12	4.29E-04
SL362022	50	28.09	-16.93	2.24E-04
SL362022	60	16.97	-26.9	1.25E-04
SL362022	75	334.14	-20.43	6.98E-05
SL362022	90	41.68	-1.38	5.59E-05
SL362162	0	336.3	60.1	5.38E-03
SL362163	10	341.4	58.9	3.29E-03
SL362164	15	359.7	46.4	2.00E-03
SL362165	20	4.4	6.4	1.04E-03
SL362166	25	17.7	0.4	5.07E-04
SL362167	30	14.5	-7.8	4.13E-04
SL362168	40	12.8	-19.7	3.56E-04
SL362169	50	18.6	-30.8	2.02E-04
SL362170	60	23.1	-37.5	1.32E-04
SL362171	75	29.8	-24.4	9.71E-05
SL362172	90	356.0	-35.7	4.02E-05
SL440202	5	9.5	41.1	4.34E-03
SL440202	10	15.8	39.2	3.97E-03
SL440202	15	17.8	33.7	3.53E-03

SL440202	20	13.8	18.1	2.68E-03
SL440202	25	30.0	23.6	1.66E-03
SL440202	30	18.8	24.7	1.22E-03
SL440202	40	17.9	11.0	7.83E-04
SL440202	50	36.6	16.6	3.75E-04
SL440202	60	35.1	18.0	1.97E-04
SL440202	75	15.3	6.8	1.80E-04
SL440202	90	46.9	21.6	1.10E-04
SL440202	105	75.6	-63.0	1.61E-05
SL440573	5	194.3	44.2	1.58E-02
SL440573	10	211.9	61.5	9.04E-03
SL440573	15	188.8	71.0	3.74E-03
SL440573	20	178.1	66.7	5.22E-04
SL440573	25	23.5	67.2	3.37E-04
SL440573	30	29.9	41.9	2.18E-04
SL440573	40	21.9	24.2	1.59E-04
SL440573	50	4.6	12.5	6.21E-05
SL440573	60	18.3	14.7	1.05E-04
SL442322	5	321.5	55.44	1.02E-02
SL442322	10	328.46	55.89	8.75E-03
SL442322	15	346.19	53.36	6.84E-03
SL442322	20	349.94	31.15	3.89E-03
SL442322	25	351.77	41.79	2.44E-03
SL442322	30	1.98	38.8	1.99E-03

SL442322	40	3.43	24.16	1.40E-03
SL442322	50	9.15	32.39	9.13E-04
SL442322	60	9.82	27.23	6.76E-04
SL442322	75	6.19	18.13	5.27E-04
SL442322	90	26.81	36.52	3.10E-04
SL442322	105	22.44	51.92	1.29E-04
SL560362	10	339.63	17.5	2.24E-03
SL560362	15	335.95	22.47	1.54E-03
SL560362	20	350.07	20.44	1.23E-03
SL560362	30	347.48	7.93	8.20E-04
SL560362	40	328.67	13.45	3.10E-04
SL560362	50	339.71	32.59	1.68E-04
SL560362	60	5.63	12.59	1.05E-04
SL560362	75	310.46	-32.09	1.23E-04
SL560553	10	7.54	2.28	2.16E-03
SL560553	15	7.83	12.3	1.02E-03
SL560553	20	355.03	17.91	7.47E-04
SL560553	30	355.05	11.35	4.77E-04
SL560553	50	1.65	14.25	2.58E-04
SL560553	60	25.01	9.1	1.36E-04
SL560553	75	344.06	46.55	1.24E-04

Appendix C

Densities, Chargeabilities, resistivities, p-wave velocities, acoustic impedances, magnetic susceptibilities and NRMs are reported with regards to the drill hole ID and depth from which the samples were obtained from.

HOLEID	Depth	Density	Chargeability	Resistivity	Pwave	AI	Magsusc	*NRM*
KP-13-01	4.1	3135.55	4.19	4016.44	6986.30	21.91	8294.00	*1062.77*
KP-13-01	4.2	3165.57	1.60	6329.61	7192.59	22.77	8309.00	*2532.31*
KP-13-01	4.3	3203.46	1.00	10024.35	7120.67	22.81	7596.00	*2651.24*
KP-13-01	4.4	3202.88	7.27	22.94	7812.00	603.72		
KP-13-01	17.1	3061.21	3.99	3990.60	6106.52	18.69	17907.00	*4450.84*
KP-13-01	17.2	2966.94	2.50	5285.70	6278.36	18.63	17152.00	*571.96*
KP-13-01	17.3	2952.97	1.72	5113.95	6479.94	19.14	18327.00	*3613.42*
KP-13-01	17.4	2952.19	2.30	6183.82	6546.87	19.33	16492.00	*2245.32*
KP-13-01	33.1	3031.68	3.20	5738.44	6053.79	18.35	19353.00	*4577.27*
KP-13-01	33.2	3063.82	4.99	3410.46	6183.83	18.95	20055.00	*8432.38*
KP-13-01	33.3	3053.35	2.87	6346.55	6020.66	18.38	18796.00	*4875.20*

KP-13-01	33.4	3328.29	5.50	3905.58	5699.24	18.97	19787.00	*3513.92*
KP-13-01	51.1	2822.33	22.94	2232.89	6319.03	17.83	33774.00	*16185.63*
KP-13-01	51.2	2948.75	35.71	1556.20	6164.00	18.18	30047.00	*1628.01*
KP-13-01	51.3	2843.97	3.78	4556.42	6423.49	18.27	35217.00	*2179.34*
KP-13-01	51.4	2850.99	6.98	18.81	34667.00	324.12		
KP-13-01	56.1	2776.45	5.28	6146.29	6605.67	18.34	36157.00	*3451.66*
KP-13-01	56.2	2759.85	3.23	9182.13	6407.99	17.69	31471.00	*942.18*
KP-13-01	56.3	2797.93	7.20	6494.11	6135.86	17.17	35414.00	*4292.05*
KP-13-01	56.4	2826.75	7.94	8905.94	6820.47	19.28	33095.00	*34.04*
KP-13-01	72.1	2975.91	3.48	3999.42	6430.41	19.14	37697.00	*31.57*
KP-13-01	72.2	3042.76	5.45	3258.32	6341.32	19.30	33523.00	*30.60*
KP-13-01	72.3	2952.28	4.64	3506.96	6377.59	18.83	35494.00	*52.57*
KP-13-01	72.4	2891.43	6.02	18.58	34645.00	33.88		
KP-13-01	91.1	3146.40	4.68	3902.28	6271.64	19.73	240.00	*151.47*
KP-13-01	91.2	2731.50	6.73	6495.12	17.74	238.00	22.40	

KP-13-01	91.3	3287.31	2.73	5188.44	6274.51	20.63	245.00	*17.69*
KP-13-01	91.4	250.00	0.01					
KP-13-01	98.1	3007.08	7.31	2950.21	6270.33	18.86	485.00	*162.47*
KP-13-01	98.2	2495.46	5.85	3758.82	6088.26	15.19	1094.00	*3552.82*
KP-13-01	98.3	2898.52	9.93	2380.77	5860.17	16.99	775.00	*425.01*
KP-13-01	98.4	1199.00	4.93					
KP-13-01	118.1	2724.74	1.36	6745.06	6451.27	17.58	181.00	*80.46*
KP-13-01	118.2	5.18	3.70	6552.02	187.00	39.29		
KP-13-01	118.3	3444.58	6.66	171.00	54.91			
KP-13-01	118.4	6617.92	16.00	1613.35				
KP-13-01	137.1	2981.74	4.02	10742.33	6246.43	18.63	13665.00	*6932.77*
KP-13-01	137.2	2931.68	3.87	7092.08	6621.54	19.41	9646.00	*10223.09*
KP-13-01	137.3	2956.64	3.87	6135.02	6910.20	20.43	26891.00	*12154.97*
KP-13-01	137.4	2981.41	5.93	8167.04	6695.96	19.96	12483.00	*5588.24*
KP-13-01	146.1	3176.49	1.72	9187.01	7174.46	22.79	17947.00	*3494.65*

KP-13-01	146.2	3167.89	1.35	6641.07	7113.40	22.53	16932.00	*5367.69*
KP-13-01	146.3	3074.64	3.14	6054.33	6873.71	21.13	22884.00	
KP-13-01	146.4	3157.87	2.35	5456.73	6876.10	21.71	21696.00	*5012.30*
KP-13-01	161.1	2877.06	4.72	6964.94	6589.55	18.96	12621.00	*10521.52*
KP-13-01	161.2	2972.51	13.54	4856.44	6813.12	20.25	16651.00	*6336.20*
KP-13-01	161.3	2939.80	5.65	6005.37	6712.71	19.73	14978.00	*8526.07*
KP-13-01	161.4	6960.87	10.00	3056.18				
KP-13-01	171.1	2737.94	1.10	5416.19	5435.42	14.88	66891.00	*1440.21*
KP-13-01	171.2	2705.26	3.21	7376.21	5501.26	14.88	33948.00	*1356.37*
KP-13-01	171.3	2517.66	3.67	4214.12	4496.03	11.32	6067.00	*168.49*
KP-13-01	171.4	2537.97	5.58	14.65	16205.00	2392.77		
KP-13-01	174.1	3139.03	1.55	11244.54	6862.35	21.54	17733.00	*2444.25*
KP-13-01	174.2	3047.29	1.81	8835.02	6740.06	20.54	17663.00	*2180.03*
KP-13-01	174.3	3019.95	1.81	9026.50	6757.47	20.41	18033.00	*2962.92*
KP-13-01	174.4	3066.68	2.09	7385.30	18497.00	6232.58		

KP-13-01	186.1	3176.35	2.21	4965.30	6974.60	22.15	29549.00	*8174.44*
KP-13-01	186.2	3131.12	3.82	7696.39	6166.25	19.31	28753.00	*7.42*
KP-13-01	186.3	3086.79	6.30	7155.03	6563.15	20.26	25862.00	*12.27*
KP-13-01	186.4	5903.38	2.00	1798.21				
KP-13-01	196.1	3316.97	1.14	8154.16	6825.35	22.64	1271.00	*490.98*
KP-13-01	196.2	3231.32	1.11	10075.72	6807.16	22.00	1842.00	*1164.46*
KP-13-01	196.3	3080.75	1.21	6657.39	7084.14	21.82	2646.00	*184.47*
KP-13-01	196.4	3211.69	3.06	7141.33	7217.31	23.18	804.00	*511.81*
KP-13-01	226.1	3432.05	33.00	1411.75	6873.04	23.59	44205.00	*17697.00*
KP-13-01	226.2	2795.72	21.01	1409.72	6954.69	19.44	83657.00	*2572.77*
KP-13-01	226.3	4036.48	15.60	2442.42	6664.79	26.90	84963.00	*6.73*
KP-13-01	226.4	2220.83	13.53	6198.27	7227.80	16.05	58662.00	*162.32*
KP-13-01	230.1	2646.28	1.75	6470.09	5822.38	15.41	12085.00	*828.34*
KP-13-01	230.2	2695.57	3.39	6006.56	5618.32	15.14	18068.00	*57.80*
KP-13-01	230.3	2640.63	1.96	5039.11	5581.72	14.74	3534.00	*103.99*

KP-13-01	230.4	2649.39	4.74	3890.91	5229.05	13.85	3381.00	*99.06*
KP-13-01	257.1	3078.33	9.05	3467.37	6470.42	19.92	40407.00	*2043.30*
KP-13-01	257.2	3155.17	13.49	3888.74	6531.68	20.61	63241.00	*30761.79*
KP-13-01	257.3	3058.93	12.47	5098.19	6451.34	19.73	56995.00	*3313.20*
KP-13-01	257.4	3057.96	8.23	5723.03	6394.34	19.55	76413.00	*12000.65*
KP-13-01	277.1	2519.06	3.25	5363.17	5811.05	14.64	6974.00	*175.64*
KP-13-01	277.2	2570.77	1.59	7241.79	5582.20	14.35	6968.00	*31.01*
KP-13-01	277.3	4.02	4.29	5656.30	4821.00	91.38		
KP-13-01	277.4	6149.04	5.00	61.49				
KP-13-01	293.1	2667.52	1.58	6022.04	5855.22	15.62	14448.00	*141.36*
KP-13-01	293.2	2724.54	3.35	5363.12	5745.09	15.65	13269.00	*113.16*
KP-13-01	293.3	2685.46	2.33	6996.68	5887.30	15.81	13408.00	*327.99*
KP-13-01	293.4	2611.78	1.21	7026.98	5644.33	14.74	13998.00	*81.16*
KP-13-01	330.1	3005.91	6.33	3384.91	5715.97	17.18	9047.00	*889.25*
KP-13-01	330.2	2544.97	9.70	2230.79	5763.51	14.67	13704.00	*68.19*

KP-13-01	330.3	2914.71	7.22	2443.99	5928.10	17.28	3551.00	*745.24*
KP-13-01	330.4	2548.27	9.47	2073.21	6953.00	5061.64		
KP-13-01	344.1	3050.92	14.69	6821.86	6988.34	21.32	31701.00	*10230.71*
KP-13-01	344.2	3061.84	11.18	3504.29	6361.66	19.48	28925.00	*4968.66*
KP-13-01	344.3	3063.06	13.17	10309.21	7026.95	21.52	28607.00	*11777.11*
KP-13-01	344.4	3113.46	11.56	6390.74	6864.41	21.37	27720.00	
KP-13-01	352.1	11.60	34.18	6686.49				
KP-13-01	352.2	13.66	48.27	6172.36				
KP-13-01	352.3	15.16	36.33	6578.43				
KP-13-02	6.1	2986.15	2.95	5245.88	6699.00	20.00	11138.00	*4395.23*
KP-13-02	6.2	2.95	51.99	6763.72	5119.00	1055.72		
KP-13-02	6.3	3041.45	2.95	6225.37	6428.78	19.55	2228.00	*1126.18*
KP-13-02	6.4	2347.67	11.00	5642.88				
KP-13-02	22.1	5.13	37.37	5331.69				
KP-13-02	22.2	3.58	67.45	5197.37				

KP-13-02	22.3	5.20	69.87	4661.07				
KP-13-02	22.4	3.52	55.40	5794.78				
KP-13-02	24.1	4.95	28.97	6157.94				
KP-13-02	24.2	4.79	34.16	7314.87				
KP-13-02	24.3	7.53	30.35	5840.21				
KP-13-02	24.4	4.11	69.18	7319.65				
KP-13-02	27.1	3079.72	12.19	6253.14	5014.86	15.44	12259.00	*31667.43*
KP-13-02	27.2	2991.13	7.40	6445.40	5195.71	15.54	17438.00	*678.75*
KP-13-02	27.3	3003.74	5.10	3441.36	6821.73	20.49	3158.00	*664.12*
KP-13-02	27.4	3005.13	2.24	8657.57	3048.00	4298.36		
KP-13-02	45.1	3136.90	2.61	4325.97	7060.92	22.15	8810.00	*4474.71*
KP-13-02	45.2	3071.34	2.39	6595.68	7067.79	21.71	8928.00	*6013.57*
KP-13-02	45.3	3154.89	1.27	10418.33	7193.09	22.69	9954.00	*5777.22*
KP-13-02	45.4	3115.73	1.34	11389.30	7065.81	22.02	9638.00	*2846.42*
KP-13-02	62.1	3083.40	1.90	6890.33	6424.29	19.81	5706.00	*2499.61*

KP-13-02	62.2	3049.98	1.70	6505.39	6278.64	19.15	5349.00	*14.30*
KP-13-02	62.3	3076.88	3.34	4368.32	6208.65	19.10	5433.00	*1540.78*
KP-13-02	62.4	6904.83	52.00	9323.01				
KP-13-02	72.1	3063.62	2.00	6079.47	6864.85	21.03	3563.00	*2845.07*
KP-13-02	72.2	2993.66	1.54	4973.81	6986.97	20.92	3594.00	*3478.20*
KP-13-02	72.3	3019.04	1.92	7626.96	6916.60	20.88	4675.00	*3922.56*
KP-13-02	72.4	6935.54	59.00	340.65				
KP-13-02	84.1	3119.86	3.80	7530.51	7064.33	22.04	14867.00	*16392.66*
KP-13-02	84.2	3154.52	3.97	4743.84	7150.23	22.56	14873.00	*9239.69*
KP-13-02	84.3	3166.95	2.43	8414.34	7049.65	22.33	17927.00	*12425.24*
KP-13-02	84.4	3157.84	2.48	9477.24	6948.55	21.94	17335.00	*2549.89*
KP-13-02	106.1	3159.67	2.78	7665.65	5912.77	18.68	6849.00	*3525.81*
KP-13-02	106.2	3000.48	2.09	9623.35	5399.95	16.20	5554.00	*18.56*
KP-13-02	106.3	2841.98	1.58	5841.41	6654.28	18.91	4353.00	*19.20*
KP-13-02	106.4	3017.34	2.33	5195.97	6944.69	20.95	5454.00	*2200.73*

KP-13-02	112.1	3111.74	26.88	1923.81	5954.35	18.53	20162.00	*16101.18*
KP-13-02	112.2	3015.66	24.84	2644.08	6114.06	18.44	19343.00	*4431.89*
KP-13-02	112.3	3081.84	30.34	2720.50	6477.09	19.96	19464.00	*30441.69*
KP-13-02	112.4	3113.42	29.14	2011.68	6284.20	19.57	20251.00	*17272.05*
KP-13-02	128.1	3163.90	3.92	4167.49	7224.37	22.86	23489.00	*26717.55*
KP-13-02	128.2	3245.91	2.06	9434.22	6937.04	22.52	23730.00	*21169.44*
KP-13-02	128.3	3265.28	6.47	7215.84	5810.42	18.97	27754.00	*20504.12*
KP-13-02	128.4	3276.63	1.93	9191.27	6701.59	21.96	24955.00	*10283.88*
KP-13-02	131.1	2947.52	3.92	4237.21	6187.89	18.24	2741.00	*2930.46*
KP-13-02	131.2	2848.93	2.96	8621.13	6701.44	19.09	5094.00	*1151.19*
KP-13-02	131.3	13.70	4047.31	6288.66	11455.00	4675.55		
KP-13-02	131.4	18.57	3516.02	19555.00	3506.59			
KP-13-02	145.1	3030.26	14.03	5639.02	7063.89	21.41	23183.00	*57099.37*
KP-13-02	145.2	2955.53	42.88	2131.73	7058.82	20.86	35106.00	*668.15*
KP-13-02	145.3	10.07	6413.00	2965.00	6554.58			

KP-13-02	145.4	4.51	6413.00	6377.00	9813.64			
KP-13-02	158.1	3051.93	4.29	6243.04	6905.59	21.08	39459.00	*24666.03*
KP-13-02	158.2	2821.87	4.29	5813.75	7040.11	19.87	40238.00	*2649.91*
KP-13-02	158.3	2951.01	29.14	3808.86	7145.52	21.09	14081.00	*8956.57*
KP-13-02	158.4	39078.00	512.01					
KP-13-02	168.1	2797.80	5.41	4573.84	6358.70	17.79	15661.00	*1650.81*
KP-13-02	168.2	2847.23	6326.37	18.01	16483.00	574.21		
KP-13-02	168.3	2832.27	3.24	2765.09	6046.69	17.13	14914.00	*1746.52*
KP-13-02	168.4	3.91	5925.03	14119.00	204.27			
KP-13-02	188.1	3104.33	10.01	5774.88	5537.29	17.19	43908.00	*13091.82*
KP-13-02	188.2	3156.53	9.80	4958.16	5459.62	17.23	43113.00	*10259.42*
KP-13-02	188.3	3123.16	10.69	6484.50	5320.61	16.62	43006.00	*10927.65*
KP-13-02	188.4	3158.13	9.98	5785.52	5327.19	16.82	42409.00	*1778.10*
KP-13-02	205.1	2935.18	3.37	7534.35	6894.81	20.24	31737.00	*6325.11*
KP-13-02	205.2	4.00	5896.81	6756.00	30371.00	1668.61		

KP-13-02	205.3	3028.90	4.52	3682.12	6384.13	19.34	34787.00	*9305.40*
KP-13-02	205.4	3066.01	34729.00	6866.04				
KP-13-02	208.1	2979.84	6.15	7269.19	6379.40	19.01	29139.00	*1449.88*
KP-13-02	208.2	3099.16	10.45	4786.05	5164.88	16.01	36014.00	*8491.87*
KP-13-02	208.3	3062.21	5385.91	16.49	36522.00	9625.26		
KP-13-02	208.4	3126.00	7.07	6553.78	6309.30	19.72	37039.00	*3524.15*
KP-13-02	214.1	3030.65	5.95	3721.89	6186.19	18.75	21900.00	*239.51*
KP-13-02	214.2	3139.75	3.46	5161.88	6603.72	20.73	1212.00	*651.82*
KP-13-02	214.3	3139.58	3.86	5790.38	6757.80	21.22	6768.00	*6680.90*
KP-13-02	214.4	3142.93	2.37	7088.36	5543.05	17.42	3002.00	*837.33*
KP-13-02	250.1	2690.04	2.42	4858.78	6059.28	16.30	9311.00	*543.09*
KP-13-02	250.2	2692.58	1.39	9978.95	6128.19	16.50	7917.00	*224.75*
KP-13-02	250.3	2619.35	2.04	6728.19	6044.65	15.83	8150.00	*1341.86*
KP-13-02	250.4	1.69	6942.93	10344.00	222.09			
KP-13-02	270.1	2705.60	3.13	5363.03	5976.29	16.17	14150.00	*495.97*

KP-13-02	270.2	2535.38	2.04	6349.32	6585.71	16.70	16390.00	*168.24*
KP-13-02	270.3	2589.73	2.33	6011.88	5969.63	15.46	9775.00	*484.56*
KP-13-02	270.4	2.82	6252.48	9143.00				
KP-13-03	8.1	2787.47	39.38	652.75	6492.68	18.10	176668.00	
KP-13-03	8.2	2537.03	70.06	716.72	6773.90	17.19	178888.00	
KP-13-03	8.3	53.04	639.49	6778.29	198608.00			
KP-13-03	8.4	2786.02	61.59	309.36	6734.99	18.76	238830.00	
KP-13-03	12.1	2841.47	8.47	6788.32	6650.69	18.90	29061.00	*2679.42*
KP-13-03	12.2	2033.38	12.58	5203.20	8260.87	16.80		
KP-13-03	12.3	6354.19	50144.00	1432.84				
KP-13-03	12.4	5861.61	47857.00	4978.10				
KP-13-03	15.1	2775.39	11.02	9382.37	6413.99	17.80	62344.00	*13159.81*
KP-13-03	15.2	2985.01	90.56	2489.27	6248.07	18.65	60895.00	
KP-13-03	15.3	6914.33	53994.00	6798.90				
KP-13-03	15.4	2993.30	75115.00	23998.84				

KP-13-03	20.1	3023.95	19.12	2932.76	6600.72	19.96	28473.00	*2467.35*
KP-13-03	20.2	2508.41	2.58	7400.36	6189.76	15.53	22609.00	*7659.32*
KP-13-03	20.3	3453.49	6468.06	22.34	31588.00	8818.34		
KP-13-03	20.4	6.35	3391.66	6695.15	28333.00	4324.62		
KP-13-03	34.1	3108.25	3.26	8133.73	6516.33	20.25	49027.00	*2343.77*
KP-13-03	34.2	3065.68	3.48	9151.90	6544.72	20.06	50060.00	*7496.56*
KP-13-03	34.3	3083.02	4.38	8253.25	6366.02	19.63	48306.00	*3447.19*
KP-13-03	34.4	3106.10	4.41	4301.09	6857.06	21.30	47944.00	*6609.18*
KP-13-03	50.1	3059.31	3.34	4712.26	5304.17	16.23	41555.00	*1351.33*
KP-13-03	50.2	3055.54	3.34	4823.30	5709.39	17.45	40984.00	*55297.46*
KP-13-03	50.3	2989.89	2.50	6289.02	5512.54	16.48	41448.00	*1005.66*
KP-13-03	50.4	5047.56	43906.00	12852.22				
KP-13-03	66.1	3002.60	4.82	6251.88	5648.52	16.96	37812.00	*657.98*
KP-13-03	66.2	3020.84	5580.07	16.86	38313.00	5998.88		
KP-13-03	66.3	2946.43	6.23	3390.58	5648.24	16.64	37097.00	*238.63*

KP-13-03	66.4	3.88	6856.88	6221.04	34258.00	2734.16		
KP-13-03	78.1	3044.08	5.81	4052.53	6195.82	18.86	42483.00	*132.71*
KP-13-03	78.2	3023.56	4.31	5517.56	5715.64	17.28	44625.00	*1363.84*
KP-13-03	78.3	45576.00	645.23					
KP-13-03	78.4	43077.00	5855.45					
KP-13-03	95.1	3029.90	5.73	4083.12	6589.58	19.97	37906.00	*567.88*
KP-13-03	95.2	3039.59	5952.56	18.09	38855.00	6765.85		
KP-13-03	95.3	5.61	4369.46	6293.93	41251.00	751.71		
KP-13-03	95.4	6204.51	41681.00	3536.90				
KP-13-03	109.1	3004.30	4.84	5313.46	5939.33	17.84	37575.00	*867.35*
KP-13-03	109.2	3220.68	5.21	3759.62	6108.87	19.67	35983.00	*4581.13*
KP-13-03	109.2	2979.99	6.44	4083.63	5504.20	16.40	37531.00	*1090.41*
KP-13-03	109.4	3030.19	6.27	3990.11	27531.00	4982.46		
KP-13-03	125.1	2972.39	2.95	3888.02	6557.65	19.49	27136.00	*1651.63*
KP-13-03	125.2	2978.83	2.43	2914.41	6465.47	19.26	27555.00	*6942.98*

KP-13-03	125.3	2947.86	2.57	3643.15	6681.88	19.70	27524.00	*1608.16*
KP-13-03	125.4	2998.34	4.44	2820.25	41625.00	5477.70		
KP-13-03	138.1	3067.37	5.41	4030.42	6330.02	19.42	43210.00	*1203.70*
KP-13-03	138.2	6425.19	40211.00	7374.91				
KP-13-03	138.3	2932.09	5.10	3492.51	6386.14	18.72	42835.00	*1278.03*
KP-13-03	138.4	2954.60	5.41	4603.55	6507.94	19.23	38397.00	*7605.54*
KP-13-03	154.1	5.26	6148.52	6199.62	37256.00	1212.86		
KP-13-03	154.2	6327.56	38085.00	4176.46				
KP-13-03	154.3	6624.69	37457.00	1095.26				
KP-13-03	170.1	2974.91	1.86	7291.44	6738.49	20.05	23850.00	*1009.76*
KP-13-03	170.2	2943.10	2.05	7645.27	6853.80	20.17	24081.00	*4142.63*
KP-13-03	170.3	2919.23	1.70	6445.75	6735.94	19.66	30031.00	*829.93*
KP-13-03	170.4	6621.17	23684.00	2675.05				
KP-13-03	187.1	2853.34	4.20	8088.94	6691.14	19.09	25490.00	*621.81*
KP-13-03	187.2	2979.00	3.76	6110.27	6622.68	19.73	25401.00	*3053.84*

KP-13-03	187.3	2998.60	6.32	4230.08	7572.63	22.71	24204.00	*972.97*
KP-13-03	187.4	2936.76	4.77	5793.35	6711.05	19.71	28714.00	*2836.80*
KP-13-03	199.1	2973.71	2.01	5504.09	5701.40	16.95	27598.00	*952.55*
KP-13-03	199.2	2980.31	3.64	5614.22	6015.28	17.93	23960.00	*4058.97*
KP-13-03	199.3	2959.25	2.34	4864.51	5603.99	16.58	23086.00	*1012.54*
KP-13-03	199.4	2931.50	2.01	6814.86	5741.34	16.83	49368.00	*2924.62*
KP-13-03	209.1	3013.95	3.64	5779.16	4932.82	14.87	47354.00	*1766.14*
KP-13-03	209.2	3046.16	2.88	6551.98	5392.83	16.43	48965.00	*7432.17*
KP-13-03	209.3	3035.69	5.08	3603.78	5047.80	15.32	49484.00	*2261.32*
KP-13-03	209.4	3050.10	3.59	4793.68	5310.86	16.20	2904.00	*5634.09*
KP-13-03	214.1	2670.97	4.12	3162.40	5301.48	14.16	3350.00	*45.69*
KP-13-03	214.2	2783.66	4.02	3700.42	5665.29	15.77	3144.00	*209.15*
KP-13-03	214.3	2642.26	4.22	3733.37	5445.59	14.39	2931.00	*46.97*
KP-13-03	214.4	4.30	3795.19	10218.00	102.55			
KP-13-03	236.1	2620.05	2.58	7129.91	5785.47	15.16	8507.00	*46.89*

KP-13-03	236.2	2657.56	3.90	5120.02	5660.42	15.04	11072.00	*114.61*
KP-13-03	236.3	2607.34	1.97	5939.41	5683.17	14.82	12926.00	*76.65*
KP-13-03	236.4	2661.50	2.44	6812.74	5365.46	14.28	3500.00	*166.55*
KP-13-03	254.1	2824.42	5.14	3144.60	6162.00	17.40	3781.00	*36.01*
KP-13-03	254.2	2812.82	2.85	4688.75	5384.80	15.15	4762.00	*85.10*
KP-13-03	254.3	2823.69	5.34	3180.27	6260.21	17.68	4450.00	
KP-13-03	254.4	2796.58	2.25	5849.19	6252.89	17.49		
B-05-15	9.1	2737.82	11.34	5732.17	6374.00	17.45	1590.52	*1854.53*
B-05-15	9.2	2932.63	18.08	4299.88	6426.39	18.85	18.30	*3.82*
B-05-15	9.3	2932.63	4.71	4929.78	6476.24	18.99	7.48	*0.82*
B-05-15	9.4	6.05	0.28					
B-05-15	18.1	1498.60	336.88					
B-05-15	18.2	1846.68	698.43					
B-05-15	18.3	2665.69	7.22	4467.68	1692.85	275.39		
B-05-15	18.4	1481.81	256.34					
B-05-15	29.1	2737.82	222.08	2774.06	1253.27	258.18		
B-05-15	29.2	1180.37	504.94					
B-05-15	29.3	2737.82	162.09	2021.80	1151.96	365.35		
B-05-15	43.1	6948.01	2912.22	926.36				
B-05-15	43.2	6447.96	3026.97	773.02				

B-05-15	43.3	6343.40	2865.35	653.83				
B-05-15	43.4	6292.46	2792.77	697.37				
B-05-15	49.1	2737.82	8.99	5328.59	1827.66	159.13		
B-05-15	49.2	2884.34	6.74	6158.30	751.61	279.39		
B-05-15	49.3	3044.30	3.88	6664.95	1240.06	129.89		
B-05-15	49.4	2749.91	4.90	5634.14	6798.56	18.70	1187.06	*290.26*
B-05-15	53.1	4287.16	399.36					
B-05-15	53.2	2949.01	57.10	1931.97	6455.84	19.04	4326.47	*629.72*
B-05-15	53.3	3776.22	56.04	1721.27	6778.17	25.60	4700.01	*863.90*
B-05-15	53.4	3892.61	382.22					
B-05-15	62.1	2353.66	1162.83					
B-05-15	62.2	3741.87	6.42	5758.35	6710.01	25.11	2385.02	*457.85*
B-05-15	62.3	3054.66	15.53	4364.94	6232.84	19.04	2040.21	*827.42*
B-05-15	62.4	6937.65	1364.44	268.52				
B-05-15	73.1	1501.79	195.28					
B-05-15	73.2	3025.67	62.62	2907.76	1567.52	163.03		
B-05-15	73.3	3311.16	9.78	6086.99	6372.90	21.10	1651.87	*247.68*
B-05-15	73.4	2272.02	408.13					
B-05-15	75.1	3311.16	7.96	5434.85	5926.29	19.62	12.25	*0.14*
B-05-15	75.2	21.33	0.48					
B-05-15	75.3	2644.05	63.60	2941.85	17.90	0.35		
B-05-15	75.4	20.61	0.32					
B-05-15	86.1	5428.14	2147.31					

B-05-15	86.2	5268.75	3899.22					
B-05-15	86.3	6096.72	5522.28	155.81				
B-05-15	86.4	2644.05	7295.75	3721.11				
B-05-15	90.1	6207.28	5553.80	1141.10				
B-05-15	90.2	6177.27	4612.39					
B-05-15	90.3	3913.77	6272.48	24.55	6185.01	3419.05		
B-05-15	90.4	4031.80	764.28					
B-05-15	96.1	6426.28	5751.31	1283.87				
B-05-15	96.2	4867.52	1510.87					
B-05-15	96.3	6896.35	5043.94	1472.30				
B-05-15	96.4	6748.81	3200.31					
B-05-15	100.1	3387.83	0.00	542.21	6324.88	21.43	150.16	*116.39*
B-05-15	100.2	2559.88	3.34	5568.15	6370.33	16.31	88.17	*15.14*
B-05-15	100.3	2539.95	6.44	4755.85	5450.79	13.84	333.99	*21.84*
B-05-15	103.1	6986.62	4608.41	1339.50				
B-05-15	103.2	6750.51	3948.08	2982.33				
B-05-15	103.3	7307.24	4268.38	772.34				
B-05-15	109.2	2540.90	3.66	3718.20	6233.23	15.84	1712.75	*3249.25*
B-05-15	109.3	3289.63	72.10	2062.05	1093.55	668.34		

B-05-15	109.4	3289.63	24.24	4270.63	119.21	5.08		
B-05-15	124.1	3289.63	0.00	4973.62	583.46	71.31		
B-05-15	124.2	6699.89	392.16	62.28				
B-05-15	124.3	275.66	49.85					
B-05-15	124.4	2958.12	6.96	4244.50	6911.76	20.45	267.14	*36.52*
B-05-15	139.1	993.53	73.04					
B-05-15	139.2	2971.69	4.25	4754.49	6292.53	18.70	620.47	*74.44*
B-05-15	139.3	2956.39	2.08	6856.18	6330.13	18.71	304.22	*37.53*
B-05-15	139.4	2941.95	4.67	5443.12	6121.78	18.01	678.64	*83.69*
B-05-15	146.1	2954.72	38.50	2093.55	6868.17	20.29	428.53	*99.73*
B-05-15	146.2	3122.38	5.11	4901.13	835.80	236.80		
B-05-15	146.3	2828.74	1200.51					
B-05-15	146.4	3122.38	7.02	5099.88	6957.53	21.72	413.72	*120.76*
B-05-15	153.1	2903.68	6.82	4049.16	6651.50	19.31	4507.35	*1074.89*
B-05-15	153.2	3426.34	4.42	6829.62	1069.20	316.70		

B-05-15	153.3	3426.34	5.97	5051.66	7383.35	25.30	683.97	*371.10*
B-05-15	153.4	646.49	195.23					
B-05-15	157.1	3361.90	50.64	2794.79	6265.40	21.06	6298.80	*1801.30*
B-05-15	157.2	3111.94	4.20	4974.52	7003.63	21.79	2002.49	*1002.02*
B-05-15	157.3	6829.90	4296.84					
B-05-15	157.4	5723.77	1581.32					
B-05-15	163.1	2868.56	4.14	7269.98	6848.15	19.64	793.47	*322.02*
B-05-15	163.2	3200.29	5.16	5937.36	6438.67	20.61	1038.25	*357.88*
B-05-15	163.3	3171.61	6.22	5591.99	6751.01	21.41	2356.69	*1288.53*
B-05-15	163.4	2127.74	477.59					
B-05-15	169.1	8972.13	1532.08					
B-05-15	169.2	3287.44	89.43	369.23	5202.18	17.10	5441.83	*4281.15*
B-05-15	169.3	3050.93	49.40	536.57	5938.94	18.12	8751.62	*6030.67*
B-05-15	169.4	3176.27	75.36	652.31	6255.24	19.87	3595.95	*1118.13*
B-05-15	173.1	1499.00	425.00					

B-05-15	173.2	3308.29	3.49	5380.43	6532.87	21.61	2694.02	*2072.16*
B-05-15	173.3	3284.25	22.14	3800.54	5422.50	17.81	6143.39	*2649.94*
B-05-15	173.4	3284.25	77.82	2901.53	6123.15	20.11	3968.77	*1838.64*
B-05-15	179.1	6676.40	1780.74					
B-05-15	179.2	4608.26	1902.43					
B-05-15	179.3	4110.90	2098.16					
B-05-15	179.4	3582.26	1065.39					
B-05-15	196.1	5532.83	2666.09	1379.53				
B-05-15	196.2	3513.45	4.59	4444.66	4106.70	14.43	535.48	*151.78*
B-05-15	196.3	4634.04	1154.92					
B-05-15	208.1	3244.57	9.80	4219.12	6679.14	21.67	1931.51	*598.12*
B-05-15	208.2	3426.14	9.47	5327.11	7031.34	24.09	2125.60	*1653.28*
B-05-15	208.3	1372.16	914.81					
B-05-15	208.4	3403.15	4.05	5479.94	7235.16	24.62	1144.96	*313.35*
B-05-15	214.1	3348.72	5.50	4030.35	6634.87	22.22	719.62	*706.82*

B-05-15	214.2	3283.05	7.66	5109.33	6635.17	21.78	512.40	*257.18*
B-05-15	214.3	3261.25	4.34	4130.35	604.07	59.83		
B-05-15	214.4	3769.83	1812.09					
B-05-15	223.1	3105.52	8.42	3437.83	6797.90	21.11	1184.91	*619.92*
B-05-15	223.2	3051.56	3.81	3908.29	6894.98	21.04	1407.89	*840.65*
B-05-15	223.3	3366.71	33.34	4066.37	7344.12	24.73	2126.55	*825.04*
B-05-15	223.4	3336.09	55.82	3115.10	278.12	88.68		
B-05-15	227.1	6910.70	769.67	166.42				
B-05-15	227.2	3336.09	6.05	5234.92	369.72	157.72		
B-05-15	227.3	3305.20	2.71	6591.74	1478.39	675.20		
B-05-15	227.4	1074.85	549.93					
B-05-15	232.1	3272.52	7.28	4117.17	7084.94	23.19	1788.19	*556.36*
B-05-15	232.2	3288.24	7.42	3877.34	6794.08	22.34	1664.44	*838.11*
B-05-15	232.3	597.63	709.35					
B-05-15	232.4	372.02	716.84					

B-05-15	237.1	2478.60	618.91					
B-05-15	237.2	2567.97	532.26					
B-05-15	237.3	3164.76	6.04	5300.02	6647.89	21.04	1972.17	*403.49*
B-05-15	237.4	2968.29	6.67	5521.42	6992.44	20.76	2298.36	*338.57*
B-06-16	4.1	3033.61	51.04	2583.77	5221.41	15.84	8370.05	*3497.50*
B-06-16	4.2	3527.02	71.80	2550.11	5376.01	18.96	5569.47	*1679.05*
B-06-16	4.3	3451.38	9.09	5032.04	5288.42	18.25	5978.90	*1920.34*
B-06-16	4.4	6488.38	7857.41	2549.64				
B-06-16	15.1	2405.79	667.60					
B-06-16	15.2	3139.65	424.28					
B-06-16	15.3	3256.95	1051.77					
B-06-16	15.4	2867.58	481.08					
B-06-16	34.1	1170.67	317.37					
B-06-16	34.2	786.39	593.93					
B-06-16	34.3	2078.09	1416.76					
B-06-16	34.4	1866.65	3230.76					
B-06-16	51.1	3451.38	116.86	2384.00	6602.53	22.79	4381.78	*1502.28*
B-06-16	51.2	3765.44	216.31	1785.01	7014.84	26.41	4207.50	*858.07*
B-06-16	51.3	3659.13	947.32					
B-06-16	51.4	3741.00	90.26	1981.99	4317.64	1088.04		
B-06-16	56.1	6379.09	2402.98					

B-06-16	56.2	3558.96	75.98	2877.94	6537.67	23.27	4870.30	*1555.06*
B-06-16	56.3	3606.03	78.19	1445.43	6383.20	23.02	7625.52	*3960.34*
B-06-16	63.1	3748.19	5.97	5358.50	7381.49	27.67	632.24	*459.72*
B-06-16	63.2	3161.20	10.84	4188.56	7356.25	23.25	510.81	*359.59*
B-06-16	63.3	359.21	141.50					
B-06-16	63.4	423.03	390.61					
B-06-16	87.1	3085.79	3.15	5561.16	4690.37	14.47	506.35	*171.59*
B-06-16	87.2	817.02	171.84					
B-06-16	87.3	2966.65	9.52	5119.38	5514.87	16.36	1071.35	*301.60*
B-06-16	87.4	829.75	263.71					
B-06-16	99.1	3147.20	7.47	3741.67	6324.13	19.90	1346.77	*330.17*
B-06-16	99.2	1785.56	1065.85					
B-06-16	99.3	2257.14	925.01					
B-06-16	104.1	772.62	397.72					
B-06-16	104.2	2190.69	763.11					
B-06-16	104.3	3147.20	4.21	6972.96	773.41	363.41		
B-06-16	121.1	3168.83	5.79	5270.88	6406.25	20.30	1165.65	*162.83*
B-06-16	121.2	1135.01	129.65					
B-06-16	121.3	2995.10	4.45	7090.71	5746.87	17.21	1019.15	*119.76*
B-06-16	133.1	2770.11	3.79	5558.71	1434.15	219.06		

B-06-16	133.2	1480.86	521.86					
B-06-16	133.3	2976.10	4.64	5143.21	6996.16	20.82	1079.47	*222.88*
B-06-16	133.4	2970.56	4.14	6208.41	6914.89	20.54	1164.94	*232.53*
B-06-16	143.1	2960.21	3.97	6344.05	6612.82	19.58	940.69	*131.11*
B-06-16	143.2	2981.64	1.73	7277.67	6715.58	20.02	1175.36	*142.96*
B-06-16	143.3	3019.77	14.69	3642.57	6050.61	18.27	415.71	*66.05*
B-06-16	143.4	472.45	70.58					
B-06-16	152.1	2978.47	83.23	2198.25	913.47	263.36		
B-06-16	152.2	960.82	224.18					
B-06-16	152.3	975.70	286.68					
B-06-16	152.4	895.96	217.95					
B-06-16	173.1	2947.40	3.94	4879.33	7851.29	23.14	1510.78	*460.11*
B-06-16	173.2	2962.58	5.40	5091.22	7772.93	23.03	1660.46	*457.31*
B-06-16	173.3	2962.58	6.74	5634.40	6980.39	20.68	1239.10	*353.51*
B-06-16	173.4	1420.06	229.90					

B-06-16	182.1	2962.58	4.30	5596.57	6930.47	20.53	1528.60	*202.43*
B-06-16	182.2	6275.61	1478.63	159.76				
B-06-16	182.3	658.90	158.26					
B-06-16	182.4	3031.51	5.53	6013.86	7020.92	21.28	661.77	*182.59*
B-06-16	186.1	3033.75	20.74	5199.73	6536.56	19.83	3564.36	*1722.63*
B-06-16	186.2	3326.27	45.44	4657.05	6004.06	19.97	1300.62	*588.36*
B-06-16	186.3	3332.98	27.55	4676.76	2643.57	883.34		
B-06-16	186.4	1635.64	1002.05					
B-06-16	191.1	3047.18	4.77	5500.75	5937.21	18.09	1813.17	*573.00*
B-06-16	191.2	3248.54	7.06	4781.83	5347.57	17.37	519.56	*365.81*
B-06-16	191.3	6433.25	2948.59	1256.95				
B-06-16	191.4	5500.56	662.54					
B-06-16	212.1	3128.56	4.51	5357.80	6583.55	20.60	322.05	*196.82*
B-06-16	212.2	311.47	119.34					
B-06-16	212.3	1315.34	366.10					

B-06-16	212.4	2827.63	43.31	3736.97	1338.02	416.10		
B-06-16	215.1	2827.63	5.72	5258.45	6946.11	19.64	1941.53	*223.82*
B-06-16	215.2	3124.40	3.22	9227.13	2093.69	348.36		
B-06-16	215.3	2872.02	6.08	5229.46	6846.15	19.66	1957.61	*450.22*
B-06-16	215.4	2872.02	6.75	5126.09	1856.46	403.03		
B-06-16	239.1	2872.02	4.80	4947.97	6686.11	19.20	81.96	*44.79*
B-06-16	239.2	119.45	120.30					
B-06-16	239.3	52.68	121.33					
B-06-16	239.4	141.01	123.00					
B-06-16	253.1	3001.81	3.71	6740.75	6626.71	19.89		
B-06-16	253.2	2883.14	6.59	4725.04	6563.03	18.92		
B-06-16	261.3	2883.14	55.87	3354.14	6917.21	19.94		
B-06-16	261.4	6733.83						
B-06-16	269.1	2855.02	58.19	5842.53	6687.79	19.09	3309.87	*8.91*
B-06-16	269.2	268.57	6.88					

B-06-16	269.3	2855.02	35.56	4313.22	7638.16	21.81	2963.55	*7.57*
B-06-16	269.4	3067.48	8.85					
B-06-16	276.1	2855.02	4.69	4192.90	6862.63	19.59	1220.40	*2070.24*
B-06-16	276.2	5.83	5286.07	6340.34	1456.03	30.89		
B-06-16	276.3	2962.67	1377.89	2179.53				
FD-13-34	8.1	1737.10	772.34					
FD-13-34	8.2	1542.53	226.22					
FD-13-34	8.3	1903.18	358.59					
FD-13-34	25.1	2856.55	4.41	4864.18	6647.87	18.99	3185.81	*217.58*
FD-13-34	25.2	2852.54	75.58					
FD-13-34	25.3	2757.68	367.39					
FD-13-34	25.4	1201.06	303.60					
FD-13-34	34.1	2790.72	3.00	4943.64	8772.23	417.54		
FD-13-34	34.2	7280.95	357.44					
FD-13-34	34.3	5964.65	579.31					

FD-13-34	34.4	5939.03	90.65					
FD-13-34	38.1	3154.14	2051.58					
FD-13-34	38.2	3345.84	2775.69					
FD-13-34	38.3	5715.18	2819.54					
FD-13-34	38.4	3148.33	2022.20					
FD-13-34	51.1	3722.06	54.72	2947.41	6972.48	25.95	5623.59	*288.49*
FD-13-34	51.2	6452.24	6682.52	423.35				
FD-13-34	51.3	6990.81	476.56					
FD-13-34	51.4	6182.30	477.60					
FD-13-34	59.1	3386.01	55.63	2243.61	6434.68	21.79	4344.30	*1486.64*
FD-13-34	59.2	6508.97	1708.98					
FD-13-34	59.3	3086.34	1107.96					
FD-13-34	59.4	11266.27	799.21					
FD-13-34	76.1	3036.32	7.32	7072.40	7034.42	21.36	2784.18	*1176.81*
FD-13-34	76.2	3036.32	7.04	7340.76	6855.97	20.82	2262.47	

FD-13-34	76.3	3028.25	7.89	7028.80	6506.39	19.70	2317.70	
FD-13-34	78.1	3015.39	7.65	8904.40	6669.51	20.11	2256.10	*746.55*
FD-13-34	78.2	3035.65	7.62	9887.69	6755.67	20.51	2399.50	*155.01*
FD-13-34	78.3	3065.99	5.51	10076.13	6663.82	20.43	2411.52	*115.16*
FD-13-34	101.1	3026.03	6.54	9410.64	6618.06	20.03	1610.57	*98.67*
FD-13-34	101.2	3093.42	31.02	4825.69	6742.64	20.86	2091.62	*59.54*
FD-13-34	144.1	3061.57	6.18	7331.08	6738.44	20.63	2076.42	*57.74*
FD-13-34	144.2	3117.20	14.89	4592.36	6836.59	21.31	2004.00	*34.44*
FD-13-34	144.3	6679.94	2150.98	22.76				
FD-13-34	166.1	3132.76	7.98	7950.45	6519.68	20.42	2034.00	*65.94*
FD-13-34	166.2	3142.60	9.13	9086.15	6745.71	21.20	2020.55	*124.48*
FD-13-34	166.3	3097.55	8.55	7301.66	6652.58	20.61	1850.18	*100.55*
FD-13-34	188.1	3088.61	7.91	10217.82	6716.20	20.74	2172.07	*133.27*
FD-13-34	188.2	3154.36	7.81	7730.39	6703.99	21.15	2110.08	*114.98*
FD-13-34	188.3	3155.86	7.79	9208.71	6746.47	21.29	2105.78	*91.74*

FD-13-34	202.1	2040.61	88.26					
FD-13-34	202.2	1860.44	80.76					
FD-13-34	202.3	2393.21	78.48					
FD-13-34	203.1	3131.49	98.31	3315.41	7121.54	22.30	3971.48	*63.40*
FD-13-34	203.2	3724.56	93.26	2198.50	7020.70	26.15	3901.93	*67.76*
FD-13-34	203.3	3733.94	7002.41	26.15	3779.30	78.56		
FD-13-34	220.2	3730.60	6.12	6999.10	6388.43	23.83		
FD-13-34	220.3	3068.01	29.92	6299.34	6613.62	20.29		
FD-13-34	220.4	3030.13	10.77	8910.06	6643.91	20.13		
FD-13-34	237.1	3137.71	60.36	3707.11	7674.69	24.08	18436.52	*232.32*
FD-13-34	237.2	3296.44	50.36	1638.13	6701.48	22.09	18891.43	*3073.37*
FD-13-34	237.3	19515.66	5129.26					
FD-13-34	237.4	6973.98	15796.98	2644.95				
FD-13-34	245.1	3692.11	29.95	1907.54	6994.22	25.82	12324.18	*3583.75*
FD-13-34	245.2	3479.48	54.01	3180.12	6423.75	22.35	8412.00	*298.61*

FD-13-34	245.3	3479.48	969.54	7034.12	24.48	11726.52	1383.48	
FD-13-34	245.4	3505.57	77.14	2019.45	7228.29	25.34	15524.91	*2734.00*
FD-13-34	248.1	3674.90	46.25	2383.73	6641.07	24.41	8568.52	*953.73*
FD-13-34	248.2	3435.18	30.34	2585.95	6556.43	22.52	7302.66	*1334.90*
FD-13-34	248.3	3296.62	72.68	2370.59	6736.73	22.21	7641.53	*915.24*
FD-13-34	248.4	3317.02	20.74	5105.43	6752.27	22.40	2260.17	*550.90*
FD-13-34	254.1	3020.06	29.49	4057.66	6662.28	20.12	4916.98	*840.06*
FD-13-34	254.2	3158.71	29.42	5413.67	6806.90	21.50	636.27	*229.97*
FD-13-34	254.3	3158.71	4577.84	1105.22				
FD-13-34	254.4	3424.13	6040.02	1484.50				
FD-13-34	266.1	60.20	4093.71	5315.13	7406.86	1245.06		
FD-13-34	266.2	54.06	3477.28	7097.67	5074.20	767.96		
FD-13-34	266.3	3232.14	59.87	2499.23	6185.13	19.99	8648.41	*1048.27*
FD-13-34	266.4	3623.00	50.01	2188.18	6738.66	24.41	7160.30	*1054.81*
FD-13-34	275.1	3334.13	29.06	4533.22	7222.54	24.08	3340.35	*435.45*

FD-13-34	275.2	3252.49	8.50	4033.21	6901.10	22.45	2790.58	*213.15*
FD-13-34	275.3	3049.08	12.87	6442.61	6967.49	21.24	1744.22	*97.54*
FD-13-34	275.4	7657.08	7630.22					
FD-13-34	282.1	2885.88	30.93	1669.96	7146.71	20.62	16929.22	*2041.11*
FD-13-34	282.2	3461.29	39.26	1790.28	12431.45	1525.17		
FD-13-34	282.3	17568.03	511.91					
FD-13-34	282.4	3710.45	2098.52					
FD-13-34	286.1	3389.95	27.21	4642.93	6804.07	23.07	2833.81	*647.43*
FD-13-34	286.2	2980.05	3.84	7177.53	6739.13	20.08	1129.38	*525.28*
FD-13-34	286.3	1058.45	10.07					
FD-13-34	286.4	1617.85	186.86					
FD-13-34	296.1	2932.87	34.45	2732.13	6250.69	18.33	7538.35	*485.18*
FD-13-34	296.2	3444.84	48.48	4032.18	5295.13	18.24	3141.56	*1811.62*
FD-13-34	296.3	6162.97	420.40					
FD-13-34	296.4	4177.95	1181.01					

FD-13-34	306.1	3295.06	41.51	3840.71	6259.98	20.63	1175.64	*1295.65*
FD-13-34	306.2	2906.99	29.88	4486.61	6855.80	19.93	226.81	*571.59*
FD-13-34	306.3	270.27	24.17					
FD-13-34	306.4	2917.90	4.38	4918.45	6615.07	19.30	573.61	*28.17*
FD-13-34	311.1	2944.45	10.41	4074.88	6596.07	19.42	4051.59	*23.41*
FD-13-34	311.2	3147.10	4.16	4753.47	6401.89	20.15	762.75	*560.76*
FD-13-34	311.3	3214.08	8.48	4325.20	6484.02	20.84	1074.34	*123.66*
FD-13-34	311.4	3198.74	9.61	4662.51	7700.31	24.63	3065.55	*72.34*
FD-13-34	323.1	3135.69	7.78	5527.55	6440.39	20.20	2204.62	*551.55*
FD-13-34	323.2	3477.21	1750.77	427.84				
FD-13-34	323.3	2006.73	286.68					
FD-13-34	323.4	3305.24	7084.39	578.83				
FD-13-34	328.1	33.18	3538.67	7237.87	4894.64	1370.33		
FD-13-34	328.2	17.19	5765.88	5961.44	7727.50	1504.76		
FD-13-34	328.3	6922.89	2089.45					

FD-13-34	328.4	6982.68	1236.18					
FD-13-34	333.1	3265.47	58.17	3141.54	6260.03	20.44	4095.18	*1801.65*
FD-13-34	333.2	3306.10	6.42	5270.95	6746.92	22.31	2348.56	*282.97*
FD-13-34	333.3	3191.41	4.45	6182.22	6326.11	20.19	1359.80	*183.58*
FD-13-34	333.4	3113.89	65.80	1767.46	5567.67	17.34	1445.55	*214.38*
M-07-238	15.1	3005.43	4.76	3880.70	6641.09	19.96	1826.28	*4446.62*
M-07-238	15.2	3012.49	4.61	3562.17	6603.40	19.89	1162.05	*3583.92*
M-07-238	15.3	3008.01	6509.62	19.58	1138.01	20167.64		
M-07-238	15.4	2995.86	6584.13	19.73	1437.14	2887.30		
M-07-238	18.1	3269.31	106.84	166.81	6394.93	20.91	73826.75	*372233.29*
M-07-238	18.2	3506.07	48.21	662.50	6865.54	24.07	49614.43	*159257.15*
M-07-238	18.3	3563.52	63.98	561.08	6933.65	24.71	52385.27	*105073.26*
M-07-238	18.4	3497.52	50.74	728.68	6865.50	24.01	61518.18	*2276.38*
M-07-238	27.1	3021.25	3.83	5960.15	6622.06	20.01	1099.66	*335.42*
M-07-238	27.2	3008.46	3.27	4345.08	6742.91	20.29	3905.03	*907.60*

M-07-238	27.3	2999.90	3.53	5572.94	6621.20	19.86	10933.96	*13794.45*
M-07-238	27.4	3002.14	3.83	6291.76	6523.56	19.58	7272.43	*360.28*
M-07-238	48.1	3013.06	2.28	6282.71	7297.64	21.99	22564.19	*400.24*
M-07-238	48.2	3005.22	2.88	5603.45	6497.33	19.53	20815.32	*319.75*
M-07-238	48.3	3026.23	2.39	6536.47	6599.94	19.97	13741.99	*1875.22*
M-07-238	61.1	3391.09	65.50	489.26	6552.41	22.22	365.81	*372233.29*
M-07-238	61.3	3483.68	49.97	533.48	6363.64	22.17	2986.61	*159257.15*
M-07-238	61.3	3327.39	72.54	134.03	6381.22	21.23	5331.82	*105073.26*
M-07-238	61.4	3293.34	89.51	640.27	6000.52	19.76	8846.00	*2276.38*
M-07-238	61.5	3573.91	55.79	655.56	5591.17	19.98	878.93	*159257.15*
M-07-238	61.6	3599.01	6614.94	23.81	3554.51	189257.15		
M-07-238	76.1	2997.84	3.92	4292.76	6760.40	20.27	4952.38	*8081.57*
M-07-238	76.2	2993.89	4.58	5828.16	5483.03	16.42	4219.50	*5300.74*
M-07-238	76.3	2972.29	4.52	6560.71	5679.47	16.88	365.81	*7346.19*
M-07-238	76.4	2997.56	3.65	6325.02	5885.20	17.64	2986.61	*2895.06*

M-07-238	76.5	2988.08	4.83	4686.50	6198.10	18.52	5331.82	*3538.02*
M-07-238	76.6	3041.72	6571.02	19.99	8846.00	3347.65		
M-07-238	85.1	3341.21	6367.92	21.28	163999.00	45600.55		
M-07-238	85.2	3369.98	10.86	6271.78	21.14	219120.00	82619.42	
M-07-238	85.3	3268.61	14.30	2131.07	6367.92	39.43	347945.00	*46845.16*
M-07-238	85.3	3304.22	19.40	1656.62	6035.06	19.94	256723.00	*74676.29*
M-07-238	85.4	1385.11	15.62	2043.56	6278.48	8.70	259723.00	
M-07-238	85.6	3274.83	1712.04	5926.80	19.41	259723.00	7268.27	
M-07-238	104.1	3067.52	17.11	1847.19	6377.23	19.56	321074.34	*4948.17*
M-07-238	104.2	3020.07	3.89	5840.41	5745.94	17.35	73869.30	*6345.68*
M-07-238	104.3	3032.44	2.80	4479.87	5596.46	16.97	172038.94	*3541.96*
M-07-238	104.4	3049.14	4.11	6966.53	5485.00	16.72	357110.88	*5137.44*
M-07-238	104.5	3025.29	4.78	4664.67	5764.21	17.44	193415.11	*5735.77*
M-07-238	104.6	3049.89	5610.68	5163.21	15.75	193415.11	6403.08	
M-07-238	115.1	23.53	1122.78	197590.00	5248.97			

M-07-238	115.2	3245.82	16.16	1194.55	169654.00			
M-07-238	115.3	20.34	1080.83	4802.79	173872.00			
M-07-238	115.4	38.62	890.45	120990.00	14488.86			
M-07-238	115.5	51.82	538.60	6731.30	145648.00	24202.38		
M-07-238	115.6	120967.00	13793.62					
M-07-238	130.1	27.78	671.98	4201.14	248903.00	2800.42		
M-07-238	130.2	3294.51	5.22	1307.42	6546.02	21.57	66792.00	*10553.72*
M-07-238	130.3	3538.00	45.60	348.16	6864.46	24.29	378363.00	*32701.49*
M-07-238	130.4	3482.01	35.42	872.81	6753.93	23.52	200700.00	*1666.68*
M-07-238	146.1	3397.00	2.43	1550.50	7901.00	2850.16		
M-07-238	146.2	2871.51	30.25	1640.27	85380.00	263.28		
M-07-238	146.3	2998.38	5927.42	17.77	78380.00	208.19		
M-07-238	146.4	2830.55	75450.00	617.49				
M-07-238	146.5	71380.00	8915.21					
M-07-238	146.6	5223.25	85680.00	12775.17				

M-07-238	158.1	3162.68	1.64	6502.94	7045.39	22.28	11759.57	
M-07-238	158.2	3214.53	2.48	6378.50	6976.74	22.43	12828.17	
M-07-238	158.3	3196.61	2.51	5737.65	7212.36	23.06	12815.89	
M-07-238	158.4	3195.35	7257.42	23.19	16075.37			
M-07-238	158.5	3217.12	1.89	7016.88	7122.00	22.91	12319.97	
M-07-238	158.6	3240.67	2.49	3533.46	7081.44	22.95	8164.31	
M-07-238	179.1	3194.43	1.24	6035.54	7236.32	23.12	8471.31	
M-07-238	179.2	3246.52	2.29	7217.49	7129.80	23.15	24908.00	
M-07-238	179.3	3245.04	3.35	3682.67	8166.01			
M-07-238	179.4	3240.93	1.74	6871.24	7224.11	2.35	8358.44	
M-07-238	179.5	3235.70	3.32	4329.03	15854.61			
M-07-238	185.1	3243.44	16.19	645.74	6363.16	20.64	9234.63	
M-07-238	185.2	3192.87	6166.46					
M-07-238	185.3	10263.92						
M-07-238	185.4	6806.63	4859.07					

M-07-238	185.5	3261.99	6368.80	20.77	5449.50			
M-07-238	185.6	21178.17						
M-07-238	198.2	2956.00	53.43	762.07	6052.00	17.89	173582.00	*18971.67*
M-07-238	198.1	3486.64	39.75	1329.39	6694.51	23.34	95268.00	*6665.77*
M-07-238	198.2	3405.05	68.53	498.72	6337.09	21.58	170732.00	*21802.24*
M-07-238	198.3	3348.12	84.65	651.17	7637.43	25.57	160734.00	*8599.76*
M-07-238	198.5	3357.25	6672.14	22.40	160623.00	6013.46		
M-07-238	211.1	3058.68	9.61	1149.27	6054.90	18.52	107666.00	*5433.45*
M-07-238	211.2	3015.09	12.69	1149.05	5939.61	17.91	86096.00	*3985.69*
M-07-238	211.3	13.78	835.14	5890.55	163907.00	12076.11		
M-07-238	211.4	3263.95	12.30	1102.14	117673.00	4998.19		
M-07-238	211.5	3151.91	11.21	810.52	5680.00	17.90	141805.00	*9154.01*
M-07-238	211.6	3222.68	67.20	583.43	6465.75	20.84	131805.00	*608.03*
M-07-238	217.1	2962.63	5.04	1693.67	5914.72	17.52	3354.00	*1251.11*
M-07-238	217.2	2915.36	2.94	1930.07	28077.00	1599.84		

M-07-238	217.3	2879.08	7.17	1693.14	6017.79	17.33	10004.00	*287.08*
M-07-238	217.4	3015.49	3.03	1842.25	15678.00	1078.45		
M-07-238	217.5	2893.96	3.01	1436.75	5787.46	16.75	13456.00	*585.72*
M-07-238	217.6	2931.33	6049.75	17.73	14890.00	273.86		
M-07-238	221.1	2976.68	5.70	2312.66	5917.55	17.61	8539.00	*1051.28*
M-07-238	221.2	3.19	1436.80	8760.00	606.80			
M-07-238	221.3	2761.97	3.41	1335.37	6375.26	17.61	5129.00	*575.04*
M-07-238	221.4	4567.00	414.88					
M-07-238	221.5	2829.20	3412.00	518.94				
M-07-238	221.6	2974.56	6319.96	18.80	6789.00	594.99		
M-07-238	225.1	2836.90	5.09	1392.12	6752.87	19.16	8207.00	*7843.27*
M-07-238	225.2	2746.33	4.54	1539.94	4581.00	26873.00		
M-07-238	225.3	4228.00	360.38					
M-07-238	225.4	2931.34	1172.68	4312.00	2204.37			
M-07-238	225.5	4.68	6608.74	2367.00	9185.67			

M-07-238	243.1	3213.68	14.13	925.88	6287.08	20.20	4244.40	
M-07-238	243.2	21.91	806.61	4401.57	12795.82			
M-07-238	243.3	2800.64	3797.56					
M-07-238	243.4	3286.04	5909.09	19.42	8881.09			
M-07-238	243.5	5864.62	10250.22					
M-07-238	243.6	4903.56	813.81					
M-07-238	259.1	2832.63	17.11	1799.10	4878.05	13.82	32122.00	*763.42*
M-07-238	259.2	4.22	1680.22	7308.00	638.49			
M-07-238	259.3	2886.64	12.05	1366.35	4940.22	14.26	9514.00	*510.30*
M-07-238	259.4	2776.90	5.67	1619.61	5594.29	15.53	10296.00	*3797.07*
M-07-238	259.5	2920.28	5.80	1419.25	5563.19	16.25	9296.00	*10797.22*
M-07-238	259.6	2951.10	2.15	1483.98	6059.11	17.88	8456.00	*1215.55*
M-07-238	272.1	3.62	1677.57	22745.00	1054.72			
M-07-238	272.2	10.06	1387.19	56083.00	7948.43			
M-07-238	272.3	2925.29	13.85	1270.27	5481.71	16.04	4553.00	*1011.51*

M-07-238	272.4	7.44	1502.33	6228.67	45678.00	10954.28		
M-07-238	272.5	2996.15	5.02	1347.05	54123.00	1697.88		
M-07-238	272.6	2910.43	6905.57	20.10	67890.00	38573.81		
M-07-238	314.1	3616.10	58.36	309.84	6590.11	23.83	54237.00	*18289.46*
M-07-238	314.2	77.80	370.33	147869.00	35807.64			
M-07-238	314.3	3438.78	13.82	1375.14	5964.44	20.51	301816.00	*3409.93*
M-07-238	314.4	3243.69	58.96	630.52	6292.54	20.41	42013.00	*3160.46*
M-07-238	314.5	3324.65	6971.47	23.18	48787.00	14796.11		
M-07-238	314.6	3257.49	5907.98	19.25	132296.00	413.18		
M-07-238	325.1	4.98	1203.81	7161.00	243.72			
M-07-238	325.2	2745.53	9.99	1440.80	4381.11	12.03	7530.00	*328.60*
M-07-238	325.3	2739.10	4.35	1421.34	4517.33	12.37	11612.00	*469.15*
M-07-238	325.4	2737.99	3.68	1532.90	4457.74	12.21	8634.00	*325.18*
M-07-238	325.5	2739.03	2.94	1539.12	4595.74	12.59	8403.00	*289.02*
M-07-238	325.6	2723.60	7890.00	3066.33				

M-07-238	334.1	3022.35	8.25	1493.07	5853.18	17.69	111961.00	*2493.84*
M-07-238	334.2	3166.33	11.21	1131.62	6559.39	20.77	130327.00	*550.13*
M-07-238	334.3	3018.01	6.30	1372.54	6065.75	18.31	54588.00	*3681.21*
M-07-238	334.4	3122.55	12.94	1278.03	5885.08	18.38	149632.00	*2412.12*
M-07-238	334.5	3162.13	35.90	484.32	6189.95	19.57	123452.00	*15010.23*
M-07-238	334.6	5485.44	134567.00	352.05				
M-07-238	340.1	2752.55	3.73	5413.89	5030.95	13.85	304.57	
M-07-238	340.2	2732.61	3.43	4513.47	5089.97	13.91	372.57	
M-07-238	340.3	2764.94	4.33	3655.22	4675.69	12.93	154.19	
M-07-238	340.4	2754.54	3.69	4147.07	4979.83	13.72	254.27	
M-07-238	340.5	2752.98	4.13	5271.52	5088.29	14.01	183.09	
M-07-238	340.6	2762.88	5342.65	14.76	84.28			
M-07-238	348.1	2814.50	5.88	3793.67	4513.26	12.70	107.06	
M-07-238	348.2	2828.17	6.47	3976.27	4367.58	12.35	108.40	
M-07-238	348.3	2800.89	6.33	2549.15	4872.75	13.65	110.75	

M-07-238	348.4	6.95	3622.48	4650.75				
M-07-238	348.5	2835.20	6.08	1898.94	4116.94	40.02		
M-07-238	348.6	6.96	3493.33	4356.65	954.90			
M-07-239	12.1	3000.02	3.53	4379.16	6733.76	20.20	222.98	*1476.21*
M-07-239	12.2	2965.96	4.45	3901.00	6398.84	18.98	275.72	*821.67*
M-07-239	12.3	2940.77	6623.34	1.95	253.86	35990.24		
M-07-239	16.1	3609.26	37.07	566.07	6633.48	23.94	10604.29	*30670.91*
M-07-239	16.2	74.46	548.64	6274.28	9829.12	17401.43		
M-07-239	16.3	3548.56	89.51	673.55	6821.80	24.21	8764.14	*2948.65*
M-07-239	21.1	3030.75	3.10	4607.11	6598.96	20.00	3243.08	*3881.90*
M-07-239	21.2	3019.22	3.68	4270.93	6747.90	20.37	1373.25	*3055.97*
M-07-239	21.3	1952.12	2.07	6801.16	6724.14	13.13	1197.86	*3592.52*
M-07-239	21.4	3051.22	6680.69	20.38	1114.06	152106.12		
M-07-239	29.1	3593.76	230.83	296.09	6885.25	24.74	56767.34	*217133.30*
M-07-239	29.2	3459.00	54.83	796.42	6716.67	23.23	54381.73	*39891.20*

M-07-239	29.3	2924.04	72.65	434.07	6436.31	18.82	27443.52	*116041.72*
M-07-239	29.4	3267.95	239.13	216.67	6276.06	20.51	40443.33	*352859.44*
M-07-239	29.5	3279.33	106.76	255.43	7296.66	23.93	63295.48	*397121.69*
M-07-239	29.6	84779.52	20100.83					
M-07-239	33.1	3029.62	3.89	1727.56	6717.60	20.35	5325.07	*21739.09*
M-07-239	33.2	3.98	1858.91	6362.92	9033.10			
M-07-239	33.3	4.46	1331.01	11817.20	12679.54			
M-07-239	33.4	2941.48	6637.12	19.52	5107.02	7567.86		
M-07-239	33.5	3018.59	6854.46	20.69	4343.80			
M-07-239	39.1	33.82	1289.01					
M-07-239	39.2	28.13	1173.48					
M-07-239	39.3	24.71	1702.12					
M-07-239	45.1	34.36	1310.22	34115.47				
M-07-239	45.2	3855.14	63.98	1410.57	7526.60	20032.43		
M-07-239	45.3	3616.91	43.99	1765.40	7268.32	26.29	4007.48	*24587.24*

M-07-239	45.4	3521.90	7262.53	25.58	3589.93	3479.19		
M-07-239	47.1	3193.98	2.92	4705.31	7174.78	22.92	366.17	*2897.43*
M-07-239	47.2	3212.27	4.07	4032.22	7127.02	22.89	312.72	*3556.31*
M-07-239	47.3	3211.02	2.39	6606.08	7109.56	22.83	421.67	*4097.71*
M-07-239	47.4	3203.68	7188.35	23.03	350.31	6697.33		
M-07-239	57.1	3499.29	50.89	915.09	6464.81	22.62	5583.82	*15095.12*
M-07-239	57.2	3404.08	61.27	948.85	6891.53	23.46	4911.18	*3898.46*
M-07-239	57.3	37.39	809.50	7141.29	41082.88			
M-07-239	57.4	3575.35	6722.87	24.04	5553.65	7639.96		
M-07-239	67.1	3007.36	3.41	6542.32	6522.67	19.62	1726.74	*6004.61*
M-07-239	67.2	2.39	6682.57	1375.62	4403.08			
M-07-239	67.3	3019.69	3.13	6856.25	6803.36	20.54	1462.34	*6960.73*
M-07-239	67.4	3033.33	5933.89	18.00	1161.25	133266.34		
M-07-239	70.1	3301.94	16.63	2036.79	5415.00	17.88	55851.28	*91592.87*
M-07-239	70.2	60572.68	129768.16					

M-07-239	70.3	3371.66	5512.70	18.59	51692.80	72389.80		
M-07-239	70.4	3101.44	59652.54	98804.75				
M-07-239	70.5	3222.69	44671.63					
M-07-239	70.6	3029.09	6419.16	19.44	9968.76			
M-07-239	79.1	2905.85	2.15	1648.35	5677.27	16.50	6719.25	*5949.48*
M-07-239	79.2	2853.90	5.94	1346.01	5360.53	15.30	5124.23	*2204.03*
M-07-239	79.3	2821.22	4.54	1453.95	5683.04	16.03	3098.64	*2703.33*
M-07-239	79.4	2948.94	1.85	1955.34	5526.79	16.30	3290.08	*3418.77*
M-07-239	79.5	2949.42	2.34	1775.12	5543.81	16.35	3110.98	*4410.13*
M-07-239	79.6	2872.88	3.41	1975.81	6392.99	18.37	3291.13	*146868.30*
M-07-239	87.1	3424.96	31.62	411.13	44487.00	100688.51		
M-07-239	87.2	3441.64	21.95	629.37	5971.49	20.55	52858.69	*86565.42*
M-07-239	87.3	3204.13	30.31	510.07	3272.38	10.49	44351.82	*131306.11*
M-07-239	87.4	3239.17	17.37	723.01	6556.63	21.24	43179.90	*91869.51*
M-07-239	87.5	3166.97	21.79	508.04	6200.00	19.64	43749.32	*89885.51*

M-07-239	87.6	3322.76	27.87	423.82	5908.40	19.63	49027.09	
M-07-239	87.7	25.45	886.94	116178.91				
M-07-239	101.1	3273.76	51.52	423.35	6345.53	20.77	57449.30	*101070.62*
M-07-239	101.2	3297.08	15.62	1176.82	6499.21	21.43	46336.00	*104370.58*
M-07-239	101.3	3314.39	35.85	790.04	6416.00	21.27	51332.31	*56381.59*
M-07-239	101.4	3212.07	17.56	698.40	5932.46	19.06	37088.13	*116027.61*
M-07-239	101.5	3304.86	20.52	656.99	6147.74	20.32	38758.78	*49173.69*
M-07-239	101.6	3224.22	5719.84	18.44	26017.35	30529.15		
M-07-239	105.1	37.06	468.87	32886.44	134796.72			
M-07-239	105.2	3205.27	50.16	315.70	77972.60	240475.37		
M-07-239	105.3	3419.12	16.26	1129.06	94593.15	37356.00		
M-07-239	105.4	3273.76	22.39	826.42	6281.16	20.56	51913.52	*137650.90*
M-07-239	105.5	3420.19	6528.53	22.33	45490.73	126167.10		
M-07-239	105.6	3342.03	6044.55	20.20	45115.58	92280.59		
M-07-239	110.1	16.89	1718.09	37922.06	56395.44			

M-07-239	110.2	3201.81	21.23	1140.93	6450.75	20.65	22604.62	*38522.49*
M-07-239	110.3	3133.24	64.18	687.28	6313.20	19.78	48335.78	*122180.92*
M-07-239	110.4	3242.09	26.77	935.82	50544.05	107155.02		
M-07-239	110.5	3252.17	6260.78	20.36	22413.22	97619.44		
M-07-239	110.6	3445.83	6630.79	22.85	37545.33	826.61		
M-07-239	121.1	2937.28	5.84	1032.65	5197.34	15.27	272.33	*95.48*
M-07-239	121.2	2999.05	6.64	1021.93	5283.17	15.84	136.17	*94.17*
M-07-239	121.3	2957.56	8.11	1046.67	5040.16	14.91	174.18	*60.09*
M-07-239	121.4	2952.94	5.47	959.60	5109.52	15.09	177.03	*64.17*
M-07-239	121.5	5.18	1202.77	204.84	111.34			
M-07-239	121.6	2906.11	5182.54	15.06	211.44	42927.43		
M-07-239	141.1	2866.63	5.16	1409.17	5675.68	16.27	6476.00	*27570.47*
M-07-239	141.2	2870.33	7.09	1719.64	5491.11	15.76	7745.14	*36580.27*
M-07-239	141.3	2929.83	27.43	1588.61	5949.49	17.43	7394.55	*9333.34*
M-07-239	141.4	3051.59	8.94	1585.35	5400.18	16.48	7954.25	*7034.71*

M-07-239	141.5	3007.64	2.43	1661.68	5437.31	16.35	2876.37	*9031.40*
M-07-239	141.6	3009.80	9.46	1377.75	5413.11	16.29	5887.00	*20929.54*
M-07-239	157.1	2960.21	7.34	1472.06	6352.67	18.81	11743.24	*22380.28*
M-07-239	157.2	2955.20	10.35	1079.53	6273.17	18.54	9736.67	*33745.45*
M-07-239	157.3	2919.99	16.65	1575.09	6157.11	17.98	13213.98	*20691.73*
M-07-239	157.4	2988.34	10.79	1919.48	6291.15	18.80	12777.89	*17480.76*
M-07-239	157.5	28.52	1066.66	6192.41	5934.19	15191.15		
M-07-239	157.6	6784.54						
M-07-239	198.1	2749.76	5.32	4347.48	4821.73	13.26		
M-07-239	198.2	2735.89	3.68	5143.09	5118.13	14.00		
M-07-239	198.3	2734.98	5293.19	14.48				
M-07-239	198.4	2674.41	6005.22	16.06	290.34			
M-07-239	228.1	2912.60	5.88	3535.02	5051.38	14.71	221.91	*188.10*
M-07-239	228.2	2919.86	4.26	3260.18	5433.59	15.87	384.17	*219.55*
M-07-239	228.3	2911.14	5.44	4102.68	5166.01	15.04	288.75	

M-07-239	228.4	2925.57	4.71	4045.73	5264.65	15.40	234.76	*163.00*
M-07-239	248.1	2740.14	6.32	2846.86	5594.23	15.33	99.28	*33.73*
M-07-239	248.2	2762.79	5.33	4476.36	5241.06	14.48	96.14	*91.53*
M-07-239	248.3	2771.35	5.00	4445.48	5302.47	14.70	88.39	*201.75*
M-07-239	348.4	2830.51	7.15	2845.42	4949.41	14.01	94.73	
M-07-249	13.1	3702.88	43.93	447.85	6854.11	25.38	6626.14	
M-07-249	13.2	3618.64	70.03	1088.39	6718.51	24.31	6397.49	
M-07-249	13.3	49.72	762.58	6150.34	3925.76			
M-07-249	24.1	3723.37	37.01	576.79	6220.33	23.16	12970.24	
M-07-249	24.2	3730.94	6289.10	2.35	10953.23			
M-07-249	24.3	3744.01	6387.98	23.92	13713.32			
M-07-249	24.4	3753.74	6405.73	24.05	11237.78			
M-07-249	30.1	64.41	767.95					
M-07-249	30.2	3179.77	71.44	772.02	6353.42	20.20		
M-07-249	30.3	3620.31	43.04	758.25	6308.80	22.84		

M-07-249	30.4	3621.70	45.82	598.45	6313.74	22.87	165269.16	
M-07-249	41.1	63.70	548.66	6668.66	267891.00	176051.81		
M-07-249	41.2	3588.75	188.77	387.58	6977.43	25.04	321556.00	
M-07-249	41.3	39.07	1126.27	6173.86	335656.00	488757.06		
M-07-249	41.4	71.94	342.07	6768.43	234509.00	152014.15		
M-07-249	41.5	3370.46	60.21	576.53	6676.14	22.50	278509.00	*132087.91*
M-07-249	41.6	53.91	587.91	7014.93	236789.00	5302.32		
M-07-249	56.1	3265.49	9.16	1876.79	6745.19	22.03	2515.83	*8123.60*
M-07-249	56.2	3280.41	11.61	2277.23	6885.49	22.59	1846.72	*10259.11*
M-07-249	56.3	3261.52	12.44	2076.50	6939.92	22.63	2199.06	*3073.09*
M-07-249	56.4	3293.57	11.55	2088.23	7106.40	23.41	1719.46	
M-07-249	56.5	4.19	1489.27	13826.28				
M-07-249	63.1	3562.84	4.89	2269.30	7346.30	91.45	1139.93	*11849.54*
M-07-249	63.2	3062.84	2.58	3684.93	7457.57	22.84	2818.27	*17870.33*
M-07-249	63.3	3183.30	2.07	2321.37	7003.03	22.29	2120.84	*15106.61*

M-07-249	63.4	3093.71	2.23	3372.00	6902.63	21.35	2999.16	*7552.80*
M-07-249	72.1	3508.00	7.87	1948.71	7294.34	25.59	301.74	*20191.15*
M-07-249	72.2	3443.62	10.00	1431.30	7273.04	25.05	243.00	*3017.42*
M-07-249	72.3	3400.86	7050.56	23.98	253.94	5975.26		
M-07-249	72.4	3365.88	6674.82	22.47	253.55	222904.85		
M-07-249	82.1	3239.67	59.72	894.42	6873.22	22.27	110341.00	*284392.37*
M-07-249	82.2	60.47	1110.95	5640.51	253449.00	271875.85		
M-07-249	82.3	86.03	156789.00	47038.22				
M-07-249	82.4	47.97	1279.88	204567.00	97839.65			
M-07-249	82.5	3109.49	107.80	990.03	6818.95	21.20	256789.00	*226614.97*
M-07-249	82.6	6997.49	189457.00	1550.79				
M-07-249	86.1	3144.32	24.08	2443.68	6447.22	20.27	599.85	*8436.20*
M-07-249	86.2	3143.28	18.37	2760.31	6436.08	20.23	626.99	*1692.38*
M-07-249	86.3	3119.29	20.97	3737.29	6484.69	20.23	503.66	*1395.61*
M-07-249	86.4	3144.12	21.66	3988.58	6523.84	20.51	493.57	*114169.55*

M-07-249	92.1	13484.06	309670.00	262226.95				
M-07-249	92.2	155164.00	95629.49					
M-07-249	92.3	13387.00	286826.00	111384.75				
M-07-249	92.4	305903.00	123327.35					
M-07-249	92.5	12298.07	290456.00	144052.16				
M-07-249	92.6	305678.00						
M-07-249	108.1	3099.82	5147.20	15.96				
M-07-249	108.2	3098.36	5.28	3444.67	5261.42	16.30		
M-07-249	108.3	3077.38	4.88	2224.42	4931.59	15.18		
M-07-249	108.4	3087.23	4691.54	14.48	3528.64			
M-07-249	119.1	8678.00	11208.93					
M-07-249	119.2	2931.44	5.78	1527.00	5965.83	17.49	8863.00	*11349.97*
M-07-249	119.3	3.48	1492.30	5663.68	8745.00	5220.81		
M-07-249	119.4	2887.07	7.79	1483.83	5659.64	16.34	8190.00	*7230.15*
M-07-249	119.5	3.28	1492.30	5652.99	8456.00	10070.59		

M-07-249	119.6	2847.37	3.88	1981.88	5128.89	14.60	7850.00	*2255.54*
M-07-249	126.1	2.33	2576.98	10516.00	1663.58			
M-07-249	126.2	2.00	1803.16	5595.00	4537.13			
M-07-249	126.3	10.68	1830.30	6192.89	15100.00	7912.53		
M-07-249	126.4	6.20	1517.56	6299.48	22041.00	90307.83		
M-07-249	126.5	4.68	1613.79	6963.00	2259.58			
M-07-249	126.6	6428.57	12345.00	40998.24				
M-07-249	137.1	10.30	1351.87	14567.00	327193.45			
M-07-249	137.2	2969.40	4.40	1375.45	8901.00	85338.93		
M-07-249	137.3	2911.24	10985.00	8397.88				
M-07-249	137.4	5316.52	105224.00	62604.58				
M-07-249	137.5	9901.00	41562.69					
M-07-249	137.6	10678.00	6210.71					
M-07-249	150.1	2908.69	28.63	1996.79	1828.77	4358.79		
M-07-249	150.2	3066.13	15.10	1289.36	6443.66	19.76	2671.30	*9277.67*

M-07-249	150.3	10.45	1448.14	3531.82	4696.12			
M-07-249	150.4	2868.63	6342.32	18.19	4763.11	14160.23		
M-07-249	150.5	2958.51	6212.99	18.38	3255.05	911.04		
M-07-249	150.6	2934.52	6607.85	19.39	831.54	47.14		
M-07-249	157.1	2845.48	9.35	1194.99	5990.13	17.04	199.47	*2273.29*
M-07-249	157.2	20.35	1077.20	6092.75	1322.73	3904.33		
M-07-249	157.3	3053.41	20.81	1184.96	6327.95	19.32	2038.24	*823.99*
M-07-249	157.4	2835.58	6353.62	18.02	2043.49	3755.47		
M-07-249	157.5	3059.05	7276.81	22.26	19956.69	12642.05		
M-07-249	157.6	3034.99	6633.49	20.13	4323.09	475831.42		
M-07-249	166.1	3452.86	72.47	425.77	6313.22	21.80	110949.42	*1118.84*
M-07-249	166.2	2789.46	4.77	1609.44	6098.65	17.01	983.71	*2231.30*
M-07-249	166.3	8.41	1215.19	6626.07	3619.37	19640.52		
M-07-249	166.4	2707.06	5.37	1456.66	6255.48	16.93	4715.37	*20256.66*
M-07-249	166.5	2780.23	20.11	1617.85	5780.92	16.07	5580.37	*10070.98*

M-07-249	166.6	2756.57	7.76	1521.53	6181.82	17.04	3282.00	*66463.95*
M-07-249	173.1	25.93	1164.09	25400.98	5460.38			
M-07-249	173.2	3024.93	30.08	780.85	5545.07	16.77	29350.47	*12210.32*
M-07-249	173.3	67.17	509.71	4300.13	441.94			
M-07-249	173.4	2455.18	195071.51					
M-07-249	173.5	3419.36	6875.71	23.51	48609.79	216947.22		
M-07-249	173.6	3476.99	6126.95	21.30	73126.73	5685.53		
M-07-249	184.1	4.54	1693.25	2440.41	17820.03			
M-07-249	184.2	13.75	1747.44	10223.69	15814.49			
M-07-249	184.3	1865.98	6886.62					
M-07-249	184.4	11349.32	25667.49					
M-07-249	184.5	2901.00	7122.02	20.66	1508.09	6616.48		
M-07-249	184.6	2847.30	5796.25	16.50	5584.13	31724.98		
M-07-249	209.1	2775.77	4.75	1565.25	5787.86	16.07	2084.60	*64569.79*
M-07-249	209.2	2927.99	5.10	1303.85	6081.84	17.81	4935.09	*37657.90*

M-07-249	209.3	2875.79	2.64	1728.35	5904.48	16.98	2494.30	*16357.77*
M-07-249	209.4	2915.54	3.34	1691.26	5594.16	16.31	1960.93	*25358.45*
M-07-249	209.5	2947.88	5.15	1148.03	6050.52	17.84	6291.39	*9780.66*
M-07-249	209.6	2917.27	9.81	1834.61	6144.44	17.92	6867.55	*7673.42*
M-07-249	225.1	5.14	1420.10	5169.72	13099.76			
M-07-249	225.2	2834.01	6.38	1224.31	5110.50	14.48	10408.51	*8701.04*
M-07-249	225.3	48.58	744.19	7947.68	468194.20			
M-07-249	225.4	14.61	1481.03	67715.38	31480.03			
M-07-249	225.5	9.37	1495.51	17029.35	130219.65			
M-07-249	225.6	2798.84	5689.57	15.92	21867.11	31715.38		
M-07-249	232.1	3049.51	8.48	1527.74	6642.25	20.26	13715.93	*31288.46*
M-07-249	232.2	3104.98	6.47	1642.64	18292.11	51628.12		
M-07-249	232.3	5.62	1105.72	30399.72	36431.45			
M-07-249	232.4	3083.96	22702.29	17167.53				
M-07-249	232.5	3093.78	6363.64	19.69	16473.01	26726.62		

M-07-249	232.6	3157.12	5860.56	18.50	17320.77	142038.88		
M-07-249	245.1	2976.75	15.46	1385.94	5348.95	15.92	40303.02	*93187.75*
M-07-249	245.2	3078.80	11.26	1526.73	35176.65	72752.01		
M-07-249	245.3	3021.37	12.00	1260.03	5493.03	16.60	32111.77	*36746.07*
M-07-249	245.4	3029.53	6.47	1338.64	5664.88	17.16	25784.88	*94989.17*
M-07-249	245.5	2979.58	21.66	1356.50	6427.34	19.15	34755.25	*51303.13*
M-07-249	245.6	2914.14	5.31	1566.50	33108.69	66800.13		
M-07-249	256.1	13.63	1142.74	60790.70	36585.25			
M-07-249	256.2	2840.04	3.92	1310.88	5002.09	14.21	15453.08	*13555.34*
M-07-249	256.3	2780.95	11.17	1289.22	7453.21	9828.45		
M-07-249	256.4	2899.19	5048.85	15215.14				
M-07-249	256.5	2772.20	4591.48	12.73	7353.75	106052.78		
M-07-249	256.6	2897.69	4913.03	14.24	21320.94			
M-07-249	267.1	2800.18	3.58	5445.36	4817.19	13.49		
M-07-249	267.2	2749.87	5.65	3607.18	4395.91	12.09		

M-07-249	267.3	2743.25	5.62	3554.51				
M-07-249	267.4	5.08	3712.60	4293.75				
SL-13-32	9.1	3265.07	15.62	1405.74	6901.54	22.53	95351.00	*18505.01*
SL-13-32	9.2	3281.15	8.66	903.15	5928.23	19.45	94875.00	*41067.27*
SL-13-32	9.3	82556.00						
SL-13-32	15.1	3360.44	11.19	882.24	8439.28	28.36	141335.00	*8211.92*
SL-13-32	15.2	3051.03	21.48	647.65	6684.03	20.39	93284.00	
SL-13-32	15.3	3043.14	29.73	590.34	6845.85	20.83	64910.00	*46373.06*
SL-13-32	15.4	3067.78	15.27	1036.92	5421.39	16.63	79104.00	*23053.26*
SL-13-32	15.5	2907.11	6143.70	17.86	112904.00			
SL-13-32	30.1	2948.96	24.03	528.97	6713.84	19.80	44574.00	*4382.44*
SL-13-32	30.2	2957.98	7.37	645.80	6806.20	20.13	76309.00	*12093.40*
SL-13-32	30.3	2917.60	9.23	651.00	6770.32	19.75	111253.00	*21704.80*
SL-13-32	46.1	3179.37	99.13	251.07	6815.81	21.67	189555.00	*45252.69*
SL-13-32	46.2	3042.72	114.75	276.37	6998.22	21.29	236404.00	*48.05*

SL-13-32	46.3	3148.55	37.48	413.44	6324.67	19.91	257232.00	*66428.27*
SL-13-32	54.1	3127.85	33.67	630.09	6453.69	20.19	247550.00	*41033.15*
SL-13-32	54.2	3246.57	23.46	642.05	6644.54	21.57	213041.00	*33.69*
SL-13-32	54.3	3215.59	35.32	384.52	6718.70	21.61	216431.00	
SL-13-32	54.4	6820.24	158589.00					
SL-13-32	63.1	2736.55	4.12	694.70	6036.57	16.52	664.00	*50.80*
SL-13-32	63.2	2687.28	1.88	906.64	6088.26	16.36	721.00	*107.68*
SL-13-32	63.3	2727.06	3.79	716.31	5980.57	16.31	824.00	*0.16*
SL-13-32	63.4	2688.57	2.47	809.10	6140.26	16.51	687.00	
SL-13-32	71.1	2971.18	8.63	777.43	7100.55	21.10	75921.00	*36084.53*
SL-13-32	71.2	2.16	988.97	7183.32	31551.00			
SL-13-32	71.3	2898.51	14.91	850.88	7062.54	20.47		
SL-13-32	71.4	2895.34	5369.83	15.55	151709.00	669.88		
SL-13-32	87.1	3272.97	105.31	228.16	6749.59	22.09	266269.00	*6379.69*
SL-13-32	87.2	3414.88	6767.85	23.11	547395.00	77727.20		

SL-13-32	87.3	3329.71	23.91	556.62	7224.83	24.06	208923.00	*81917.40*
SL-13-32	87.4	3664.55	6407.71	23.48	481086.00			
SL-13-32	88.1	2941.52	25.52	729.93	6715.37	19.75	184936.00	*56573.38*
SL-13-32	88.2	2794.63	2.25	958.79	6427.28	17.96	17098.00	
SL-13-32	88.3	3030.24	8.50	914.29	6349.92	19.24	24875.00	
SL-13-32	88.4	2922.29	6.37	739.35	6987.11	20.42	50678.00	*15.56*
SL-13-32	111.1	2827.62	29.10	228.79	6178.83	17.47	459.00	*0.04*
SL-13-32	111.2	2768.75	3.56	366.53	5952.09	16.48	397.00	*88.95*
SL-13-32	111.3	2768.92	644.27	6165.14	17.07	481.00	22.87	
SL-13-32	111.4	2738.91	3.26	631.55	5912.99	16.20	921.00	*14.53*
SL-13-32	114.1	2709.37	4.81	692.31	5830.65	15.80	2333.00	*83.52*
SL-13-32	114.2	2699.48	5.33	812.40	5339.57	14.41	444.14	
SL-13-32	114.3	2804.36	6013.72	16.87	1020.00	41.56		
SL-13-32	128.1	2713.80	3.67	1037.01	6408.45	17.39	729.00	*1046.31*
SL-13-32	128.2	2713.20	4.00	801.24	6229.67	16.90	977.00	*2.70*

SL-13-32	128.3	2808.93	14.72	703.32	6197.67	17.41	1840.00	
SL-13-32	128.3	2738.02	2.63	869.85	6485.07	17.76	3760.00	*4433.96*
SL-13-32	149.1	2961.86	6.40	673.96	6644.54	19.68	84201.00	
SL-13-32	149.2	2963.76	3.10	1003.31	6853.81	20.31	85783.00	*17391.40*
SL-13-32	149.3	2977.84	2.11	1009.11	6841.19	20.37	91048.00	*8.70*
SL-13-32	149.4	2961.37	5.49	696.48	6748.51	19.99	7784.23	
SL-13-32	149.5	3.22	887.71					
SL-13-32	152.1	3152.76	13.21	652.01	7785.60	24.55	125566.00	*0.87*
SL-13-32	152.2	3258.69	16.39	726.78	6566.03	21.40	82603.00	*25987.46*
SL-13-32	152.3	3166.02	4.08	780.87	6228.26	19.72	232322.00	*32324.51*
SL-13-32	152.4	3237.53	25.60	632.91	6545.45	21.19	94251.00	
SL-13-32	167.1	3200.78	6.29	760.68	7012.28	22.45	76088.00	*38620.26*
SL-13-32	167.2	3122.51	5.85	772.44	6878.53	21.48	200440.00	*20.82*
SL-13-32	167.3	3267.71	40.97	525.72	6760.29	22.09	295392.00	*23206.95*
SL-13-32	167.4	32.69	477.45	5800.07	94326.00			

SL-13-32	171.1	2985.93	3.56	678.68	6920.90	20.67	124592.00	*18134.17*
SL-13-32	171.2	3019.70	3.64	795.69	6834.56	20.64	108012.00	*11055.83*
SL-13-32	171.3	2991.11	2.22	961.55	6779.09	20.28	134974.00	*49121.70*
SL-13-32	171.4	2991.42	3.73	769.96	6766.74	20.24	123603.00	*31134.26*
SL-13-32	182.1	3314.60	29.22	625.15	6960.60	23.07	183120.00	*125.12*
SL-13-32	182.2	3328.22	4.09	690.89	6612.63	22.01	66287.00	*5197.21*
SL-13-32	182.3	3098.94	15.74	681.92	6875.22	21.31		
SL-13-32	182.4	3198.17	6.94	752.10	6980.72	22.33	35714.00	
SL-13-32	199.1	3001.94	17.99	936.35	6472.34	19.43	220145.00	*4723.56*
SL-13-32	199.2	2916.02	23.25	530.33	6770.49	19.74	69115.00	*99752.62*
SL-13-32	199.3	3149.42	45.81	293.82	6227.39	19.61	206889.00	*55726.15*
SL-13-32	199.4	3236.26	6219.51	20.13	78317.00			
SL-13-32	202.1	3078.99	10.87	501.10	5673.87	17.47	102950.00	*10.04*
SL-13-32	202.2	3192.21	14.93	355.98	5483.78	17.51	48912.00	*9125.15*
SL-13-32	202.3	3273.32	18.77	337.32	5934.17	19.42	77260.00	*26149.82*

SL-13-32	202.4	3127.23	9.18	491.26	227622.00			
SL-13-32	218.1	3350.73	15.43	531.18	6940.62	23.26	234776.00	*20845.28*
SL-13-32	218.2	3319.14	14.32	435.50	6945.12	23.05	62334.00	*50.08*
SL-13-32	218.3	3173.71	3.74	612.87	7001.40	22.22	315894.00	*6503.48*
SL-13-32	218.4	3162.34	9.19	600.09	6620.85	20.94	54139.00	
SL-13-32	237.1	2794.29	3.98	728.18	6109.28	17.07	10777.00	*588.84*
SL-13-32	237.2	2806.33	2.96	719.36	6055.44	16.99	4570.00	*2069.53*
SL-13-32	237.3	2826.46	4.61	658.09	6245.56	17.65	13637.00	
SL-13-32	237.4	2802.23	4.25	615.03	6117.02	17.14	8254.00	
SL-13-32	243.1	2730.35	6.56	914.09	6207.45	16.95	13991.00	*11455.16*
SL-13-32	243.2	2704.17	5.23	754.73	6123.77	16.56	15158.00	*15.61*
SL-13-32	243.3	2720.62	6.59	837.55	6207.83	16.89	13866.00	*21.19*
SL-13-32	243.4	2678.90	3.05	921.87	6203.82	16.62	13161.00	*6136.25*
SL-13-32	250.1	2693.35	2.63	890.79	6007.00	16.18	29284.00	*1238.40*
SL-13-32	250.2	2677.45	1.24	1055.12	6128.42	16.41	40571.00	*1352.15*

SL-13-32	250.3	2692.83	2.62	671.01	6026.35	16.23	17436.00	*1.36*
SL-13-32	250.4	2664.28	6141.95	16.36	15707.00	5127.22		
SL-13-36	12.1	3479.22	59.11	477.85	6938.78	24.14	11829.17	*10508.16*
SL-13-36	12.2	3191.34	15.62	1662.97	6716.68	21.44	19800.00	*885.24*
SL-13-36	12.3	29.23	1240.87					
SL-13-36	20.1	3148.92	26.94	883.34	6934.73	21.84	12650.00	*7485.58*
SL-13-36	20.2	33.07	1563.44					
SL-13-36	20.3	52.66	492.92	6896.25	13700.00	9181.61		
SL-13-36	24.1	3295.19	23.72	1206.80	6677.24	22.00	13972.50	*1570.73*
SL-13-36	24.2	3382.33	14.18	1558.17	6660.92	22.53	30565.83	*680.86*
SL-13-36	24.3	3166.89	6721.22	21.29	23180.83	3806.80		
SL-13-36	93.1	3183.28	56.05	567.51	6574.68	20.93	11260.00	*2687.42*
SL-13-36	93.2	3201.18	51.59	637.23	6453.50	20.66	11159.17	*4.92*
SL-13-36	93.3	3188.00	60.95	476.71	6582.14	20.98	11235.00	*1747.81*
SL-13-36	169.1	2774.02	4.65	1759.86	5945.54	16.49	4742.50	*199.88*

SL-13-36	169.2	2774.66	1.29	3052.39	5924.52	16.44	3445.83	*200.14*
SL-13-36	169.3	11.48	1299.68	6108.07	4181.67			
SL-13-36	186.1	3107.22	28.59	1105.91	6713.79	20.86	23364.17	*10669.02*
SL-13-36	186.2	3083.48	27.00	1066.63	6694.29	20.64	23188.33	*8.42*
SL-13-36	186.3	3083.67	16.92	2153.43	6664.76	20.55	25021.67	*6586.04*
SL-13-36	202.1	3035.80	18.67	1181.30	6459.14	19.61	19652.50	*13148.37*
SL-13-36	202.2	3022.91	17.46	1051.36	6387.06	19.31	19699.17	
SL-13-36	216.1	3076.91	9.56	1299.99	6264.54	19.28	19969.17	*4162.64*
SL-13-36	216.2	3055.38	6.40	1125.01	6363.39	19.44	19795.83	*4.57*
SL-13-36	220.1	3234.43	6748.41	21.83	12822.50			
SL-13-36	226.1	2717.26	2.60	1287.99	6190.98	16.82	2982.50	*135.11*
SL-13-36	226.2	2724.30	3.78	1668.96	6122.72	16.68	2848.33	*172.24*
SL-13-36	226.3	2715.53	7.69	1395.24	6267.49	17.02	2765.83	*349.25*
SL-13-44	10.1	3303.38	123941.00	17250.90				
SL-13-44	14.2	3231.83	55.24	871.76	71305.00	18336.48		

SL-13-44	20.1	2985.89	23.94	1213.41	6377.95	19.04	6907.50	*5893.06*
SL-13-44	20.2	2964.60	18.30	1605.39	6101.61	18.09	6928.33	*1559.77*
SL-13-44	20.3	2974.84	8.10	1398.04	4050.99	12.05	7152.50	*2444.72*
SL-13-44	39.1	2824.29	4.14	1649.89	6366.13	17.98	73.42	*48.02*
SL-13-44	39.2	2897.31	3.60	1719.08	6347.52	18.39	63.00	*82.24*
SL-13-44	39.3	2835.59	2.93	3163.42	6475.02	18.36	96.67	
SL-13-44	57.1	3303.38	45.97	596.55	6474.80	21.39	19080.00	*11365.20*
SL-13-44	57.2	3231.83	31.05	894.23	6527.51	21.10	19115.00	*30.19*
SL-13-44	57.3	3238.43	46.01	651.61	6550.55	21.21	22218.33	*38.96*
SL-13-44	69.1	3137.01	10.45	817.75	6649.15	20.86	129329.00	
SL-13-44	69.2	3160.98	7.26	974.63	7057.18	22.31	106659.00	
SL-13-44	69.3	50.54	393.12	6582.68	209985.00			
SL-13-44	76.1	2680.84	2.64	1016.47	3707.00			
SL-13-44	76.3	2834.04	7.87	1016.42	7315.69	20.73	115071.00	*23.11*
SL-13-44	77.2	3382.17	6733.00	32010.20				

SL-13-44	77.3	2868.59	6490.35	18.62	47593.00	4795.53		
SL-13-44	87.1	2885.30	12.59	906.46	6663.79	19.23	74776.00	*13599.15*
SL-13-44	87.2	2892.10	17.57	765.29	6502.82	18.81	101430.00	*18668.47*
SL-13-44	87.3	2932.79	18.85	566.54	6411.76	18.80	76439.00	*20555.57*
SL-13-44	90.1	2931.25	6.80	1896.48	6641.07	19.47	3766.67	*2276.67*
SL-13-44	90.2	2836.74	2.39	1466.05	6464.70	18.34	5909.17	*1269.28*
SL-13-44	90.3	2862.16	3.76	1650.05	6614.77	18.93	4787.50	
SL-13-44	100.1	2873.57	7.91	1831.03	6727.27	19.33	58129.00	*16175.59*
SL-13-44	100.2	3010.61	5.47	1019.34	6708.46	20.20	80433.00	*7222.03*
SL-13-44	100.3	2941.11	16.18	779.53	6763.98	19.89	4814.13	
SL-13-44	112.1	3331.11	83.22	313.00	6565.97	21.87	321120.00	*46491.56*
SL-13-44	112.2	3479.36	41.02	199.81	6322.11	22.00	441644.00	
SL-13-44	112.3	3393.60	3.14	950.66	6434.22	21.84	447835.00	
SL-13-44	116.1	2791.12	2.11	1188.76	6216.22	17.35	42023.00	*3069.62*
SL-13-44	116.2	56.04	194.08	6396.71	43318.00			

SL-13-44	116.3	4.83	638.68	42547.00	4.84			
SL-13-44	127.1	8.62	953.65	5649.19	161016.00			
SL-13-44	127.2	2845.28	35.74	564.23	6522.45	18.56	71475.00	*25.54*
SL-13-44	127.3	2845.16	13.12	1084.69	6908.38	19.66	119214.00	*52669.29*
SL-13-44	132.1	3236.67	440066.00					
SL-13-44	137.1	3284.79	17.66	493.44	7085.93	23.28	304950.00	*119484.16*
SL-13-44	137.3	3240.41	11.28	711.06	7246.44	23.48	163076.00	
SL-13-44	155.1	3123.10	4.32	1379.24	7665.00	23.94	6316.00	*4409.69*
SL-13-44	155.2	3011.13	11.68	694.47	6530.76	19.67	14243.00	*4.94*
SL-13-44	155.3	6.40	529.53	7398.24	1.48			
SL-13-44	163.1	5.97	1011.03	6806.55	87752.00	31.08		
SL-13-44	163.2	3263.86	24.24	660.16	6717.72	21.93	127078.00	*36024.98*
SL-13-44	177.1	3258.16	6.94	1107.08	6104.07	19.89	74328.00	*3190.10*
SL-13-44	177.2	3230.98	31.86	733.79	6113.68	19.75	84629.00	*5773.37*
SL-13-44	177.3	3230.43	17.26	732.91	6221.80	20.10	99998.00	*23079.02*

SL-13-44	190.1	3190.68	15.51	640.29	6716.69	21.43	97963.00	*35569.16*
SL-13-44	190.2	3151.61	54.26	518.49	6975.68	21.99	94421.00	*5246.52*
SL-13-44	198.2	3219.73	7782.47	25.06	51475.00	11.83		
SL-13-44	198.3	3284.51	6885.55	22.62	90246.00			
SL-13-44	204.2	2805.21	608.59	6887.10	19.32	27090.00	18715.22	
SL-13-44	204.3	2827.42	6.69	756.45	6818.60	19.28	106708.00	*28.31*
SL-13-44	217.1	3263.78	17.28	786.63	6202.96	20.25	111678.00	*14377.98*
SL-13-44	217.2	42.42	886.34	6733.87	100939.00	12855.23		
SL-13-44	217.3	43.97	580.03	6779.43	6652.37			
SL-13-44	232.1	3284.14	14.96	443.87	6894.60	22.64	8013.33	*6048.10*
SL-13-44	232.2	3005.30	14.10	828.89	4901.96	14.73	8952.50	*11525.47*
SL-13-44	232.3	5860.34	27.55	673.74	7078.79	41.48	3440.83	*4.53*
SL-13-44	234.1	3215.66	6839.76	21.99	104517.00	49024.35		
SL-13-44	234.2	3199.34	6418.21	20.53	106030.00	28344.50		
SL-13-44	234.3	122215.00						

SL-13-44	246.3	3067.15	14037.14					
SL-13-44	256.1	3088.26	2.40	1389.19	6192.43	19.12	108990.00	*35.66*
SL-13-44	256.2	3161.69	9.51	778.39	5327.51	16.84	134501.00	*39.82*
SL-13-44	256.3	2927.19	52.13	405.25	6176.47	18.08		
SL-13-44	256.4	3159.35	46.03	477.05	6909.99	21.83		
SL-13-44	277.1	2707.34	24.43	596.69	7454.87	20.18	14481.67	*16149.40*
SL-13-44	277.2	3312.44	53.43	497.17	7102.60	23.53	13903.33	*14319.47*
SL-13-44	277.3	3313.98	50.60	492.81	6991.60	23.17	14127.50	*18813.74*
SL-13-44	277.4	3334.93	7115.03	23.73	123632.00	16279.49		
SL-13-44	297.1	2704.98	40.69	453.30	5729.56	15.50	5427.00	*1.94*
SL-13-44	297.2	2685.97	3.64	875.86	5468.27	14.69	6366.00	
SL-13-44	297.3	3.37	857.82	5943.33				
SL-13-56	6.1	2994.24	6.34	734.68	6845.20	20.50	1882.50	*545.00*
SL-13-56	6.2	3003.60	2.82	1444.34	6801.29	20.43	1717.92	*506.95*
SL-13-56	6.3	2993.90	5.01	1616.98	6731.44	20.15	1871.67	*292.12*

SL-13-56	12.1	3311.05	6749.20	22.35	13752.50	8.35		
SL-13-56	14.1	2752.73	1.83	1293.07	6548.32	18.03	3988.33	*533.76*
SL-13-56	19.1	2996.93	4.82	1885.23	6721.22	20.14	4319.17	*16.85*
SL-13-56	19.2	2910.81	18.54	1365.83	6371.61	18.55	3754.17	*4987.75*
SL-13-56	19.3	2936.77	18.60	1259.74	6382.98	18.75	4203.33	
SL-13-56	36.1	2889.13	8.96	2862.83	6604.10	19.08	6271.67	*3107.27*
SL-13-56	36.2	2875.03	4.53	1402.34	6599.32	18.97	4666.67	*2511.28*
SL-13-56	36.3	2972.24	6803.28	20.22	4779.17	1032.50		
SL-13-56	44.1	2749.20	8.42	2093.61	6600.62	18.15	3300.00	*361.58*
SL-13-56	44.2	2716.84	7.28	1764.16	6708.61	18.23	3931.25	*724.66*
SL-13-56	55.1	2882.30	14.55	1775.84	6553.17	18.89	4627.50	*2566.63*
SL-13-56	55.2	2919.92	6.54	1876.90	6608.52	19.30	4621.67	*1092.42*
SL-13-56	55.3	2839.50	6.59	1460.03	6590.59	18.71	4980.00	*2139.57*
SL-13-56	66.1	3023.35	7.59	1838.83	6829.84	20.65	11653.33	*3123.05*
SL-13-56	66.2	2974.56	15.12	1704.67	6747.06	20.07	10232.50	*1960.05*

SL-13-56	66.3	3016.52	10.62	1642.62	6645.91	20.05	9066.67	*716.27*
SL-13-56	76.1	3633.23	11.94	1349.98	6656.13	24.18	38763.33	*3232.11*
SL-13-56	76.2	52.21	319.56	6785.71	22887.50	16885.08		
SL-13-56	99.1	3277.14	6.44	1195.12	6285.07	20.60	16310.17	*2642.78*
SL-13-56	99.2	2915.22	71.71	357.48	6430.74	18.75	8880.00	*1750.67*
SL-13-56	99.3	3117.88	7.25	1571.45	6382.40	19.90	22088.33	*5787.41*

Curriculum Vitae

Name:	Hiruni Gunawardana
Post-secondary Education and Degrees:	University of Western Ontario London, Ontario, Canada 2010-2015 B.Sc. Honors Geology
Honours and Awards:	Dean's Honor List -The University of Western Ontario 2013-2015
Related Work Experience	Teaching Assistant The University of Western Ontario 2015-2017 Research Assistant 2013 (May-August) Research Assistant 2014 (May – August) Geological Field Assistant 2015 (June- August)

Publications:

Gunawardana, H. (2016). Paleomagnetism of the Devonian McAras Brook Formation, Avalonia revisited, AGS Colloquium (Abstract)

Gunawardana, H., McCausland, P.J.A., Good, D.J. and McBride, J. (2017) Use of anisotropy of magnetic susceptibility to analyze magmatic petrofabrics in Cu and PGE bearing gabbroic units of the Marathon Cu-PGE deposit, Ontario (Poster Abstract). PDAC Colloquium, Toronto, Canada, March 1-4, 2017

Gunawardana, H., McCausland, P.J.A., Good, D.J. and McBride, J. (2017) Use of anisotropy of magnetic susceptibility to analyze magmatic petrofabrics in Cu and PGE bearing gabbroic units of the Marathon Cu-PGE deposit, Ontario (Poster Abstract). RoundUp poster session, Vancouver, Canaga, January, 2017